CONSTRUCTION ENGINEERING OF STEEL TUB-GIRDER BRIDGE SYSTEMS FOR SKEW EFFECTS

A Dissertation
Presented to
The Academic Faculty

by

Juan Manuel Jimenez Chong

In Partial Fulfillment
of the Requirements for the Degree of
Doctor of Philosophy in the
School of Civil and Environmental Engineering

Georgia Institute of Technology
May 2012

CONSTRUCTION ENGINEERING OF STEEL TUB-GIRDER BRIDGE SYSTEMS FOR SKEW EFFECTS

Approved by:

Dr. Donald W. White, Advisor
School of Civil and Environmental Engineering
Georgia Institute of Technology

Dr. Lawrence F. Kahn
School of Civil and Environmental Engineering
Georgia Institute of Technology

Dr. Roberto T. Leon
School of Civil and Environmental Engineering
Georgia Institute of Technology

Dr. George A. Kardomateas
School of Aerospace Engineering
Georgia Institute of Technology

Dr. Reginald DesRoches
School of Civil and Environmental Engineering
Georgia Institute of Technology

Date Approved: January 10, 2012

ACKNOWLEDGEMENTS

I would like to thank all those who have contributed and supported me during my doctoral studies.

Firstly, I would like to express my gratitude to my advisors Dr. Donald W. White and Dr. Roberto T. Leon for their guidance, patience, and incessant support from the beginning to the completion of this research. My gratitude also goes to my thesis committee members, Dr. Lawrence F. Kahn, Dr. Reginald DesRoches and Dr. George Kardomateas, for their valuable comments and revisions.

I would like to acknowledge the support of my colleagues on the project Cagri Ozgur and Andres Sanchez who provided invaluable help and strong complementary work to this research. I also would like to thank Yoon Duk Kim, Cliff Bishop, Akhil Sharma and, Yavuz Mentes for making the office a positive, collaborative work environment.

The research described in this thesis is a combined effort funded by the National Cooperative Highway Research Program and is a part of the Project NCHRP 12-79, Guidelines for Analytical Methods and Erection Engineering of Curved and Skewed Steel Deck-Girder Bridges. The financial support from the National Cooperative Highway Research Program (NCHRP) is gratefully acknowledged. My graduate studies were also possible by financial support from the Mexican National Council of Science and Technology (CONACYT). Their generous support enabled me to pursue my graduate education as the sole professional focus during my tenure as a graduate student.

I would like to thank my family and especially my parents Gumesindo and Minerva for their constant encouragement and unconditional support.

None of this would have been possible without the unconditional support, love, patience, and sacrifice of my loving wife Itzel Noriega. She made this enterprise possible and worthwhile from the very first beginning and will continue beyond its conclusion.

TABLE OF CONTENTS

LIST OF TABLES

LIST OF FIGURES

SUMMARY

Closed structural sections, such as those having circular, rectangular or trapezoidal shape, possess high rotational rigidity when compared to open sections such as I-girders. The high torsional rigidity of closed sections makes them ideal for use in highly curved bridges. In this case, the geometry of the bridge results in large torsional forces. Because of structural efficiency and economy reasons, most of these closed-section bridges consist of a trapezoidal cross-section, with a top concrete slab and bottom and side steel plates. The slab is cast after the steel is erected and thus a system of internal diaphragms and braces is necessary to stabilize the system during erection. During the steel erection and the early stages of the concrete deck placement, the section can be considered as quasi-closed as the top concrete flange has not been cast or is not yet effective.

During steel erection, undetermined and/or large torsional forces and/or displacements may result in fit-up problems requiring large stresses to overcome. During concrete deck placement, the undetermined displacements can affect the control of the deck thickness and the final deck geometry, such as the alignment of deck joints and the matching of stages in phased constructions projects.

Due to the interactions between their various components, the behavior of curved and skewed tub-girder bridges is significantly more complex than that of straight bridges. When skewed supports are used in tub-girders, the interaction of the girder bending rotations and the displacement constraints induced by the skewed support diaphragms causes twisting of the girders at the supports. These twist rotations introduce additional torques into the system. Both curvature and skew can cause design and construction difficulties, especially at the supports, where the corresponding steel dead load deflections and the large torsional stiffness of the girders may lead to large fit-up forces. Currently, the general understanding of the level of sophistication of analysis models required to properly predict forces and deformations of curved and/or skewed bridges during construction is limited. The development of guidelines regarding the sufficiency

of simplified methods of structural analysis is the overall motivation and objective of this dissertation.

This research addresses the construction load effects due to skew and due to combined skew and curvature and develops design recommendations and analytical tools for the construction engineering of tub-girder bridges. The effects of skew and curvature are studied by examining the results for different levels of analysis for 18 representative bridges. These bridges reflect the range of bridge curvature and skew used in current practice. By comparing the output from simplified analysis methods to validated refined 3D FEA solutions, general conclusions are developed as to when the simplified methods provide sufficient results.

An important original contribution of this research is that the data generated constitutes the first systematic study on a large set of curved and skewed tub-girder bridges using consistent refined 3D FEA models to model construction forces and deformations. As such, the results of this research can serve as a benchmark for current and future improvements in methods of analysis and design for the construction engineering of curved and skewed tub-girder bridges. In the current research, this data has been used in both straight and curved tub-girder bridges to:

- Develop a simplified 1D analysis method to account for the effect of skew on girder twist rotations and internal torques,
- Evaluate the effect of skew on component forces, and propose improved simplified procedures to capture these effects,
- Identify interactions between components and develop improved simplified analysis methods to account for these effects,
- Establish limits for when the improved 1D and 2D simplified methods of analysis are sufficient for construction engineering analysis, and
- Identify sources of steel erection fit-up problems, and to develop guidelines for estimation of the fit-up forces.

CHAPTER I.

INTRODUCTION

1.1 Problem Statement

The quasi-closed geometry of tub-girder bridges provides high rotational rigidity, which makes these systems ideal when high torsional loads are expected. In addition, tub-girder bridge systems have advantages in terms of span range, durability and aesthetics compared to other types of steel girder bridges. Because of structural efficiency and economy reasons, tub-girder bridges consist of a trapezoidal cross-section, with a top concrete slab and bottom and sloped side steel plates (Figure 1.1). A system of internal cross-frames, diaphragms and flange lateral bracing is required to stabilize the system during erection and concrete deck casting. During the steel erection, the section can be considered as quasi-closed as the top concrete deck has not been cast. The torsional forces and associated displacements due to curvature, skew or eccentric loads may result fit-up problems during erection and/or in large stresses or geometry control problems during erection and concrete deck placement.

The bracing system is essential because, in addition to providing stability, it provides strength and stiffness to the tub-girders. This results in large forces being transferred to and from the plate girder system. In consequence, the bracing interaction with the girders results in a complex behavior that needs to be analyzed.

In practice, the analysis of tub-girders often is performed via simplified methods that require additional analytical tools to evaluate the contribution of the bracing components to the girder behavior. As the complexity of the system increases with the use of skewed supports, the traditional simplified analysis methods may not be capable of correctly predicting the behavior, and the bridge analysis may require the use of refined 3D finite element analysis methods. However, the benefits of the quasi-closed section properties of the tub-girders are significant when the bridge system must withstand high torsional loads with a small number of girders. Tub-girder systems are ideal for bridge

configurations demanding high torsional stiffness such as in curved interchange ramps and long spans subjected to torsional loads due to skew or large eccentric loading.

Figure 1.1. Tub-girder bridge under construction at the Marquette Interchange, Milwaukee, WI. (Courtesy of T. Shkurti, HNTB).

At the bridge supports, the tub-girder rotations generally are driven by the major-axis bending. The in-plane stiffness of solid plate support diaphragms constrains the girder rotations to occur about the bearing line. When the bearing line is perpendicular to the girders, only major-axis bending rotations occur at the supports and the girder twisting is essentially constrained to be zero. However, when a bearing line is skewed, the constraint from the support diaphragms forces the girders to twist at the supports. These imposed twist rotations induce additional girder torques and twist rotations within the bridge span.

Tub-girder systems are particularly well suited for applications requiring high torsional stiffness. Despite the large tub-girder stiffness, which results in smaller displacements, overcoming construction displacements to fit-up the steel components may require relatively large forces. The displacements during construction are affected by the curvature and skew. The use of skewed supports is often avoided in tub-girder bridges due to the potential for fit-up problems during the steel erection and the lack of guidelines for designers as to the level of sophistication of the analysis required to properly predict

the forces and deformations during construction. The development of simplified analytical tools for the early design process, and guidelines for using various simplified analysis procedures, is the overall motivation and objective of this dissertation.

1.2 Current Status

In current practice (2011), tub-girder systems can be analyzed at basically three levels of increasing sophistication as indicated in Figure 1.2. The first level is known as the 1D Line-Girder method (Fig. 1.2a). In this approach, the individual bridge girders are modeled as individual straight beams. This method uses a simplified approach to estimate the moments resulting from curvature, and the skew effects often are not included prior to the work presented in this dissertation. The second method is known as 2D-Grid analysis (Fig. 1.2b). This approach models the bridge as a horizontal grid of beam elements, capturing directly many of the overall curvature and skew effects. When using either of these simplified methods, the forces acting in the tub-girder bracing and other components are not directly modeled in the analysis. Rather, these component forces are estimated by separate component force equations. The component force equations are based on fundamental strength of materials idealizations and work with the girder major-axis bending moments and the torques from the structural analysis as input. A few of the equations depend on the girder vertical displacements and twist rotations from the structural analysis. The accuracy of the estimates depends on the ability of the simplified analysis methods to capture these quantities. In addition, of course, the accuracy of the estimates also depends on the accuracy of the strength of materials idealizations used in the development of the component force equations. The 1D and 2D methods are recognized as simplified approaches that cannot capture all of the potentially important effects. However, they are preferred due their ease of use for design. Clearly, there are cases where they fail to adequately predict the behavior and more refined methods are needed. There are also cases where these methods are sufficient. It is important generally for the engineer to utilize an appropriate analysis model for the task at hand. This research seeks to better quantify the accuracy associated with the various approximations.

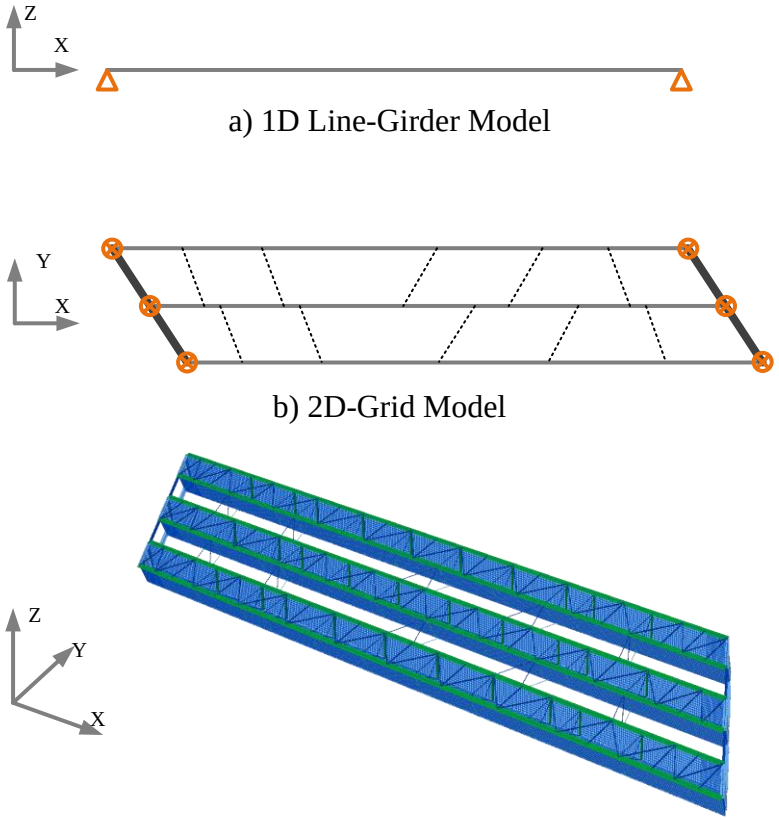

Figure 1.2. Models for 3D FEA, 2D-grid, and 1D line-girder levels of analysis.

The last level of analysis depicted in Fig. 1.2 is a refined 3D Finite Element Analysis or 3D FEA (Fig. 1.2c). This type of analysis directly represents each component of the bridge including the main girder plates and the secondary bracing elements at their actual positions. The 3D FEA approach is a much more detailed analysis, both in terms of the number of elements utilized and the detailed information needed for the definition of all the components. This method offers the significant advantage of directly providing stresses and deformations without further processing. Nevertheless, 3D FEA is not widely adopted due to its inherent greater complexity both in model preparation and checking and in handling of the large volume of data output.

This research addresses the construction load effects due to skew, and due to combined skew and curvature, and develops analytical tools for the construction engineering of tub-girder bridges. The effects of skew and curvature on the accuracy of simplified analysis methods are studied by examining the results for different levels of

analysis of increasing sophistication for 18 different bridges. These bridges reflect the range of tub-girder bridge curvature and skew observed and expected in design practice. By studying the bridge behavior and evaluating the simplified analysis methods against validated refined 3D FEA, general conclusions are developed as to the accuracy of simplified analysis results.

1.3 Objectives and Scope

1.3.1 Objectives

The objective of this research is to provide design guidelines and analytical tools for the construction engineering of curved and/or skewed tub-girder bridges. This research intends to evaluate methods of determining the construction load effects due to curvature and skew on an independent and combined basis. Both curvature and skew can cause design and construction difficulties, especially at the supports, where the corresponding deflections and/or distortions may lead to fit-up difficulties.

1.3.2 Scope

This research focuses on tub-girder bridge systems with the following characteristics:

- Two or more trapezoidal open section girders with a top flange lateral bracing system,
- Single celled girders with internal cross-frames to control distortion.
- Straight or horizontally curved girders,
- Radial or skewed supports,
- Simple or continuous-spans, and
- Non-integral piers and abutments.

Emphasis is placed on the analysis of steel erection and concrete deck placement stages prior to the concrete providing composite strength to the system. This research does not address the wide range of additional overall considerations for the complete analysis and design of tub-girder bridges, such as the design of the structure in its final constructed condition for vehicular live load effects.

1.4 Original Contributions

An important original contribution of this research is that the data generated constitutes the first systematic study to model construction forces and deformations in a large set of curved and skewed tub-girder bridges using consistent refined 3D FEA models. As such, the results of this research can serve as a benchmark for current and future improvements in methods of analysis and design for the construction engineering of curved and skewed tub-girder bridges. In the current research, this data has been used in both straight and curved tub-girder bridges to:

- Develop a simplified 1D analysis method to account for the effect of skew on girder twist rotations and internal torques,
- Evaluate the effect of skew on component forces, and propose improved simplified procedures to capture these effects,
- Identify interactions between components and develop improved simplified analysis methods to account for these effects,
- Establish limits for which improved 1D and 2D simplified methods of analysis are sufficient for construction engineering, and
- Identify sources of steel erection fit-up problems, and develop guidelines for estimation of the fit-up forces.

1.5 Organization

The overall thesis organization is as follows. Chapter 2 begins by describing the tub-girder system components and by providing a brief review of previous studies that address the effects of curvature and skew in tub-girder bridges. Chapter 2 then presents a more detailed discussion of the three main types of analysis described in Section 2.2 in order to identify both the strengths and weaknesses of each method and opportunities for improvements in the 1D and 2D methods.

Chapter 3 presents proposed improvements to the 1D and 2D methods for tub-girder bridges with skewed supports. These improvements are based on a simple mechanics of materials approach to evaluate the influence of skew on tub-girder responses. The effects of skewed supports on the tub-girder cross-section distortions are

considered negligible because the torque originates discretely at the supports. At these locations, the solid plate diaphragms distribute the reaction forces and induce predominantly a St. Venant torque in the girders. The localized effects of forces from the top flange lateral bracing (TFLB) system are re-evaluated to include an additional effect, referred to as "sawtooth" stresses, which can lead to significant localized increases in the top flange longitudinal normal stresses.

Chapter 4 discusses the selection of a large set of existing and parametric study tub-girder bridges utilized for this research. In total, 28 tub-girder bridges were analyzed using 3D FEA to evaluate the bridge behavior under a wide range of geometric parameters including skew and curvature. Eighteen of these bridges were analyzed using simplified analysis methods. This set of bridges was used to evaluate the simplified analysis methods against refined 3D FEA to identify sources of errors and highlight needed improvements in the simplified methods.

Chapter 5 uses the analytical studies from Chapter 4 to evaluate the estimation of the torsional moment due to skew by the simplified analysis methods presented in Chapter 3. In addition, this chapter evaluates the accuracy of the simplified analysis methods on the stresses, displacements, and component force estimations.

Chapter 6 studies various tub-girder construction engineering considerations. Simplified equations are presented to evaluate the forces needed to overcome displacement incompatibilities due to steel dead load deflections during the steel erection. In addition, this chapter discusses practices recommended by Helwig et al. (2007) to limit the deck cross-section distortion during concrete deck placement. Lastly, a proposed analysis procedure is given for cases when twin bearings are used. The effect of skewed supports on each of the above considerations is discussed.

Lastly, Chapter 7 summarizes the contributions of this research and further research needs are described.

Appendix A provides the detailed 3D FEA, 2D-grid and 1D line-girder results of five tub-girder bridges. Appendix B shows a validation of the component force equations by comparing simplified procedure results to refined 3D FEA analysis for a published

benchmark model of a tub-girder system. Appendix C presents the layouts of the existing bridges collected in this research. Appendix D gives brief summaries of the 3D FEA results for the 18 analytical study bridges considered in this research.

CHAPTER II.

BACKGROUND

2.1 Tub-Girder Bridge Systems

Figure 2.1 shows a common configuration of a twin tub-girder system labeling the most common components described below. A tub-girder is a quasi-closed trapezoidal single celled box system consisting of two sloped webs, two top flanges, and one bottom flange connecting the webs. The girder webs can be stiffened longitudinally and transversely and the bottom flange can be longitudinally stiffened. The tub-girder is braced at the top flanges by a horizontal truss known as top flange lateral bracing system (TFLB system) and transversally by plate diaphragms and cross-frames. Multiple tub-girder systems typically are connected externally at the supports by plate diaphragms and by cross-frames at intermediate locations along the span. However, generally cross-frames or diaphragms may be utilized at either location. Plate diaphragms are referred to in this research as end diaphragms when located at the abutments and as support diaphragms when located at intermediate piers. The diaphragms and cross-frames are referred as internal if they are located inside the tub-girder and external if they connect adjacent girders.

The top horizontal truss is used to provide bracing to the top flanges and acts similar to an effective solid top flange plate, thus establishing the quasi-closed properties of the girders. This truss also provides stiffness to the system under major-axis bending. The truss is composed of diagonals and struts. Single diagonal systems with Warren and Pratt layouts as well as X-type two-diagonal layouts are common.

The cross-frames are composed of a top-chord, diagonals and bottom-chord. The internal cross-frame layout uses inverted-V-type cross-frames without a bottom-chord in the majority of the cases, but can have a bottom chord member attached to the bottom flange or to bottom flange longitudinal stiffeners, and also can use an X-type layout. The external cross-frames use V-type or X-type layout. V-type cross-frames are the most common configuration.

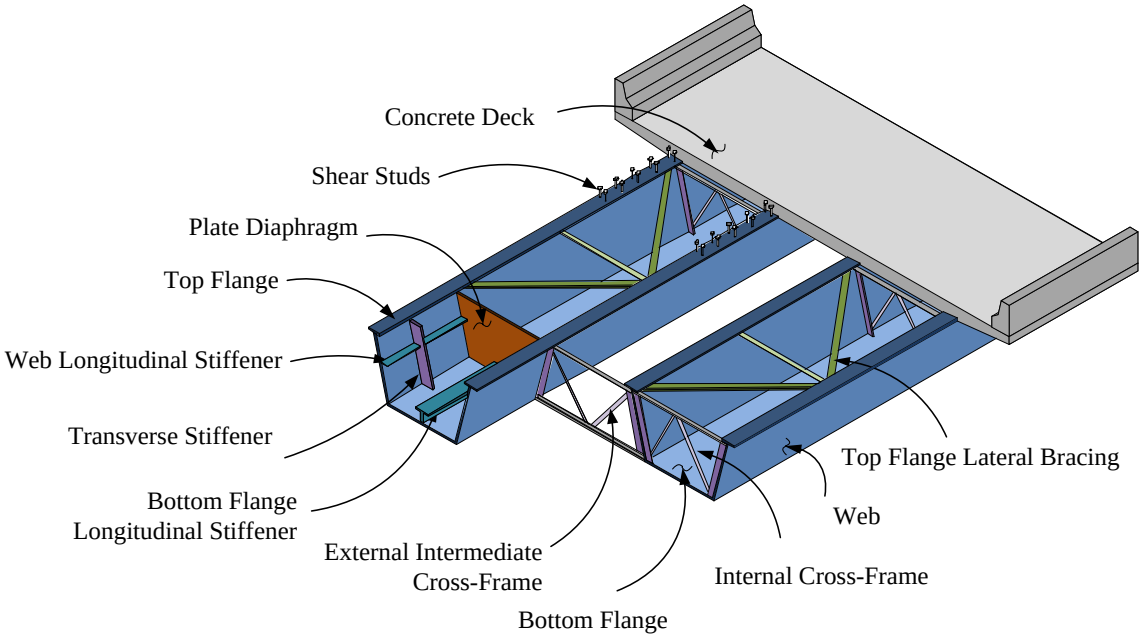

Figure 2.1. Components of a tub-girder system.

Internal plate diaphragms are stiffened at their top and external diaphragms at their top and bottom. These stiffeners are commonly known as the diaphragm flanges. For typical configurations where these components are relatively deep compared to their length, the main function of such elements is to stiffen the diaphragm rather than to provide bending strength. The plate diaphragms are commonly stiffened at the support points and around access holes.

The tub-girder system is completed by a reinforced concrete deck that provides composite strength to the bridge. To achieve the composite strength, shear studs are used at the top flanges to connect the concrete deck. During concrete placement, prior to hardening of the concrete, the steel tub-girders provide the entire system strength. This can be a critical stage of the bridge for the design of the bracing components. Once the composite strength is achieved, the bracing of the steel tub-girder by the TFLB system and by any external intermediate diaphragms often is regarded as unnecessary. The support diaphragms or cross-frames are still essential to distribute the end reactions to the girders and resist the overall torsion of the girders, and the intermediate internal cross-frames are essential to restrain girder cross-section distortion under the torsional loads.

2.1.1 Literature Review

The earliest studies of tub-girder bridges are based on analysis simplifications that permit estimates of the quasi-closed girder section torsional properties. However, the estimation of the bracing components behavior, such as the top flange lateral bracing system, requires additional component force equations. Various studies have been conducted to develop component force equations, which transform the major-axis bending and torsional moments, or the girder displacements and rotations from the analysis, into the bracing component forces. The importance on the estimation of the component forces is due to the importance of the bracing to the strength and stiffness of the entire system. The bracing components are an essential part of the overall structural system.

The analysis simplifications on tub-girder bridges are based on developments by Dabrowski (1968) and Kollbrunner and Basler (1969). These developments consider the top flange lateral bracing system as an equivalent plate. This method, known as the "Equivalent Plate Method", permits the estimation of the torsional behavior of quasi-closed box- and tub-girders as equivalent closed sections allowing the use of simplified analysis.

Tung and Fountain (1970) introduced the "M/R Method" as a simplified analysis procedure to estimate the torsional effects due to horizontal curvature in box girders. The method estimates the effects of horizontal curvature as an equivalent distributed torsional moment equal to the major-axis bending moment M divided by the radius of curvature R. The combined use of the M/R and Equivalent Plate approximations are key developments for the simplified analysis of tub-girder systems.

University of Houston, University of Texas at Austin, and Texas Department of Transportation research has had a major impact in the development of bracing component force equations. Helwig et al (2007) provide a comprehensive compendium of the research in this area, including Fan and Helwig (1999 and 2002) and Fan (1999) both focused on improving the top flange lateral bracing and cross-frame component force equations. Li (2007) studied the effect of partial depth end diaphragms and conducted

parametric analyses addressing skew effects. Li recommended several basic factors to adjust the girder torsional moments to account for the influence of skew. Topkaya and Williamson (2003) developed 3D FEA software for analysis of curved tub-girder bridges during construction.

Additional experimental and field studies have been developed by Chen (1999) on the buckling of tub girders with top flange bracing, and by Chen et al. (2005) on bracing forces and stay-in-place metal deck forms. Cheplak et al. (2002) and Memberg et al. (2002) focused on field studies for the assessment of external intermediate cross-frames. The accuracy of the developments by Fan and Helwig were reassessed by Kim (2004) and Kim and Yoo (2006). These researchers recommended the calculation of additional contributions to the bracing component forces from cross-section distortion effects.

The combined efforts of the National Highway Institute (NHI) and the National Steel Bridge Alliance (NSBA) have provided recent developments in the area of tub-girder bridges including general design guidelines by Coletti et al. (2005) and the development of design examples for tangent and curved bridges by the National Highway Institute (NHI, 2007 & 2011). Also, the National Steel Bridge Alliance (NSBA, 2006) has published recommended guidelines for design details on tub-girder bridges as well as guidelines for general structural analysis of steel girder bridges, including tub-girder bridges (NSBA, 2011).

El-Tawil and Okeil (2004) analyzed a set of curved tub-girder bridges to investigate the warping-related stresses. The analytical studies by El-Tawil and Okeil assumed that the bridges had an internal cross-frame system to help resisting the distortional loads. Under these assumptions, El-Tawil and Okeil concluded that warping had little effect on both shear and normal stresses in all the cases on their study. Previously, Heins (1975) reached the same conclusion after studying warping in bridge tub-girders by evaluating the forces necessary to restore warping deformations on an open tub-girder section.

With the exception of Li (2007) all the previous developments address only tangent and curved bridges with radial supports. Li addressed skew effects via a

parametric study of simple-span bridges with one span length, five curvature configurations and one skewed support with six different skew angles. Li provided insight on the additional torsional moments due to skew. However, the mechanism by which the skewed supports modify the bridge behavior was not directly identified and studied.

The use of skewed supports in tub-girder bridges typically is avoided in current practice since their effects are not well understood and the potential for fit-up problems is high because of their torsional stiffness. This dissertation builds on the previous research by focusing on a detailed evaluation of the skew effects on straight and horizontally curved tub-girder bridges.

2.1.2 Tub Girders

The tub girders are composed of two top flanges, two webs and one bottom flange. The main trapezoidal cross-section geometry (girder depth, tub width and separation) often is kept constant while the plate thickness is varied along the bridge length. The tub-girders are oriented with the bridge cross slope to simplify the design and detailing of the girders. Bridges with cross section changes other than the plate thicknesses are not considered in the analytical studies of this research.

The open girder tops (with a TFLB system) allow fabrication advantages over closed box sections and the sloped webs help reduce the bottom flange width while maintaining the spacing at the top to support the concrete deck. The web slope typically is limited to 1-to-4 to reduce the transverse shear on the web. AASHTO (2010) provides various proportioning guidelines for tub-girders.

2.1.3 Bracing Elements

The bracing elements in a tub-girder are used primarily to carry loads caused by bending and torsion. They also help in preventing cross-section distortion.

Two types of bracing are used in a tub-girder system: the internal bracing which provides stability and resists cross-section distortion and the external bracing used to control the relative displacements between tub-girders. The top horizontal truss and the

internal cross-frames are considered as internal bracing. The external intermediate cross-frames are considered as external bracing as they interconnect girders at places other than the supports. Plate diaphragms also serve as bracing elements but they are used more often as support elements to distribute the reaction forces.

2.1.3.1 Top Flange Lateral Bracing

The horizontal top truss provides bracing to the top flanges and creates a pseudo-closed box. This truss is often connected to the top flanges and is to be referred in this dissertation as top flange lateral bracing (TFLB). The TFLB system provides a path for the shear flow due to St. Venant torsion. This is analogous to what would happen in closed boxes but one side of the box (the top) is open and the force flow on that side of the box is only through the bracing member. The TFLB also helps resist the force effects due to bending as it interacts with the top flanges directly. The torsional stiffness of the quasi-closed tub-girder system is in the order of a thousand times larger than in a comparable I-girder. This characteristic makes the tub-girder system ideal for high torsional loadings such as those experienced by long and narrow bridges and some skewed bridges.

The TFLB system is composed of diagonals and struts. The truss can have different panels using single or multiple diagonals. The single diagonal truss types can follow Warren and Pratt layouts. The multiple diagonal truss panels are X-type. Different behavior is achieved by using a different truss layouts and therefore the selection of the TFLB system should consider the effects of load distribution, local and girder effects and the cost of fabrication.

The TFLB typically is modeled as an equivalent plate in order to compute the St. Venant torsional properties of the tub-girder system. Kollbrunner and Basler (1969) provide equations to transform the system in an equivalent plate for different truss types. These characteristics are used for simplified analysis methods. The approach for the use of such equations is discussed in Section 2.2.1.2.

The length between the connection points of the TFLB truss to the top flanges is known as the TFLB panel.

2.1.3.2 Internal Cross-Frames

The internal cross-frames are transverse elements that provide stiffness in their planes, and help resist distortional loads and prevent cross-section distortion during fabrication, transportation, construction and service. During construction the girders typically are lifted and temporally supported at these cross-frame locations. This practice reduces the chances of distorting the girder cross-section and it distributes the self-weight loads to the system.

The cross-frames are composed of a top chord and diagonals and use inverted-V or X-type layouts. The components of the cross-frames are connected to the girder at connection plates welded normal to the webs, these plates also serve as web transverse stiffeners.

The internal cross-frames typically are spaced every two panels, but other configurations exist. AASHTO (2010) limits the spacing to a maximum of 40 ft.

2.1.3.3 External Intermediate Cross-Frames

External intermediate cross-frames are used to connect the adjacent girders at intermediate locations along the span of the bridge. These cross-frames control the vertical displacements and girder locations to prevent distortion of the general layout of the bridge during the concrete deck placement. Once the concrete deck has hardened, the deck provides additional stiffness to the tub-girder system, eliminating the need for the external cross-frames. For this reason the external cross-frames are often seen as temporary elements which can be removed. The use of external-intermediate cross-frames is often unnecessary as the tub-girder vertical and twisting stiffness is sufficient to limit the relative girder displacements within an acceptable tolerance.

The behavior of the external intermediate cross-frames depends mainly on the tub-girder stiffness. As mentioned before, these cross-frames control the relative displacements between girders and for that reason the acting forces can be estimated by assuming that the cross-frame is relatively rigid in its plane.

Section 2.3.3 discusses the modeling techniques considered in this research for the estimation of external intermediate cross-frame forces.

The external intermediate cross-frames can use any type of V- or X-type layouts. The V-type is the most common as this reduces the unbraced length of the bottom-chord.

External cross-frames can also be used at the supports. In the common practice however, full height solid plate diaphragms are used because of their larger stiffness .

2.1.3.4 Diaphragms

AASHTO (2010) defines a diaphragm as a "vertically oriented solid transverse member connecting adjacent longitudinal flexural components or inside a closed-box or tub section to transfer and distribute vertical and lateral loads and to provide stability to the compression flanges". For tub-girders these can be internal or external. Internal diaphragms are located at the interior of the tub-girder while the external are located in between adjacent girders. Diaphragms used at the abutments are referred to in this research as end diaphragms. When used at intermediate piers in continuous-span bridges, they are referred to as support diaphragms and often have stiffened access holes to allow inspection. Diaphragms can also be used instead of regular cross-frames at internal intermediate locations but the use is not as common as the regular cross-frames since they pose complicated connection details and may make the tub-girder inspection more difficult. Plate diaphragms do not provide significant restraint against girder cross-section warping as their out of plane stiffness is limited.

Reduced height diaphragms have been used in practice but these have been shown to be inefficient as they may not provide enough in-plane stiffness at the girder ends (Li, 2004). Li recommended that the solid plate diaphragms should be as deep as practicable. Li analyzed a set of parametric bridges via 3D FEA and showed that partial depth end diaphragms were poor at limiting the end twist rotations. Li's parametric studies showed that connecting the external diaphragm flanges to the girders had little impact on the bridge response for aspect ratios (length/height) less than approximately three.

Diaphragm web plates typically are vertically and horizontally stiffened. The vertical stiffeners are located at the bearing location to help distribute the support reaction. The top of the internal diaphragm and the top and bottom of the external diaphragm the diaphragms are horizontally stiffened, these stiffeners are known as diaphragm flanges however, these elements are used only to stiffen the plate and the flanges are often unconnected to the girders.

For simplified analysis purposes, this research shows that the internal diaphragms often may be regarded as rigid elements in their planes. This idealization and the analytical evidence for it is discussed in Section 3.1.1.1.

2.1.4 Curvature and Skew Conventions

The following developments assume the following conventions to specify curvature and skew and the associated signs for the torques and rotations.

- All curved bridges are oriented concave upward in their plan view with the center of curvature located toward the top of the page.
- The skew angles are measured with respect to a line perpendicular to the bridge centerline, i.e., a support line with no skew has a zero skew angle.
- Counterclockwise skew angles are positive.

The characteristics and limitations of the analysis methods are discussed in the following section. The tools necessary to obtain the bracing component forces from the 1D and 2D results are discussed in Section 2.3. The bracing component forces are based on the bending and torsional moments, as well as in some cases, on the girder vertical displacements and rotations.

2.2 Methods of Structural Analysis

In broad terms, three different levels of analysis are employed in bridge design practice. The first one is referred to as a 1D line-girder analysis, the second as a 2D-grid and the third as 3D Finite Element Analysis. The following subsections discuss these methods of analysis.

2.2.1 1D Line-Girder Analysis

The most basic method for analysis is the line-girder analysis. Its simplicity allows the designer to perform basic design and provide preliminary member sizes for subsequent refinement. In some cases, the line-girder method can be sufficient depending on the characteristics of the bridge but in general tub-girder bridges are complex systems requiring advanced understanding of the behavior of the multiple components.

The line-girder method assumes straight girders acting independently from each other, that is, the interaction between girders is ignored. The effects of elements interconnecting the girders must be analyzed separately to obtain a coarse estimate of their behavior and their effect on the full system.

Tub-girders are assumed as single line elements whose loads are assumed to be applied on the girder centerlines. The girders are expected to behave as boxes and the torsional characteristics given by the top flange lateral bracing contribution is included in the girder properties as described in Section 2.2.1.2. The single girders are analyzed as simply-supported or continuous-span beams depending on the nature of the bridge.

The loads during steel erection and concrete placement are based typically on tributary areas including the girder self-weight, weight of the deck, formwork and overhangs. The load is applied as a distributed load at the girder centerline and any effects of eccentric loading are added as an additional torsional moment applied to the girders. For live load analysis, the system behaves as a composite section and the AASHTO (2010) provides a set of recommendations for live load distribution similar to those used for other girder systems.

The line-girder method directly provides only vertical displacements and major-axis bending moments. Supplementary calculations are needed to estimate the effects of curvature and skew. Supplementary equations also are used for calculation of the forces in the multiple bracing components of the tub-girder system. Curvature effects are included in the analysis as described by the M/R Method (Tung and Fountain, 1970). These authors provide an estimate of the distributed torsional loads and their effects can be found via integration or by the conjugate beam method. Skewed supports have an

impact on the girder lengths, which correspondingly influences the relative girder stiffnesses. Furthermore, the skew affects the torsional moment distributions. The developments presented in Chapter 3 provide a simplified method to include the additional torsional effects which otherwise would not be included in a 1D analysis.

Sections 2.3 summarize the calculations commonly utilized to extend the line-girder method results to estimate the bracing component forces, such equations are valid for 1D and 2D methods.

2.2.1.1 Mechanics of Curvature

The girders' quasi-closed behavior makes tub-girder systems ideal for configurations that require a high torsional stiffness and strength such as highly curved and relatively narrow configurations. The parametric cases studied in this research are assumed mostly to be narrow bridges and have span length to deck width ratios larger than five. This limit corresponds to a minimum span length of 150 ft typically for tub-girder bridges, and a minimum deck width of 30 ft for a one or two lane bridge.

The top flange lateral bracing system in tub-girder bridges provides a quasi-closed configuration for the development of the St. Venant torsion. Internal cross-frames are placed to limit the cross-section distortion. The warping normal stress effects are small in typical tub-girder bridges as reported by Heins (1975) and Okeil and El-Tawil (2004). The torsional behavior of tub-girders permits the estimation of the torsional effects using the M/R Method (Tung and Fountain, 1970). In contrast, individual I-girders perform poorly to carry torsional loads and their torsional capacity is usually neglected. The effects of curvature on I-girder systems can be estimated with the V-Load Method (USS, 1965) as shear forces on the cross-frames.

The following discussion explains the quasi-closed characteristics of tub-girders and the origin of the torsional moments induced by the horizontal curvature. This development is used to incorporate the curvature effects as a distributed torque in simplified line-girder analyses. The equations for estimating the component bracing forces account for the horizontal curvature effects via the use of the equivalent distributed torque M/R.

2.2.1.2 Quasi-Closed Section Model

Tub-girders physically are not closed sections. The top of the girder is left open to facilitate construction and reduce material. A truss, framework or lattice at the top of the girder replaces the top plate and provides the equivalent effect of a plate connecting the top flanges. This allows tub-girders to be considered as closed or quasi-closed sections provided that the TFLB system is capable of transferring the torsional effects.

Dabrowski (1968) and Kollbrunner and Basler (1969) developed equations to estimate the contribution of the top truss into the system to be replaced as a fictitious equivalent plate known as the Equivalent Plate Method. The equivalent plate thickness can be determined for different truss layouts and cross-sectional areas of the diagonals and struts.

This method provides a simplified way to estimate the torsional properties of the tub-girder as a closed box section. The equations and associated dimensions for different top flange lateral bracing truss layouts are shown in Figure 2.2.

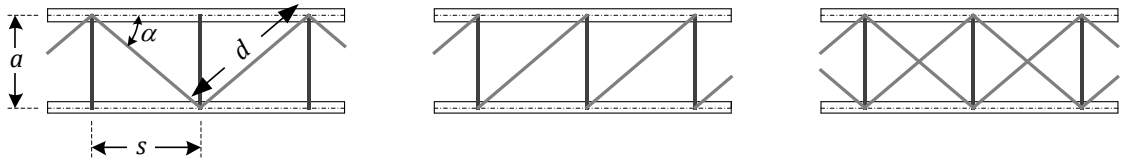

Warren Layout

$$t^* = \frac{E}{G}\frac{sa}{\left[\frac{d^3}{A_d} + \frac{2s^3}{3A_f}\right]}$$

Pratt Layout

$$t^* = \frac{E}{G}\frac{sa}{\left[\frac{d^3}{A_d} + \frac{a^3}{A_s} + \frac{2s^3}{3A_f}\right]}$$

X-type Layout

$$t^* = \frac{E}{G}\frac{sa}{\left[\frac{d^3}{2A_d} + \frac{s^3}{6A_f}\right]}$$

A_d = Cross section area of diagonal
A_f = Cross section area of the top flange
A_s = Cross section area of strut
E = Modulus of elasticity
G = Shear modulus
a = Tub top width (Strut length)
d = Diagonal length
s = Panel length
t^* = Equivalent plate thickness
α = Diagonal angle

Figure 2.2. Equivalent plate thickness for the top flange lateral bracing system.

The equations shown in Figure 2.2 represent the most common layouts used in tub-girder systems with equal top flange dimensions. Other layouts can be found in Kollbrunner and Basler (1969). These equations assume that the truss elements are simply and concentrically connected to the tub-girder plates. For eccentrically connected

elements, Heins (1975) provides a set of equations for a modified equivalent plate thicknesses.

The Equivalent Plate Method allows the estimation of the girder torsional constant as

$$J = K_T = \frac{4A_0^2}{\sum_i b_i / t_i} \tag{2.1}$$

where A_0 is the area enclosed by the tub-girder, and b_i and t_i are the width and thickness of the plates. The warping contribution to the torsional resistance is negligible when compared to the St. Venant contribution in tub-girders and is often ignored when estimating the torsional resistance.

The torsional constant is of the order of 100 to 1000 times that of a comparable I-girder section, making tub-girders ideal for supporting large torsional loads. Under this assumption, the M/R Method, discussed in the next section, permits the evaluation of the torsional moment along the length of a tub-girder.

2.2.1.3 The M/R Method

The M/R method is a simplified tool for estimating the torsional effects due to curvature in general box-girders. This method, which was first introduced by Tung and Fountain (1970), applies an equivalent distributed torsional moment M/R to an individual girder, where M is the major-axis bending moment and R is the radius of curvature. This method assumes that each of the box-girders in the bridge cross-section deforms independently of the other girders for a given span. That is, any interaction between the girders due to their interconnection via the bridge deck and/or intermediate external diaphragms is neglected. The assumptions behind the method are explained by Figure 2.3 where a free-body diagram is shown for a box girder differential segment *ds*.

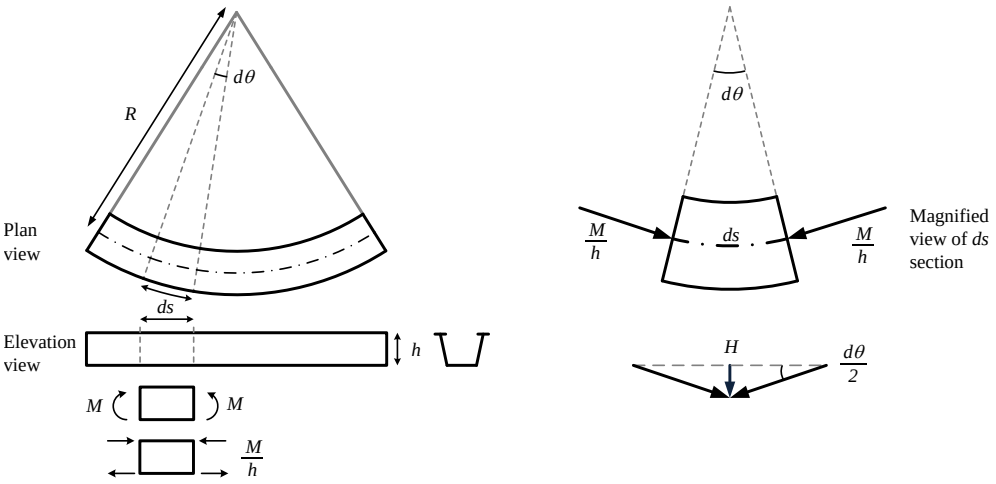

Figure 2.3. Force equilibrium at an infinitesimal curved section.

The unbalanced flange force H due to curvature at a given segment ds, which is the arc length of the angle $d\theta$, is

$$H = 2\left(\frac{M}{h}\frac{d\theta}{2}\right) = \frac{M}{h}\frac{ds}{R} \tag{2.2}$$

By dividing both sides of the equation by ds, one obtains the equivalent distributed lateral loads q applied at the top and bottom of the section

$$q = \frac{H}{ds} = \frac{M}{h}\frac{ds}{R}\frac{1}{ds} = \frac{M}{Rh} \tag{2.3}$$

These loads produce the equivalent distributed torsional moment M/R shown in Fig. 2.4.

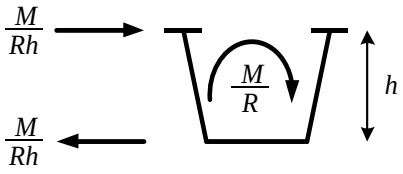

Figure 2.4. M/R torsional moment.

2.2.1.4 Torsional Moment Due to Curvature

Given the M/R method assumption that no interactions occur between the girders along the span length, the internal torsional moment at a given position s can be found as

$$T_C(s) = T_{C0} - \int_0^s \frac{M(s)}{R} ds \tag{2.4}$$

where *M(s)* is the distribution of the major-axis bending moment along the length. T_{C0} is the torsional moment at $s = 0$ given by

$$T_{C0} = \frac{1}{L}\int_0^L \frac{M(s)}{R}(L - s) ds \tag{2.5}$$

For a simple-span bridge with a constant radius of curvature *R*, subjected to uniformly distributed vertical load *w*, the corresponding internal torsional moment is

$$T_C(s) = \frac{wL^3}{24R} - \frac{ws^2(3L - 2s)}{12R} \tag{2.6}$$

Based the conventions utilized in this research (see Section 2.1.3.4), the bridge would be shown in plan with its center of curvature at the top of the page. The internal torsional moment would start at the left-hand support with a positive value and would vary according to the above cubic polynomial, ending at the right-hand support with an equal but negative torsional moment. The girder would twist such that the top flange to bottom flange relative vertical displacement, referred to in this thesis as the layover of the girder, moves away from the center of curvature. The sign of these layovers and the corresponding twist rotations is assumed positive.

For multiple continuous-spans the M/R procedure requires the assumption that the torsion in each span is independent of the other adjacent spans. This is a reasonably good assumption for ordinary radially-supported tub-girder bridges, since the girder torsional response is dominated by St. Venant torsion and twisting is essentially restrained at each of the supports. The above equations are then applied to each span of the bridge. The integration is commonly carried out numerically.

The simple-span curved tub-girder bridge NTSCR1 (the bridge designations are discussed in Chapter 4), which has a span length $L = 150$ ft and radius of curvature $R = 400$ ft, is shown in Figure 2.5. Each girder of the bridge is subjected to a distributed vertical load of $w = 2.84$ kip/ft. The torsional moment distribution can be estimated by

means of Eq. 2.6 and is shown in Figure 2.6 for Girder 1 (the girder on the outside of the curve).

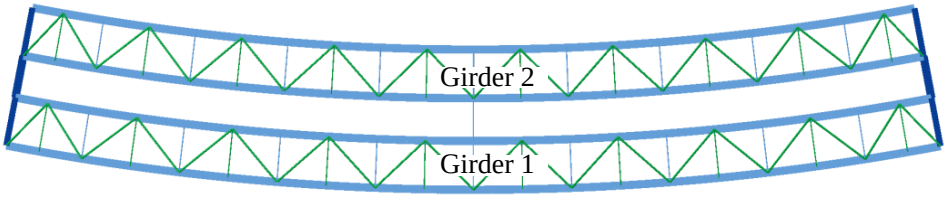

Figure 2.5. NTSCR1 Bridge Layout.

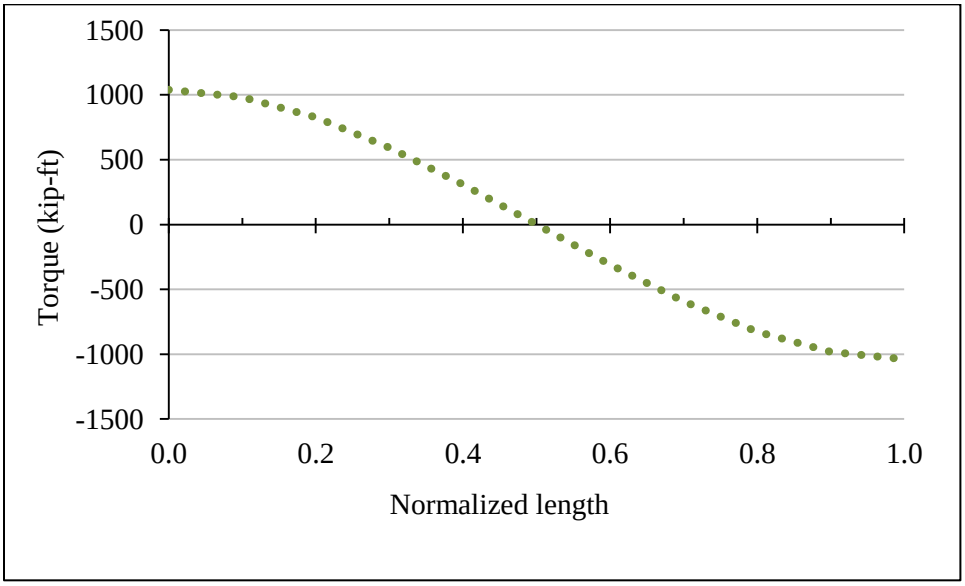

Figure 2.6. NTSCR1 Torsional moments for Girder 1.

2.2.1.5 Curvature Induced Twist Rotation

Tung and Fountain (1970) also developed a simplified approach to evaluate the girder twist rotations along the length of the girder. The girder twist rotation at the position s due to the horizontal curvature $1/\underline{R}$, $\phi_{x,C}(s)$, is proportional to the girder vertical displacement $\Delta(s)$ and is estimated as

$$\phi_{x,C}(s) = \frac{1}{R}\left(1 + \frac{EI}{GJ}\right)\Delta(s) \tag{2.7}$$

where E and G are the steel elastic and shear modulus, I is the moment of inertia and J is the St. Venant torsional constant of the girder.

The estimate given by Eq. 2.7 assumes that the girder twist is zero at the support line. This is typically a sufficient approximation at abutments or piers with external and/or internal diaphragms or cross-frames oriented normal to the girders. For skewed supports, this assumption is modified by the introduction of an additional twist rotation, discussed in Chapter 3.

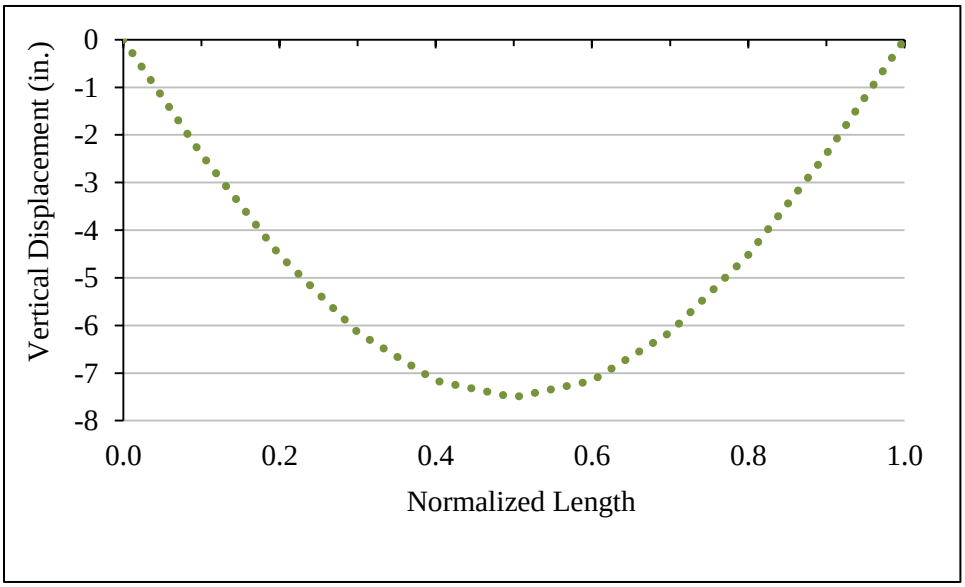

Figure 2.7. Centerline vertical displacements for Girder 1.

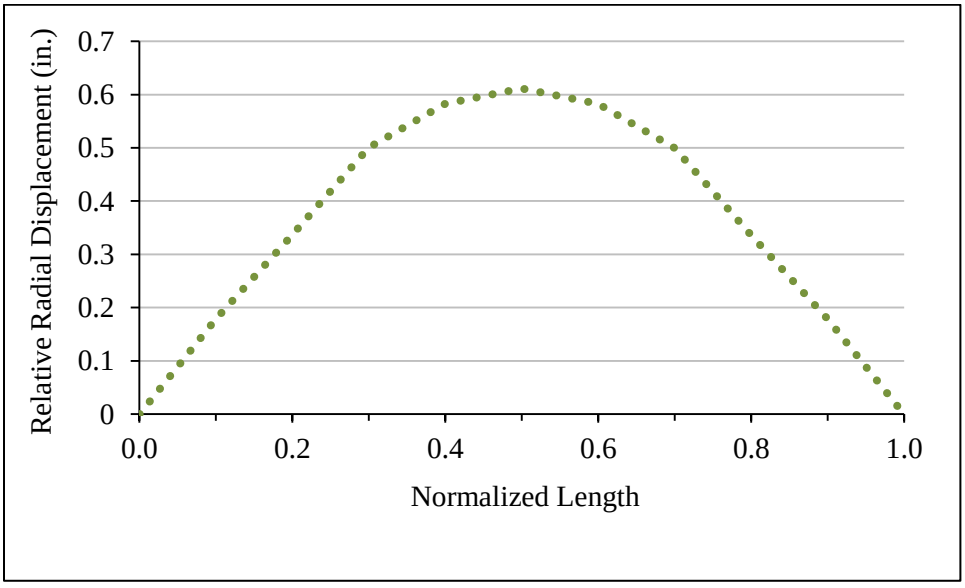

Figure 2.8. Relative radial displacements for Girder 1.

Figure 2.8 illustrates the top to bottom flange relative radial displacements determined from the twist rotation given by Eq. 2.7 and the vertical displacements shown in Figure 2.7 for the NTSCR1 bridge.

Appendix A, Section A.1, provides detailed results of the M/R Method for the torsional and relative lateral displacements of this bridge, and compares to the results obtained from the 3D FEA and 2D-grid methods. The M/R Method torsional moments show good agreement in distribution and magnitude with the other analysis methods for the NTSCR1 bridge.

2.2.1.6 Previous Research on Skew Effects in Tub-Girder Bridges

Li (2004) analyzed a set of parametric curved tub-girder bridges to study the effects of the skewed supports on the bracing elements. The parametric studies conducted by Li consisted of simple-span bridges with one span length, five curvature configurations and one skewed support with six different skew angles.

While a curved radially-supported tub-girder bridge would exhibit a symmetrical distribution of the bracing forces, skewed bridges show a shift in the internal forces, i.e. the forces in the bracing do not vary symmetrically along the span. To address this effect, Li (2004) recommended an approach in which the torsional moment obtained from a hypothetical radially-supported bridge is increased by specified percentages to obtain the internal torsional moment in the corresponding skewed bridge. The recommended percentages are based on fitting to maximum results from the parametric studies. The mechanism that causes the increased torque was not evaluated in Li's research.

The developments in the following chapter address the skew effects based on a mechanistic evaluation of the girder/diaphragm interaction. This approach provides a clear understanding of the effects of skew as well as a method to directly include these effects in the tub-girder component force equations.

2.2.2 2D-Grid Analysis

The 2D-grid method is possibly the most commonly used simplified approach for tub-girder bridge analysis in current practice. The method is capable of directly modeling important geometric characteristics such as horizontal curvature and skewed supports. In

the 2D-grid method, the girders typically are analyzed as line elements with two nodes per element and three degrees of freedom (DOF) per node: two rotational, which capture the major-axis bending (DOF 2 and 5) and torsional (DOF 3 and 6) responses and one translational (DOF 1 and 4) that captures the displacements normal to the plane containing the grid, (see Fig. 2.9). Tub-girders are idealized as single beams with bending and torsional properties that reflect the characteristics of the internal bracing components from the quasi-closed section model discussed in Section 2.2.1.2. In addition, the external bracing components are modeled in the grid. All the girders, external cross-frames and external diaphragms are modeled at their centerlines in the plan of the structure, and all of these components are assumed to be located in a common horizontal plane and connected together at this common elevation. Vertical offsets and depth of the elements are ignored, meaning that all the bearings, girders, external cross-frames and diaphragms are modeled at the same elevation. This is the source of the name "2D-grid."

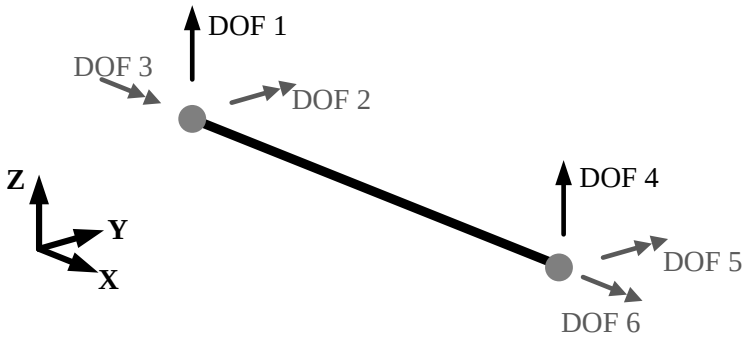

Figure 2.9. Schematic representation of the general two-node element implemented in computer programs for 2D-grid analysis of tub-girder bridges.

Although practically any structural analysis software can be used to perform a 2D-grid analysis, commercial software specialized in bridge design is most commonly used for the grid approach mainly due to the live load analysis capabilities as well as phased construction analysis. In this research the MDX package (MDX Software 2011), as well as, the LARSA software (LARSA, 2011) are used for the analysis studies conducted using 2D-grid models. In the remainder of this dissertation, the LARSA and MDX programs are referred to as Program 1 (P1) and Program 2 (P2), respectively.

It is possible to modify the basic 2D-grid approach to obtain a better approximation to the system behavior, by including additional degrees of freedom or adding eccentricities or offsets in some members. When additional degrees of freedom are included, the method may be referred to as a 2D-Frame model. A 2D-Frame model uses six degrees of freedom at each node, but all the elements are still modeled in the same plane. This approach typically is used in general purpose structural analysis software. Given the most common models, the displacements at each of the three additional degrees of freedom at each node are all zero in the 2D-Frame model, and hence the results are theoretically identical to those of the basic 2D-grid model. Therefore, this model may also be referred to as a 2D-grid approach.

When the engineer models the actual eccentricity of the bridge deck and includes a shell FEA model of the composite deck, the procedure is commonly referred to as a Plate and Eccentric Beam (PEB) model. A PEB model provides a specific representation of the centerline elevation of the girders and actual elevation of the concrete deck. The deck is modeled using shell finite elements and the girders are modeled with frame elements, offset relative to the deck and having six degrees of freedom per node. The PEB approach provides substantial benefits for live load analysis, since the deck surface is modeled by shell elements, while maintaining a relatively small total number of degrees of freedom in the overall model via the frame element representation of the steel girders. .

The LARSA Software implements the 2D-grid model and outputs displacements, bending and torsional stresses that permit the estimation of the bracing forces via the component force equations presented in Section 2.3. The MDX Software implements the Plate and Eccentric Beam approach. However, the composite action given by concrete deck is not included in these studies. This renders the model as a basic 2D-grid solution for stages not including the composite action of the concrete deck. The MDX Software input requires detailed characteristics of the bracing elements to support the bracing force calculations internally. Under certain conditions, the torsional response of tub-girder bridges is captured relatively well by the 2D methods, as they can model skew and curvature and capture their effects directly. In other cases, the 2D methods can exhibit

some inaccuracies in their representation of the behavior of the external intermediate cross-frames and diaphragms and, in consequence, may fail to accurately capture the effects of skew and curvature.

2.2.2.1 Conventional 3D-Frame

A 3D-Frame model is an extension of the 2D-grid models when the frame elements include the vertical offset and use six degrees of freedom per node. The girders and external cross-frames are modeled at their actual centroidal elevations. Rigid offsets are used to include locate all the components and the bearings at their actual elevations. The cross-frames are still modeled as frame elements using equivalent stiffnesses.

Similar to the 2D methods, the torsional response of the quasi-closed section is also captured relatively well by conventional 3D-frame elements. Therefore, the 3D-frame method is reasonably accurate provided that the tub-girder internal bracing systems are properly designed to provide sufficient torsional stiffness. However, there are a number of approximations of the 3D-Frame model that can potentially lead to some loss of accuracy. These include:

- Conventional 3D-frame elements typically do not account for differences between the shear center axis and the centroidal axis in their formulation, and
- The width and depth ratio of the tub-girder cross-sections is typically very similar to the length and depth of the external cross-frames. However, the 3D-frame model represents all of these components as line elements. The finite size of girder cross-section within the "nodal" regions is not explicitly modeled.

It should be noted that these approximations also apply to the more common 2D-grid analysis models.

With respect to the second bullet point above, the transfer of shear and moment from the external cross-frames or diaphragms to the tub-girders involves internal diaphragms or cross-frames in the girder cross-section, as shown in Fig. 2.10. The detailed force transfer between the external and internal cross-frame, the webs, the top flanges and the bottom flanges involves more degrees of freedom than included in the

3D-frame models. Therefore, some type of simplified idealization is necessary for 2D-grid, 2D-frame and 3D-frame models to represent the detailed responses in these regions. If the internal cross-frames or diaphragms at these locations have any significant flexibility within their plane, the resulting deformations cause distortion of the corresponding tub-girder cross-section.

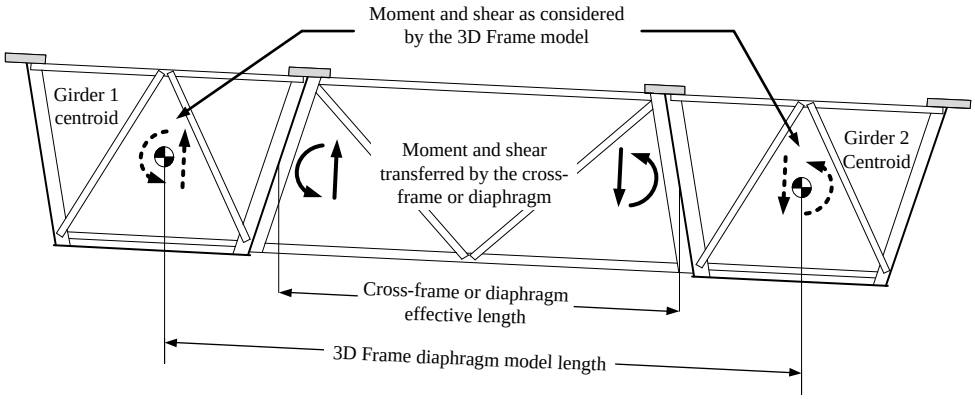

Figure 2.10. Moment and shear force transfer from the external cross-frames or diaphragm to the tub-girders.

2.2.3 3D Finite Element Analysis (FEA)

A 3D Finite Element Analysis (FEA) is a model where the superstructure is modeled fully in three dimensions and all of the components are represented at their nominal physical geometric locations using their nominal physical dimensions. Combinations of shell, truss and beam elements are commonly used to represent the bridge components. Diverse 3D FEA implementations are possible for modeling bridge systems. The approach used for this research is discussed in detail below.

For the purpose of this research the individual girder flanges are modeled using beam, shell or solid type elements, the girder webs are modeled using shell or solid type elements, the cross-frames or diaphragms are modeled using truss, beam, shell or solid type elements as appropriate, and, although its strength and stiffness is not included in the analysis in this research, the concrete deck can be modeled using shell elements. The three-dimensional elastic finite element analyses conducted in this research involve the use of:

- A general-purpose 4-node quadrilateral Reissner-Mindlin (shear-deformable) shell element for modeling tub-girder webs, and tub-girder bottom flanges. The tub-girder webs and bottom flanges are modeled at skewed bearing lines by "fanning" the geometry of the quadrilateral elements.
- A compatible 2-node shear-deformable beam element for modeling tub-girder top flanges, bearing stiffeners, connection plates, intermediate transverse stiffeners, longitudinal stiffeners, and the "lips" of tub-girder bottom flanges extending outside of the webs.
- A 2-node shear-deformable beam element for modeling of cross-frame chords. The cross-frame chords are modeled at their physical location through the depth of the structure. Their connections into the girders are modeled generally using multi-point constraints so that the FEA discretization through the depth of the webs does not have to be adjusted to place nodes at the specific cross-frame chord depths.
- A 2-node truss element for modeling of cross-frame diagonals, and for modeling of top flange lateral bracing.

Figure 2.11 shows a segment of a twin tub-girder bridge unit illustrating these finite element representations on the various structural steel components. The nearer web has been removed to facilitate the visualization of the interior components.

The girder webs are modeled between the centerlines of the girder flanges in the above model. The flanges are at the correct physical depth in all cases, and the model of the web has an overlap of t_f /2 with the flange areas, (See Fig. 2.12). The resulting additional web area is on the order of the steel area from web-flange fillet welds. The web-flange fillet welds are otherwise not explicitly included in the model. At transitions in girder flange thicknesses, the centerline of the flange elements shifts with the change in thickness, therefore, the depth of the girder web also shifts with changes in the flange thickness in the FEA model (See Fig. 2.12). The average of the two flange thicknesses is used within a one-element transition length at any change in the flange thickness. This transition element is located on the side of the transition with the larger area.

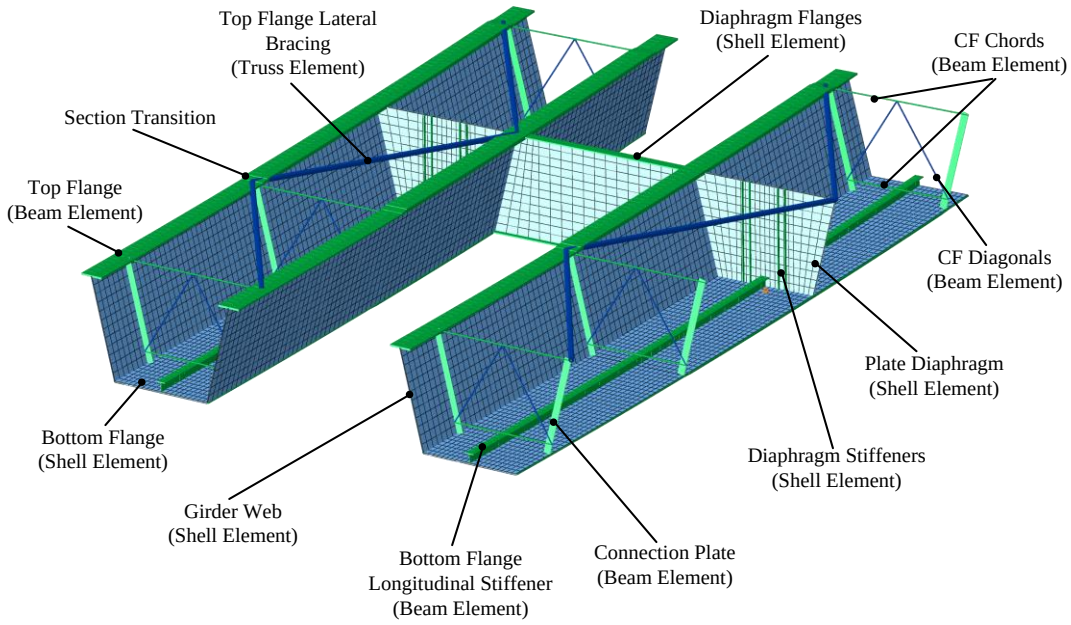

Figure 2.11. Example of the 3D FEA modeling approach on a segment of a twin tub-girder bridge unit (nearer web not visible).

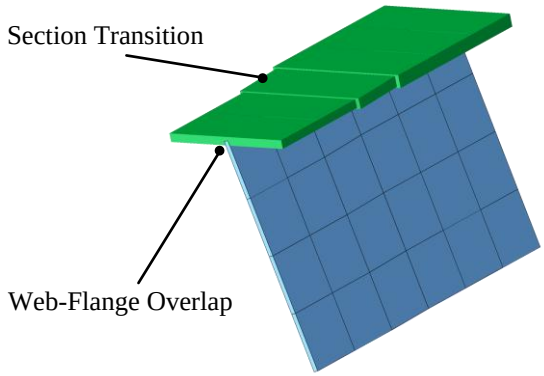

Figure 2.12. FEA Model Detail at flange section transition.

In addition to the above, the 3D FEA modeling approach employed in this research invokes the following idealizations:

- Similar to the above modeling idealizations, all beam and truss elements representing bracing members are connected directly into the work point locations at the mid-thickness of the girder webs, or in the case of flange-level lateral bracing at the web-flange juncture.

- The support bearings are modeled as a point vertical support at the intersection of the bottom flange and an end diaphragm. A rigid rectangular patch with dimensions equal to those of the sole plate is modeled on the bottom flange. The girder model is generally free to rotate about the point support location. Horizontal displacement constraints representing guided bearings are placed at the point support location, where applicable.
- The substructure is modeled as a rigid support, including any temporary towers for construction.
- Uplift at the bearings is modeled, where it is allowed, by using a "one-directional" support.
- Both geometrically linear (linear elastic) and geometrically nonlinear (second-order elastic) behavior of the elements is considered. The second-order amplification of the displacements and internal forces typically is small in tub-girder bridge systems, however.
- Superelevation, grade and vertical curves are not included in the models. It is believed that in most situations in practice, the bridge response to vertical (gravity) loads during construction is not significantly influenced by these attributes.
- The weights of the structural steel components are modeled as distributed body loads of 490 pcf in all of the finite elements.
- The weights of formwork (10 psf) and the concrete slab including the reinforcing steel (150 pcf) are modeled using equivalent vertical line loads at the middle of the top flanges of the girders, based on the tributary widths. The influence of eccentric loads on the slab overhangs, supported by overhang brackets, is modeled as a force couple composed of two equal and opposite horizontal distributed loads, one at the level of the top flange and one at the level of the bottom of the overhang brackets.
- The weight of construction equipment is neglected since the accuracy of the simplified methods can be assessed without including these loads.
- Steel erection stages are modeled by activating the portion of the steel structure for that stage and "turning on" the corresponding gravity loads.

- Holding cranes are modeled as a rigid vertical point support with no horizontal restraint at the hold location.
- Tie downs are modeled as rigid point supports.

ABAQUS 6.10 (Simulia 2010) is the specific software utilized in this research for all the 3D FEA studies. Model generators were developed that permitted a streamlined comprehensive description of complete tub-girder bridge structures for this purpose. The specific ABAQUS elements utilized and the corresponding FEA discretization selected for the design analyses are as follows:

- 12 S4R shell elements are utilized through the web depth. The S4R element is a linear-order (i.e., linear displacement field) 4-node quadrilateral Reissner-Mindlin displacement-based shell element with reduced integration. For geometric nonlinear analysis, the element is formulated for large strain. The number of shell elements along the girder lengths was selected such that all the shell elements on the web have an aspect ratio close to 1.0.
- The top flanges, the various stiffeners and the cross-frame connection plates are modeled using the B31 element, which is a two-node beam element compatible with the S4R shell element.
- The bottom flanges are modeled using 20 S4R elements through their width. One B31 element is used on each side of the bottom flange to model the "lips" of the bottom flanges that projects beyond the intersection of the flange with the webs.
- The solid plate diaphragms in tub-girder bridges are modeled using S4R elements for their web and B31 elements for their flanges. The trapezoidal geometry of the diaphragm webs is represented by "fanning out" the S4R element geometries.
- The cross-frame chords also are modeled using B31 elements.
- The cross-frame diagonals as well as the top flange lateral bracing struts and diagonals are modeled using the T31 truss element. When integration of the stresses is performed these elements are switched to B31 beam elements.

It should be noted generally that geometric nonlinear elastic FEA solutions, using the above models, are utilized as the primary standard for evaluation of the different simplified 1D and 2D models in Chapter 5. In general, tub-girders exhibit a linear elastic behavior (negligible geometric non-linearity) for the bridges studies conducted in this research.

2.3 Calculation of Bracing Forces from Line-Girder and 2D-Grid Analysis Results

Due to the idealization of the tub-girders, cross-frames and diaphragms as line elements in the simplified analysis methods, the analysis of tub-girder bridges by any of the simplified methods requires component force equations to estimate the internal and external bracing response.

To ensure good accuracy in the evaluation of the bracing component forces in curved and skewed bridges, the overall bridge analysis must capture the effects of curvature and skew with good accuracy. In general, conventional 1D line-girder analysis calculations inherently do not include curvature or skewed support effects. They include a separate torsional analysis of the individual girders, via the M/R Method to account for the influence of horizontal curvature as discussed previously in Section 2.2.1. The torsional effects of skewed supports on the bracing elements are addressed in Chapter 3. The 2D-grid method is able of directly including the influence of curvature and skew, provided that the support and intermediate diaphragms and cross-frames are accurately represented in the model.

From 1D line-girder and 2D-grid analyses, the vertical displacement and major-axis bending stress estimates can be obtained easily; however, to obtain responses such as top flange lateral bending stresses and bracing component forces, the analysis results must use component force equations to account for the interaction of the bracing elements and the girder plates.

The component force equations for tub-girder bracing presented below were developed by Fan and Helwig (1999 & 2002) and Helwig et al (2007). These developments extend the research by Kollbrunner and Basler (1969) based on the internal and external mechanics of the tub-girders. To evaluate the accuracy of these component

force equations, Chapter 5 presents an evaluation of the analytical studies and Appendix A shows the detailed analytical results of five tub-girder bridges with different geometry including curvature and skew. The analytical results compare the accuracy of the simplified analysis methods for the evaluation of girder displacements, top flange stresses and top flange lateral bracing forces using the following developments and the improvements proposed in this research.

2.3.1 Top Flange Lateral Bracing Diagonals and Struts

The top flange lateral bracing (TFLB) system is considered as an equivalent plate for the purposes of determining the torsional response in the simplified methods. The TFLB system also contributes to the flexural stiffness of the girders but its contribution is usually neglected in the analysis. The TFLB is essential for the construction stages of a tub-girder bridge, especially for the deck placement when the steel girders must possess sufficient strength to resist the wet concrete load. However, once the concrete deck has hardened, the steel and concrete work together and neutral axis of the composite cross section shifts closer to the deck, minimizing the contribution of the top truss to the composite cross section but reducing the fatigue induced problems in the top truss system.

The torsion developed on the cross-section due to curvature and/or skew is carried mainly via the St. Venant shear flow, due to the closed section behavior. The idealizations discussed in Section 2.2.1.2 provide the basis to consider the tub-girders as quasi-closed sections due to their top flange lateral bracing system. Since the girders act as closed sections, the effects of warping torsion tend to be negligible. AASHTO (2010) requires the use of sufficient internal cross-frames such that distortion of the girder cross-section under torsional loads is commonly neglected, except for checking of fatigue.

The top flange lateral bracing diagonals and struts resist different effects of the bending and torsional moments, as well as horizontal loads resulting from the tub-girder sloping webs. The following sections describe the origin of the forces and discuss the component force equations for these elements.

2.3.1.1 Forces in the TFLB Diagonals

As the diagonals connect at different locations along the span length, they are subjected to associated axial strains due to the bending and torsion. Since the tub-girder is analyzed as a quasi-closed cross section, the shearing effects due to torsion T can be estimated by means of the shear flow on a closed section with enclosed area A_0 as

$$q = \frac{T}{2A_0} \tag{2.8}$$

The diagonals transmit the torsional effects between consecutive panel points of the TFLB system. The distortional forces due to torsion are assumed to be resisted by the internal cross-frames limiting the magnitude of the distortional forces that the diagonals and struts are subjected to.

For a truss system with a single diagonal in each panel, the force due to pure torsion is

$$D_{Torsion} = \frac{qa}{\sin\alpha} \tag{2.9}$$

where a is the truss width (i.e., the tub-girder width between the top flanges), and α is the angle of the diagonal measured from the flange centerlines. For a double diagonal system, the load is equally distributed between the two diagonals, resulting in a strut force of one-half that shown in Eq. 2.9 (see Fig. 2.13).

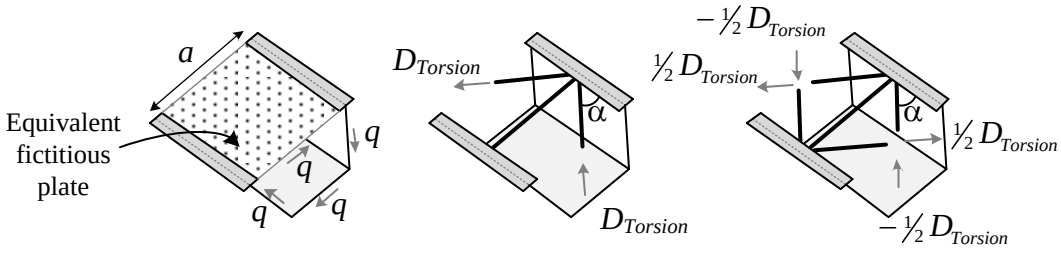

Figure 2.13. Forces on the top flange lateral bracing diagonals induced by torsion from the Equivalent Plate Method.

The top flange lateral bracing system also interacts with the girder bending since the system is subjected to the same major-axis bending strain level. The top truss is

assumed to be connected at the top flange level which is approximately true for many practical applications. This assumption results in a conservative estimate of the loads on the truss (correspondingly, it tends to over-estimate the equivalent girder stiffness). The following equations are taken from Fan and Helwig (1999) and Fan (1999). Fan (1999) also presents a solution for top trusses vertically offset from the top flange.

Since the top truss is a discrete system connected at different points along the length of the girder, the truss components resists the relative bending deformations between these locations. Figure 2.14 illustrates the calculation of the axial deformations in a diagonal (i.e., axial relative end displacements) of an X-type top flange lateral bracing system. In this figure, the diagonal is subjected to relative displacements between its ends, *u* and *v*, due to the major-axis bending of the girder, as well as the corresponding transverse strut deformations, resulting on a deformation Δ_{diag}. In contrast, Figure 2.15 illustrates the calculation of the TFLB diagonal axial deformation in a single diagonal system due to the relative flange lateral displacements at the ends of the diagonal. In this figure, v_1 is the relative lateral displacement of the girder flanges between the two ends of the diagonal. In addition, the relative lateral displacements of the ends of the diagonal are influenced by the elongation of the transverse struts, denoted by the term v_2.

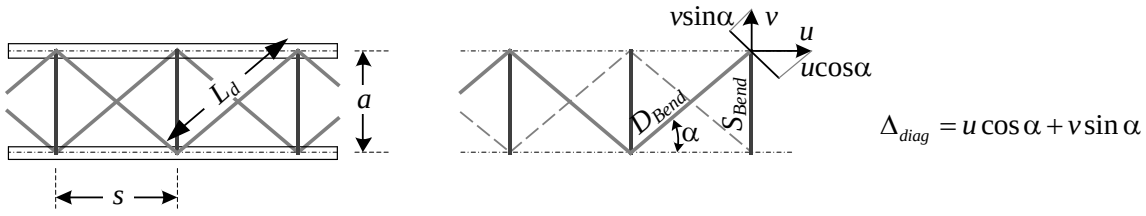

Figure 2.14. Elongation of an X-type top flange lateral bracing diagonals.

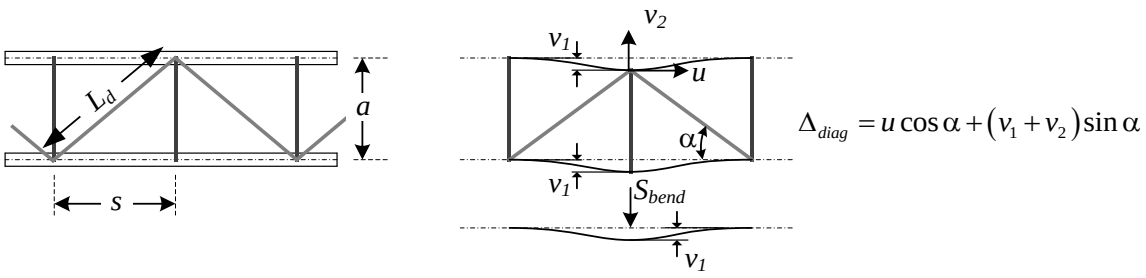

Figure 2.15. Elongation of a single-diagonal top flange lateral bracing diagonals.

The resulting forces for single diagonal and double diagonal (X-type) systems are (Fan and Helwig 1999):

$$D_{Bend} = \frac{f_b s \cos\alpha}{K_i} \tag{2.10}$$

where K_i=K_1 for a single diagonal system and K_i=K_2 for a double diagonal system:

$$K_1 = \frac{d}{A_d} + \frac{a}{A_s}\sin^2\alpha + \frac{s^2}{2b_f^2 t_f}\sin^2\alpha \tag{2.11}$$

$$K_2 = \frac{d}{A_d} + \frac{2a}{A_s}\sin^2\alpha \tag{2.12}$$

In the above equations, f_b is the average top flange major-axis stress in the truss panel, A_d and A_s are the cross sectional area of the TFLB diagonal and strut, and b_f and t_f are the top flange width and thickness. The forces induced in the truss diagonals, due to the girder major-axis bending, are a function of the stiffness of the truss and are considered on the factors K_1 and K_2.

In practice, the value K_i typically is calculated for a single set of dimensions for the entire girder length for simplicity of the calculations. The minimum value of K_i should be used in order to provide conservative estimates. The top flange lateral bracing element sizes are commonly repeated within various regions of the bridge to reduce the number of different fabrication details and the associated costs; therefore, in practice, the minimum value of K_1 often is calculated for the location with the top flange with the

largest $b_f^2 t_f$ and then used at other locations. In this research the actual K_i factors are calculated for each section.

2.3.1.2 Forces on the TFLB Transverse Struts

As mentioned previously, if the struts are not part of the internal cross-frame, they are assumed not to be subjected to significant effects of the distortional loads due to torsion or eccentric load application. The internal cross-frames are assumed to resist the entire cross-section distortional forces (i.e., the contribution to this resistance from the girder cross-section is neglected). The top flange lateral bracing struts are assumed to resist the lateral component of the vertical load *p* due to the sloping webs and equilibrate the bending effects on the diagonals. The lateral load *p* resulting from the sloping webs and the corresponding force S_{Lat} taken by the transverse struts are

$$p = \frac{w}{2}\tan\phi \tag{2.13}$$

$$S_{Lat} = ps \tag{2.14}$$

where *w* is distributed vertical load per unit length assumed to be applied at the top flanges (see Fig. 2.16) and *s* is the truss panel length measured along the girder centerline.

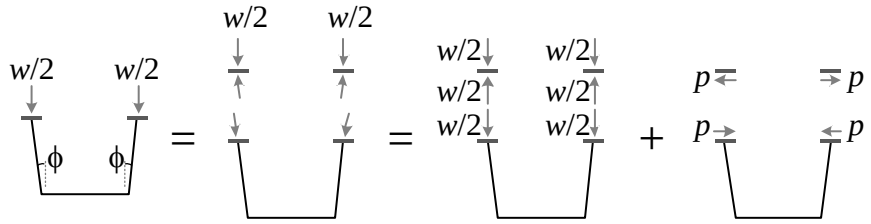

Figure 2.16. Lateral component of the distributed vertical load.

The strut equilibrates the force on the diagonal due to bending. Based on nodal equilibrium, the load S_{Bend} resulting from the bending effects on a truss with single diagonals is

$$S_{Bend} = -D_{Bend}\sin\alpha \tag{2.15}$$

The term D_{Bend} varies in every panel of the truss due to the variation of the girder bending moment along the girder length, and therefore the average between consecutive panels commonly is used. Alternatively, D_{Bend} can be calculated for the bending moment at the strut location. The average value is used for the calculations conducted in this research.

For a double diagonal system, the force on the transverse strut is obtained by summing the contribution from each of the diagonals. The struts on double X-type trusses do not transfer load to the top flange, whereas in single diagonal systems, significant lateral forces are transferred to the top flange.

For Pratt trusses, the top flange lateral bracing transverse strut is subjected to torsion effects since the shear flow in one diagonal must be transferred by the strut to develop the shear flow into the next diagonal. The force in the strut due to torsion is

$$S_{Torsion} = qa \tag{2.16}$$

2.3.1.3 Total Forces in the TFLB Diagonals and Transverse Struts

The total force on the top flange lateral bracing diagonals is the result of the additive effects of bending and torsion and must be combined to account for compression and tension. The total force on the top truss and strut are

$$D_{Tot} = D_{Torsion} + D_{Bend} \tag{2.17}$$

$$S_{Tot} = S_{Bend} + S_{Lat} + S_{Torsion} \tag{2.18}$$

To illustrate the proper combination of the effects the following example is provided.

In a tub-girder subjected to positive major-axis bending, the TFLB diagonals are subjected to compression since the top flanges shorten along the length of the girder (see Fig. 2.17a). When the girder is subjected to torsion, the diagonals, are subjected to a compression or a tension depending on their orientation (see Fig. 2.17b). Figure 2.17

shows the exaggerated flexural and torsional deformations on the TFLB system and labels the diagonals subjected to compression (C) and to tension (T).

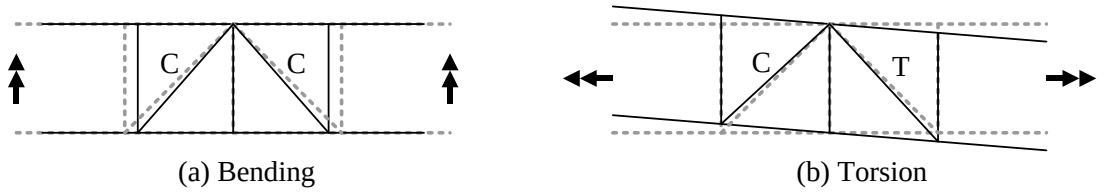

(a) Bending (b) Torsion

Figure 2.17. Effects of bending and torsion on the top flange lateral bracing diagonals.

Kim and Yoo (2006) provide an alternate set of equations for the top flange lateral bracing struts and diagonals considering the effects of the cross-section distortion. The approach by Fan and Helwig assumes that the distortional effects are controlled by the internal cross-frames only and, for simplicity, neglect the distortional effects on the top flange lateral bracing. Kim and Yoo show improved accuracy relative to the Fan and Helwig (1999 & 2002) equations compared to the 3D FEA responses. When the tub-girders do not satisfy the AASHTO (2010) requirements or high distortional loads are expected, such as in high curvature bridges with subtended angles larger than those studied in this research (larger than 21°) and high eccentric loads during construction, a more detailed analysis may be merited. In other cases, the Fan and Helwig equations are expected to provide an appropriate solution to the behavior of the bracing elements.

It should be noted that significant errors in the magnitude of the forces predicted by the component force equations still are observed as the result of the lack of accuracy of required inputs (i.e., the major-axis bending moments and the torques, particularly the torques), as discussed subsequently in Chapter 5. In addition, both the Fan and Helwig (1999 & 2002) and the Kim and Yoo (2006) benchmarks are based on single curved girders. Since interconnected tub-girder systems are subjected to a more complex behavior due to the force interactions between the girders, significant errors can be introduced due to corresponding inaccuracies in the internal force calculations. The errors addressed by Kim and Yoo are expected to be small compared to the errors due to other effects. Therefore, the evaluation of the component forces in this research uses the Fan and Helwig developments.

2.3.2 Internal Cross-Frames

The main function of the internal cross-frames on tub-girder bridges is to control the cross-section distortion produced by the distortional loads assumed to act on the box due to curvature and other applied eccentric loads.

Regarding the distortional load due to curvature, the M/R distributed torque, by definition, originates from the lateral component of the axial forces in the curved girder flanges. Since the top flanges are located in the extreme points of the cross section and the amount of material is greater, it is assumed that the web contribution to resist the axial load is negligible. This yields a pair of forces with magnitude $M/(Rh)$ applied on the top and bottom of the girder. The corresponding couple can be decomposed into pure torsion and distortional forces on the cross-section. The torques due to eccentric vertical loads during construction (see Fig. 2.18), also can be subdivided into pure torsion and distortional forces on the cross-section. In the equations developed by Fan and Helwig (2002) for inverted-V internal cross-frame forces, the cross-section distortional forces from these two contributions are resisted by the internal cross-frame forces

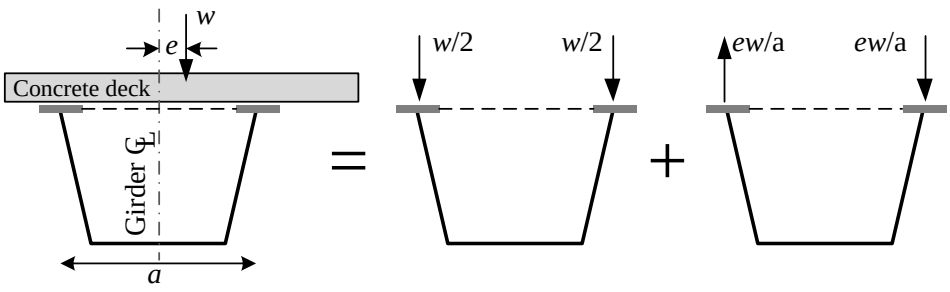

Figure 2.18. Eccentric concrete deck load.

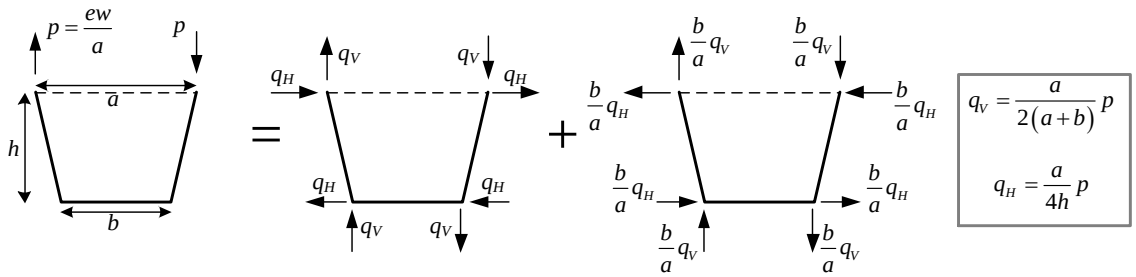

a) Distortional forces due to eccentric vertical load

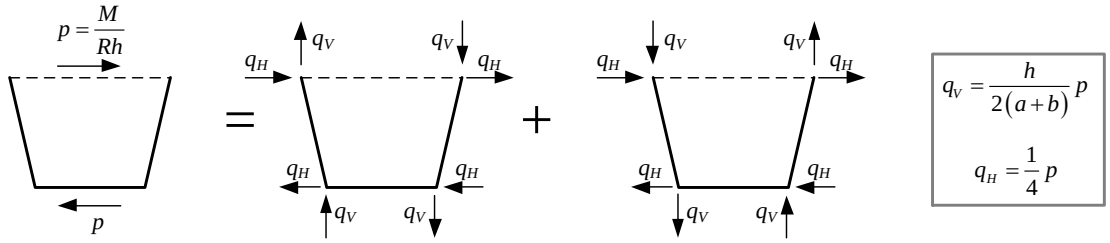

b) Distortional forces due to *M*/*Rh* lateral load

Figure 2.19. Distortional forces due to eccentric vertical load and *M*/*Rh* lateral load.

The horizontal curvature and eccentric vertical load effects produce loads that can be represented as pure torsional and distortional distributed forces. Figure 2.19 illustrates the applied distributed loads and the mechanical equivalent components at the corners of the tub cross section. The distortional distributed forces are assumed to be resisted only by the internal cross-frames and the top flange lateral bracing strut is assumed not affected by the distortional loads. Kim and Yoo (2006) propose a set of equations for the top flange lateral braces including these distortional components. Kim and Yoo's developments show that the Fan and Helwig (2002) equations provide unconservative estimates in some cases. However, Fan and Helwig equations still provide conservative estimates of the strut forces when compared to the 3D FEA analysis of the bridges studied in this dissertation. This is due to other compensating effects.

Equations 2.19 and 2.20 show the resulting forces on the cross-frame top chord *S* and on the diagonal *D*. The plus/minus signs represent the reversibility of the forces since there are two chord sections and two diagonals in the cross-frame.

$$S = \pm \frac{s_K b}{4A_0}\left(\frac{b}{a}ew - \frac{M}{R}\right) \tag{2.19}$$

$$D = \pm \frac{s_K L_{DK}}{2A_0} \left(\frac{M}{R} - \frac{b}{a} ew \right) \tag{2.20}$$

In these equations s_K is the cross-frame spacing, usually twice the top truss panel length, L_{DK} is the length of the internal cross-frame diagonal, a and b are the top and bottom width of the cross-frame, assumed to match the tub-girder dimensions, M is the major-axis bending moment at the cross-frame location, R is the girder radius of curvature, and A_0 is the girder cross-section enclosed area.

Equation 2.19 provides one positive and one negative result. These are due to the equilibrium with the diagonal force from Eq. 2.20. Since the top chord usually doubles as a TFLB strut, the forces on the top chord from Eq. 2.19 should be added with the effects of the force, S_{Tot}, calculated on the previous section.

2.3.3 External Intermediate Cross-Frames

The external intermediate cross-frames are used to sufficiently maintain the geometry of the overall cross section of the bridge during construction. They limit the girder displacements and rotations between adjacent girders and can facilitate girder erection but require additional forces for placement potentially increasing the erection fit-up problems. In general these elements can be avoided for bridges where the girder relative displacements, Δ_{rel}, are sufficiently small such that the slab elevations and the deck thicknesses are within specified tolerances (see Figure 2.20).

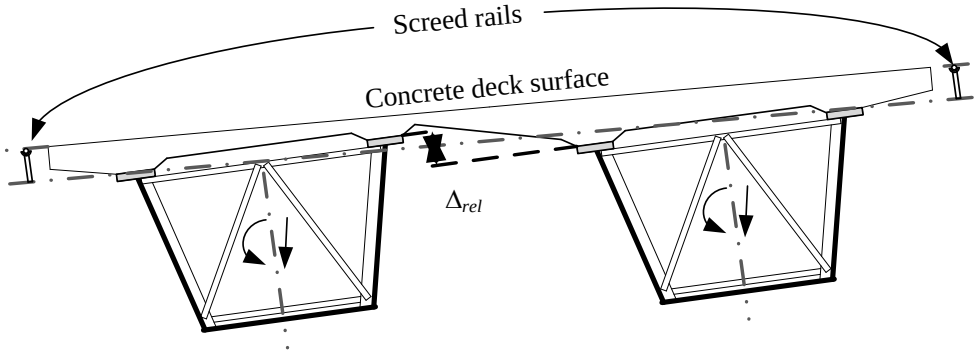

Figure 2.20. Slab profile due to independent deflections of two tub-girders. .

The forces on the external cross-frames are induced by the tendency for the girders to independently to displace and rotate as shown in Fig. 2.20. To estimate these forces, Helwig et al. (2007) developed equations based on the assumption that the external cross-frames experience forces proportional to the independent girder rotations and the relative vertical displacements that occur at their positions if the cross-frames were not present.

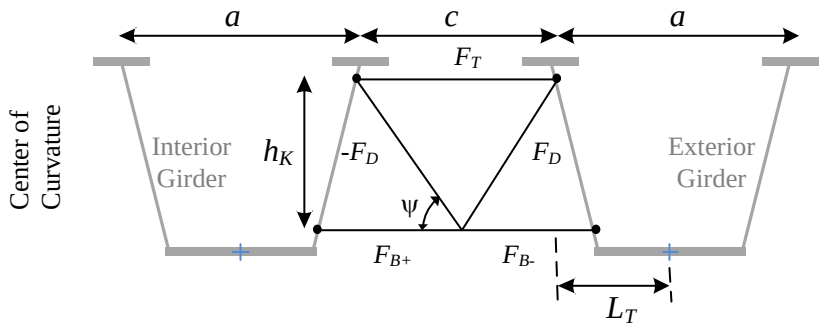

Figure 2.21. External intermediate cross-frame forces.

The forces on the external cross-frame diagonals, F_D, and top and bottom chords, F_T and F_B, are expressed as (Helwig et al., 2007):

$$F_D = 4GJ\,\frac{\left(L_i\phi_{w,ext} + L_e\phi_{w,\text{int}} - K_{e1}\Delta_{w,rel}\right)}{K_{e2}} \tag{2.21}$$

$$F_T = \frac{4GJ\left(\phi_{w,ext} - \phi_{w,\text{int}}\right) - F_D L_K\left(L_e - L_i\right)}{h_k\left(L_i + L_e\right)} \tag{2.22}$$

$$F_B = \pm F_D\cos\psi - F_T \tag{2.23}$$

where the variables in these equations are

$$L_K = h_K\cos\psi + L_T\sin\psi \tag{2.24}$$

$$K_{e0} = 1 + \left(1 + \frac{EI}{GJ}\right)\left(1 - \cos\frac{\beta_0}{2}\right) \tag{2.25}$$

$$K_{e1} = \frac{L_i + L_e}{a + c} \tag{2.26}$$

$$K_{e2} = K_{e0} K_{e1} \frac{L_i^3 + L_e^3}{12\left(EI/GJ\right)} \sin\psi + 2L_i L_e L_K \tag{2.27}$$

The other terms involved in the calculations are as follows (see Fig. 2.21): c is the tub spacing along the girder length, ψ is the external cross-frame diagonal angle, h_K is the top to bottom chord distance, L_T is the external cross-frame top chord distance to girder centerline and β_0 is the span subtended angle. Figure 2.22 illustrates the internal and external girder centerline lengths, L_i and L_e, and Figure 2.23 illustrates the relative vertical displacement between girders at the external cross-frame location, $\Delta_{w,rel}$ (Δ_{rel} in Fig. 2.20) and the internal and external girder twist rotations, $\phi_{w,ext}$ and $\phi_{w,int}$. Helwig et al. (2007) also provide equations to estimate the relative vertical displacement and rotations for simple-span bridges.

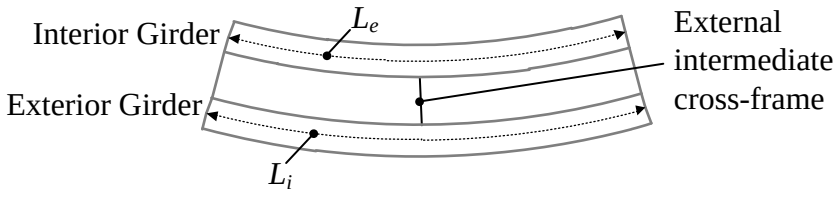

Figure 2.22. Girder lengths for the external intermediate cross-frame component force equations.

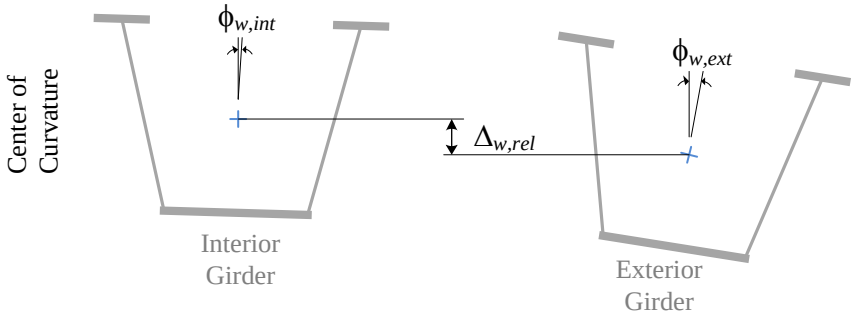

Figure 2.23. Girder twist rotations and relative vertical displacement for the external intermediate cross-frame component force equations.

The girder rotations and relative vertical displacements are obtained by analyzing a model of the bridge without the external intermediate cross-frames attached to the girders. This provides information to determine if external cross-frames are necessary.

Helwig et al. (2007) suggest a maximum girder relative vertical displacement $\Delta_{critical} = 0.5$ in for Δ_{rel} in Fig. 2.20. Bridges with $\Delta_{w,rel}$ less than $\Delta_{critical}$ do not require external intermediate cross-frames. In practice, Δ_{rel} can be accommodated to some extent in the girder cambers and/or in the girder haunch depths; therefore, the external intermediate cross-frames often may not be necessary provided that the deflections are estimated accurately. However, it should be noted that the relative displacements, Δ_{rel}, vary as the concrete is placed along the length of the bridge. The external intermediate cross-frames help limit these displacements, thus facilitating the deck thickness and slab elevation control.

When internal intermediate cross-frames are used these must be placed only at locations where they align with internal cross-frames so that the loads can be transferred through an appropriate path and fatigue effects are avoided. AASHTO (2010) requires this. Skewed external cross-frames must be avoided since the sloped webs would require a warped cross-frame to fit the geometry. A possible solution requires skewing the internal cross-frames so that the cross-frames are collinear but this practice brings additional complexity due to the geometric characteristics of the tub-girders.

The forces from the external cross-frames can have a significant effect on the internal cross-frame forces in the vicinity of the external cross-frames. These additional forces are not addressed in the development of the component force equations summarized in Section 2.3.2. A separate analysis must be performed for the internal and external cross-frame truss system to properly capture these forces on the internal cross-frame. In typical practice with the use of simplified analysis methods, the internal cross-frame forces are calculated by considering the force paths to develop the forces from the external cross-frames in an approximate analysis solely within the plane of the external and internal cross-frames. It should be noted that the influence of the external cross-frames on the TFLB forces is captured inherently by the input of the major-axis bending moments and the torques from a 2D-grid analysis that includes the external cross-frames.

Appendix A, Section A.1.8, shows the step by step implementation of the above equations for the estimation of the external intermediate cross-frame forces under total dead load and steel dead load for a simple-span curved bridge. The first set of forces is useful for design purposes and the second for the evaluation of the fit-up forces during steel erection. Additionally, the cross-frame forces are used to evaluate the effect on the girder torsional moment distribution.

2.3.4 Solid Plate Diaphragms

Solid plate diaphragms are typically used at the girder supports within the girder cross-sections and externally between adjacent tub-girders. Internal diaphragms serve the purpose of distributing the reactions from the support to the girder. The external diaphragms are essential to developing the support reactions to provide torsional equilibrium to the system. For a tub-girder bridge to perform as a system, the external diaphragms must be able to transfer the shears and moments between the girders associated with reacting the girder torques, and they must be stiff enough to limit the twist rotations at the ends of the girders. .

The tub-girder diaphragm strength and stiffness requirements are based on the shear force resulting from the girder end torques. For a twin tub-girder system with a single bearing on each tub, the diaphragm shear force, V_d, is calculated based on the girder end torsional moments, T_1 and T_2, as:

$$V_d = \frac{T_1 + T_2}{L_d} \tag{2.28}$$

where L_d is the distance between the centerline of the bearings (see Fig. 2.24).

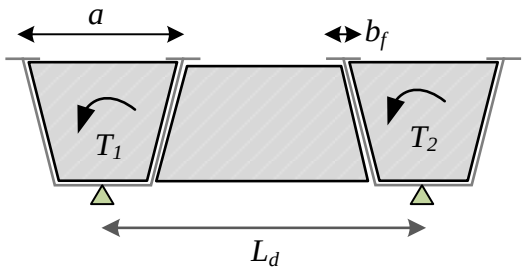

Figure 2.24. Support diaphragm dimensions for strength and stiffness requirements.

Basic rules for sizing of the support solid plate diaphragms of bridges composed of two tub-girders, as recommended by Helwig et al. (2007) are as follows. The first diaphragm requirement is based on the shear strength. Since the diaphragm aspect ratio is often less than five, the behavior is dominated by shear. The required diaphragm web area required for shear strength may be estimated as

$$A_{d,strength} = \frac{T_1 + T_2}{L_d \left(0.58 F_y\right)} \tag{2.29}$$

based on the assumption that the web is sufficiently stocky and/or stiffened such that it can develop its full plastic shear strength, where T_1 and T_2 are the factored torques under the governing LRFD load combination. The second requirement is based on limiting the relative displacement of the girders at the support lines. Helwig et al. (2007) suggest a maximum allowable relative vertical displacement Δ_{rel} of 0.5 inches (see Figure 2.20). Based on this criterion, the area required to satisfy the stiffness requirement is given by

$$A_{d,stiffness} = \frac{\left(T_1 + T_2\right) x_r}{0.0125 G L_d} \tag{2.30}$$

where $x_r = \left(a + b_f\right)/2$. Figure 2.24 illustrates the dimensions a and b_f.

The above requirements assume two tub-girder systems. For systems with more than two girders, the shear force, V_d, in the diaphragms should be evaluated separately.

2.3.5 Top Flange Lateral Bending Stresses

Lateral bending stresses are induced in the tub-girder top flanges by the lateral component of the vertical force in the web as well as horizontal curvature effects. Estimates of these stresses are

$$f_{\ell,p} = \frac{0.6 p s^2}{b_f^2 t_f} \tag{2.30}$$

(Fan and Helwig, 1999) and

$$f_{\ell,M/Rh} = \frac{0.6Ms^2}{Rhb_f^2 t_f} \tag{2.31}$$

(similar to the flange stress associated with AASHTO (2010) Eq. C46.1.2.4b-1) respectively. These two components of lateral bending are based on a lateral distributed load or equivalent lateral distributed load, w_ℓ, applied over the unbraced length equal to the panel length *s*, and the estimation of the maximum flange lateral bending moment as $w_\ell s^2/10$.

A third contribution to the top flange lateral bending is caused by interaction of the top flanges with the TFLB system under major-axis bending of the girder. Figure 2.25 shows diagrams of these interactive forces developed by Fan and Helwig (1999). For a Warren configuration of the TFLB system, the interactive forces are as shown in Fig. 2.25a. For this case, the force in both diagonals due to the major-axis bending is taken as D_{Bend}, from Eqs. (2.10) and (2.11), the transverse struts are subjected to the force $S_{Bend} = -D_{Bend}\sin\alpha$, from Eq. (2.15), and the force *Q* is equal to S_{bend}. Joint equilibrium at each end of the transverse struts requires the transfer of a lateral forces equal to S_{bend} to the top flanges in alternating directions as shown in the figure.

In double diagonal (X-type) TFLB systems (Fig. 2.25b), the struts are assumed to resist the full transverse component of the load from the diagonals. Therefore, the strut force is taken as $S_{bend} = -2D_{Bend}\sin\alpha$. The top flanges are not subjected to any significant lateral forces in these systems.

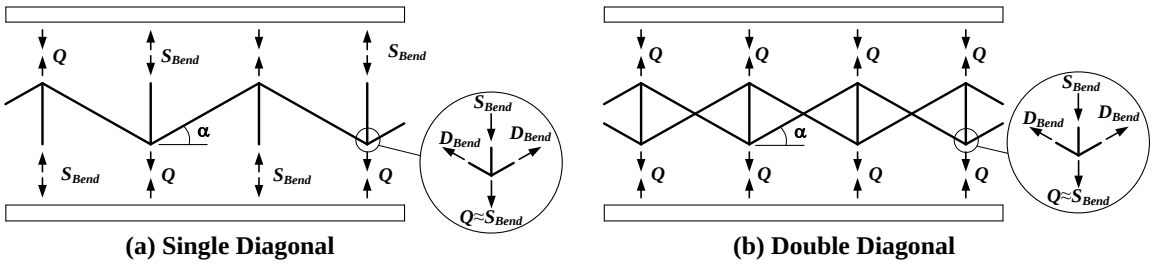

(a) Single Diagonal **(b) Double Diagonal**

Figure 2.25. Simplified interactive forces between top flange lateral bracing and top flange: (a) Single diagonal (Warren truss), (b) Double diagonal.

Based on the above estimates, an additional contribution to the flange lateral bending of

$$f_{\ell,Bend} = \frac{1.5s}{b_f^2 t_f} S_{Bend} \tag{2.32}$$

is present in the Warren TFLB systems. For X-type systems, the top flange lateral bending due to the major-axis bending of the girder is negligible.

Generally, the total top flange lateral bending stress is calculated by superimposing the above components as

$$f_{\ell,Tot} = f_{\ell,p} + f_{\ell,M/Rh} + f_{\ell,Bend} \tag{2.33}$$

The interactive forces in Pratt-type TFLB configurations are different than shown above. A general approach considering these interactive forces is addressed in Chapter 3. In addition, the Chapter 3 developments account for the variability of the torsional moments along the length of the bridge and the effects of on the major-axis stresses of the top flange.

In Appendix B, a validation study is performed for as example single tub-girder system presented by Fan and Helwig (1999). The results of the component force equations are compared with a 3D FEA implementation of the same model. This example is a single curved three-span girder subjected to distributed vertical load. The component force equations provide a good match to the results of the 3D FEA for this problem. However, it should be noted that various complexities often occur in tub-girder bridges, due to the presence of external intermediate cross-frames, eccentric loads, and skewed supports. Chapter 5 discusses the detailed effects of these factors on the accuracy of simplified calculations of the girder torques and their effects of the bracing force estimates.

CHAPTER III.

IMPROVEMENTS TO SIMPLIFIED ANALYSIS METHODS

3.1 Mechanics of Skew

The effects of skewed supports on plate girders can be evaluated by considering the girder major-axis bending rotations and the approximate displacement constraint provided by the diaphragms. The basic approximation is that the end diaphragms are effectively rigid in their own planes, but are able to rotate freely with respect to the support line. The interaction of the girder major-axis bending rotations and the displacement constraint provided by the skewed support diaphragms causes the girders to twist such that the top flanges displace laterally (i.e., lay over) with respect to the bottom flange. In summary, the overall effects of skewed supports on the girders can be explained as a torsional moment induced by the relative twist between the girder supports due to the displacement constraints from diaphragms placed along the skewed bearing lines.

3.1.1 Simplified Evaluation of the Effects of Skew on Tub-Girders

For the estimation of the effects of skew using a 1D analysis approach, the method described below is based on the assumption that the external end diaphragms act rigidly in their planes, as well as the assumption of negligible interaction between the external intermediate cross-frames and the girders.

3.1.1.1 Rigid Diaphragm Hypothesis

Two types of diaphragms are used for tub-girder bridges: internal and external. The internal diaphragms are located within the cross-section of the tub-girders and are connected to the girder along its entire perimeter. They are typically end diaphragms. The external diaphragms are located at the support lines between adjacent girders and are connected at their sides to the webs of the girders. The main purpose of the external diaphragms is to restrain deformations in their own plane such that the bridge torsional reactions are developed at the bearing lines, and the overall torsional rotation of the tub-

girders is restrained. The internal diaphragms prevent cross-section distortion and the external diaphragms develop the forces between the girders.

The diaphragms in tub-girder bridges are solid-plate components that typically have relatively short lengths compared to their depth. Therefore, they are typically stiff components capable of resisting loads acting on the plane of the diaphragm with relative small deformations compared to their out of plane behavior. The diaphragms are free to rotate with the girder ends and they provide a relatively small torsional stiffness compared to their in-plane behavior and the torsional and bending behavior of the tub-girders. To approximate the tub-girder bridge behavior, the diaphragms may be assumed rigid in their planes. Generally, they should comply with the minimum stiffness requirements such as those described on Section 2.3.4 for this assumption to be valid.

Internal diaphragms typically are continuously welded to the webs and to the bottom flange and participate integrally with the behavior of the external diaphragms. External diaphragms are bolted to the webs and may be connected to the internal diaphragm top flange as discussed in NSBA (2006), where recommended design details including external diaphragm connections are addressed. For aspect ratios less than about five, the external diaphragms rely predominantly on their shear stiffness to resist and transmit the loads. For tub-girders AASHTO (2010) recommends a distance center to center of flanges of adjacent tub-girders of 80 to 120 percent of the tub-girder width. This restriction often limits the depth to average length ratio to less than five.

Analyses on 3D FEA models performed for the development of this dissertation show that variations in the thickness of the end diaphragms have a small effect on the overall torque due to skew. Table 3.1 summarizes the results of sensitivity studies performed on two tub-girder bridges (see Fig. 3.1): a straight and skewed bridge (NTSSS1) and a radially supported curved bridge (NTSCR1) with radius R equal to 400 ft. Both are simple-span bridges with 150 ft of length. The bridge name designations are introduced subsequently in Chapter 4. Generally speaking, the satisfaction of basic strength and stiffness requirements such as those discussed in Section 2.3.4 would not permit this wide of a variation in the diaphragm thickness.

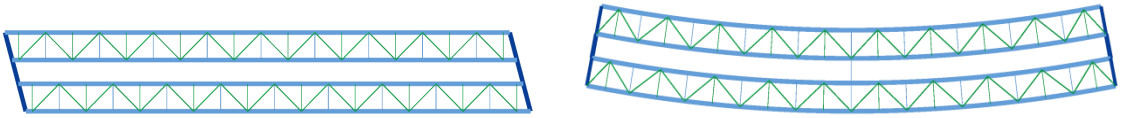

a) NTSSS2 **b) NTSCR1**

Figure 3.1. Diaphragm sensitivity study bridges.

Table 3.1. Diaphragm thickness sensitivity results.

Bridge	Thickness from Eq. 2.30 (in)	Diaphragm thickness (in)	3D FEA Maximum Torque (kip-ft)
NTSSS2	0.75	0.3125	1074
		0.625	1076
		2	1076
NTSCR1	0.75	0.3125	1002
		0.625	1003
		2	1004

In summary, the diaphragm thickness has negligible effect on the internal torques in the bridges studied in this dissertation, Bridges fulfilling strength and stiffness recommendations such as those in Section 2.3.4 are expected to behave similarly.

3.1.1.2 Matrix Stiffness Analysis

In this section, a skewed tub-girder and diaphragm system is analyzed as a 2D-Grid model using the direct stiffness approach. The grid model is shown in Figure 3.2. For simplicity, the model is assumed to be composed of single line elements located at the component centerlines. The grid corresponds to a simply supported straight girder system with unequal skewed support angles α and β. The element numbering, degrees of freedom (DOF) and assumed bending and torsional characteristics and lengths (I_i, J_i, L_i) are as shown in Figure 3.2.

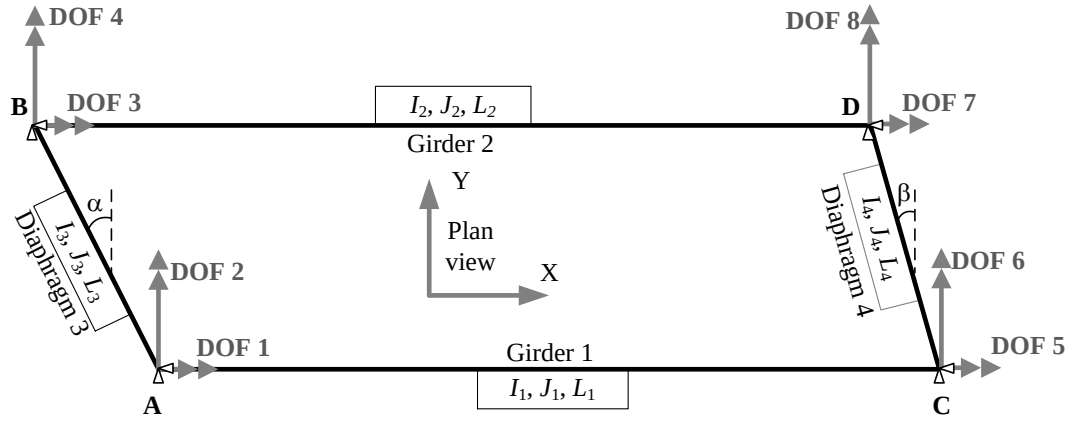

Figure 3.2.Grid model of a skewed tub-girder system.

The girders are assumed to be dominated by St. Venant torsional behavior and their properties are calculated by means of the Equivalent Plate Method. For simplicity, the diaphragms are modeled as line elements framing between the girder centerlines, neglecting the detailed behavior of the internal end diaphragms.

The general loading condition is assumed as a uniform distributed vertical load, *w*, applied to the girders. Figure 3.3 shows the stiffness development for Node A and degrees of freedom 1 and 2. *E* and *G* are the elastic and shear modulus, respectively.

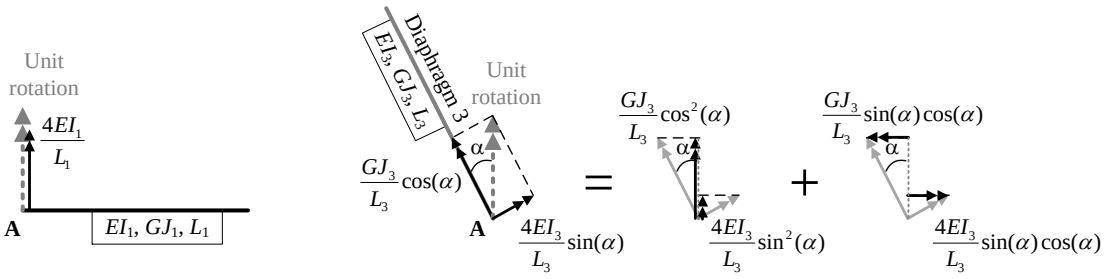

Figure 3.3. Stiffness development for Node A.

The torsional moment on the girder originates from the interaction of the girder major-axis bending rotation (Fig. 3.3a) and the rotation of the skewed diaphragm about the skewed bearing line (Fig. 3.3b). This coupling is evidenced in the contribution to the global stiffness from the diaphragm at Node A,

$$K_{12} = \frac{4EI_3}{L_3}\sin(\alpha)\cos(\alpha) - \frac{GJ_3}{L_3}\sin(\alpha)\cos(\alpha) \tag{3.1}$$

i.e., the moment about the global degree of freedom 1 from the diaphragm, due to a unit rotation about the global degree of freedom 2. Global degree of freedom 1 is associated with the twisting of the girder, and global degree of freedom 2 is associated with the major-axis bending of the girder.

The full system response involves the interaction of multiple degrees of freedom. In order to obtain a relationship between the major-axis bending moment and the torsional moment of the girder, the stiffness matrix for the system shown in Figure 3.2 is developed and solved for two simplified cases: parallel skew ($\alpha = \beta = \theta$) and one skewed support ($\alpha = \theta$, $\beta = 0$).

For the analysis, the stiffness problem $K \cdot d = F$ is solved. K is the 8 by 8 stiffness matrix for the rotational degrees of freedom shown in Figure 3.2, d is the twist and bending rotations vector and F includes fixed end bending moments from the applied distributed load, m, as the only actions.

The parallel skew configuration allows a simple approach resulting in equal girder and diaphragm lengths set to $L_1 = L_2 = L_g$ and $L_3 = L_4 = L_d$. The girder and diaphragm bending and torsional properties are set to $I_1 = I_2 = I_g$, $J_1 = J_2 = J_g$, $I_3 = I_4 = I_d$ and $J_3 = J_4 = J_d$. The displacement solution for the parallel skew has two unique terms that, with respect to the girder degrees of freedom, correspond to bending rotation ϕ_y and the twist rotation ϕ_x. The solution does not involve the diaphragm torsional stiffness because the equal girder loads and girder and diaphragm lengths makes the girders rotate equal amounts about the support line, resulting in zero twisting of the diaphragms. The rotations ϕ_y and ϕ_x are given by the equations

$$\phi_y = \frac{1}{2}\frac{L_g\cos^2(\theta) + \frac{GJ_g}{3E}\frac{L_d}{I_d}}{EI_g\cos^2(\theta) + \frac{1}{3}GJ_g\frac{I_g}{L_g}\frac{L_d}{I_d} + GJ_g\sin^2(\theta)}m \tag{3.2}$$

$$\phi_x = -\frac{1}{2}\frac{L_g \sin(\theta)\cos(\theta)}{EI_g \cos^2(\theta) + \frac{1}{3}GJ_g \frac{I_g}{L_g}\frac{L_d}{I_d} + GJ_g \sin^2(\theta)} m \tag{3.3}$$

In the above equations, if the diaphragm is assumed rigid within its plane, the term containing L_d/I_d may be considered negligible. In addition, when comparing $\sin^2(\theta)$ and $\cos^2(\theta)$, the term $\sin^2(\theta)$ is small for the relatively limited skew angles used in tub-girder bridges. By neglecting this term, the major-axis bending restraint that the skewed diaphragm offers to the girder, i.e. partial end moment fixity, is ignored.

These two assumptions, and the fact that the fixed end moment m can be written in terms of the applied distributed vertical load, w as $wL_g^2/12$, allow the above equations to be simplified to

$$\phi_y = \frac{wL_g^3}{24EI_g} \tag{3.4}$$

$$\phi_x = -\phi_y \tan(\theta) \tag{3.5}$$

The girder torsional moment equation from the stiffness approach is:

$$T_g = \frac{GJ_g}{L_g}\frac{L_g \sin(\theta)\cos(\theta)}{EI_g \cos^2(\theta) + \frac{1}{3}GJ_g \frac{I_g}{L_g}\frac{L_d}{I_d} + GJ_g \sin^2(\theta)} m \tag{3.6}$$

By the application of the above simplifications, the girder torque can be reduced to

$$T_g = -\frac{GJ_g}{L_g} 2\phi_x \tag{3.7}$$

This solution shows the mixed effect of skew at both ends, i.e. total twist equal to $2\phi_x$. For the case with only one skewed support, the girder and diaphragm lengths differ along with the applied end fixed moment. For simplicity, these lengths may be assumed

equal to provide a simplified estimate. However, this assumption neglects the important geometric effects of skew on the girder lengths, such as changes in the relative bending stiffness between girders, girder end rotations and interaction with the diaphragm.

The diaphragm interaction was addressed previously and ruled out for the equal skew case because the girders would tend to rotate the same amount, making the diaphragm rotate rigidly about the bearing line and have zero twisting and zero internal torque. In the case of one skewed support or general unequal skew, the difference in the Girder 1 and Girder 2 lengths results in the girders not rotating the same amount in major-axis bending at the support. Therefore, relative end twists occur at the end diaphragms, and the internal torque in the end diaphragms is no longer zero. However the end diaphragms do not provide significant twist restraint as their rotational stiffness is relatively small when compared to the girder major-axis bending and torsional properties. Based on the assumption that this restraint is negligible, a simplified solution for the single skewed support case is equal to half to that of Eq. 3.7 or:

$$T_S = -\frac{GJ_g}{L_g}\phi_x \tag{3.8}$$

The kinematic approach shown in Section 3.1.2 gives the same results. Both approaches rely on the assumption of rigid diaphragm behavior, as discussed in Section 3.1.1.1.

3.1.1.3 Neglecting the Interaction with External Intermediate Diaphragms

Tub-girders typically have few or no external intermediate cross-frames connecting adjacent girders. When present, these cross-frames control the girder relative displacements and redistribute the torsional effects. However, the maximum girder torsional response is expected when no external intermediate cross-frames are present. Therefore, ignoring the effects of these cross-frames provides a conservative estimate of the girder overall torsional effects.

In one design approach for tub-girder bridges recommended by (Helwig et al, 2007), the external intermediate cross-frames are ignored in the simplified analyses. The tub-girders are then designed to withstand all loads from this analysis, and the cross-

frames are later added, if necessary, to limit the relative vertical displacement of adjacent girders during the deck placement. The external intermediate cross-frame design forces are estimated as a function of the girder displacements without the consideration of the external cross-frames in the simplified model.

The external intermediate cross-frames are often unnecessary since the tub-girders can be designed to support the loads independently and the girder relative displacements are sufficiently small.

Analytical observations on 3D FEA models show that, once the external intermediate cross-frames are placed, shear forces are transferred though them depending on the tendency for girder to girder relative vertical displacements. These shear forces tend to reduce the torques in the girders, meaning that the interaction of the external cross-frames can be safely neglected in the estimation the girder torques.

3.1.2 Skew Induced Torque

As an alternative to the solutions in Section 3.1.1.2, the effect of skewed supports on the girder torques in tub-girder bridges can be estimated by a few simplified mechanistic models. The basic kinematic assumptions are discussed in Section 3.1.1.1, i.e., the external diaphragms at the supports are effectively rigid in their own plane, and provide relatively little restraint to the tub-girders in their out-of-plane direction. Furthermore, the external diaphragms are often I-sections and therefore their torsional stiffness is relatively small compared to the tub-girders.

In a non-skewed configuration, as the girder deflects vertically it rotates about the support bearing, assuming a single bearing for each girder. Correspondingly, the diaphragms, acting as rigid plates, rotate about the lines connecting the bearings. When the support line is skewed, the diaphragm, acting approximately as a rigid plate in its own plane, forces the girders to twist to maintain compatibility (see Fig. 3.4).

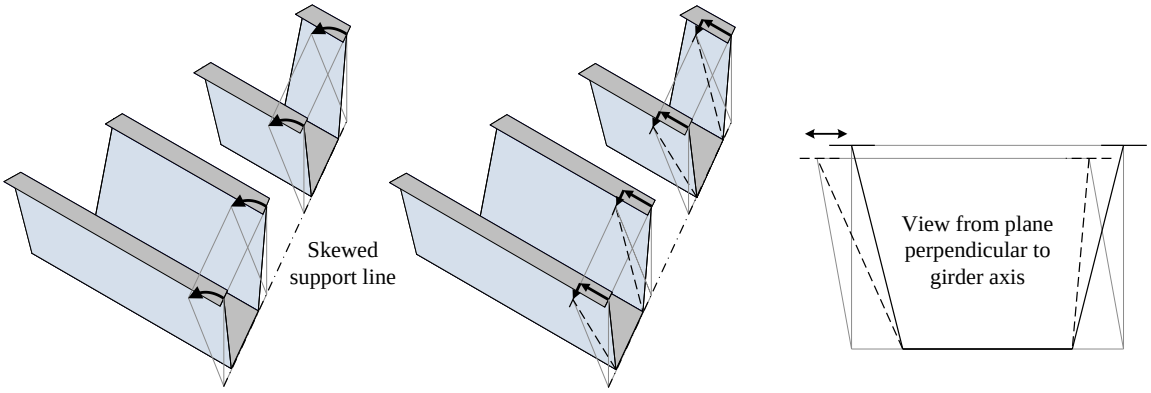

Figure 3.4. Lateral displacements due to rotation about the line of the support in a tub-girder bridge.

The support diaphragms may be idealized essentially as rigid components in their own plane and as highly flexible components out of their plane. Given the rigid in-plane assumption, the diaphragm rotation has two components relative to the axis of the girders, one corresponding to the major-axis bending rotation of the girders and one corresponding to twist rotation of the girders (see Fig. 3.5).

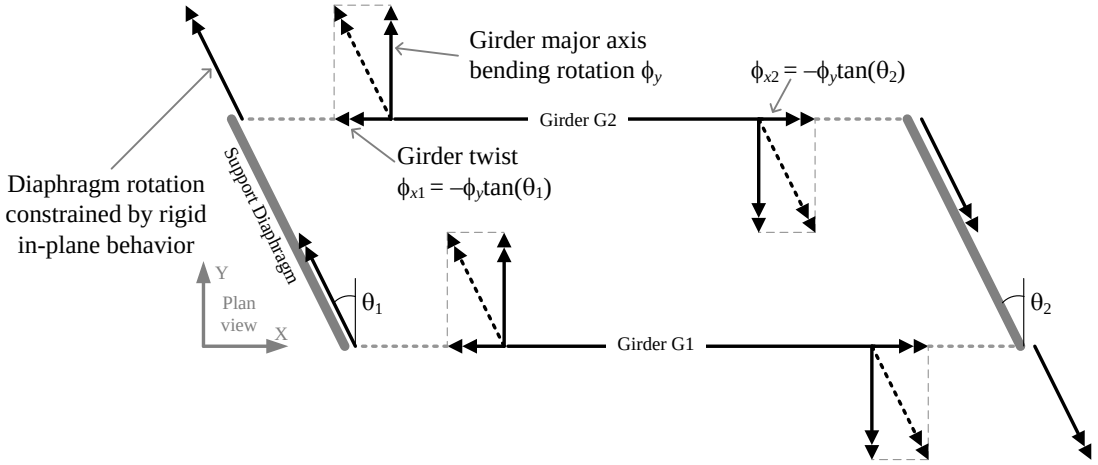

Figure 3.5. Rigid diaphragm rotation mechanism at a skewed support of a tub-girder bridge.

The girder end twist rotations at each support can be estimated by Eq. 3.5 as $\phi_x = -\phi_y \tan\theta$ in terms of the major-axis bending rotation ϕ_y and the support skew angle θ, as shown by Eq. 3.8 and Fig. 3.5. The girder torques then are estimated by multiplying

the girder torsional stiffness *GJ/L*, by the total girder twist rotation $\phi_{x1}+\phi_{x2}$. The resulting torsional moment due to skewed supports is

$$T_S = -\frac{GJ}{L}\left(\phi_{y1}\tan\theta_1 + \phi_{y2}\tan\theta_2\right) \tag{3.9}$$

Figure 3.6 shows two configurations, one with parallel skew and one with an equal and opposite skew angle. Figure 3.6a illustrates the behavior for the parallel skew case. In this situation the girders experience twist rotations in opposite directions at the two supports. This produces a constant torque in the girders. Figure 3.6b illustrates the case when the skew angles are equal and opposite in sign. In this special case, the girder ends twist the same amount and in the same direction. This results in rigid body girder rotation and zero internal torque in the girders. Other skew configurations would result in unequal twist of the ends, resulting in a constant torque proportional to the relative angle of twist between the girder ends.

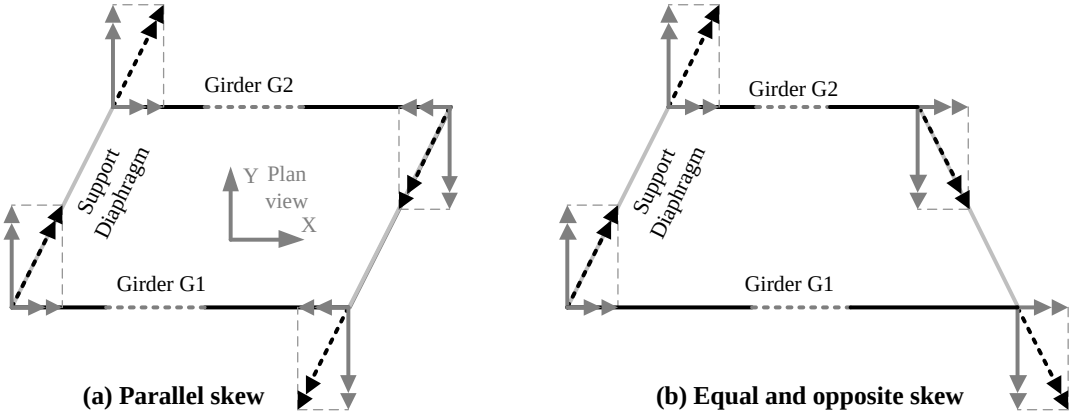

Figure 3.6. Girder end rotations in a tub-girder bridge with parallel skew of the bearing lines and with equal and opposite skew of the bearing lines.

The assumption that the end diaphragms are rigid in their own plane, combined with the assumption that the girders are simply-supported at their ends, produces an upper-bound estimate of the relative angle of twist between the girder ends. This can be used with a torsional model of the individual girders, in a line-girder analysis, to obtain an upper-bound estimate of the tub-girder torques due to the skew.

As an example, the above procedure is applied to estimate the torsional moments in the simple-span straight and skewed tub-girder bridge NTSSS2. This bridge is a twin tub-girder system with a span of L = 150 ft and parallel skewed supports of $\theta = 30°$. The bridge framing plan is shown in Figure 3.7. The naming conventions for the different study bridges is discussed subsequently in Chapter 4.

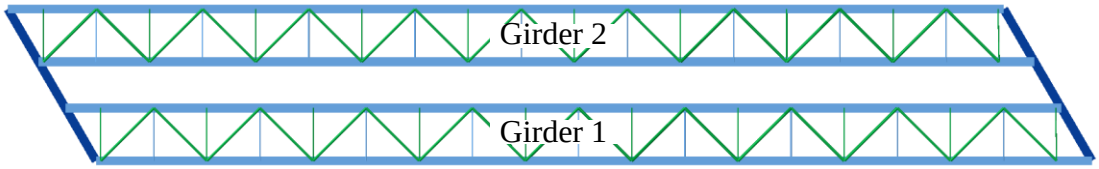

Figure 3.7. Plan view of NTSSS2.

For a simple-span bridge example, the terms in the torque due to skew, given by Eq. 3.9, can be substituted as $\phi_{y1} = \phi_{y2} = wL^3/(24EI)$. The estimate of the torsional moment due to skew results equal to $T_S = wL^2GJ\tan\theta/(24EI)$ where w is the vertical distributed load, I and J are the bending and torsional properties of the tub-girder and E and G are the material elastic properties. By the use of the ratio E/G = 2.6 the torsional moment in a simple-span single tub-girder can be estimated as $T_S = wL^2J\tan\theta/(64.2I)$.

A support with positive skew angle, such as the supports in NTSSS2, tends to introduce a positive torque into the girders at the support, although the actual girder internal torque induced by skew depends on the skew angle at both girder ends. The effect of two skewed supports with positive skew has additive effects on the girder torque. The total internal torque in the girders, due to skew, is constant along the length of the girders according to the simplified analysis approximations.

Figure 3.8 illustrates the torsional moments in Girder 1 of Bridge NTSSS2 obtained from the integration of the 3D FEA stresses, the 2D-grid model and the equation estimates of the torsional moment T_s due to skew.

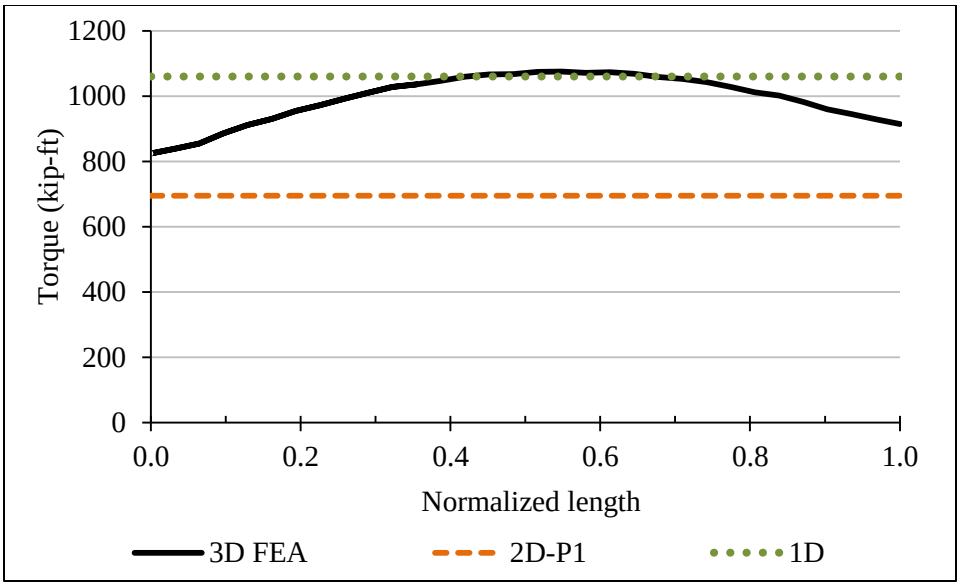

Figure 3.8. Comparison of the torsional moments in Girder 1 of Bridge NTSSS2 predicted using refined and approximate analysis methods.

Eq. 3.9 provides an upper bound estimate of the torsional response and is close to the torque from the 3D FEA. Several factors impact the accuracy of the torsional moment estimates. In this example, the non-constant 3D FEA torsional moment diagram is due to the effect of interactive forces from the bracing components. The smaller torsional moment estimate from the 2D-grid analysis is the result of the additional flexibility of the support end diaphragm which is modeled with increased length from the girder centerlines ignoring the regions inside the girder. The 3D FEA in Section 3.1.1.1 showed that the torsional moment is insensitive to the diaphragm thickness, however, the modeling of the diaphragm by a 2D-grid predicts a larger diaphragm flexibility. A better approach in a 2D-grid is to model the diaphragm as a rigid frame element.

The parabolic-like distribution of the torsional moment from the 3D FEA in Figure 3.8 is the result of additional internal torsional moments with a parabolic-like distribution. The shape also suggests correlation with the girder major-axis bending moment. This is evidence that the internal moments are caused by the TFLB strut lateral forces which follow a similar distribution as shown in Figure A.24 in Appendix A. The effects of these interactive forces on curved bridges are relatively minor when compared to the girder torques due to curvature and are not noticeable in the torsional moment

distribution in typical curved bridges. Section A.2.5 in Appendix A discusses these effects in more detail.

Given an estimate of the tub-girder torques, one should consider the moment equilibrium between the tub-girder and the support diaphragm as shown in Fig. 3.9. If the diaphragm is assumed to have negligible torsional stiffness, it can balance the tub-girder torque only via an internal major-axis bending moment. In turn, the tub-girder has to supply a major-axis bending component at its end such that moment equilibrium is satisfied at the joint. This in turn affects the overall vertical bending deflections of the tub-girder. This additional effect on the vertical bending deflections typically is neglected in the above types of hand calculations and the results at this stage taken as a coarse line-girder estimate of the tub-girder bridge response.

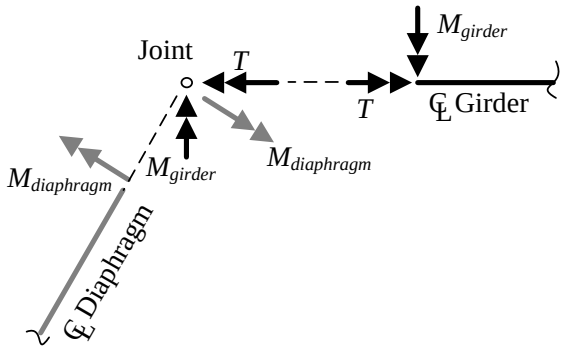

Figure 3.9. Idealization of moment equilibrium at the joint between a tub-girder and its support diaphragm.

In bridges that contain intermediate external diaphragms, which are usually provided to control the relative displacements between the girders potentially that may influence the slab thickness profile as illustrated in Fig. 2.20, the behavior is more complex potentially necessitating more than a line-girder analysis to properly account for the coupling of the tub-girders by the intermediate diaphragms. For simplicity, Helwig et al. (2007) recommend the design of the tub-girder bridges for their final constructed condition assuming no intermediate external diaphragms or cross-frames, followed by the provision of external cross-frames solely to control the profile of the slab thickness during the placement of the concrete deck. They provide equations for sizing the external

intermediate cross-frames based solely on the criterion of controlling the slab thickness profile (see Section 2.3.3).

Appendix A, Sections A.1.5 and A.5.5, illustrate detailed results including the implementation of the equations for the torsional moment due to skew for the NTSSS2 bridge and an additional existing straight bridge. The skew estimates assume a constant girder internal torque as discussed above. The equations provide reasonable conservative estimates of the torsional moments. However, differences are noticed due to the interaction of the different bridge components, such as the effect of the bracing and external intermediate cross-frame forces. The ETSSS2 bridge has several skewed external intermediate cross-frames and, in consequence, the bridge exhibits large differences in the torque estimates compared to the 3D FEA results. The differences are attributed to the girder interactions caused by the bridge having several external intermediate cross-frames. The developments described in this section assume independent girder behavior for the estimation of the torsional effects. The torsional effects from the interaction between girders due to the presence of external intermediate cross-frames should be included for a more accurate prediction of the behavior.

3.1.3 Skew Induced Twist Rotation

The torsional moment due to skew is assumed constant along the length of the girder span and the twist rotation follows a linear variation along the length of the girder.

For the general case, for a span with skewed supports at both ends, the twist rotation due to skew can be estimated as

$$\phi_x(s) = \phi_{x1} - \left(\phi_{x1} - \phi_{x2}\right)\frac{s}{L} \tag{3.10}$$

where $\phi_x(s)$ is the estimated twist rotation at a distance s from the left support, ϕ_{x1} and ϕ_{x2} are the twist rotations at the left and right supports respectively, estimated by means of Eq. 3.5, and L is the span length.

The above developments presented for the estimation of the skewed support effects on the girders assume that the girder torques and twist rotations are the only

components impacted by the skew. This provides a simplified approach to include the effects of skew in the bracing equations discussed in Chapter 2, which depend directly on the torsional moments (i.e., the equations for the TFLB forces and the internal cross-frame forces), or the twisting rotations (i.e., the equations for the external intermediate cross-frame forces).

As an example, the bridge NTSSS2 girder 1 top to bottom flange relative lateral displacements are estimated by means of Eq. 3.10 as $h\tan\phi_x$, where h is the girder depth. Figure 3.10 illustrates the Girder 1 relative lateral displacements obtained from the 3D FEA, 2D-grid and the equation estimates.

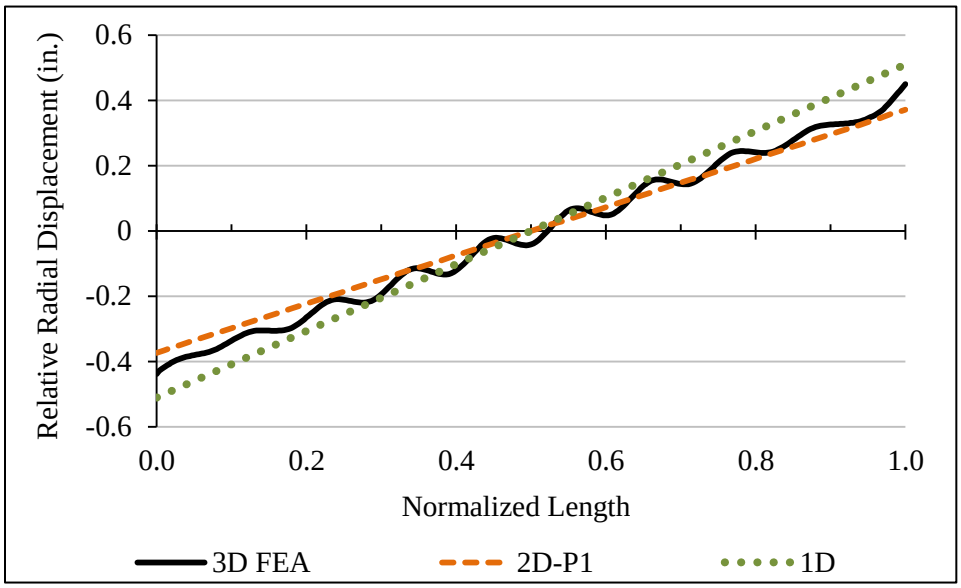

Figure 3.10. Comparison of relative lateral displacements in Girder 1 of Bridge NTSSS2 predicted using refined and approximate analysis methods.

Eq. 3.10 provides an appropriate estimate of the girder twist rotations, and in consequence, the relative lateral displacements between the top flanges and the bottom flange of the girders. The small differences between the 3D FEA and the simplified analysis methods are caused by the inability of the 1D and 2D to estimate the behavior at the unbraced flange locations between the TFLB panel points.

In Appendix A, Sections A.1.2 and A.5.2 illustrate the top to bottom flange relative radial displacements calculated from the twist rotation given by Eq. 3.10 for the

simple-span straight bridges NTSSS2 and the ETSSS2. The results show good agreement with the 3D FEA and 2D-grid in the general distribution and magnitude.

The effects of potential cross-section distortion on the components that depend on the distortional loads (i.e., the internal cross-frames) should be studied in general. The following section discusses the response due to skewed supports on single box girders in order to evaluate the influence of skew on the distortional loads.

3.1.4 Cross-Section Distortion Due to Skew

Bridge tub-girders are subjected to well-known distortional effects associated with the torsion due to horizontal curvature effects and eccentric applied loads. In order to control the box distortion, internal cross-frames are used at relatively short distances along the girder lengths to resist these deformations..

In the previous subsection, the girder torsion due to skewed supports was discussed. By definition, this torsional moment originates from the interaction of the girder major-axis bending rotations and the restraint from the bearing-line diaphragms. The girder-diaphragm interaction produces a discrete torque at the skewed support as the result of the girder twist. The resulting behavior is approximately an additional constant internal torque that must be summed with the torques due to the horizontal curvature effects.

At the supports, internal solid plate diaphragms are used to distribute the reaction forces and girder torsional moments. These internal solid plate diaphragms prevent cross-section distortion and, therefore, the torque due to skew is introduced into the girders effectively as just a St. Venant torque.

In order to provide an example of the magnitude of the distortion due to skew, two square simple-span box-girders are subjected to vertical loads to study the effects of the torque on the cross-section distortion. The two geometries studied are a straight and skewed box-girder (Fig. 3.11a) and a horizontally curved box-girder (Fig. 3.11b). The span lengths are L_{as} = 150 ft and are subjected to loads comparable to those of an actual tub-girder bridge subjected to the weight of wet concrete. The square box depth, D, is equal to $L_{as}/25$ and the web thickness is selected so that $D/t_w \leq 150$. This results in

D = 72 in and t_w = 0.5 in. The top and bottom flanges thicknesses are assumed equal with t_f = 0.5 in. The straight girder is subjected to a skewed end equal to θ = 30° and the curved girder has a curvature comparable to those used on the parametric cases selected on Chapter 4, equal to R = 400 ft. One inch thick solid plate end diaphragms are used at the supports for the box. No internal cross-frames are used in the box to evaluate the possibility of distortion. The vertical load on the girders is equal to w = 0.2 kip-in and is applied at the top flange-web juncture locations as two 0.1 kip-in distributed loads. This load represents an approximate load for steel plus concrete deck self-weight on a tub-girder bridge with similar geometry.

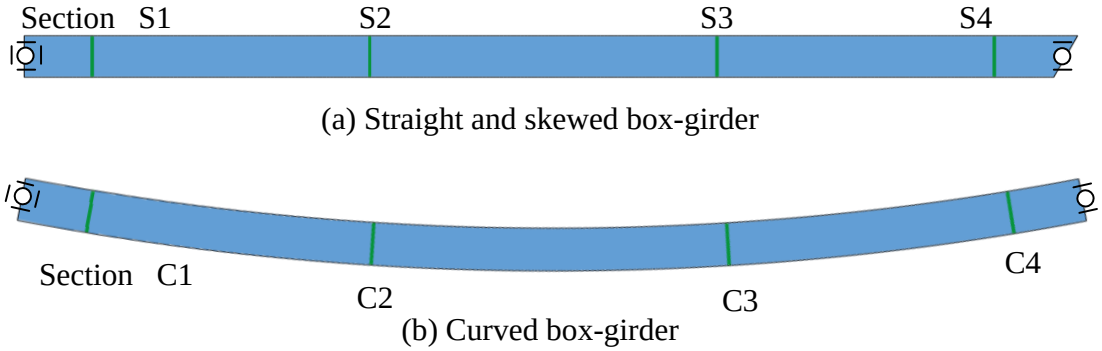

(a) Straight and skewed box-girder

(b) Curved box-girder

Figure 3.11. Straight and skewed and curved box-girders plan view.

The box-girders are supported continuously at the bearing lines restricting vertical displacement but allowing rotations with respect to the support line. Additional translational supports are added to provide stability to the analysis as schematically shown in Figure 3.11.

The resulting cross-section cross section deformations for each of the box-girders, obtained from a geometric non-linear 3D FEA, is illustrated in Figures 3.12 and 3.13. The cross-section deformed shapes correspond to the cross-sections located along the length of the bridge as shown in Figure 3.11. Neither of the box-girders has internal cross-frames. This causes significant cross-section distortions in Fig. 3.12, but not in Fig. 3.13.

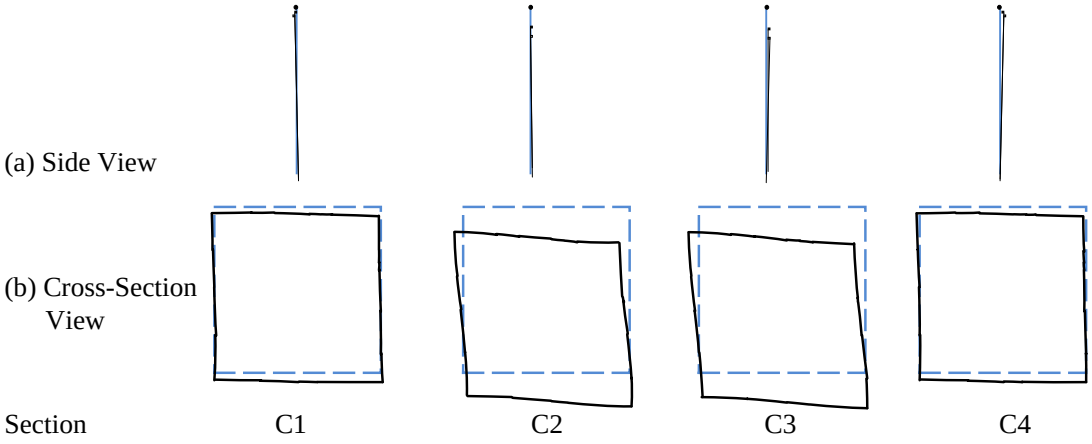

Figure 3.12. Deformed shapes for different cross-sections along the length of the curved box-girder.

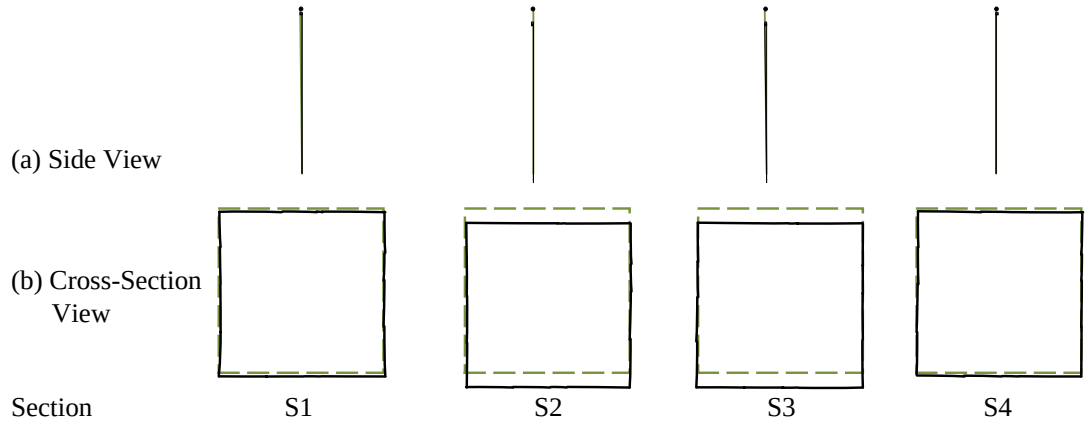

Figure 3.13. Deformed shapes for different cross-sections along the length of the straight and skewed box-girder.

The curved girder is expected to exhibit significant cross-section distortion due to the equivalent distributed lateral load effects *M/(Rh)* as shown in Figure 2.4. This couple can be subdivided into a St. Venant torque component plus a cross-section distortional component of forces as discussed by Fan and Helwig (2002). Figures 3.12a and 3.12b show negligible warping of the cross-sections out of plane and clear evidence of the cross-section distortion respectively. In the AASHTO (2010) design procedures, these distortional effects are prevented by the use of internal cross-frames. The distortional forces on the tub-girder internal cross-frames are the loads required to bring the cross-sections back to essentially an undistorted configuration at the internal cross-frame locations.

In contrast, Figures 3.13a and 3.13b show the cross-section warping and distortion for the straight and skewed girder. The straight and skewed girder is subjected to torsional loads due to the girder bending rotation and the constraint provided by the skewed support and end diaphragm. The effects of the cross-section distortion are clearly small. Therefore, the influence on the internal cross-frames is expected to be negligible.

When comparing the behavior of both girder systems, it is noticeable that the curved bridge is affected significantly by the cross-section distortion associated with the equivalent torsional loading due to the horizontal curvature. The evidence presented, supports that the skew causes negligible effects on the in-plane cross-section distortion. For both the curved and skewed cases, the cross-section out of plane deformation (i.e., the warping of the cross-sections) is negligible.

3.2 Combined Curvature and Skew Effects

3.2.1 Torsional Moment and Twist Rotation Due to Combined Effects

Curvature and skew contribute to the overall torsional moments and twist rotations in different amounts depending on the geometry of the bridge. The girder internal torques and twist rotations due to skewed supports add and/or subtract with the corresponding torques and twist rotations due to horizontal curvature. For 1D analysis the torsional moments and twist rotations may be estimated as

$$T(s) = T_C(s) + T_S \tag{3.11}$$

$$\phi_x(s) = \phi_{x,C}(s) + \phi_{x,S}(s) \tag{3.12}$$

where $T_C(s)$ is given by Eq. 2.5 (or Eq. 2.6 for a simple-span bridge), T_S is given by Eq. 3.9, $\phi_{x,C}(s)$ is given by Eq. 2.7 and $\phi_{x,S}(s)$ is given by Eq. 3.10. Equations 3.9 and 3.10 assume a skew angles measured with respect to a line perpendicular to the bridge centerline, i.e., an curved bridge with radial supports has zero skew angle.

When the skew on the left support is positive (counter-clockwise orientation from the non-skewed configuration), the top flange moves to the top of the page relative to the bottom flange. For consistency with the curvature effects, a positive skew at this support

causes a negative twist rotation and layover. For positive skew at the right support, the girder rotations and layovers are in the opposite direction, and are taken as positive. For the simple-span curved bridge with positive skew at the left support shown in Fig. 3.14, the skew causes a negative rotation at the left-hand support (i.e., the top flange to moves toward the center of curvature), while there is essentially zero rotation at the right-hand . The twist rotation due to the skew varies essentially in a linear fashion along the girder lengths. The horizontal curvature causes a positive twist rotation with a parabolic-like distribution within the span, zero rotation at the supports, and a maximum rotation at the midspan.

As an example, the above procedure is applied to estimate the torsional moments in the simple-span curved and skewed tub-girder bridge shown in Fig. 3.14. NTSCS29. The bridge, designated NTSCS29, is a twin tub-girder system with a span of L = 225 ft and one skewed support with $\theta = 15.7°$. This bridge has two external intermediate cross-frames at 0.31 and 0.69 of the full span length..

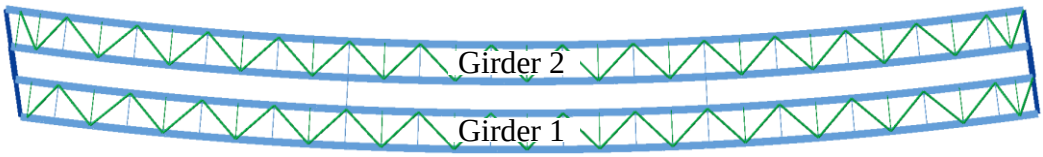

Figure 3.14. Plan view of NTSCS29.

Figure 3.15 illustrates the torsional moments in Girder 1 (the outside girder with respect to the center of curvature) obtained by the M/R Method estimates with the torsional moment T_S due to skew, by a 2D-grid analysis, and by integration of the 3D FEA stresses. The external cross-frames in this bridge influence the torsional response via the vertical shear forces they transmit between the girders as well as the corresponding internal moments. In the case where the external intermediate diaphragms exist, the approximate equations still give an estimate of the internal torques sufficient for design.

The top to bottom flange relative lateral displacement predictions are shown in Fig. 3.16. The results are shown from the 3D FEA, 2D-grid and 1D line-girder calculations. The effects of skew are accounted for via Eqs. 3.11 and 3.12 in the 1D line-

girder analysis method The results show good agreement on the estimation of the skew effects at the left support. The differences in the predictions by the 1D method along the length of the bridge are caused by the lack of consideration of external intermediate cross-frames in the M/R Method and in the procedures developed for evaluating the girder internal torques due to skew.

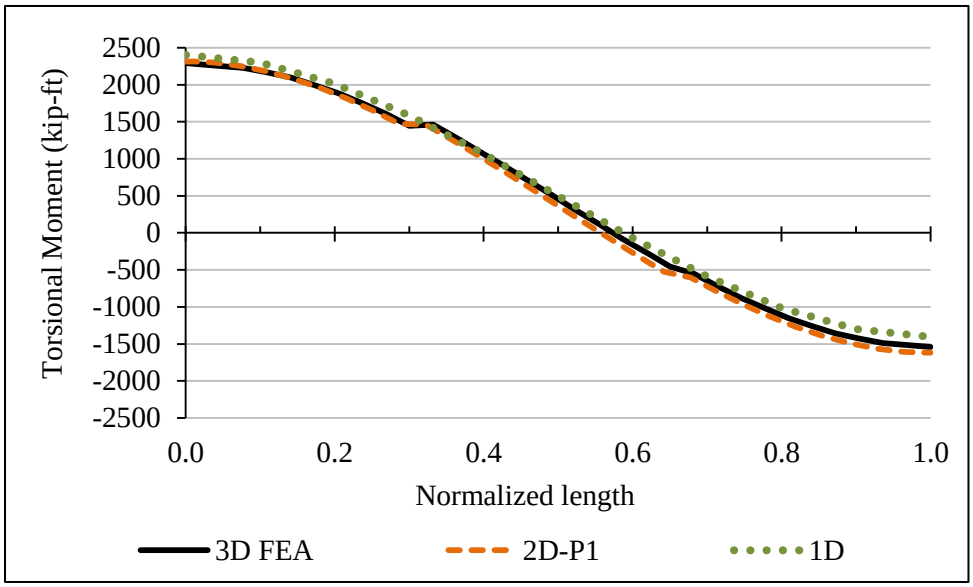

Figure 3.15. Comparison of torsional moments in Girder 1 of Bridge NTSCS29 predicted using refined and approximate analysis methods.

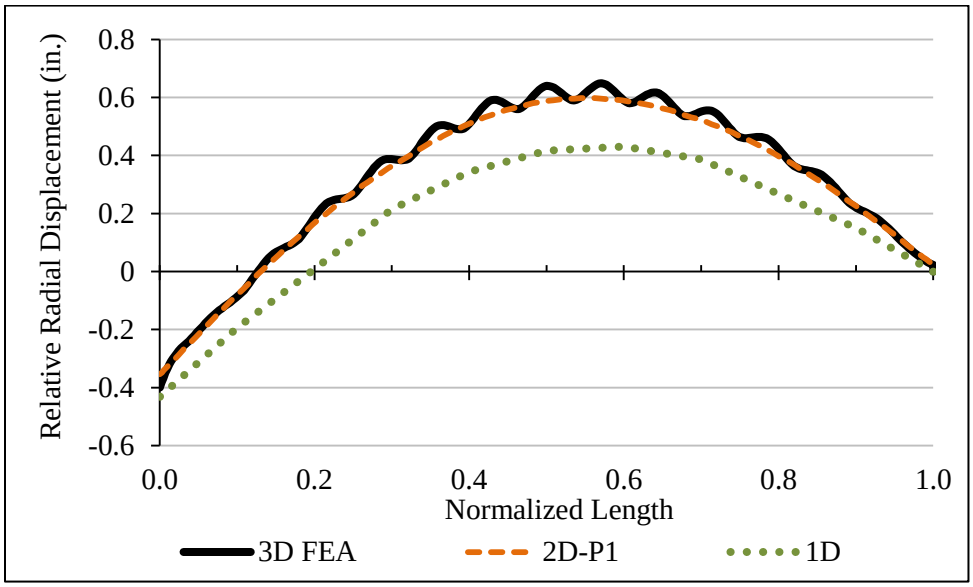

Figure 3.16. Comparison of relative lateral displacements in Girder 1 of Bridge NTSCS29 predicted using refined and approximate analysis methods.

The following development builds on the above estimates to evaluate the magnitude of the approximately constant internal torque due to skew relative to the maximum internal torque due to curvature in a simple-span bridge. The ratio of these torques is referred to as the skew-curvature torsion index. A simplified equation is developed that explains the relationship of this index to the girder torsional and bending properties, the horizontal curvature, and the skew angles.

3.2.2 Skew-Curvature Torsion Index

The constant girder torque due to skew can be estimated by means of the Eq. 3.9 for a span with two skewed supports with angles θ_1 and θ_2. For a simple-span bridge, one can substitute $\phi_{y1} = \phi_{y2} = wL^3/(24EI)$ into this equation. Recognizing the ratio $E/G = 2.6$, the torque due to skew may be written as

$$T_S = \frac{wL^2 J}{64.2I}(\tan\theta_1 + \tan\theta_2) \tag{3.13}$$

The distribution of the internal torque due to curvature is given by Eq. 2.6 for a simple-span bridge. The maximum torque due to curvature, which occurs at the supports, is

$$T_{C0} = \frac{wL^3}{24R} \tag{3.14}$$

Based on the above estimates, the ratio of the constant torque from the skew to the maximum torque due to curvature, referred to in this work as the "Skew-Curvature Torsion Index,"

$$I_{SC} = \frac{T_S}{T_{C0}} \tag{3.15}$$

may be written as

$$I_{SC} = \frac{J}{I}\frac{\tan\theta_1 + \tan\theta_2}{2.675\alpha} \tag{3.16}$$

where α is the subtended angle L/R, I and J are the girder moment of inertia for major-axis bending and St. Venant torsion constant respectively, and θ_1 and θ_2 are the skew angles at the supports.

The I_{SC} index from Eq. 3.16 is derived for simple-span bridges. For continuous-span bridges, Eq. 3.14 provides a conservative estimate of the maximum torque due to the horizontal curvature. Therefore, Eq. 3.16 can be applied for continuous-spans to conservatively characterize the combined effects of curvature and skew.

The Skew-Curvature Torsion Index can be used to determine the amount that the torque due to curvature should be incremented by to account for the effect of skew. It also can be used to understand the relative torsional effects from skew and from horizontal curvature as a function of I and J.. If the torque due to curvature, T_C, is known, the total torque can be estimated as

$$T = T_C + I_{SC} T_{C0} \tag{3.17}$$

Section 2.1.4 provides simple rules for the correct use of the signs for the combined effects of curvature and skew. A curved bridge concave upward in the plan view with a counterclockwise (positive angle) skewed support from the radial line experiences a larger torsional moment at its left-hand support, while at the right-hand support, the total girder torque is reduced.

For a given subtended angle of a span and skew angles of the bearing lines, the amount of torque due to skew depends on the ratio of J/I of the girder. For smaller J/I values, the torque contribution from the skew is smaller.

Figure 3.17 shows the variation of I_{SC} as a general function of the span subtended angle L/R for several different values of skew at the left-hand abutment of a simply-supported bridge with girders having a ratio J/I = 0.63. The point within the plot corresponding to the NTSCS29 bridge, where the girder J/I ratio is 0.63, also is indicated. The NTSCS29 bridge has a skew angle of 15.7° at the left support and 0° at the right, the span length is 225 ft and the radius of curvature is 820 ft. Therefore, the subtended angle of the span is L/R = 0.274. The resulting value of I_{SC} is 0.24. The skew contribution to the

total torque of the bridge is approximately 24 % of the torque due to curvature at the supports. For this specific example, the torque due to curvature at the supports is T_{C0} = 1904 kip-ft. Therefore, the internal torque diagram due to curvature should be shifted upward an amount $I_{SC} \times T_{C0}$ = 459 kip-ft. This is a conservative estimate since the interaction of the external intermediate cross-frames is ignored in the development of the underlying equations.

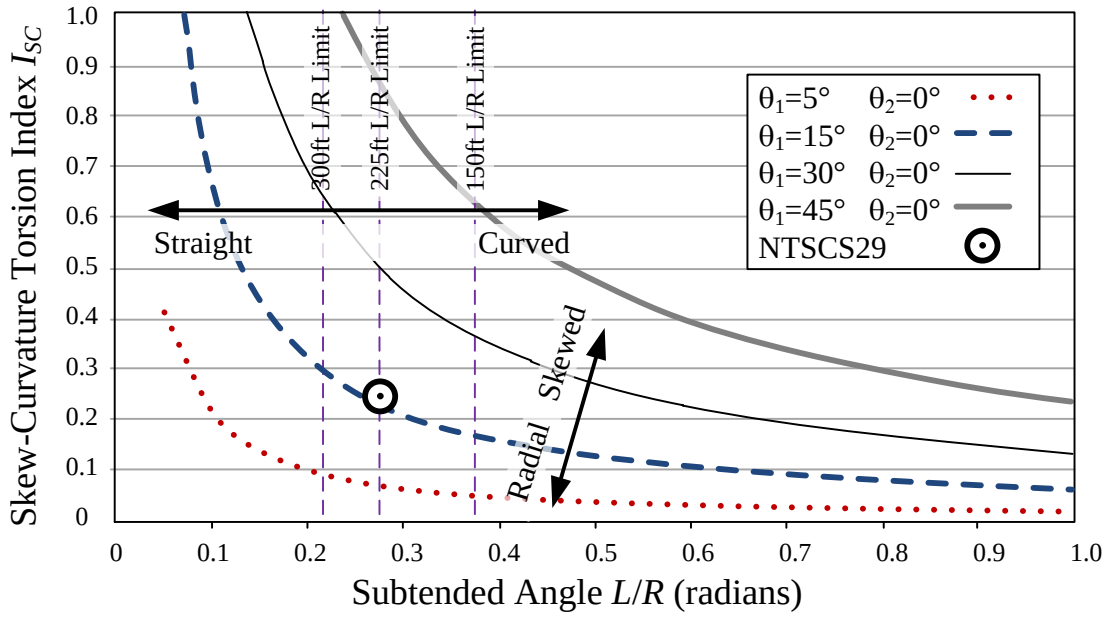

Figure 3.17 I_{SC} index values for different tub-girder geometries and J/I = 0.63.

The limit on the subtended angles for three different span lengths (150 ft, 225 ft and 300 ft) from the parametric bridge sets used in this research (see Chapter 4) are indicated as vertical lines in the above plot. Based on these lines, one can observe that for longer spans, the maximum L/R tends to be smaller; hence, the potential importance of skew is larger. Of course, for a nearly straight bridge, the I_{SC} index can be a relatively large number.

The skew-curvature torsion index in Figure 3.17 is applicable only for J/I = 0.63. The figure shows the influence of span length, curvature and skew. Larger values of J/I would result on the curves for a given skew shifting upwards, i.e., the ratio increases.

This occurs because, as torsional stiffness increases with respect to the bending stiffness, larger torques are generated in the girders for a given major-axis bending rotation at the supports.

The topics discussed in this section confirm that the skew effects become less important for bridges with larger curvature. It also provides tools (Eq. 3.16 and 3.17) to evaluate the importance of skew in a curved bridge.

3.3 Continuous-Span Bridges

Skewed support lines generally impose a twist rotation proportional to the major-axis bending rotation and skew angle (see Eq. 3.5). Support diaphragms on radial bearing lines restrain the girder twists and, consequently, these are assumed as torsionally fixed supports.

For evaluating the skew effects in continuous-span bridges, Eq. 3.5 is applicable to determine the girder twist at each support, and Eq. 3.9 is applicable to determine the torque within each span. The twist rotation induced by skew varies essentially in a linear fashion between the supports as given by Eq. 3.10. The torsional reactions at the interior supports of a continuous-span bridge are obtained by summing the end torques from the two adjacent spans. The girder internal torsional moments do not transfer from one span to the next, since St. Venant torsion dominates. For radial intermediate supports in a continuous-span bridge, the twist rotation at the interior support is essentially zero. Also, if diaphragms are utilized at interior skewed supports, the twist rotation is proportional to the major-axis bending rotation of the girder over the support. Some torsional-flexural coupling between the spans can occur in this case, since the major-axis rotation on a given span can be resisted by both the flexural and torsional rigidity of the adjacent span at an interior support. However, in many situations, diaphragms would not be used at interior bearing lines on tub-girder bridges.

For intermediate skewed piers the skew induced twist rotations are also proportional to the bending rotation at the support. This means that in a continuous-span bridge, the intermediate skewed pier causes two equal in magnitude but opposite in sign torsional moments in the spans adjacent to the pier (assuming that skewed diaphragms

are present at the interior bearing line). For spans with similar span length, the major-axis bending rotation at the pier may be small, and consequently, the torsional rotation at the pier is small regardless of the span length or skew angle. This behavior occurs for typical twin girder systems with a skewed interior supports. However, for wide tub-girder bridges, the girder lengths can vary significantly due to a skewed support; therefore, for similar span lengths with intermediate skewed pier, the torques on the fascia girders may not be negligible due to this length variation.

The support diaphragm is essential for the above described behavior to be true. For bridges where the support diaphragm is omitted at the skewed interior pier, the torsional moment due to this skewed support skew is negligible.

The above procedure is applied below to estimate the internal torques in a two-span continuous curved and skewed tub-girder bridge NTCCS22. The top flange lateral bracing layout is illustrated in Figure 3.18. The left abutment of the bridge is skewed 20.1° and it is parallel to the radial intermediate pier. The right abutment is oriented radially. This layout has one skewed and one radial span and provides insight into the effect of skew in continuous-span bridges. The results presented in this section are shown for Girder 1 (the outside girder with respect to the center of curvature).

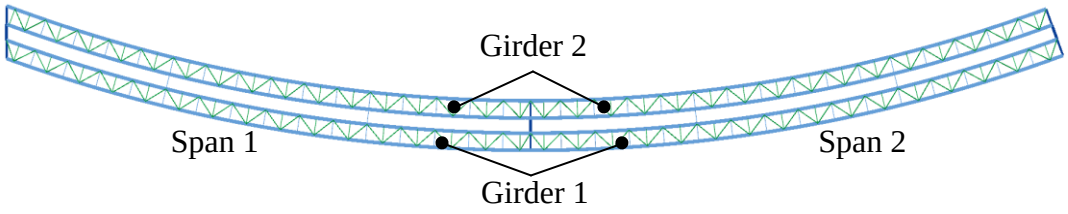

Figure 3.18. Plan view of NTCCS22.

In the above example, the intermediate pier acts as a torsionally fixed support since the skew only affects the skewed span. Figure 3.19 shows the torsional moment distribution in Girder 1 of the bridge for the three levels of analysis. The 3D FEA torsional moment is the result of the integration of the 3D FEA stresses. The 2D-grid results are obtained by modeling the curvature and skewed supports. The 1D line-girder estimations are based on Equation 3.8 and on the assumption that the skew only affects the left span. The torsional moment distribution in Figure 3.19 is nearly antisymmetrical,

but differs only on the left span by an additional constant torque. This additional constant torque is estimated accurately by the 1D method equations as 325 kip-ft.

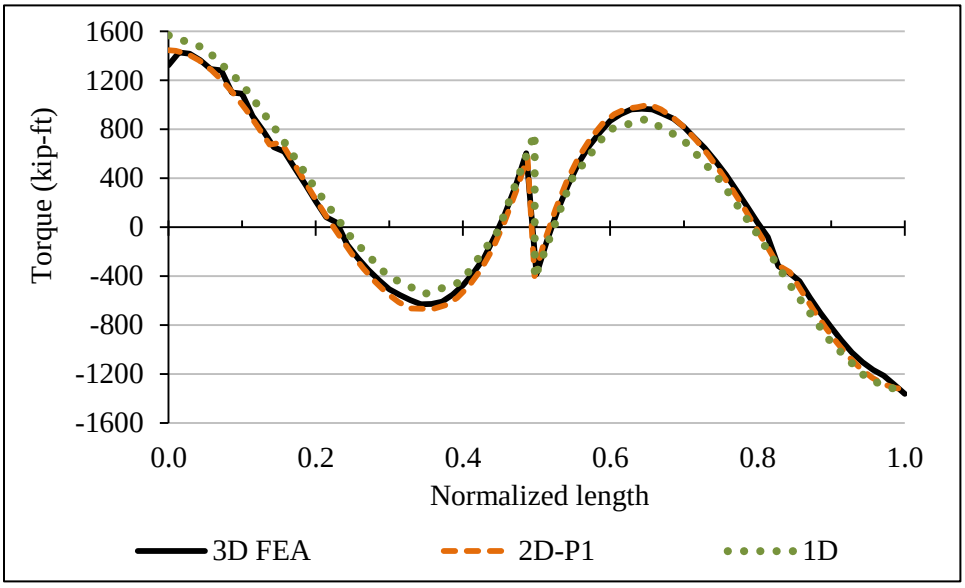

Figure 3.19. Comparison of the torsional moments in Girder 1 of Bridge NTCCS22 predicted using refined and approximate analysis methods.

Figure 3.20 illustrates the top to bottom flange relative radial displacements as estimated by the 3D FEA, 2D-grid and 1D analysis methods. In this case, the skew causes a layover at the left-hand support. Equation 3.5 provides an estimate of the girder layover, which then varies linearly along the left-hand span to a value of zero at the intermediate pier. This layover may be superimposed on the girder twist rotations due to the horizontal curvature, calculated using Eq. 2.7 from the M/R method.

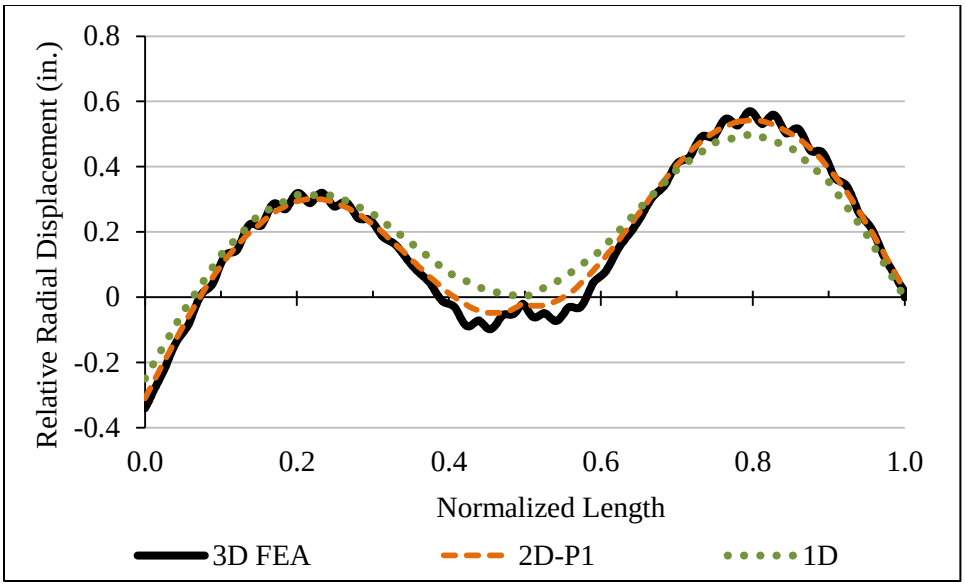

Figure 3.20. Comparison of relative lateral displacements in Girder 1 of Bridge NTCCS22 predicted using refined and approximate analysis methods.

These estimations show good agreement between the three analyses methods and indicate that the effect of the left-hand support skew is localized to the left span and has little effect on the right span. The developments presented in this dissertation allow an estimate of the effects using the 1D line-girder method.

3.4 Skew Effects on Component Force Estimates from Line-Girder and 2D-Grid Analysis

Recommendations based on this research are provided in this section to include the effects due to skewed supports on the estimation of the tub-girder component forces. In the following subsections the bracing equations presented in Chapter 2 are scrutinized to include the effects of skew where applicable. In general, the main factor related to skew in the equations is the additional girder torque due to skew.

3.4.1 Effects of Skewed Supports on the Top Flange Lateral Bracing

For line-girder analysis, the internal torque on the girder due to curvature can be estimated via the M/R Method and the internal torque due to skewed supports as the T_s torsional moment as discussed in Section 3.1.2. The combined torque due to curvature plus skew, given by Eq. 3.11, is then input into Eq. 2.8 for the calculation of the shear flow.

2D-Grid methods estimate the effects of skew on the girder internal torques by direct modeling. This approach requires modeling the girders at their centerlines, which can cause an under-estimation of the diaphragm stiffness due to the additional length between the girder centerlines compared to the actual diaphragm length. It is recommended to model a rigid link inside the girder cross-section or model the diaphragm as a rigid element since the diaphragm behaves mostly rigid due to its aspect ratio and multiple stiffener components.. This allows for a better estimate of the skewed support mechanism and a better estimation of the girder torque.

3.4.2 Effects of Skewed Supports on Internal Cross-Frames

The source of the girder internal cross-frame forces is predominantly the restraint of distortion of the tub-girder cross-sections. However, as discussed in Section 3.1.4, the skewed supports do not cause any significant distortional loads when internal support diaphragms are present. Therefore, skewed supports may be assumed to cause only pure torsional (St. Venant torsional) behavior when evaluating the internal cross-frame forces.

3.4.3 Effects of Skewed Supports on External Intermediate Cross-Frames

The equations for the forces in the external intermediate cross-frames depend directly on the individual girder rotations and the relative vertical displacement. When 2D-grid methods are used, the estimates of the girder rotations and displacements are readily available including the skew effects. For 1D line-girder analysis, the girder rotations must include the effect of skewed supports as presented on Section 3.1.3. These require the evaluation of the support rotation and the assumption of a linear variation of the twist along the span length as described by Eq. 3.10. Curved and skewed bridges require the superposition of the skew and curvature rotations as presented on Section 3.2.1. Equation 3.12 describes the superposition of the twist rotations due to curvature and skew.

3.4.4 Effects of Skewed Supports on External Support Diaphragms

Skewed supports have a direct effect in the amount of torque required to design the diaphragms for strength and stiffness. On straight bridges, the skew produces approximately constant torques to the girders as discussed in Section 3.1.2. The

magnitude of the torsional moments is given by Eq. 3.9. On curved and skewed bridges, the torque at the support may be increased or reduced by the skew depending on the geometry. Section 3.2.1 discusses the combined effects and Eq. 3.11 provides an estimate of the torques including the effects of skew. The skewed supports directly affect the input for the diaphragm force equations.

3.4.5 Effects of Skewed Supports on Top Flange Lateral Bending Stresses

The top flange lateral bending stresses are not directly affected by the skewed supports; however, the forces acting on the flanges are affected by the torsional moments which should be calculated accordingly to include the effects of skew. Additional effects on the top flange axial stresses are discussed in detail in the next section, which addresses the interactive forces coming from the top flange lateral bracing system.

3.5 Top Flange Stresses and Localized Effects from the TFLB System

Tub-girders are subjected to a combination of stresses originating from the girder major-axis bending and torsion. The girder top flanges are subjected to the effects of the equivalent lateral forces corresponding to the horizontal curvature as well as to lateral forces from the horizontal component of vertical forces in the sloping webs. Additionally, the top flanges take forces from the TFLB system components. In certain cases the TFLB components are connected eccentrically to the flanges, resulting in decreased stiffness of the TFLB system and local stresses at the connections due to the eccentric bending moments.

3.5.1 Average Major-Axis Bending Stresses

The top flange lateral bracing truss contributes to the girder major-axis bending resistance due to the compatibility of deformations. Ignoring the contribution of the top truss is generally expected to result in conservative estimates of the flange average axial stresses and it is usually the preferred practice. The analytical studies indicated that neglecting the contribution for the TFLB still provides accurate results. Section 3.6.2 illustrates the average major-axis bending stresses estimated by means of this procedure and how they compare to other interactive effects. The top flange axial stress is traditionally calculated as

$$f_b = \frac{M}{S_{x,top}} \tag{3.18}$$

where $S_{x,top}$ is the girder section modulus for the top flange ignoring the action of the top truss. The axial stress given by Eq. 3.18 is referred as the average axial stress in the following developments, since the stresses on the top flange also are affected by the interactive forces coming from the top flange lateral bracing diagonals for curved and/or skewed bridges which are subjected to torsion. For straight, non-skewed bridges, this "saw-tooth" effect is typically small. However, neglecting the top truss additional interactive "saw-tooth" effects in curved and/or skewed bridges may yield significantly unconservative estimates.

The additional effects of the interactive forces should be added to the average axial stress. A methodology to include them in the simplified analysis methods is presented in the following section.

3.5.2 Sawtooth Major-Axis Bending Stresses

As discussed previously in Section 2.3.5, for the purposes of the top flange lateral bending stresses, D_{Tot} is assumed to be the same value in adjacent panels when evaluating the equilibrium at a given nodal location of the TFLB truss. This assumption results on D_{Bend} being the only force acting laterally onto the girder flange. However, a more accurate way to estimate the actual forces acting in the top flange is by using the total forces in the diagonals, $D_{Tot,i}$ and $D_{Tot,j}$ (see Figure 3.21).

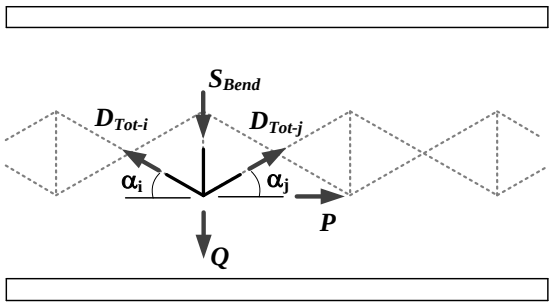

Figure 3.21. Total interactive forces between top flange lateral bracing and top flange for Warren and X-type layouts.

From Figure 3.21, the forces P and Q result

$$P = D_{Tot,i}\cos\alpha_i - D_{Tot,j}\cos\alpha_j \tag{3.19}$$

$$Q = D_{Tot,i}\sin\alpha_i + D_{Tot,j}\sin\alpha_j - S_{Bend} \tag{3.20}$$

The total force on the diagonal, D_{Tot}, is dominated by the torsional component, $D_{Torsion}$ (Eq. 2.9), for curved and/or skewed bridges. This is illustrated in Appendix A for five bridges where the forces D_{Tot} along the length of the bridge follow a distribution similar to the torsional moment diagram. In this case, the forces on the diagonals alternate from tension to compression in adjacent panels.

For Warren and X-type top truss systems, where the two diagonals meet at the same work point, and under the assumption that the diagonals forces vary a moderate amount due to the reduced panel size, it can be conservatively assumed that $D_{Tot,i}\sin\alpha_i + D_{Tot,j}\sin\alpha_j \approx 0$ Consequently, $Q \approx S_{Bend}$ for Warren cases and $Q \approx 0$ for X-type diagonals as discussed previously on Section 2.3.5. However, the effects are additive for the load *P* in Fig. 3.21, which results on a concentrated longitudinal force acting on the top flange.

For Pratt configurations, such as the one shown in Figure 3.22, only one diagonal connects at the truss work point and therefore

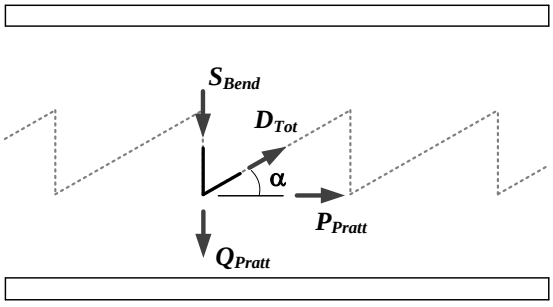

Figure 3.22. Total interactive forces between top flange lateral bracing and top flange for Pratt layout.

$$P_{Pratt} = D_{Tot}\cos\alpha \tag{3.21}$$

$$Q_{Pratt} = D_{Tot}\sin\alpha - S_{Bend} = D_{Torsion}\sin\alpha = qa \tag{3.22}$$

The axial force P_{Pratt} is calculated for the only diagonal acting at the working point. The lateral force Q_{Pratt} reduces to qa since the other projection components simplify. In Eq. 3.22 q is the shear flow defined by Eq. 2.8 and a is the truss width or tub-girder width at the top.

The effect of the load P is noticeable on the top flange axial stresses at the work points where the diagonals connect. The resulting top flange axial stresses distribution follows a sawtooth shape with the average axial stress approximately equal to f_b from 3.18, as shown in Fig. 3.23. Conventional line-Girder and 2D-grid methods do not include this effect and report just the stresses from Eq. 3.18 as f_b.

For straight and skewed bridges, the forces on the diagonals are dominated by the force from the constant girder torques. For these types of bridges, the sawtooth stress magnitude is approximately constant throughout the span length. For curved bridges the sawtooth stress varies as a function of the internal torsional moment. This leads to a maximum sawtooth stress close to the supports and a minimum at the midspan.

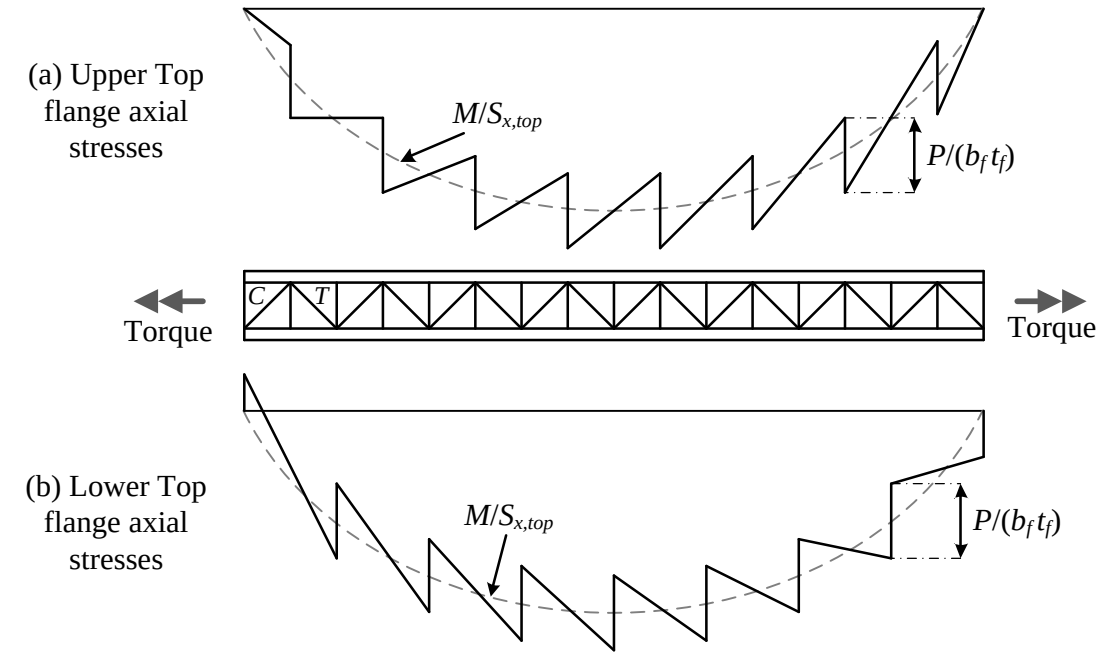

Figure 3.23. Top Flange sawtooth major-axis bending stresses due to the top flange lateral bracing interactive forces.

The force P causes a reduction of the flange axial stress on one side of a work point and an increase on the other side. For simplicity it can be assumed that half of the force P acts as compression and the other half as tension. Therefore, the top flange maximum axial stress can be calculated at the TFLB work points as

$$f_{b,TFLB} = f_b \pm \frac{P}{2b_f t_f} \tag{3.23}$$

3.5.3 Application Examples

3.5.3.1 Straight and Skewed Bridge

The following straight and skewed tub-girder bridge is analyzed by a 2D-grid method. The bridge is the simple-span straight and skewed tub-girder bridge NTSSS2. The bridge is a twin tub-girder system with a span of L = 150ft. The bridge framing plan is shown in Figure 3.24.

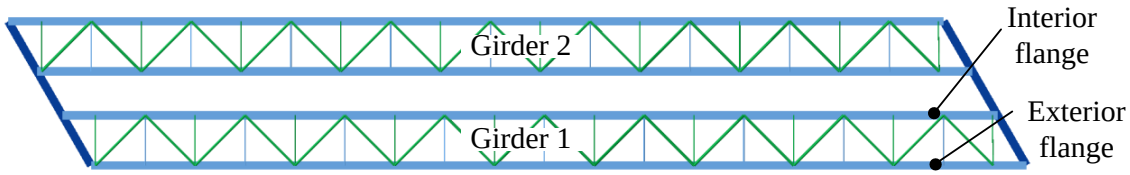

Figure 3.24. Plan view of NTSSS2.

The average top flange stresses are readily calculated from the major-axis bending moment and girder cross-section elastic section modulus. For this case, the TFLB system interacts with the top flange stresses and it is expected that the force P is proportional to the bending moments and, in greater measure, to the torsional moments. The torsional moments are approximately constant for the skewed and straight bridge configuration. Therefore, an approximately constant sawtooth stress is expected. The sawtooth stress is smaller at the first and last truss points, where only one diagonal connects. For the rest of the bridge span, the average P force is 140 kip which for a top flange with dimensions b_f = 16 in and t_f = 0.875, results on a sawtooth stress of 10 ksi or a total stress modification equal to $f_b \pm 5$ ksi at the work points of the truss. The increase/decrease of the stress is assumed to be equal in tension and compression on each side of the work

point. The average P is used in the above discussion because these forces vary slightly from panel to panel in the 2D-grid analysis.

Figure 3.25 shows the resulting sawtooth stresses added to the average stresses reported from a 2D-grid analysis for the exterior flange of the girder on the outside of the curve. Figure 3.26 shows the stresses for the interior flange of the same girder. In the figure, the average stresses and the results from a 3D FEA are also shown. The horizontal axis of the plot is the normalized span length, which varies from zero to 1.0. The figures show a good agreement with the behavior of the top flange stresses and show a significant increase of the maximum stresses at the center of the span.

3.5.3.2 Curved Bridge

The case studied above shows the effects under approximately constant torque which results in an approximate uniform sawtooth size. This torsional moment distribution is characteristic only of straight and skewed bridges. Curved bridges are subjected to a different torsional distribution and generally have their maximum torsional moment close to the supports and a minimum close to the center of the span. This results in a corresponding variation of the sawtooth stresses, with a minimum $P/(2b_f t_f)$ at the center of the span and a maximum near the ends of the span. .

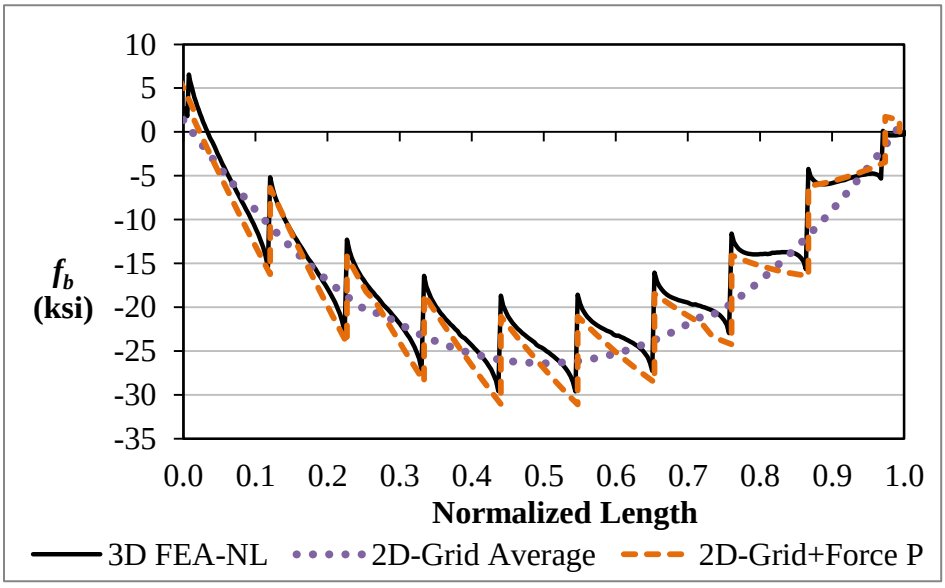

Figure 3.25. Girder 1 exterior top flange major-axis stresses and top flange lateral bracing interactive forces for Bridge NTSSS2.

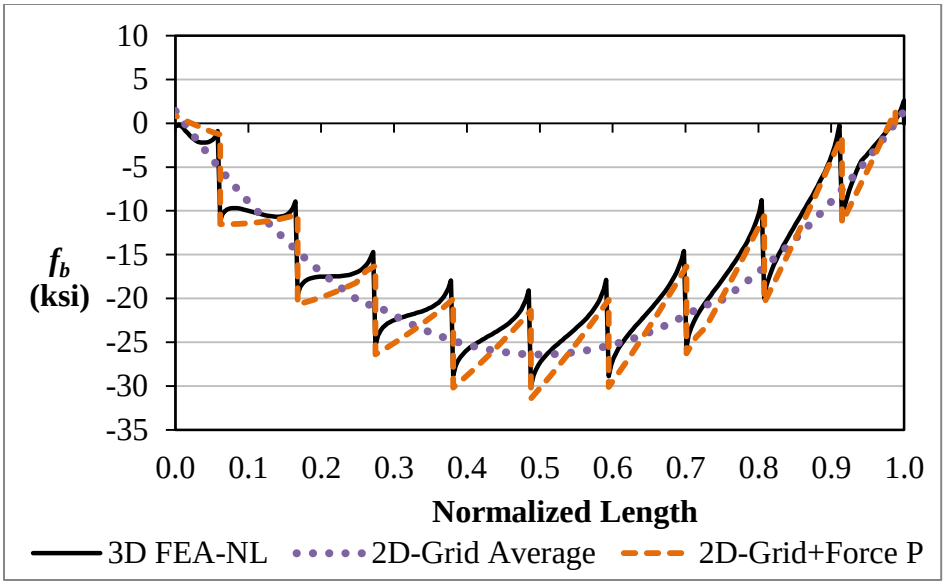

Figure 3.26. Girder 1 interior top flange major-axis stresses and top flange lateral bracing interactive forces for Bridge NTSSS2.

To illustrate this effect a simple-span curved tub-girder bridge with radial supports is analyzed. The bridge is designated as NTSCR1. This bridge is a twin tub-girder system with a span of L = 150ft and radius R = 400 ft. The bridge framing plan is shown in Figure 3.27.

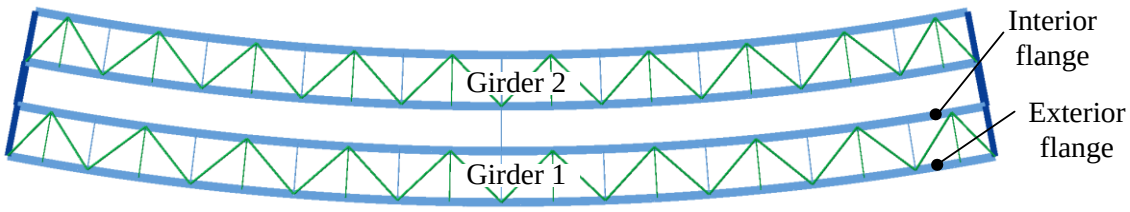

Figure 3.27. Plan view of NTSCR1.

The major-axis bending responses for the top flanges of the girder on the outside of the curve are shown in Figures 3.28 and 3.29. In these figures, the sawtooth size decreases at the center span and it is a maximum close to the supports. This distribution has smaller impact on the maximum top flange axial stress than the corresponding distribution in straight and skewed bridges. However, in cases where the flanges are transitioned to a smaller size as a result of the smaller stresses, the larger saw-tooth stresses in the regions with small major-axis bending stress may have an important impact on the proportioning of the smaller flange sizes.

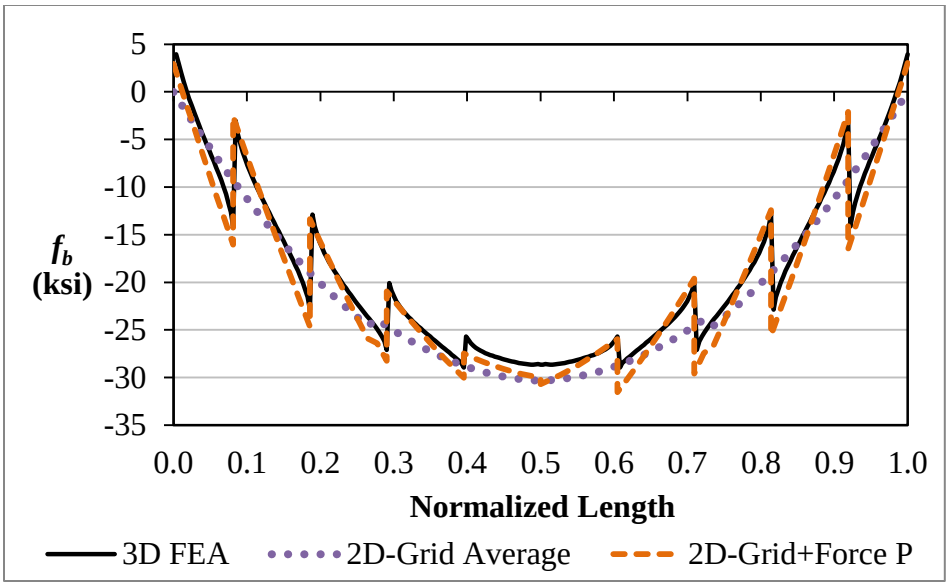

Figure 3.28. Girder 1 exterior top flange major-axis stresses and top flange lateral bracing interactive forces for Bridge NTSCR1.

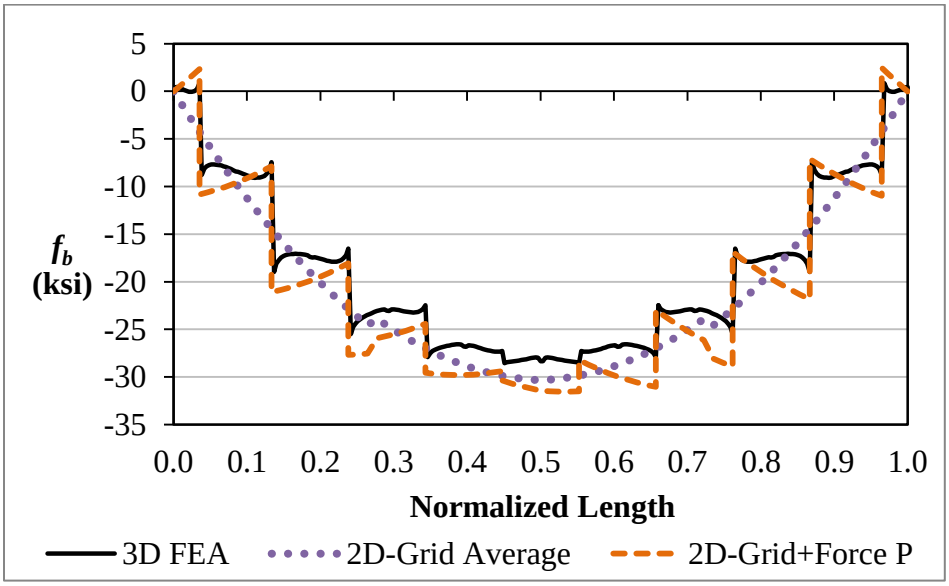

Figure 3.29. Girder 1 interior top flange major-axis stresses and top flange lateral bracing interactive forces for Bridge NTSCR1.

The interaction of the TFLB system with the top flange generally causes localized increases in the flange normal stresses on one side of the TFLB work points. In general, these are most noticeable in straight and skewed bridges.

3.6 Summary of Component Force Calculations

The top truss in tub-girders creates a quasi-closed condition which significantly increases the girder torsional stiffness and strength. To estimate this behavior in a simplified way, Kollbrunner (1966) developed the Equivalent Plate Method in which the top truss is replaced by an equivalent plate of a given thickness depending on the top truss characteristics. Tang and Fountain, (1970) developed the M/R Method to estimate the torsional effects on a curved girder. To account for the effects of skew, the developments in Sections 3.1, 3.2 and 3.3 provide estimates of the torsional effects on skewed bridges. The top flange bending response, all bracing elements forces, and the bearing-line diaphragm strength and stiffness requirements are calculated using component force equations based on the girder geometry and the stress resultants from the overall analysis (Fan and Helwig, 1999 & 2002 and Helwig et al, 2007).

The following sections provide a summary of the force equations for the different tub-girder bridge components. Sections 3.6.1 and 3.6.2 present the required input depending on the level of analysis and the Equivalent Plate Method to model the tub-girder torsional behavior. Sections 3.6.3, 3.6.4 and 3.6.5 present the forces for Warren, X-type and Pratt top flange lateral bracing systems. Sections 3.6.6 and 3.6.7 summarize the external intermediate cross-frame force equations and the strength and stiffness requirements for the support diaphragms. Section 3.6.8 lists the variable definitions used in the equations.

Appendix A presents the detailed results of these calculations for five tub-girder bridges. This appendix shows the results of the 1D line-girder analysis method, including the skew effects as previously described where applicable. The results from a 2D-grid analysis and a 3D FEA are also included. A detailed assessment of the errors in the evaluation of the displacements, stresses and bracing forces is presented in Chapter 5.

3.6.1 Input

Major-Axis Bending Moment, M

The girder major-axis bending moment distribution is directly obtained from 1D or 2D analysis.

Torque, T

The girder torsional moment for 2D analysis is directly obtained from the analysis. For 1D analysis the torsional moment distribution is calculated independently for each girder and each span.

At a location *s*, the torsional moment due to curvature is given by:

$$T_{C0} = \frac{1}{L}\int_0^L \frac{M(s)}{R}(L-s)\,ds$$

$$T_C(s) = T_{C0} - \int_0^s \frac{M(s)}{R}\,ds$$

Concentrated torques are applied to the girders from the skewed supports. The girder internal torque from the skew in each span is obtained by determining a twist rotation at each end of the span (ends 1 and 2) and then multiplying the total relative twist between the two ends by the St. Venant torsional stiffness *GJ*/*L*. The resulting constant torque in a given span due to skewed supports is given by:

$$T_S = -\frac{GJ}{L}(\phi_{y1}\tan\theta_1 + \phi_{y2}\tan\theta_2)$$

The total torque is equal to the sum of the torque due to curvature and due to skew:

$$T(s) = T_C(s) + T_S$$

Vertical Displacements, Δ

The vertical displacements are directly obtained from the 1D or 2D analysis.

Girder Twist Rotations, ϕ

The girder twist rotations for 2D analysis are directly obtained from the analysis. For 1D analysis the twist rotation distribution is obtained as follows.

At a location *s*, the twist rotation due to curvature is given by:

$$\phi_{x,C}(s) = \frac{1}{R}\left(1 + \frac{EI}{GJ}\right)\Delta(s)$$

The twist rotation due to skew is calculated at each support by the equation

$$\phi_{xi} = -\phi_{yi}\tan(\theta_i)$$

and the distribution along the span length is assumed to vary linearly as

$$\phi_{x,S}(s) = \phi_{x1} - (\phi_{x1} - \phi_{x2})\frac{s}{L}$$

The total girder twist rotations are equal to the sum of those due to curvature and those due to skew:

$$\phi_x(s) = \phi_{x,C}(s) + \phi_{x,S}(s)$$

Average Major-Axis Bending stress

$S_{x,top}$ does not include contribution from TFLB system.

$$f_b = \frac{M}{S_{x,top}}$$

3.6.2 Equivalent Plate Method

The Equivalent Plate Method allows the estimation of the girder torsional constant as

$$J = \frac{4A_0^2}{\sum_i b_i / t_i}$$

The top truss contribution to the system torsional behavior is estimated by replacing the truss by a fictitious equivalent plate. The equivalent plate thickness t^* can be determined for different truss layouts and cross-sectional areas of the diagonals and struts.

3.6.3 Warren TFLB Systems

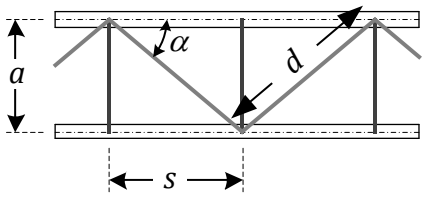

3.6.3.1 Equivalent Plate Thickness

$$t^* = \frac{E}{G}\frac{sa}{\left[\frac{d^3}{A_d} + \frac{2s^3}{3A_f}\right]}$$

3.6.3.2 TFLB Diagonal Forces

Torsion contribution

$$q = \frac{T}{2A_0}$$

$$D_{Torsion} = \frac{qa}{\sin\alpha}$$

Bending contribution

$$K_1 = \frac{d}{A_d} + \frac{a}{A_s}\sin^2\alpha + \frac{s^2}{2b_f^2 t_f}\sin^2\alpha$$

$$D_{Bend} = \frac{f_b s\cos\alpha}{K_1}$$

Other contributions

The lateral components of the transverse forces in the inclined girder webs are assumed to be developed entirely by the TFLB struts.

The influence of distortion on the TFLB diagonal forces is assumed to be negligible.

Total TFLB Diagonal Forces

$$D_{Tot} = D_{Torsion} + D_{Bend}$$

3.6.3.3 TFLB Strut Forces

Torsion contribution

$$S_{Torsion} = D_{Tot,i}\sin\alpha_i + D_{Tot,j}\sin\alpha_j$$

This is typically neglected, and is not considered in the base calculations.

Bending contribution

$$S_{Bend} = -D_{Bend}\sin\alpha$$

Transverse load contribution

$$p = \frac{w}{2}\tan\phi$$

$$S_{Lat} = ps$$

Girder distortional contribution

$$S_{Dist} = \pm\frac{s_K b}{4A_0}\left(\frac{b}{a}ew - \frac{M}{R}\right)$$

S_{Dist} is assumed to affect the struts that also serve as internal cross-frame top chords.

The only significant girder distortions are assumed to be due to eccentricity of the vertical load *w*, and due to the horizontal curvature effects.

Other contributions

At external cross-frame locations, significant TFLB strut forces may be developed. These forces should be estimated by basic principles considering the overall force paths and joint equilibrium for the bracing components.

Total

$$S_{Tot} = S_{Bend} + S_{Lat} + S_{Torsion} + S_{Dist}$$

3.6.3.4 Intermediate Internal Cross-Frame Diagonals

Distortion effects due to eccentric vertical load and due to horizontal curvature are assumed to be the only contributor to the internal cross-frame diagonal forces.

$$D = \pm \frac{s_K L_{DK}}{2A_0}\left(\frac{M}{R} - \frac{b}{a}ew\right)$$

3.6.3.5 Top Flange Lateral Bending

Major-axis bending contribution (from interaction with TFLB system)

$$f_{\ell,Bend} = \frac{1.5s}{b_f^2 t_f} S_{Bend}$$

Horizontal curvature contribution

$$f_{\ell,M/Rh} = \frac{0.6Ms^2}{Rhb_f^2 t_f}$$

Transverse load contribution

$$f_{\ell,p} = \frac{0.6ps^2}{b_f^2 t_f}$$

Total

$$f_{\ell,Tot} = f_{\ell,p} + f_{\ell,M/Rh} + f_{\ell,Bend}$$

3.6.3.6 Top Flange Major-Axis Bending Stresses

$$P = D_{Tot,i}\cos\alpha_i - D_{Tot,j}\cos\alpha_j$$

$$f_{b,TFLB} = f_b \pm \frac{P}{2b_f t_f}$$

The $P/2b_f t_f$ stress causes a reduction of the axial stress on one side of the top truss work point and an increase at the other side. Between work points the stress is assumed to vary linearly causing a sawtooth distribution.

3.6.4 X-Type TFLB Systems

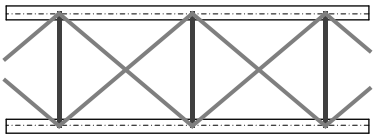

3.6.4.1 Equivalent Plate Thickness

$$t^* = \frac{E}{G}\frac{sa}{\left[\frac{d^3}{2A_d} + \frac{s^3}{6A_f}\right]}$$

3.6.4.2 TFLB Diagonal Forces

Torsion contribution

$$q = \frac{T}{2A_0}$$

$$D_{Torsion} = \frac{qa}{2\sin\alpha}$$

Bending contribution

$$K_2 = \frac{d}{A_d} + \frac{2a}{A_s}\sin^2\alpha$$

$$D_{Bend} = \frac{f_b s\cos\alpha}{K_2}$$

Other contributions

The lateral components of the transverse forces in the inclined girder webs are assumed to be developed entirely by the TFLB struts.

The influence of distortion on the TFLB diagonal forces is assumed to be negligible.

Total TFLB Diagonal Forces

$$D_{Tot} = D_{Torsion} + D_{Bend}$$

3.6.4.3 TFLB Strut Forces

Torsion contribution

$$S_{Torsion} = D_{Tot,i}\sin\alpha_i + D_{Tot,j}\sin\alpha_j$$

This is typically neglected, and is not considered in the base calculations.

Bending contribution

$$S_{Bend} = -2D_{Bend}\sin\alpha$$

Transverse load contribution

$$p = \frac{w}{2}\tan\phi$$

$$S_{Lat} = ps$$

Girder distortional contribution

$$S_{Dist} = \pm\frac{s_K b}{4A_0}\left(\frac{b}{a}ew - \frac{M}{R}\right)$$

S_{Dist} is assumed to affect the struts that also serve as internal cross-frame top chords.

The only significant girder distortions are assumed to be due to eccentricity of the vertical load *w*, and due to the horizontal curvature effects.

Other contributions

At external cross-frame locations, significant TFLB strut forces may be

developed. These forces should be estimated by basic principles considering the overall force paths and joint equilibrium for the bracing components.

Total

$$S_{Tot} = S_{Bend} + S_{Lat} + S_{Torsion} + S_{Dist}$$

3.6.4.4 Intermediate Internal Cross-Frame Diagonals

Distortion effects due to eccentric vertical load and due to horizontal curvature are assumed to be the only contributor to the internal cross-frame diagonal forces.

$$D = \pm \frac{s_K L_{DK}}{2A_0}\left(\frac{M}{R} - \frac{b}{a}ew\right)$$

3.6.4.5 Top Flange Lateral Bending

Major-axis bending contribution (from interaction with TFLB system)

$$f_{\ell,Bend} = 0$$

Horizontal curvature contribution

$$f_{\ell,M/Rh} = \frac{0.6Ms^2}{Rhb_f^2 t_f}$$

Transverse load contribution:

$$f_{\ell,p} = \frac{0.6ps^2}{b_f^2 t_f}$$

Total

$$f_{\ell,Tot} = f_{\ell,p} + f_{\ell,M/Rh} + f_{\ell,Bend}$$

3.6.4.6 Top Flange Major-Axis Bending Stresses

$$P = D_{Tot,i}\cos\alpha_i - D_{Tot,j}\cos\alpha_j$$

$$f_{b,TFLB} = f_b \pm \frac{P}{2b_f t_f}$$

The $P/2b_f t_f$ stress causes a reduction of the axial stress at one side of the top truss work point and an increase at the other side. Between work points the stress is assumed to vary linearly causing a sawtooth distribution.

3.6.5 Pratt TFLB Systems

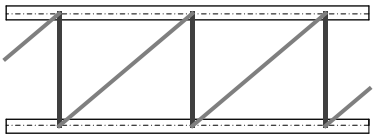

3.6.5.1 Equivalent Plate Thickness

$$t^* = \frac{E}{G}\frac{sa}{\left[\frac{d^3}{2A_d} + \frac{s^3}{6A_f}\right]}$$

3.6.5.2 TFLB Diagonal Forces

Torsion contribution

$$q = \frac{T}{2A_0}$$

$$D_{Torsion} = \frac{qa}{\sin\alpha}$$

Bending contribution

$$K_1 = \frac{d}{A_d} + \frac{a}{A_s}\sin^2\alpha + \frac{s^2}{2b_f^2 t_f}\sin^2\alpha$$

$$D_{Bend} = \frac{f_b s\cos\alpha}{K_1}$$

Other contributions

The lateral components of the transverse forces in the inclined girder webs are assumed to be developed entirely by the TFLB struts.

The influence of distortion on the TFLB diagonal forces is assumed to be negligible.

Total

$$D_{Tot} = D_{Torsion} + D_{Bend}$$

3.6.5.3 TFLB Strut Forces

Torsion contribution

$$S_{Torsion} = qa$$

Bending contribution

$$S_{Bend} = -D_{Bend}\sin\alpha$$

Transverse load contribution

$$p = \frac{w}{2}\tan\phi$$

$$S_{Lat} = ps$$

Girder distortional contribution

$$S_{Dist} = \pm\frac{s_K b}{4A_0}\left(\frac{b}{a}ew - \frac{M}{R}\right)$$

S_{Dist} is assumed to affect the struts that also serve as internal cross-frame top chords.

The only significant girder distortions are assumed to be due to eccentricity of the vertical load *w*, and due to the horizontal curvature effects.

Other contributions

At external cross-frame locations, significant TFLB strut forces may be developed. These forces are not considered in the base calculations.

Total

$$S_{Tot} = S_{Bend} + S_{Lat} + S_{Torsion} + S_{Dist}$$

3.6.5.4 Intermediate Internal Cross-Frame Diagonals

Distortion effects due to eccentric vertical load and due to horizontal curvature are assumed to be the only contributor to the internal cross-frame diagonal forces.

$$D = \pm \frac{s_K L_{DK}}{2A_0}\left(\frac{M}{R} - \frac{b}{a}ew\right)$$

3.6.5.5 Top Flange Lateral Bending

Major-axis bending contribution (from interaction with TFLB system):

$$f_{\ell,Bend} = \frac{1.5s}{b_f^2 t_f} S_{Bend}$$

Horizontal curvature contribution

$$f_{\ell,M/Rh} = \frac{0.6Ms^2}{Rhb_f^2 t_f}$$

Transverse load contribution

$$f_{\ell,p} = \frac{0.6ps^2}{b_f^2 t_f}$$

Total

$$f_{\ell,Tot} = f_{\ell,p} + f_{\ell,M/Rh} + f_{\ell,Bend}$$

3.6.5.6 Top Flange Major-Axis Bending Stresses

$$P_{Pratt} = D_{Tot}\cos\alpha$$

$$f_{b,TFLB} = f_b \pm \frac{P_{Pratt}}{2b_f t_f}$$

The $P_{Pratt}/2b_f t_f$ stress causes a reduction of the axial stress at one side of the top truss work point and an increase at the other side. Between work points the stress is assumed to vary linearly causing a sawtooth stress.

3.6.6 External Intermediate CF

$$F_D = 4GJ\frac{\left(L_i\phi_{w,ext} + L_e\phi_{w,\text{int}} - K_{e1}\Delta_{w,rel}\right)}{K_{e2}}$$

$$F_T = \frac{4GJ\left(\phi_{w,ext} - \phi_{w,\text{int}}\right) - F_D L_K\left(L_e - L_i\right)}{h_k\left(L_i + L_e\right)}$$

$$F_B = \pm F_D\cos\psi - F_T$$

Where the variables in these equations are

$$L_K = h_K\cos\psi + L_T\sin\psi$$

$$K_{e0} = 1 + \left(1 + \frac{EI}{GJ}\right)\left(1 - \cos\frac{\beta_0}{2}\right)$$

$$K_{e1} = \frac{L_i + L_e}{a + c}$$

$$K_{e2} = K_{e0}K_{e1}\frac{L_i^3 + L_e^3}{12\left(EI/GJ\right)}\sin\psi + 2L_iL_eL_K$$

3.6.7 Support Diaphragms

Strength requirement

$$A_{d,strength} = \frac{T_1 + T_2}{L_d\left(0.58F_y\right)}$$

Stiffness requirement

$$x_r = \left(a + b_f\right)/2$$

$$A_{d,stiffness} = \frac{\left(T_1 + T_2\right)x_r}{0.0125GL_d}$$

3.6.8 Variables Used in the Equations

A_0 = area enclosed by box.

$A_{D,stiffness}$ = external end diaphragm cross section area stiffness requirement.

$A_{D,strength}$ = external end diaphragm cross section area strength requirement.

A_d, A_s = cross section area of TFLB diagonal and strut.

D = internal CF diagonal axial force.

$D_{Torsion}, D_{Bend}$ = TFLB diagonals torsional and bending force components.

D_{Tot} = TFLB diagonal axial forces.

$D_{Tot,i}, D_{Tot,j}$ = TFLB diagonal axial forces in two consecutive panels.

E = steel elasticity modulus.

F_D, F_T, F_B = external CF diagonal, top and bottom chord axial forces.

F_y = steel yield strength.

G = steel shear modulus.

I = tub-girder cross-section moment of inertia.

J = St Venant tub-girder torsional constant.

K_1, K_2 = EPM constants for TFLB force calculation.

K_{e0}, K_{e1}, K_{e2} = constants for external intermediate CF force calculation.

L_d = diaphragm length between supports.

L_{DK} = length of internal CF diagonal.

L_i, L_e = internal and external girder CL lengths.

L_K = constant for external intermediate CF force calculation.

L_T = external CF top chord distance to tub centerline.

M = girder bending moment.

R = radius of horizontal curvature of girder.

$S_{Lat}, S_{Bend}, S_{Dist}, S_{Torsion}$ = TFLB struts lateral, bending, distortional and torsion force components.

S_{Tot} = TFLB strut axial forces.

$S_{x,top}$ = top flange section modulus.

T = total girder torsional moment

T_C, T_S = girder torsional moments due to curvature and skew.

T_1, T_2 = girder end torques.

a = box girder top width.

b = bottom flange width.

b_f = top flange width.

c = external CF top chord length.

d = TFLB diagonal length.

e = effective eccentricity of resultant distributed load.

f_b = average top flange major-axis bending stress.

$f_{b,TFLB}$ = top flange major-axis bending stress including the TFLB interaction.

$f_{\ell,Bend}, f_{\ell,p}$ = lateral force and major-axis bending components of lateral bending.

$f_{\ell,M/Rh}$ = influence of the horizontal curvature of the top flanges lateral force to lateral bending.

$f_{\ell,Tot}$ = total top flange lateral bending stress.

h = box girder depth.

h_d = end diaphragm depth.

h_K = external CF chords distance.

p = lateral component of the normal force *w* due the sloping webs.

q = torsion shear flow.

s = TFLB panel length.

s_K = spacing between internal CF measured along the girder length.

t_d = end diaphragm thickness.

t_f = top flange thickness.

x_r = constant for diaphragm force calculation.

w = distributed vertical load per unit length assumed to be applied at the top flange.

α = TFLB diagonal angle.

α_i, α_j = TFLB diagonal angles in two consecutive panels.

β_0 = subtended angle.

$\Delta_{w,rel}$ = relative vertical displacement between girders at external CF location.

$\phi_{w,ext}, \phi_{w,\text{int}}$ = interior and exterior girder twist rotations at CF location.

ϕ = web slope.

ψ = external CF diagonal angle.

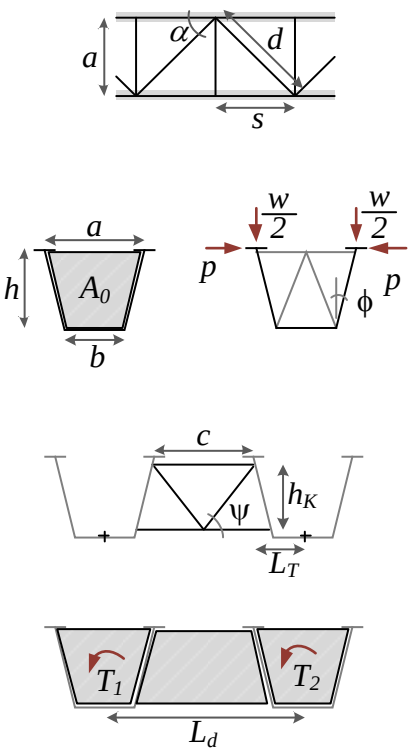

Figure 3.30. Associated dimensions for the displacement, force and stress equations for tub-girder components (two girder systems).

CHAPTER IV.

SELECTION OF STUDY BRIDGES

4.1 Introduction

The analytical studies presented in this research are a combined effort for the research project NCHRP 12-79 (NCHRP, 2011) to assess the analytical method for construction engineering of curved and skewed steel I- and tub-girder bridges. The analytical studies are focused on actual designs and parametric bridges to directly investigate the effects of geometric factors related to skew and curvature. In total, 28 tub-girder bridges are analyzed using 3D FEA and 18 of those bridges also are analyzed using simplified methods.

This chapter describes the analytical studies and the process used to characterize the bridges based in the main deck geometry. The selected bridges for the analytical studies are presented in this section.

4.2 Overview of the Research Studies

The studies presented in this research evaluate the analytical methods for a wide range of bridge structures under construction loads. The accuracy of simplified analysis methods is evaluated using actual bridge designs and a set of parametric bridges that satisfy either prior and/or current AASHTO design criteria. The parametric bridges permitted to study direct effects on certain geometric parameters.

Existing bridges were identified representing a sample of various combinations of span arrangement, span length, curvature, bridge widths and skew used in existing highway bridges. The preferred bridges had good instrumented field data or field observations and detailed construction plans to evaluate the effects during construction.

The focus of these studies were on analysis and design using appropriate practices and average practice, therefore, bridges involving generally acknowledged poor practices, extreme geometric characteristics, non-conventional support systems, etc., were not

considered. It was desired for the studies to explain when the analysis methods are not able to highlight inappropriate design details.

For the existing bridges the geometric factors influencing the analysis, design and construction of the bridges were identified and a number of levels of these factors were selected for subsequent analytical study. The following sections provide a detailed description of these steps.

4.3 Identification of Existing Bridges

Appendix C summarizes the overall characteristics of the existing tub-girder bridges collected from various owners and consultants. The figures show sketches of the overall deck plan geometry and bearing lines. The collected bridges are subdivided into the following categories:

- Simple-span, Straight, with Skewed supports (TSSS),
- Continuous-span, Straight, with Skewed supports (TCSS),
- Simple-span, Curved, with Radial supports (TSCR),
- Continuous-span, Curved, with Radial supports (TCCR),
- Simple-span, Curved, with Skewed supports (TSCS), and
- Continuous-span, Curved, with Skewed supports (TCCS).

The collected existing bridges were an aid to evaluate the range and level of geometries that should be considered within the main parametric studies of the research and to select a number of the existing bridges that best fit the research criteria for the analytical studies.

Four tub-girder bridges had measurements or field observations of some type during construction and six tub-girder bridges had detailed construction plans. Furthermore, the extent of the field measurements was generally limited.

In addition to the existing bridges, a number of useful detailed LRFD example tub-bridge designs have been published in the recent literature. Figure 4.1 summarizes the plan geometries of the collected hypothetical bridges. The straight, non-skewed bridges

in these examples were selected to serve as useful base-line problems the project calculations.

The selection of the existing and example bridges for inclusion in the Project overall parametric study is addressed in Section 4.5.

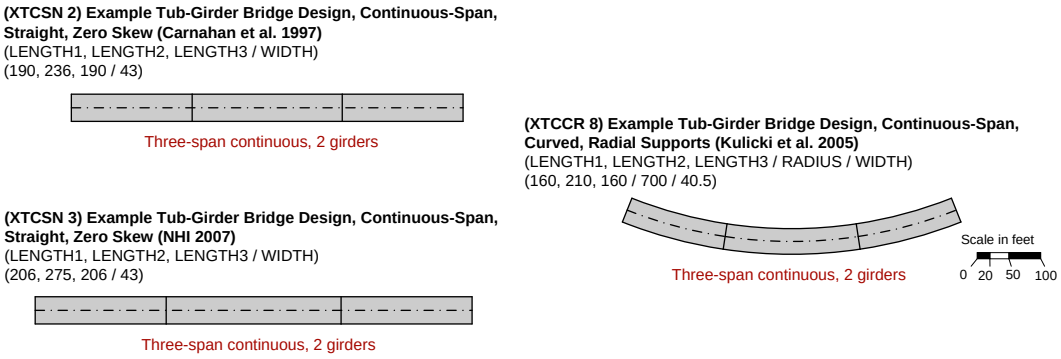

Figure 4.1. AASHTO LRFD example tub-girder bridge designs.

4.4 Selection of Geometric Factors

4.4.1 Identification of Primary Geometric Factors

4.4.1.1 Characterization of Horizontal Curvature

In this research the "Torsion Index", I_T, introduced by Ozgur (2011) is as a useful measure of the degree of curvature of the bridge spans since this parameter is closely related to the magnitude of the overall torsion that exists in the bridge (or bridge unit). The torsion index provides a characterization of horizontal curvature considering the width of the bridge which the commonly used factor L_{as}/R does not include. The index is based on the overall the tendency for uplift at the bearings, and it is also an indicator of torsion and overturning:

$$I_T = \frac{s_c}{s_c + b} \tag{4.1}$$

where s_c is the perpendicular distance between the centroid of the deck and the chord between the inside bearing locations, and b, the perpendicular distance from the centroid

(×) to the chord between the bearing locations on the outside girders. The terms in this equation are illustrated in Figure 4.2.

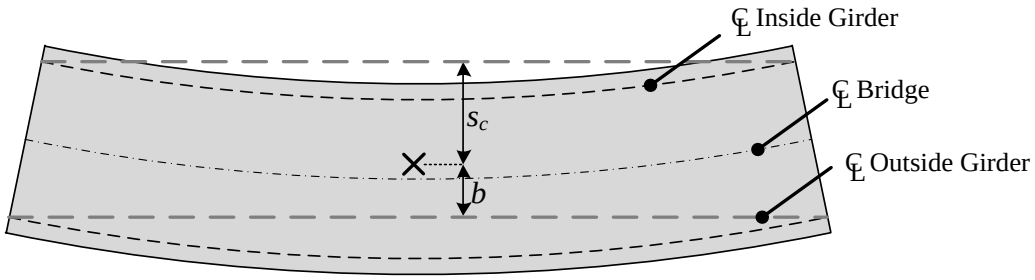

Figure 4.2. Illustration of terms for expressing I_T.

When I_T approaches 0.5 the centroid of the deck area is mid-way between the chords intersecting the outside and inside end bearings, e.g. tangent bridge. A value of $I_T = 1.0$ means that the centroid of the deck area is located at the chord line between the outside bearings. This implies that the bridge is at incipient overturning instability, by rocking about its outside bearings under uniform self-weight.

The torsion index provides indication of the potential for uplift at simple bearings and relates to the magnitude of the overall torsion that exists in the bridge span due to the eccentricity of its self-weight. Continuous-span bridges can tolerate higher indices due to the stabilizing effect of the continuity with the adjacent spans.

For simple-span radially supported tub-girder bridges, horizontal curvature values were selected by conducting basic estimates to determine the largest curvature (smallest *R*) without having uplift at the most critical bearing location(s) under nominal dead plus live loads. This value of *R* was used as the most extreme value for the horizontal curvature. This radius of curvature then was increased approximately 1.5 times to obtain cases with smaller curvature (larger *R*).

Tub-girder bridges tend to have relatively high torsion indices compared to I-girder bridges with similar deck geometry due to the shorter length between the fascia girder bearings. This resulted in lower and upper bound values of I_T equal to 0.72 and 0.87 respectively. For the more tolerant curved continuous-span bridges radially

supported tub-girder bridges, the lower and upper bound values of I_T were obtained as 0.69 and 1.14 respectively.

4.4.1.2 Characterization of Skew Pattern

There are a number of factors related to the representation of the skew pattern for practical designs. Figure 4.3 shows a number of possible combinations of θ values and skew patterns on individual curved bridge span with, radius and span length w = 30 ft, R = 400 ft and L = 150 ft. The values of skew shown are 15, 30 and one case with 10.7° to provide a parallel support configuration. The 30^o skew case is the maximum skew angle considered and, as summarized subsequently, this is close to the maximum value of the skew encountered in the existing tub-girder bridges with conventional supports shown in Appendix B. Tub-girder bridges generally tend to have smaller skew values, due to the expected sensitivity to skew effects as well as the fabrication difficulties and increased cost associated with complicated skewed connection details.

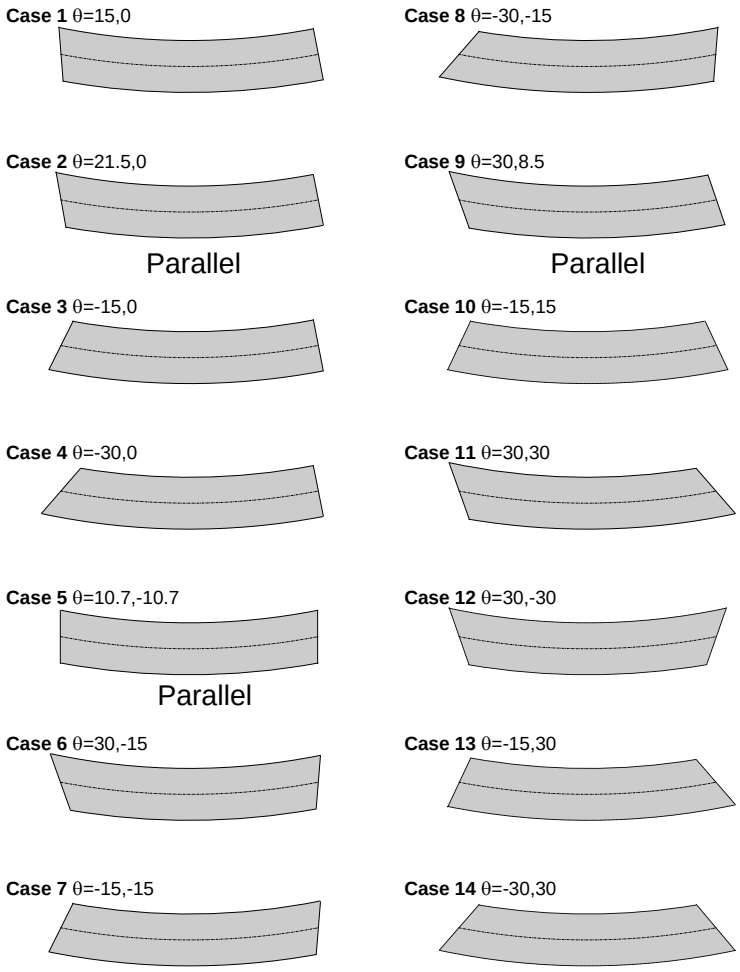

Figure 4.3. Example potential skew and horizontal curvature combinations for curved tub-girder bridge spans with w = 30 ft, L_{as} = 150 ft and R = 400 ft.

4.4.2 Synthesis of Primary Factor Ranges from the Collected Bridges

Upon perusing the distribution of the primary factors among the existing bridges, the following ranges of these factors were observed:

- Arc-span length, L_{as}
  - 139 to 205 ft (straight simple-spans with skewed supports)
  - 101 to 207 ft (curved simple-spans with radial supports)
  - 217 ft (curved simple-spans with skewed supports)
  - Only one bridge was identified as curved simple-span with skewed supports; this was the bridge ETSCS1.
  - 57.5 to 373 ft (curved continuous-spans with radial supports)
  - 153 to 332 ft (curved continuous-spans with skewed supports)

- Deck width, *w*
  - 25 to 45 ft (spans with two tub-girders)
  - 36 ft to 120 ft (spans with more than two tub-girders)
- Torsion Index, I_T
  - 0.50 to 1.14 (spans with two tub-girders; an I_T larger than 1.0 is possible due to continuity with adjacent spans)
  - 0.50 to 0.84 (spans with more than two tub-girders)
- Skew angle of the bearing lines relative to a tangent to the bridge centerline, θ
  - 0 to 12.8^o (spans with two tub-girders, excluding the ETCCS7 bridge, which had cast-in-place concrete end diaphragms and non-typical bearing details)
  - 0 to 38.9^o (spans with more than two tub-girders)
- Skew pattern
  - All the skewed spans have non-parallel bearing lines for the collected bridges that are composed of two tub-girders.
  - One curved bridge with two tub-girders (ETCCS3) has θ = 0^o & 12.8^o and a 39.0^o difference in orientation between the bearing lines.
  - One curved bridge with two tub-girders (ETCCS7) has θ = 51.8^o & 39.5^o and a 32.0^o difference in orientation between the bearing lines; however, this bridge has cast-in-place (CIP) concrete end diaphragms and non-typical bearing details.
  - Most of the skewed spans with more than two tub-girders have parallel bearing lines.
  - One curved bridge with four tub-girders (ETCCS6) has θ = 0^o & 38.9^o and a difference in orientation of 53.8^o between the bearing lines in one span.
- Type-of-span
  - Most of the collected tub-girder bridges are continuous-span.
  - Ratio of exterior-to-interior span lengths: 0.49 to 1.0
  - Ratio of adjacent interior span lengths: 0.49 to 1.0
  - Ratio of span lengths, 2-span continuous: 0.69 to 1.0
  - A fraction of the bridges with more than two tub-girders are simple-span.

The values for several additional "secondary" parameters discussed in the above, but not selected as primary factors were:

Arc-span length to deck width ratio, L_{as}/w
- 2.80 to 8.76 (radially-supported spans with two tub-girders)
- 4.66 to 10.35 (skewed spans with two tub-girders)
- 0.83 to 3.83 (skewed spans with more than two tub-girders)

- Subtended angle of the span's centerline, L_{as}/R
  - 0.0 to 0.68 radians (spans with two tub-girders)
  - 0.07 to 0.28 radians (spans with more than two tub-girders)

4.4.3 Selection of Primary Factor Ranges and Levels

Table 4.1 shows the ranges and levels of the primary factors that were selected for the main analytical studies. These primary factors are discussed in detail in the preceding sections.

The first row of Table 4.1 addresses the type of span. Three-span continuous designs with one balanced end span and one end span of equal length to the main span capture both the behavior associated with drop-in spans as well as the interactions between balanced and unbalanced continuous-spans. The potential combinations of skew arrangements become large as the number of spans is increased. Many of these combinations would have a minor effect on the final analysis accuracy assessments though, due to the fact that the influence of the skew at a particular bearing line tends to die out several spans away from this bearing line. Furthermore, long multi-span curved bridges often may have only a few skewed bearing lines because of geometry constraints at a particular location, whereas it may be possible to orient other bearing lines radially.

The second row of Table 4.1 shows the values selected for the arc-span length. The selected lengths for simple-spans were 150, 225 and 300 ft and the selected lengths for continuous-spans were 150, 250 and 350 ft. The maximum span length of L_{as} = 350 ft. was selected to match the maximum value targeted by the AASHTO (2010) Specifications. An arc-span length of L_{as} = 150 ft is a rough lower-bound value at which welded girders are generally required. Only the two interior spans of the parallel US 119 bridges over KY 1441 and Raccoon Creek in Pike Co., KY (bridge ETCCR 2) have arc-span lengths greater than 350 ft, although there are two other tub-girder bridges with spans larger than 300 ft.

The third row of Table 4.1 shows the selected deck widths for the parametric study bridges. Only 30 ft deck widths were considered in the new parametric designs for the tub-girder bridges which is representative of one- to two-lane bridges. A large number of the existing tub-girder bridges were one to two lane ramp type structures. The less common tub-girder bridges having more than two girders were addressed by including one of these existing bridge cases in the overall parametric study matrix.

Table 4.1. Primary factor ranges and levels for the main analytical study.

Factor	Tub-girder bridges
Type of span	Simple, 2-span continuous, and 3-span continuous with one balanced end span and one end span equal in length to the main center span. Use the above 3-span continuous bridges as base TCCR cases. Consider both 2- and 3-span continuous bridges for the TCSS and TCCS cases. Consider at least one 2-span continuous bridge with a significant unbalance between the span lengths.
Maximum arc-span length of bridge centerline, L_{as}	150, 225 & 300 ft. for simple-spans 150, 250 & 350 ft. for continuous-spans
Deck width, w	30 ft (1 to 2 traffic lanes + shoulders & barriers)
Torsion Index, I_T	0.72 to 0.87 for TSCR bridges 0.69 to 1.14 for TCCR bridges
Skew angle θ	15° & 30° and additional sensitivity studies with variations up to ±15° from zero skew
Skew pattern	Consider the ± combinations of skew angles using θ = 15 & 30°. Give preference to typical (i.e., non-exceptional) bridge geometries.

The combinations of L_{as} from 150 to 350 ft with w of 30 ft give a range for the arc-span length to the bridge width L_{as}/w from 5 to 11.7. It was believed that these larger values should be studied to fully address the bridge responses and analysis accuracies for these practical but more extreme geometry conditions.

The fourth row of Table 4.1 gives the selected ranges and levels for the torsion index I_T. This parameter was used in establishing the horizontal radius of curvature R for the TSCR and TCCR designs, given the arc-span length L_{as} and the deck width w. The horizontal radius of curvature obtained for the TSCR designs was then employed for other new curved TSCS parametric bridge designs. Similarly, the horizontal radius of

curvature obtained for the TCCR designs was employed for the other new curved TCCS parametric bridge designs. A maximum limit on L_{as}/R of 1.0 was imposed on the parametric designs. This limit can govern for shorter spans with wide decks and is somewhat larger than the maximum L_{as}/R of 0.68 radians for the collected existing bridges. Nevertheless, it was believed that L_{as}/R = 1.0 is a practical extreme that should be addressed in the parametric study design. Wide bridges with these larger L_{as}/R values may require special handling during the steel erection and/or deck placement.

The fifth row of Table 4.1 shows the selected ranges and levels of the skew angle θ. A value of 30^o is a reasonable maximum limit for θ for tub-girder bridges, larger values are expected for I-girder bridges.

Lastly, the sixth row of Table 4.1 explains the recommended variations of the skew pattern considered. These variations are more easily understood by showing the actual deck plan geometries for various hypothetical new bridge designs.

4.5 Selection of the Analytical Study Bridges

The following sub-sections summarize the key characteristics of the tub-girder bridges selected for the analytical studies. To arrive at the analytical study design, a full factorial design matrix involving all the above factors and levels was developed. A number of these combinations and permutations could be considered impractical or unbuildable and some prioritization of the bridges was necessary within the full range of practical designs. Furthermore, a number of bridges in which the combination of factors led to exceptional (i.e., particularly unusual) structures and designs that were very similar in one or more characteristics to other designs were eliminated.

Once these selections were completed, the library of existing bridges summarized in Appendix C was searched for bridges that matched closely with the analytical study design selections, and satisfied the criteria previously described. In a few cases, modifications were made to the analytical study design to include existing bridges that were particularly good candidates. In addition, one of the Example bridges from Fig. 4.1 was selected for inclusion in the analytical study. The remaining bridges in the study design were targeted as “New” bridges, indicating that they were to be fully designed by

the NCHRP 12-79 project team using the AASHTO LRFD Specifications and current common standards of care. The resulting final study targeted 18 total tub-girder bridges.

The following sections first discuss the base straight, non-skewed study bridges considered, followed by straight skewed simple and continuous-span cases, then simple and continuous-span curved bridges with radial supports, and finally curved and skewed simple- and continuous-span bridges. Each of these sections includes simple summary sketches of the bridge deck plan and bearing-line geometries corresponding to the designs along with a title block for each of the bridges containing:

- An identification label, composed of the letter "X" for "eXample" bridge designs followed by the symbols explained in Section 4.3, indicating the bridge category (e.g., TSSS, TCSS, etc.), and ending with the bridge number for that category. An additional category, TCSN, is introduced in Fig. 4.1. The "CSN" designation stands for Continuous-span, Straight, with Non-skewed supports.
- An identification label, composed of the letter "E" for "Existing" followed by the above symbols indicating the bridge category, and ending with the bridge number for that category, e.g., bridge "ETSSS 2" in Fig. 4.5.
- An identification label, composed of the letter "N" for "New" bridge designs followed by the above symbols indicating the bridge category, and ending with the bridge number for that category, e.g., bridge "NTSSS 1" in Fig. 4.5. A summary of the basic geometry information about the bridge, enclosed in parentheses. For instance, in Fig. 4.5, the basic geometry information includes the span length of the bridge centerline, the out-to-out width of the bridge deck perpendicular to the bridge centerline, and the skew angle with respect to centerline of the bridge for both bearing lines.

This information is conveyed symbolically in the figure caption as "(LENGTH/WIDTH/θ_1, θ_2)." The other categories have similar but different basic geometry information. The skew angle of the bearing lines is represented by the symbol θ. This angle is taken as zero when a bearing line is perpendicular to the centerline of the structure, that is, when the bearing line does not have any skew.

All of the figures referenced in the following sub-sections adopt the following conventions:

- Typical or common geometries are sketched using a solid black outline,
- Geometries considered unusual or exceptional are sketched using a black dashed outline,
- A few bridge geometries that are considered impractical or unbuildable are sketched using a solid light-grey outline.
- The deck plans for the eXample bridges are shaded and cross-hatched,
- The deck plans for the Existing bridges are shaded with a textured background,
- The deck plans for selected New bridges are shaded with a solid background,
- The bridge unit centerlines are indicated by a "dot-dash" line, and
- The different phases in phased construction bridges (i.e., bridges constructed as a number of separate longitudinal units) are delineated by dashed lines.

4.5.1.1 Straight Non-Skewed Base Comparison Case

The straight non-skewed base comparison tub-girder bridge is illustrated in Fig. 4.4. The analysis accuracy results for these cases served as useful indicators or benchmarks for decisions about the levels of accuracy sufficient for bridges with more complex geometries. XTCSN3 is selected as the base case for tub-girder bridges and is a published design example by NHI (2007).

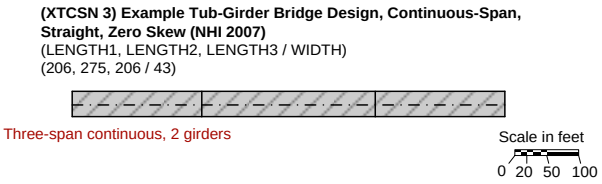

Figure 4.4. eXample Straight Non-skewed bridges used as base comparison cases, (LENGTH1, LENGTH2, LENGTH3 / WIDTH).

4.5.1.2 Simple-Span Bridges, Straight, with Skewed Supports

Figure 4.5 shows the 24 total combinations and permutations for the TSSS bridges obtained considering:

- Eight combinations of skew magnitude and pattern for the straight bridges are: {(θ_{Left}, θ_{Right}) = (15°,15°), (30°,30°), (15,0°), (15°,15°), (30°,0°), (30°,15°), (30°,-15°), (30°,-30°) },
- Three values for the length L_{as} (L_{as} = 150, 225, 300 ft), and
- One value for the deck width w (w = 30 ft)

Three of the four tub-girder bridges selected in this category have the shortest span length of 150 ft. The selection of short span cases is based on the fact that the torsional effects due to skew are likely to be larger for the shorter spans. The short span bridges selected are NTSSS1 and NTSSS2 with parallel skewed supports of 15° and 30°, and NTSSS4 with equal but opposite skew of 16°. NTSSS4 was modified to a skew angle of 16° in order to make the orientation of the supports similar to the curved and radially supported bridge NTSCR1 shown subsequently. NTSSS4 also highlights the reversed skew case discussed on Section 3.1.2 and Fig. 3.6.

In addition to the above bridges, the NTSSS10 bridge was selected to study the correlation of the span length when the skew support angle is kept constant. The NTSSS10 bridge was replaced by the existing ETSSS2 (Sylvan Bridge). The Sylvan bridge has a span length of 205 ft and was constructed in two individual longitudinal phases with deck widths of 58.7 ft and parallel skewed supports of 33.4°. Only one phase is considered for the analytical studies. Figure 4.6 show the ETSSS2 bridge phase 1 under construction and Fig. 4.7 shows the temporary external intermediate cross-frames.

4.5.1.3 Continuous-Span Bridges, Straight, with Skewed Supports

Figure 4.8 shows the combinations and permutations for the TCSS bridges for two and three continuous-span tub-girder bridges considering:

- Eight combinations of skew magnitude and pattern for the two-span straight bridges: {(θ_{Left}, θ_{Right}) = (0°, 15°,0°), (0°, 0°, 15°), (0°, 15°, 15°), (15°, 15°, 15°), (0°, 30°, 0°), (0°, 0°, 30°), (0°, 30°, 30°), (30°, 30°, 30°)},
- Two combinations of skew magnitude and pattern for the three-span straight bridges: {(θ_{Left}, θ_{Right}) = (15°, 15°, 15°), (30°, 30°, 30°)},
- Two values for the length L_{as} (L_{as} = 150, 250 ft), L_{as} = 350 ft are not shown, and

- One value for the deck width w (w = 30 ft)

None of the continuous-span tub-girder bridges shown in Figure 4.8 were selected. It was decided to focus on simple-span and continuous radially supported (curved) cases.

It was anticipated that the torsional behavior of curved and straight bridges would be very similar, due to the relatively small torsional interaction of the spans in continuous-span tub-girder bridges and the independency of the effects due to the torsional constraint given by the support system.

4.5.1.4 Simple-Span Bridges, Curved, with Radial Supports

Figure 4.9 shows the 6 combinations for the TSCR bridges obtained considering:

- Three values for the span length L_{as} (L_{as} = 150, 225, 300 ft),
- One value for the deck width w (w = 30 ft), and
- Two values of the curvature radii R for each span length.

NTSCR1 and NTSCR2 (I_T = 0.83 and 0.72) were selected to study for the effects for different curvature at the shorter span length. One bridge, NTSCR5 (I_T = 0.87), was selected to study the effect of larger span length for similar I_T.

4.5.1.5 Continuous-Span Bridges, Curved, with Radial Supports

Figure 4.10 is based on the combinations for the TCCR for three continuous-span bridges considering:

- Three values for maximum the span length L_{as} (L_{as} = 150, 250, 350 ft),
- One value for the deck width w (w = 30 ft), and
- Two values of the curvature radii R; one corresponding to the largest curvature (smallest R) without having uplift at the most critical bearing location(s) under nominal dead plus live loads and other one corresponding to the smaller curvature (larger R)

Five continuous-span tub-girder bridges were selected as this is the most common configuration for tub-girder bridges used as access ramps for highway interchanges. The extreme cases NTCCR1 and NTCCR5 were selected to provide information for sharp

curve and large span lengths while the intermediate cases were replaced by existing and example bridges (ETCCR15, XTCCR8 and ETCCR14). ETCCR15 is a six span bridge located in Milwaukee, WI and is part of the Marquette Interchange (see Figs. 4.11 and 4.12), XTCCR8 is a design example developed by Kulicki et al. (2005) and ETCCR14 is a three-span bridge instrumented and studied by Fan, (1999) located in Houston, TX.

4.5.1.6 Simple-Span Bridges, Curved, with Skewed Supports

Figure 4.13 displays the possible combinations for the TSCS (tub-girder) bridges considering:

- Twelve combinations of skew magnitude within the ranges of ±30° and two additional configurations for parallel skew previously shown in Figure 4.3,
- Two values for length, L_{as} =150 and 225 ft, L_{as} = 300 ft and their associated radius values are not shown,
- One value for the deck width w =30 ft, and
- Four values of radius of curvature R = 400, 600, 820 and 1230 ft which are selected from TSCR bridges

The selected cases (NTSCS5 and NTSCS29) have parallel supports since these configurations represent the most likely scenarios for skewed supports combining 150 and 225 ft spans and skewed supports up to 15.7°. The NTSCS5 bridge is similar to NTSSS4 shown in Figure 4.5 with reversed skew angle. NTSCS29 bridge has skew in only one support.

4.5.1.7 Continuous-Span Bridges, Curved, with Skewed Supports

Figure 4.14 shows combinations for the TCCS (tub-girder) bridges for two continuous-span bridges considering:

- Eight combinations of skew magnitude and pattern when only one support is skewed in the rage of ±30° and two additional configurations when two supports are skewed to accommodate three parallel support lines,
- Two values for the length L_{as} (L_{as} = 150, 250 ft), L_{as} = 350 ft and their associated radius values are not shown,

- Two values of the curvature radii R for each span length, and
- One value for the deck width w (w = 30 ft)

In this category several cases fall into the exceptional cases since a 30° skew for curved bridges distorts the geometry at the support lines causing undesired layouts for a narrow configuration. Two existing bridges with an intermediate skewed support were included in this category (ETCCS5a and ETCCS6) and a third case was selected NTCCS22.

NTCCS22 was selected with moderate skew of 20° at one abutment, this configuration results in two parallel support lines. ETCCS5a is located at the SR 9A and SR202 interchange in Duval Co. FL, the bridge has an intermediate skewed support of 4.8°. These two bridges bring insight about the effect of skew at an intermediate support and at the abutment.

ETCCS6 is the Magruder Blvd. bridge over I-64 in Hampton, VA shown in Fig. 4.15. The bridge is longitudinally phased with 2 tub-girders each and has a maximum skew angle of 40° at the interior phase. The bridge design does not include an external support diaphragm at the intermediate skewed support connecting the girders.

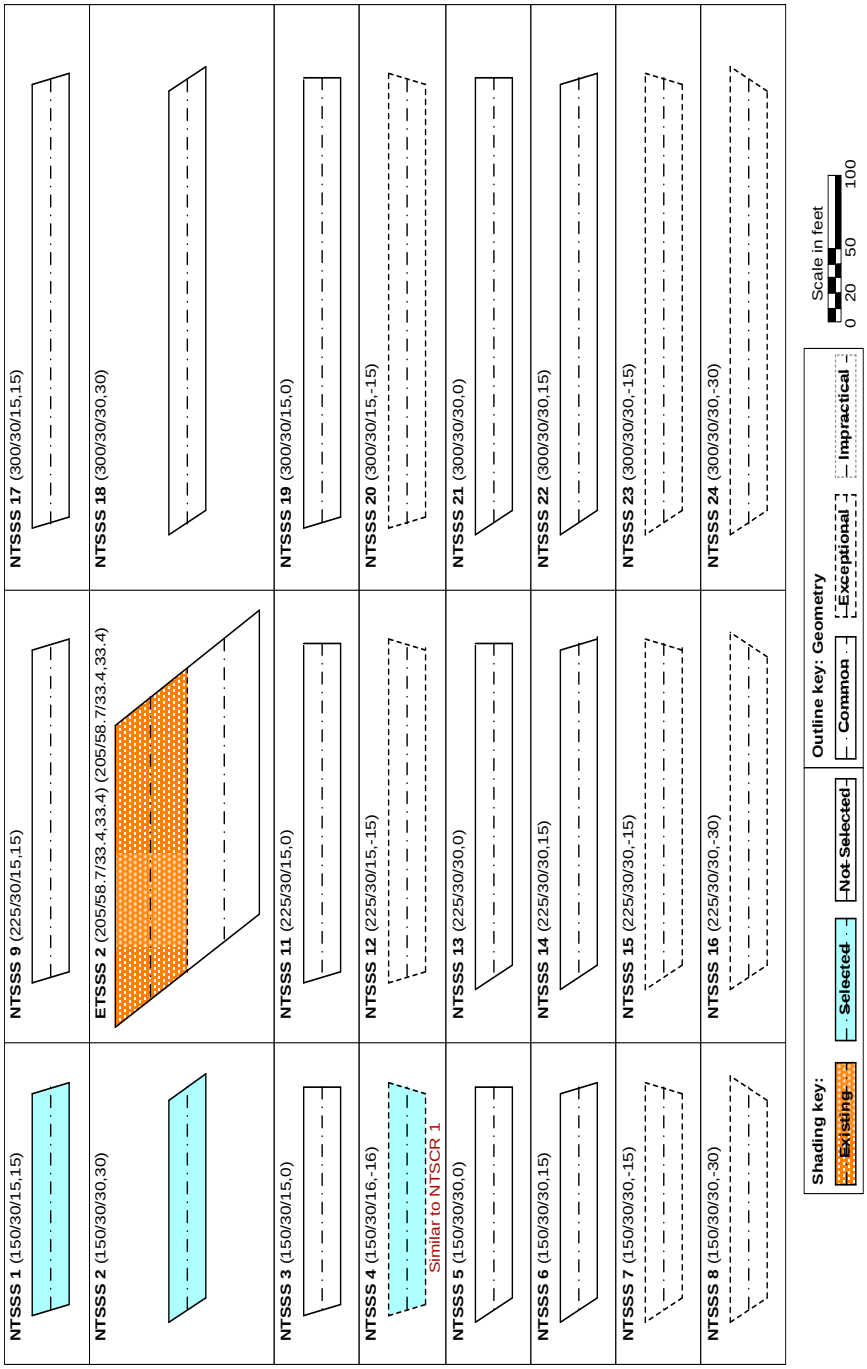

Figure 4.5. Existing and New Tub-girder bridges, Simple-span, Straight with Skewed supports, ETSSS or NTSSS (LENGTH / WIDTH / θ_{Left}, θ_{Right}).

Figure 4.6. ETSSS2, Sylvan Bridge over Sunset Hwy in Multnomah Co., OR. (Courtesy of H. Seradj, ODOT).

Figure 4.7. ETSSS2, Sylvan Bridge over Sunset Hwy in Multnomah Co., OR. (Courtesy of H. Seradj, ODOT).

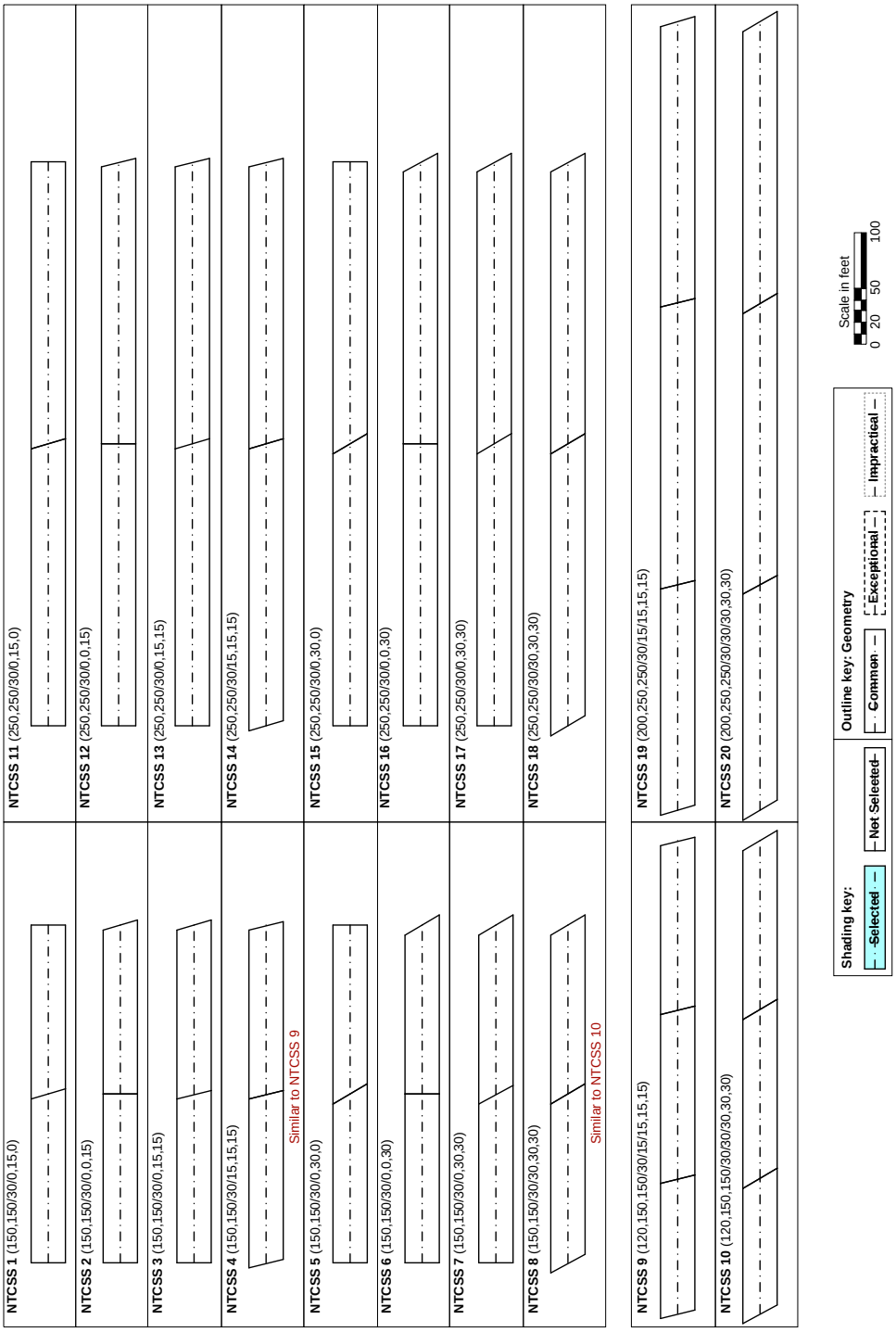

Figure 4.8. New Tub-girder bridges, Continuous-span, Straight with Skewed supports, NTCSS (LENGTH1, LENGTH2, … / WIDTH / θ_{Left}, …, θ_{Right}). The columns in the matrix for (L = 350 ft , w = 30 ft) are not shown.

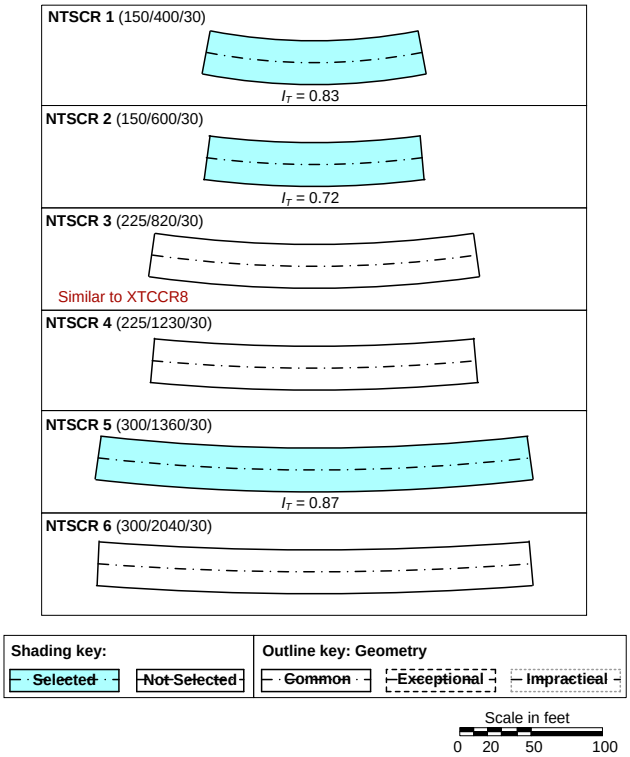

Figure 4.9. New Tub-girder bridges, Simple-span, Curved with Radial supports, NTSCR (LENGTH / RADIUS / WIDTH).

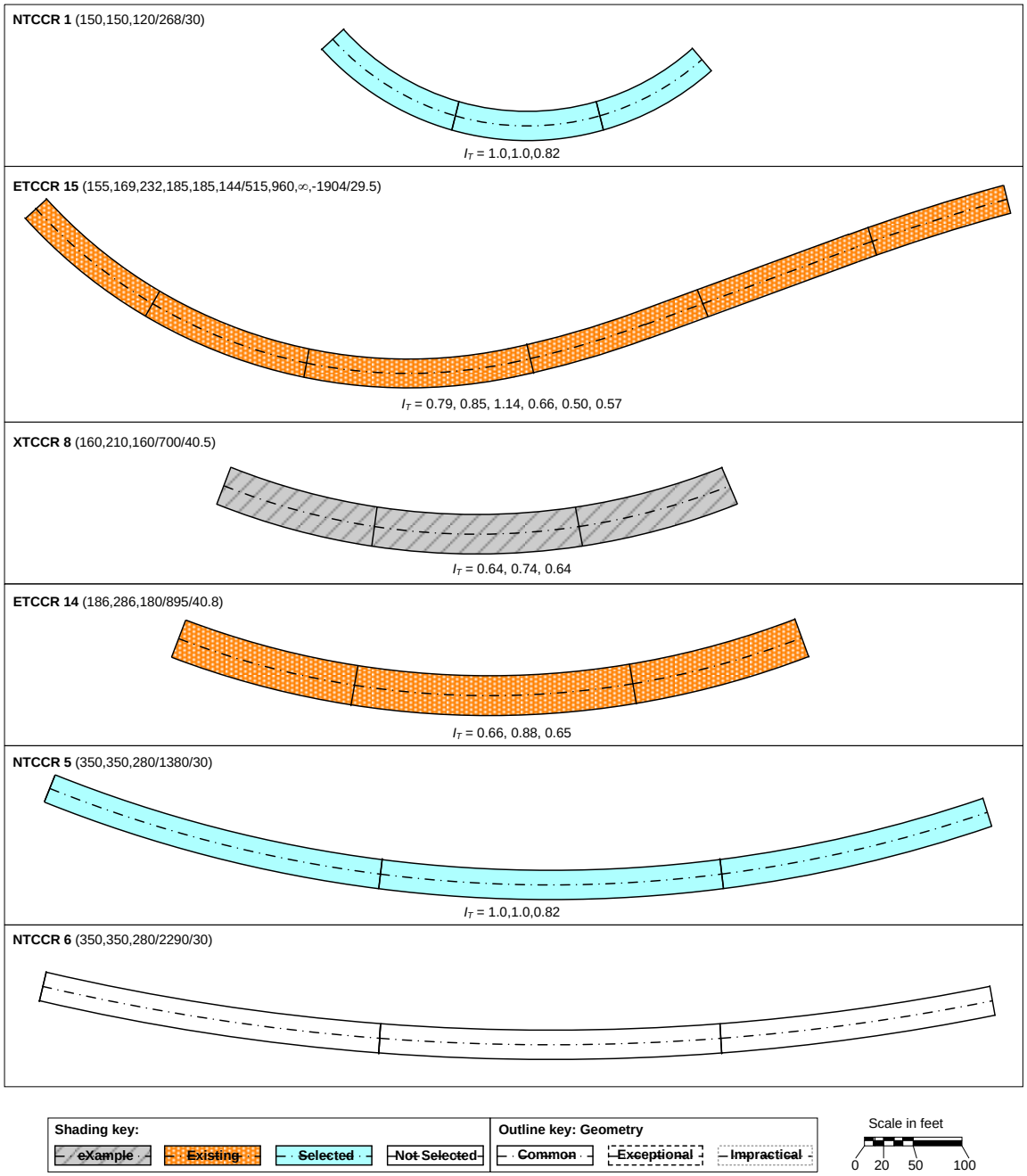

Figure 4.10. Existing, eXample and New Tub-girder bridges, Continuous-span, Curved with Radial supports, ETCCR, XTCCR or NTCCR (LENGTH1, LENGTH2, … / RADIUS / WIDTH).

Figure 4.11. ETTCR 15, Unit B-40-1122 of the Marquette Interchange, Milwaukee, WI. (Courtesy of T. Shkurti, HNTB).

Figure 4.12. ETTCR 15, Unit B-40-1122 of the Marquette Interchange, Milwaukee, WI. (Courtesy of T. Shkurti, HNTB).

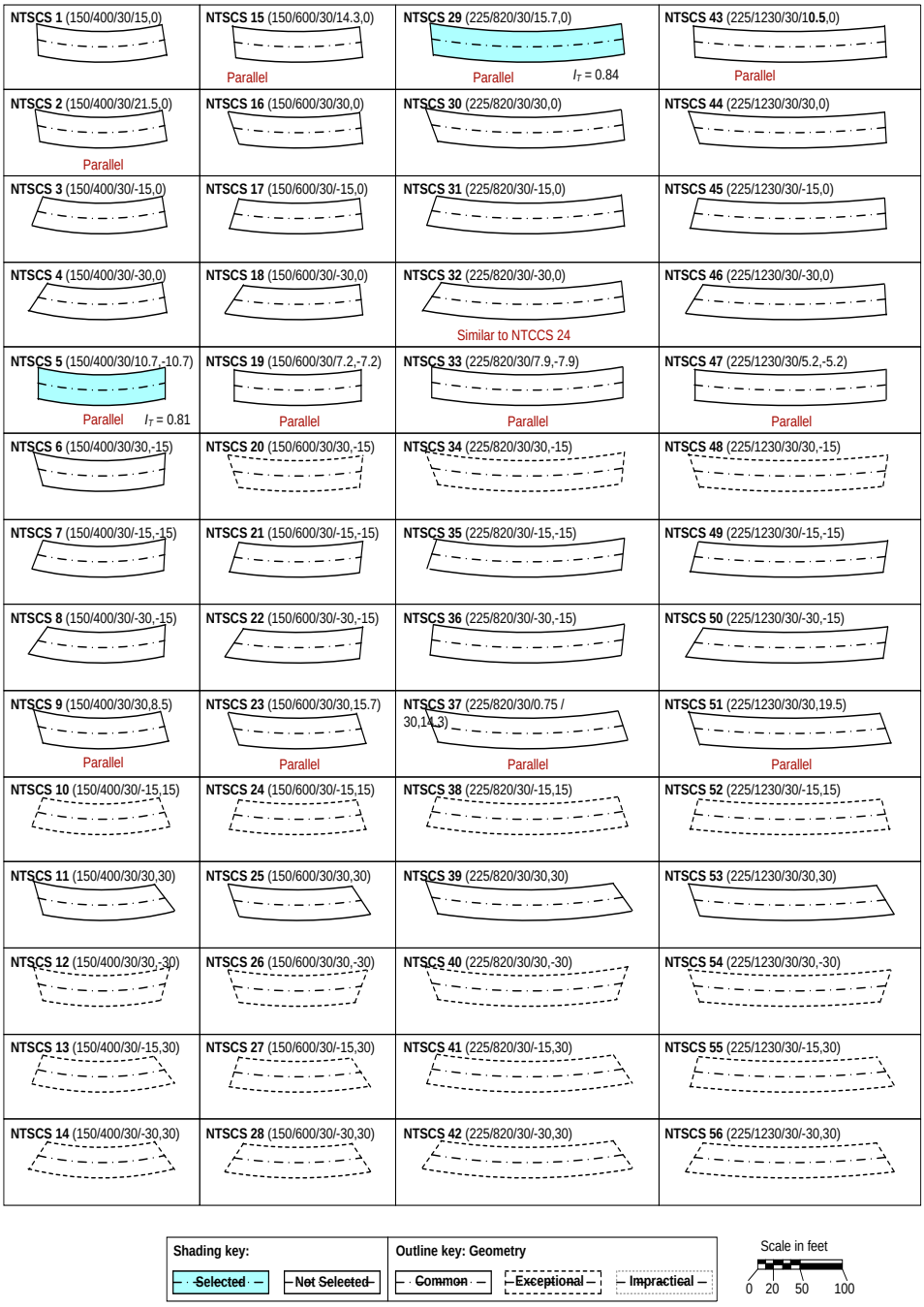

Figure 4.13. New Tub-girder bridges, Simple-span, Curved with Skewed supports, NTSCS (LENGTH / RADIUS / WIDTH / θ_{Left}, θ_{Right}). The columns in the matrix for (L = 350 ft, w = 30 ft, R = 1390 and 2085 ft) are not shown.

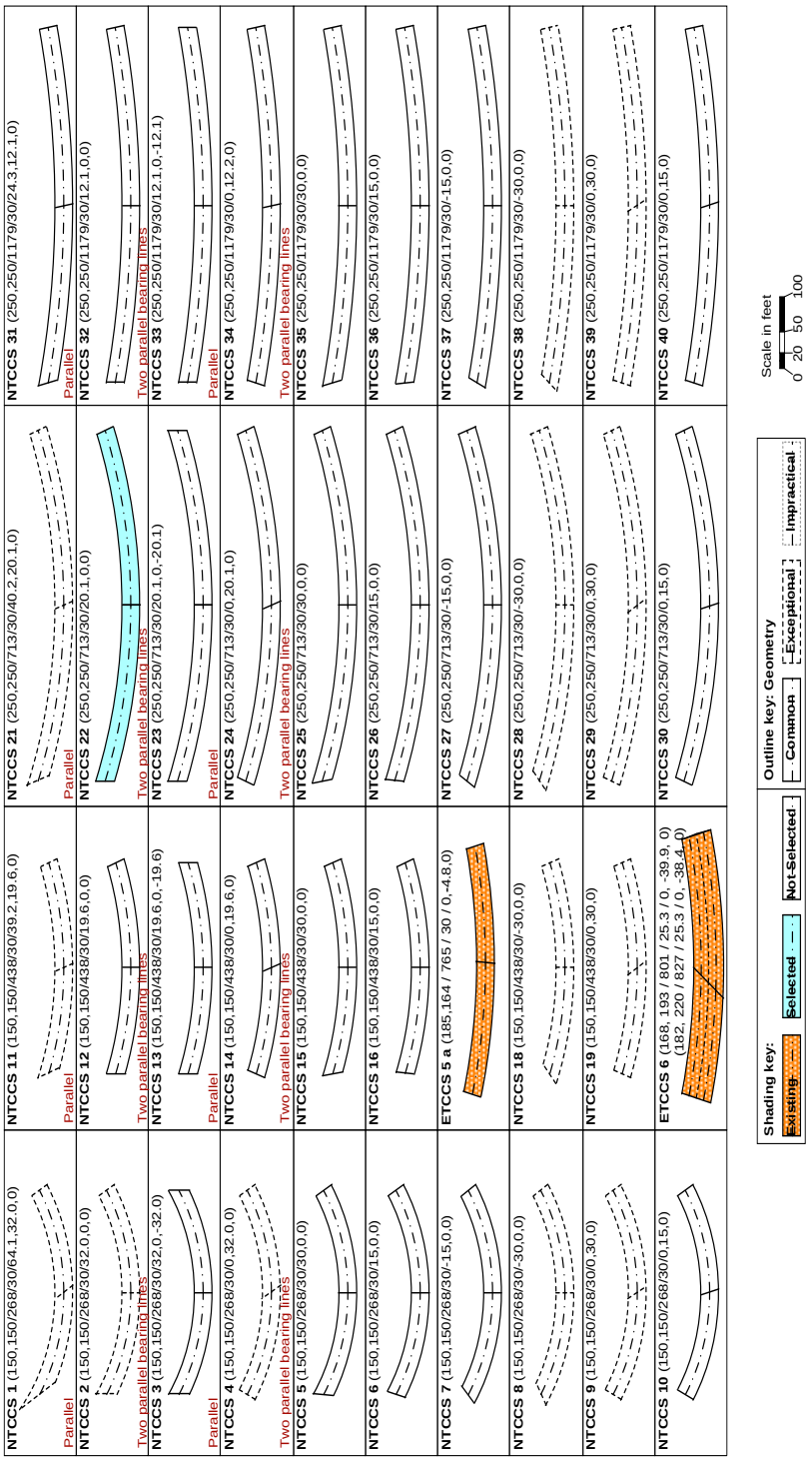

Figure 4.14. Existing and New Tub-girder bridges, Continuous-span, Curved with Skewed supports, ETCCS or NTCCS (LENGTH1, LENGTH2, … / RADIUS / WIDTH / θ_{Left}, …, θ_{Right}). The columns in the matrix for (*L* = 350 ft , *w* = 30 ft, *R* = 1380 and 2291 ft) are not shown.

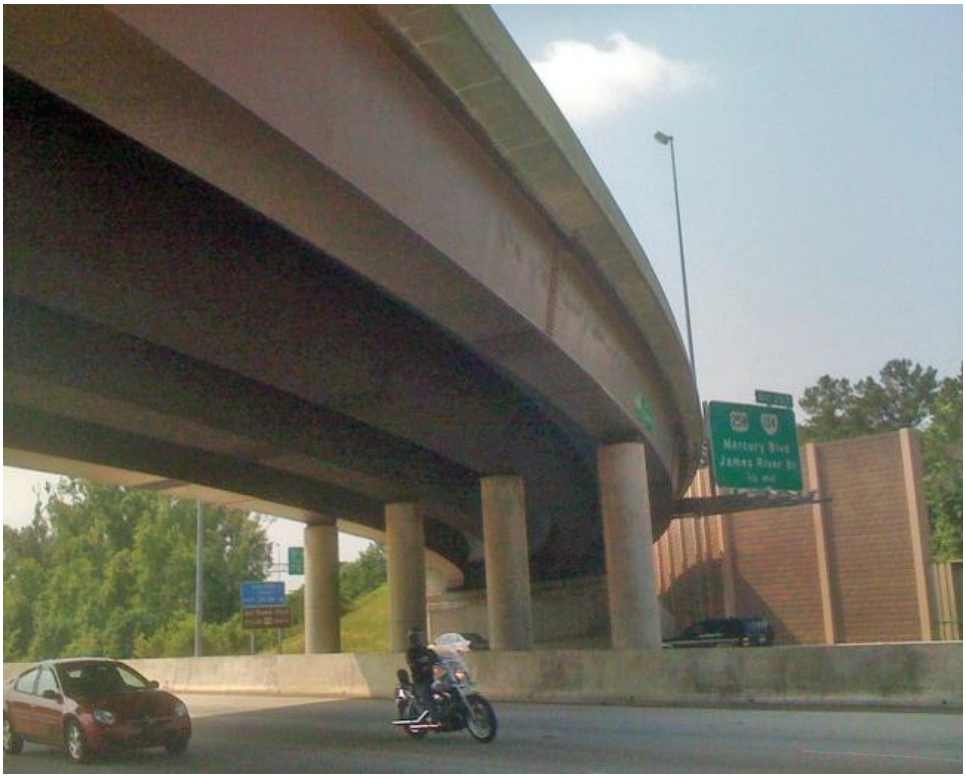

Figure 4.15. ETCCS6, Magruder Blvd. bridge over I-64 in Hampton, VA. (Courtesy of D. White).

4.5.1.8 Tub-Girder Skew Sensitivity Studies

Skew sensitivity studies were performed for six of the above tub-girder bridges to assess the impact of skew on the simplified torsional moment estimates. No changes to the tub-girder bridge original designs were made but minor modifications were made to accommodate the changes on the framing plan. The bridges and their variations are NTSSS2 (30°, 15° and 0°), NTSSS4 (16°, 10° and 0°), NTSCS5 (10.7° and 0°), NTSCS29 (15.7° and 0°), ETCCS5a (-4.8°, 0°, -10° and 10°) and NTCCS22 (20.1° and 0°). The first angle in the above parentheses corresponds to the original design. The bridge layouts of the sensitivity studies are shown in Figure 4.16.

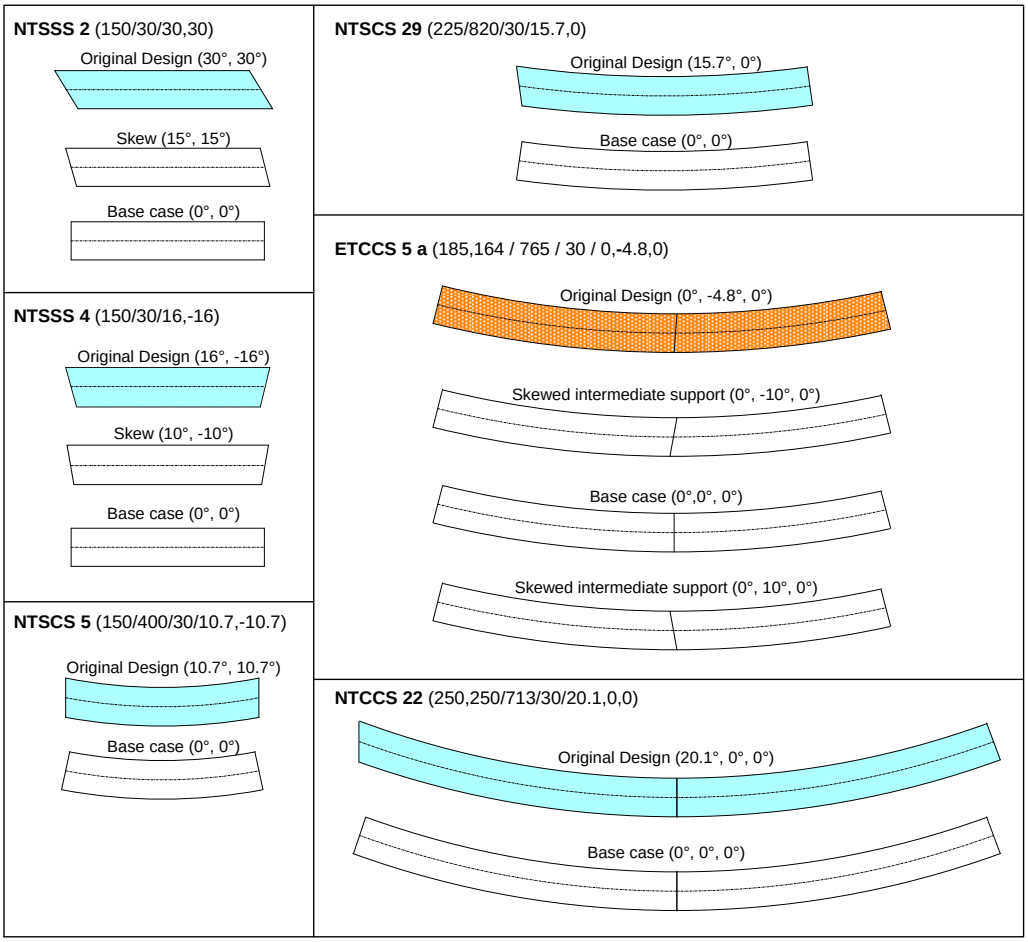

Figure 4.16. Tub-Girder sensitivity studies bridges.

4.5.2 Selected Analytical Study Bridges

Table 4.2 provides an overall summary of the number of New, Existing and eXample bridges for each of the major groups of bridges. Twenty-eight tub-girder bridges are analyzed of which, 5 are existing bridges, 2 are example bridges, 11 base parametric study designs and 10 sensitivity study bridges. Appendix C provides summaries of the most important results for each of the bridges.

Table 4.2. Overall summary of New, Existing and eXample tub-girder bridges.

Description		Cases
eXample Tub-girder, Continuous-span, Straight, No skew (Base comparison case)		1
TSSS	(ETSSS) Existing, Tub-girder, Simple-span, Straight, Skewed supports	1
	(XTSSS) eXample, Tub-girder, Simple-span, Straight, Skewed supports	0
	(NTSSS) New, Tub-girder, Simple-span, Straight, Skewed supports	3
	Total: TSSS	4
TCSS	(ETCSS) Existing, Tub-girder, Continuous-span, Straight, Skewed supports	0
	(XTCSS) eXample, Tub-girder, Continuous-span, Straight, Skewed supports	0
	(NTCSS) New, Tub-girder, Continuous-span, Straight, Skewed supports	0
	Total: TCSS	0
TSCR	(ETSCR) Existing, Tub-girder Simple-span, Curved, Radial supports	0
	(XTSCR) eXample, Tub-girder Simple-span, Curved, Radial supports	0
	(NTSCR) New, Tub-girder Simple-span, Curved, Radial supports	3
	Total: TSCR	3
TCCR	(ETCCR) Existing, Tub-girder, Continuous-span, Curved, Radial supports	2
	(XTCCR) eXample, Tub-girder, Continuous-span, Curved, Radial supports	1
	(NTCCR) New, Tub-girder, Continuous-span, Curved Radial supports	2
	Total: TCCR	5
TSCS	(ETSCS) Existing, Tub-girder, Simple-span, Curved, Skewed supports	0
	(XTSCS) eXample, Tub-girder, Simple-span, Curved, Skewed supports	0
	(NTSCS) New, Tub-girder, Simple-span, Curved, Skewed supports	2
	Total: TSCS	2
TCCS	(ETCCS) Existing, Tub-girder, Continuous-span, Curved, Skewed supports	2
	(XTCCS) eXample, Tub-girder, Continuous-span, Curved, Skewed supports	0
	(NTCCS) New, Tub-girder, Continuous-span, Curved, Skewed supports	1
	Total: TCCS	3
Total: Existing Tub-girder bridges		5
Total: eXample Tub-girder bridges		2
Total: New Tub-girder bridges		11
Total: Additional skew sensitivity studies		10
Total: Tub-girder bridges		28

CHAPTER V.

EVALUATION OF SIMPLIFIED ANALYSIS METHODS

5.1 Modeling Characteristics

Analytical studies were conducted for a wide range bridges introduced in Chapter 4 to determine the ability of the approximate 1D line-girder and 2D-grid methods of analysis to capture the behavior predicted by refined 3D FEA models.

The 1D line-girder analyses were performed using the STLBRIDGE package (Bridgesoft, Inc., 2010) along with spreadsheet calculations to include the effects of curvature using the M/R Method (Tung and Fountain, 1970) and the additional effects of skew via the developments presented in Chapter 3.

The 2D-grid models were implemented using the LARSA 4D (LARSA, 2010) and MDX (MDX Software, 2011) software packages. The 2D-grid analysis from LARSA and MDX include the curvature and skew in the grid composed of the girders, external intermediate cross-frames and diaphragms modeled at their centerlines and located in a common horizontal plane. The external intermediate cross-frames and diaphragm properties are estimated considering their bending and shear flexibility. The length of external intermediate cross-frames and diaphragm that corresponds to the region inside the girders is modeled using the same cross-section properties as the external diaphragm.

For the LARSA software and 1D line-girder solutions, torsional properties were estimated by the Equivalent Plate Method (Kollbrunner and Basler, 1969) and the bracing forces were calculated using the component force equations discussed in Chapter 2 and summarized in Section 3.6. The MDX software requires the input of the bracing components characteristics and calculates the equivalent torsional properties and bracing forces internally. The MDX software uses a relatively coarser grid to represent skewed bridges using one element between each of the top flange lateral bracing panel zones. In comparison, the LARSA models were constructed using four elements to represent the

same length. The 1D line-girder analysis relies in a constant discretization level per span of ten elements.

The sawtooth interactive force effects discussed in Section 3.5 are not included for calculation of the major-axis bending stresses and the errors are calculated for the average bending stress. The use of the average major-axis bending stresses and the modeling of the diaphragms neglecting the rigid zones within the cross-section of the girders, reflect current analysis and modeling standards of care in professional bridge design practice. The quantitative errors shown next reflect this practice and serve as motivation for the application of the analysis improvements.

5.2 Quantitative Errors

An assessment of the simplified analysis methods is obtained by identifying error measures that compare the approximate solutions to the 3D geometric nonlinear elastic FEA benchmarks. An error function is defined as the absolute difference between the benchmark 3D FEA and the approximate method solutions (see Fig 5.1). The error is calculated at each of the sampling points *i* of the approximate solution as:

$$e_i = \left| R_{FEA} - R_{APPROX} \right| \tag{5.1}$$

where R_{FEA} and R_{APPROX} are the responses being evaluated obtained by the benchmark 3D FEA and approximate methods. Linear interpolation between sampling points of the 3D FEA are calculated to estimate the approximate solution sampling point *i*.

The error function is used to calculate the normalized mean error. This index provides an overall measure of the performance of the approximate models and is calculated as:

$$\mu_e = \frac{1}{N \cdot R_{FEA,\max}} \sum_{i=1}^{N} e_i \tag{5.2}$$

where μ_e is the normalized mean error, N is the total number of sampling points along the girder length used in the approximate model, $R_{FEA,max}$ is the maximum response obtained from the 3D FEA, and e_i is the error function evaluated at point *i*. The mean error is

normalized with respect to the maximum value of the response obtained from the 3D FEA to avoid a comparison of "small numbers to small numbers." By normalizing by $R_{FEA,max}$, the influence of the load magnitude is removed from the analysis results.

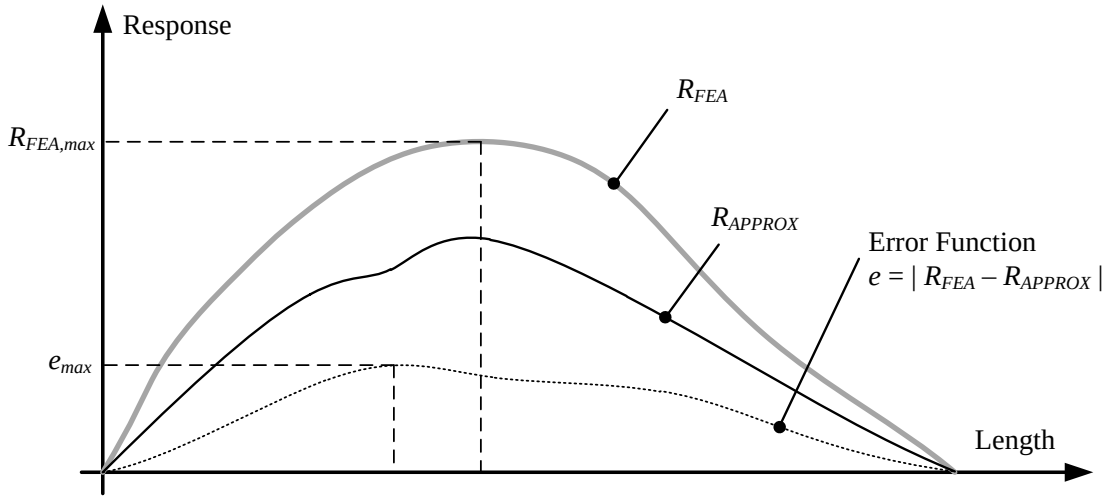

Figure 5.1. Schematic representation of the Error Function .

This procedure is applied to evaluate the normalized mean errors in the major-axis bending stresses, vertical displacements and girder torsional moments obtained for the 18 tub-girder bridges.

For the qualitative assessment of the top flange lateral bracing (TFLB) and internal cross-frame (CF) axial forces, the signed errors for the maximum response are reported. Traditionally, the dimensions of the bracing elements are kept constant along the length of the bridge since this minimizes the detailing efforts and reduces the possibility of construction errors. In consequence, the top flange lateral bracing and cross-frame components are designed for the maximum axial forces found throughout the length of the bridge. Due to this practice, the axial assessment of the analysis methods is performed by reporting the signed error for the maximum response for each of these components. The sign on the error for conservative estimates is positive and unconservative is negative. The error reporting for these components are grouped for the (1) top flange lateral bracing diagonals, (2) internal cross-frame diagonals, and (3) the combined top flange lateral bracing struts and internal cross-frame top chords.

The bridges are divided into three different groups based on their geometry. The first group corresponds to curved radially-supported bridges (labeled as "C"), the second group to straight and skewed structures (labeled as "S") and the third group contains the curved and skewed bridges studied in the project (labeled as "C & S").

Table 5.1 compares the Program P1 (LARSA) and P2 (MDX) 2D-grid and 1D analysis major-axis bending stress and vertical displacement results to the predictions obtained from geometric nonlinear elastic 3D FEA. In the table, f_b is the major-axis bending stress, Δ_z is the vertical displacement and T is the torsional moment. A mean error value is calculated for each response on each girder of the bridges. The values reported by Table 5.1 are the largest mean errors determined by inspecting the values obtained for each girder in a given bridge. The differences between the linear and geometric nonlinear 3D FEA are negligible and therefore not shown. The torsional moments results were not obtained from Program P1 (MDX) and therefore the accuracy of the results are not evaluated for this case. The mean errors for the major-axis bending stresses, vertical displacements and girder torsional moments are always positive.

Similarly, Table 5.2 compares maximum axial force results 2D-grid and 1D analysis to the predictions obtained from geometric nonlinear elastic 3D FEA. In the table, the signed errors for the maximum response are reported for the top flange lateral bracing diagonals (TFLB Diag.), internal cross-frame diagonals (CF Diag.), and the combined top flange lateral bracing struts and internal cross-frame top chords (TFLB & Top CF Strut). The errors for the bracing forces are signed: conservative estimates are positive and unconservative are negative.

An additional group is shown for the bracing forces that included the bridges using Pratt TFLB. The simplified analysis methods experience additional accuracy problems for these bridges.

Table 5.1. Tub-girder bridge percent normalized mean errors compared to geometric nonlinear elastic 3D FEA for major-axis bending stresses (f_b), vertical displacements (Δ_z) and torsional moment (T).

Group	Bridge Name	2D-Grid – P1			2D-Grid – P2		1D		
		f_b μ_e	Δ_z μ_e	T μ_e	f_b μ_e	Δ_z μ_e	f_b μ_e	Δ_z μ_e	T μ_e
C	NTSCR1	7	5	5	12	13	10	6	7
	NTSCR2	5	3	6	8	9	8	4	11
	NTSCR5	8	6	8	19	10	12	8	11
	NTCCR1	5	2	6	8	6	7	4	14
	ETCCR15	5	2	20	6	3	7	3	26
	XTCCR8	5	3	23	7	3	8	12	27
	ETCCR14	6	2	12	36	11	17	8	13
	NTCCR5	6	3	3	8	4	6	2	5
S	XTCSN3	3	2	19	5	5	6	6	23
	NTSSS1	4	5	31	11	7	5	1	18
	NTSSS4	4	1	30	6	5	7	3	53
	NTSSS2	8	7	27	19	13	11	5	10
	ETSSS2	5	2	28	10	2	9	7	30
C & S	NTSCS5	7	6	3	21	13	12	7	14
	NTSCS29	7	7	3	15	11	9	4	9
	ETCCS5a	10	6	22	5	5	6	5	29
	ETCCS6	6	2	43	22	3	7	2	33
	NTCCS22	5	4	3	8	8	6	3	11

Table 5.2. Tub-girder bridge percent errors for maximum values of responses compared to geometric nonlinear elastic 3D FEA for the bracing system forces.

Group	Bridge Name	2D-P1			2D-P2			1D		
		TFLB Diag.	CF Diag.	TFLB & Top CF Strut	TFLB Diag.	CF Diag.	TFLB & Top CF Strut	TFLB Diag.	CF Diag.	TFLB & Top CF Strut
C	NTSCR1	8	30	24	55	80	-26	33	19	-1
	NTSCR2	7	27	25	58	74	-7	33	16	5
	NTSCR5	18	36	37	61	91	75	57	17	1
	NTCCR1	12	73	21	54	87	-42	34	90	-2
	XTCCR8	1	200	171	97	265	-18	27	264	54
	ETCCR14	0	241	93	148	51	-80	140	23	48
	NTCCR5	21	71	66	49	99	10	49	60	21
S	NTSSS1	-4	NA[a]	12	165	NA[a]	17	15	NA[a]	6
	NTSSS4	23	NA[a]	13	67	NA[a]	33	-16	NA[a]	6
	NTSSS2	-15	NA[a]	18	119	NA[a]	4	22	NA[a]	15
	ETSSS2	-55	NA[a]	-18	9	NA[a]	-37	15	NA[a]	-16
C & S	NTSCS5	17	24	17	65	75	-30	40	7	-15
	NTSCS29	5	29	35	84	83	-11	14	16	-4
	ETCCS6	12	52	4	46	110	20	51	-24	9
	NTCCS22	8	73	49	97	141	3	25	107	3
Pratt TFLB	ETCCR15	0	NA[b]	-3	-41	NA[b]	-75	56	NA[b]	-19
	XTCSN3	40	NA[a]	49	-74	NA[a]	-84	48	NA[a]	58
	ETCCS5a	0	-12	-3	26	123	-40	1	4	22

[a] The component force equations summarized in Section 3.6 report negligible forces on the internal CF forces in straight tub-girders.

[b] ETCCR15 uses internal solid plate diaphragms rather than internal CF.

5.2.1 Vertical Displacements, Major-Axis Bending Stresses and Torsional Moments Accuracy Discussion

Upon inspection of the results in Table 5.1, the following important trends can be observed.

2D-Grid Solutions

Several observations can be made regarding the 2D-grid solutions from Table 5.1 for the major-axis bending stresses, vertical displacements and torsional moments:

- The 2D-grid solutions from Program 1 (P1) give better estimates than Program 2 (P2) for the major-axis bending stresses and vertical displacements in all the cases in Table 5.1 with the exception of ETCCS5a. The ETCCS5a bridge uses a Pratt TFLB which has shown low accuracy due to the internal behavior of the bracing. There is not enough information to confirm that Program 2 has better accuracy for bridges using Pratt TFLB systems.
- The major-axis bending stresses and vertical displacements do not exhibit clear differences on the errors for the different groups "C", "S" or "C & S". This means that there is no clear effect of the curvature or skew on the accuracy of the major-axis bending stresses or vertical displacements.
- Only the torsional moments form Program 1 were collected. The errors are in general larger for the "S" bridges. However, the groups "C" and "C & S" also report bridges where the errors are comparable to those on group "S".
- The torsional moment estimates for bridges ETCCR15 and XTCCR8 exhibit the largest errors in the "C" group. The ETCCR15 has an irregular TFLB layout using Pratt trusses that reverse the orientation of the diagonals at arbitrary regions of the bridge. These characteristics are believed to induce a behavior difficult to estimate. There is no clear reason why the solutions differed for bridge XTCCR8.
- For the "C & S" bridges, the torsional results are reasonably accurate for three of the bridges. The bridge ETCCS5a again reports large errors due to the Pratt TFLB system. The bridge ETCCS6 exhibits very large errors and the reason for this behavior is the lack of diaphragm at the intermediate pier.
- The torsional moment estimates for the "S" group exhibit errors larger than group "C & S". The "C & S" group bridges have smaller errors even when the independent effects of skew are expected to be comparable to those on the "S" group. However, the effects of curvature are large enough to reduce the relative differences. The reason for the reduced accuracy in the "S" bridges is explained below.

The Program 2 models include the skewed geometry in the grid and different factors affect the accuracy on the torsional moment estimations. An important reason for

the lack of accuracy is the diaphragm modeling in the grid systems. The 2D-grid approach models the diaphragms considering their bending and shear flexibility. However, the diaphragms behave more as rigid elements due to the small aspect ratio and the stiffener systems.

In addition, the internal bracing forces also influence the torsional moment accuracy. The bridges that are expected to be subjected to constant torsional moments parabolic-like distribution of the internal torsional moment. These are the result of additional internal torsional moments with a parabolic-like distribution. This is evidence that these additional internal moments are caused by the TFLB strut lateral forces which follow a similar distribution. The shape also suggests correlation with the girder major-axis bending moment or the strut force fraction originated from bending.

Other errors are attributed to the discretization level of the bridge model, however, these errors are considered minor compared to the effects discussed above.

1D Line-Girder Solutions

The 1D line-girder solutions shown in Table 5.1 exhibit the following characteristics:

- The vertical displacements and major-axis bending stress solutions are reasonably good for all the bridges and comparable to the 2D-grid results.
- For the "S" and "C & S" bridges, the 1D line-girder solutions for vertical displacements and major-axis bending stresses exhibit better accuracy than the conventional 2D-grid from Program 1 solutions in the majority of the cases, however, there is no clear reason why the solutions are better for these cases.
- The torsional moment estimates report accuracy with errors equal or less than 14 %. The torsional moment estimates for the ETCCR15, XTCCR8, ETCCS5a and ETCCS6 bridges exhibit larger errors for the same reasons discussed previously for 2D-grid solutions accuracy.
- As with 2D-gird solutions, the torsional moment estimations for the "S" group exhibit errors larger than group "C & S". The same internal bracing behavior is expected to cause errors as explained previously for 2D-grid solutions, however,

and additional reason for the reduced accuracy in the "S" bridges is explained below.

Additional errors are attributed to the effects of the external intermediate cross-frames as the 1D method is unable to capture any information about the transverse load paths in the bridge system. The external intermediate cross-frames transfer forces between girders that cause additional torsional moment to the girders. When skewed external intermediate cross-frames are used, the cross-frames connect at different relative girder lengths resulting on an increment of the transferred force between girders as the relative vertical displacements that the cross-frames control are expected to be larger. The effects of external intermediate cross-frames are again more noticeable in straight bridges as the effect in curved bridges is relatively small when compared to the overall combined skew and curvature torques.

5.2.2 Bracing Forces Accuracy Discussion

2D Grid Solutions

As with the vertical displacements and major-axis bending stresses, the 2D-grid solutions from Program 1 (P1) give better estimates than Program 2 (P2) for the top flange lateral bracing diagonals forces (TFLB Diag.), internal cross-frame diagonal forces (CF Diag.) and the combined top flange lateral bracing strut and internal cross-frame top strut (TFLB & Top CF Strut) for the majority of the cases in Table 5.2. The larger errors in Program P2 are attributed to the coarser discretization used in Program 2 and the internal process for the evaluation of the bracing forces. As the internal process is proprietary of the software there is no information to confirm the specific differences between Programs 1 and 2. Therefore the results from Program 1, which explicitly use the component force equations, are discussed.

- The TFLB Diag. forces directly depend on the major-axis bending and torsional moments and, in consequence, the errors are large for the "S" group where the torsional responses were estimated less accurately. For the "C" and "C & S" the accuracy is improved and the estimates are conservative. This means that the accuracy is largely affected by the accuracy of the torsional moment estimations.

- The CF Diag. force estimation exhibit large conservative errors for the "C" and "C & S" groups. The CF Diag. forces for the "S" group are negligible and, therefore, the errors not addressed. The CF Diag. forces are assumed to depend only on the distortional components of the applied loads. The largest distortional contribution is the *M*/*Rh* distributed lateral load which is characterized by the major-axis bending moments. As the major-axis bending stresses are captured accurately for the Program P2 it is concluded that the conservative estimates are caused by the assumption that considers that the internal cross-frames are the only elements resisting the distortional loads. In consequence, it is assumed that other bracing elements contribute to resisting the distortional loads.
- The combined TFLB & Top CF Strut. force estimations exhibit large conservative errors for the majority of the bridges with the exception of the bridges using Pratt TFLB. These bracing forces depend on a combination of the major-axis bending moment and torsional moments but in contrast to the TFLB Diag. force, which also depends on the same factors. The "S" group exhibits smaller errors which are believed to be caused by the reduced accuracy of the torsional moment estimates.
- Additional localized errors are attributed to the interaction of the external intermediate cross-frames and the internal cross-frames. At the locations that align to the external intermediate cross-frames there is transverse load path that the component force equations do not consider. This effect causes force increases in the adjacent bracing components.

The bracing estimates exhibit larger errors for the majority of the cases, some of the errors are reported as conservative. For bridges using Pratt TFLB layouts, the component force equations exhibit a poorer performance caused by the interaction of the internal components of the bracing. In all other cases, the conservatism level is reduced as the torsional moment estimations exhibit larger errors.

1D Line-Girder Solutions

The 1D line-girder solution for the bracing components in Table 5.2 exhibit larger errors than the corresponding responses by Program 1 for the 2D-gird solution. The errors are consequence of the previously discussed effects. Additional errors are caused by the

discretization level used in the 1D line-girder implementation which results on the bracing component forces not being calculated at the actual positions but at the closest tenth point.

The following section synthesizes the analysis errors to evaluate the accuracy of the simplified analysis methods using a grading scheme.

5.3 Synthesis of Errors in Major-Axis Bending Stresses, Vertical Displacements, Torsional Moments and Top Flange Lateral Bracing Forces

An arbitrary grading scheme is used to synthesize the analytical errors depending on the type of response and the consequences of the error as different ranges of error can be acceptable for the various calculations on different jobs. The first rank is selected based on the fact that most engineers would agree that analysis results that do not deviate more than 6 % from a highly refined benchmark solution are indeed highly accurate. Similarly, analysis results where the errors are larger than 30 % might be considered as highly unreliable. The specific selected error ranges are assigned letter grades based on the following criteria:

A: $\mu_e \leq$ 6 %: excellent accuracy of the analysis predictions.

B: 6 % < $\mu_e \leq$ 12 %: the analysis predictions are in "reasonable agreement" with the benchmark analysis results.

C: 12 % < $\mu_e \leq$ 20 %: the analysis predictions start to deviate "significantly" from the benchmark analysis results.

D: 20 % < $\mu_e \leq$ 30 %: the analysis predictions are poor, but may be considered acceptable in some cases

F: $\mu_e >$ 30 %: the analysis predictions are considered unreliable and inadequate for design.

Table 5.3 shows the number of bridges within specific ranges of the normalized mean errors for the major-axis bending stresses and the vertical displacements from Table 5.1. Both of the 2D-grid programs P1 and P2 are considered, as well as the 1D analysis results.

Table 5.3. Number of tub-girder bridges within specified error ranges for major-axis bending stress and vertical displacement for each of the types of bridges considered.

Type of Bridge	Number of Bridges	Error Range	Number of Bridges within Error Range							
			Major-Axis Bending Stress			Vertical Displacement			Girder Torques	
			2D-P1	2D-P2	1D	2D-P1	2D-P2	1D	2D-P1	1D
C	8	A: ≤ 6%	**6**	1	1	**8**	**4**	**5**	**4**	1
		B: 7-12%	**2**	**5**	**6**	0	3	**3**	2	**3**
		C: 13-20%	0	1	**1**	0	**1**	0	1	2
		D: 21-30%	0	0	0	0	0	0	**1**	**2**
		F: >30%	0	**1**	0	0	0	0	0	0
S	5	A: ≤ 6%	**4**	2	2	**4**	**3**	**4**	0	0
		B: 7-12%	**1**	**2**	**3**	**1**	1	**1**	0	1
		C: 13-20%	0	**1**	0	0	**1**	0	1	1
		D: 21-30%	0	0	0	0	0	0	**3**	**2**
		F: >30%	0	0	0	0	0	0	**1**	**1**
C & S	5	A: ≤ 6%	2	1	2	**4**	2	**4**	**3**	0
		B: 7-12%	**3**	1	**3**	**1**	**2**	**1**	0	**2**
		C: 13-20%	0	1	0	0	**1**	0	0	1
		D: 21-30%	0	**2**	0	0	0	0	1	1
		F: >30%	0	0	0	0	0	0	**1**	**1**

Table 5.4 shows an analogous categorization for the bracing forces errors in Table 5.2. In this case, the grading scale is signed. This means that a positive grading corresponds to a conservative estimates and unconservative otherwise.

Table 5.4. Number of tub-girder bridges within specified error ranges for the maximum values of the bracing system forces for each of the types of bridges considered.

Type of Bridge	Number of Bridges	Error Range	Number of Bridges within Error Range								
			TFLB Diag.			TFLB & Top CF Strut			CF Diag.		
			2D-P1	2D-P2	1D	2D-P1	2D-P2	1D	2D-P1	2D-P2	1D
C	7	+F: >30%	0	**7**	**6**	**4**	**1**	**2**	**5**	**7**	**3**
		+D: 21-30%	**1**	0	1	3	0	1	2	0	1
		+C: 13-20%	1	0	0	0	0	0	0	0	3
		+B: 7-12%	**3**	0	0	0	1	0	0	0	0
		+A: ≤ 6%	2	0	0	0	0	2	0	0	0
		-A: ≤ 6%	0	0	0	0	0	**2**	0	0	0
		-B: 7-12%	0	0	0	0	1	0	0	0	0
		-C: 13-20%	0	0	0	0	1	0	0	0	0
		-D: 21-30%	0	0	0	0	1	0	0	0	0
		-F: >30%	0	0	0	0	**2**	0	0	0	0
S	4	+F: >30%	0	**3**	0	0	**1**	0			
		+D: 21-30%	**1**	0	**1**	0	0	0			
		+C: 13-20%	0	0	**2**	**2**	1	**1**			
		+B: 7-12%	0	1	0	1	0	0			
		+A: ≤ 6%	0	0	0	0	1	**2**			
		-A: ≤ 6%	1	0	0	0	0	0			
		-B: 7-12%	0	0	0	0	0	0			
		-C: 13-20%	1	0	**1**	**1**	0	**1**			
		-D: 21-30%	0	0	0	0	0	0			
		-F: >30%	**1**	0	0	0	**1**	0			
C & S	4	+F: >30%	0	**4**	**2**	**2**	0	0	**2**	**4**	**1**
		+D: 21-30%	0	0	1	0	0	0	2	0	0
		+C: 13-20%	**1**	0	1	1	**1**	0	0	0	1
		+B: 7-12%	**2**	0	0	0	0	**1**	0	0	1
		+A: ≤ 6%	1	0	0	1	1	1	0	0	0
		-A: ≤ 6%	0	0	0	0	0	1	0	0	0
		-B: 7-12%	0	0	0	0	1	0	0	0	0
		-C: 13-20%	0	0	0	0	0	1	0	0	0
		-D: 21-30%	0	0	0	0	**1**	0	0	0	**1**
		-F: >30%	0	0	0	0	0	0	0	0	0
Pratt TFLB	3	+F: >30%	**1**	0	**2**	**1**	0	**1**			
		+D: 21-30%	0	**1**	0	0	0	1			
		+C: 13-20%	0	0	0	0	0	0			
		+B: 7-12%	0	0	0	0	0	0			
		+A: ≤ 6%	**2**	0	1	0	0	0			
		-A: ≤ 6%	0	0	0	**2**	0	0			
		-B: 7-12%	0	0	0	0	0	0			
		-C: 13-20%	0	0	0	0	0	**1**			
		-D: 21-30%	0	0	0	0	0	0			
		-F: >30%	0	**2**	0	0	**3**	0			

5.4 Generalized Analysis Scores

For each of the bridge groups and analysis methods in Tables 5.3 and 5.4 rows with important scores are highlighted. The row corresponding to the error range with the largest errors exhibited (i.e., worst case) for a given bridge group and analysis method is highlighted by a dark shade. In addition, the row corresponding to the most frequently occurring error range (i.e., the mode) is highlighted by a light shade, unless this range is the same as the error range with the largest errors. In Table 5.4, up to two worst case cells are highlighted for maximum positive and negative errors. These highlighted rows are used to generate final simplified scores for each of the bridge groups and analysis methods in Tables 5.5 and 5.7.

The summarized letter grades provided in Table 5.5 and 5.6 correspond to the error ranges with the largest error in Tables 5.3 and 5.4. This is because it was decided that the letter grades generally need to reflect the worst-case errors for a given category. In several cases, the specific letter grade for a given type of bridge is higher than that for a bridge type where for most of the analysis methods, the results are more accurate. In these situations, the letter grade for the bridge type where the results typically would be more accurate is used. The footnotes in Tables 5.5 and 5.6 indicate the cases where these modifications were made. Overall generalized errors are summarized for the 2D-grid from Program P1 and 1D line-girder analyses on Table 5.7.

Table 5.5. Generalized tub-girder bridge scores for girder major-axis bending stresses, torques, and displacements.

Response	Group	Worst-Case Scores		Mode of Scores	
		2D-P1	1D-Line Girder	2D-P1	1D-Line Girder
Major-Axis Bending Stresses	**C**	B	C	A	B
	S	B	B	A	B
	C&S	B	C[b]	B	B
Girder Torques	**C**	D	D	A	B
	S	**F**	**F**	D	D
	C&S	**F**	**F**	A	B
Vertical Displacements	**C**	A	B	A	A
	S	B	B	A	A
	C&S	B	B	A	A
Girder Layover at Bearing Lines	**C**	NA[a]	NA[a]	NA[a]	NA[a]
	S	B	B	A	A
	C&S	B	B	A	A

[a] Magnitudes should be negligible where properly designed and detailed diaphragms or cross-frames are present.

[b] Modified from B to C based on the score for the C bridges

Table 5.6. Generalized tub-girder bridge scores for bracing system forces and flange lateral bending stresses.

Response	Sign of Error	Group	Worst-Case Scores		Mode of Scores	
			2D-P1	1D-Line Girder	2D-P1	1D-Line Girder
TFLB Diagonal Force	Positive (Conservative)	C	D	F	B	F
		S	D	D	D	C
		C&S	D[a]	F	B	F
		Pratt TFLB System	F	F	A	F
	Negative (Unconservative)	C	--	--		
		S	F[b]	C		
		C&S	--	--		
		Pratt TFLB System	--	--		
TFLB & Top Internal CF Strut Force	Positive (Conservative)	C	F	F		
		S	C	C		
		C&S	F	F[c]		
		Pratt TFLB System	F	F		
	Negative (Unconservative)	C	--	A		
		S	C	C		
		C&S	--	C		
		Pratt TFLB System	D	D		
Internal CF Diagonal Force	Positive (Conservative)	C	F	F		
		S	NA[d]	NA[d]		
		C&S	F	F		
		Pratt TFLB System	--	F[e]		
	Negative (Unconservative)	C	--	--		
		S	NA[d]	NA[d]		
		C&S	--	D		
		Pratt TFLB System	B	--		
Top Flange Lateral Bending Stress (Warren TFLB Systems)	Positive (Conservative)	C	F	F		
		S	C	C		
		C&S	F	F[c]		
	Negative (Unconservative)	C	--	A		
		S	C	C		
		C&S	--	C		

[a] Modified from a C to a D considering the grade for the C and the S bridges.

[b] Large unconservative error obtained for bridge ETSSS2 due to complex framing. If this bridge is considered as an exceptional case, the worst case unconservative error is -15 % for NTSSS2 (grade = C).

[c] Modified from a B to an F considering the grade for the C bridges.

[d] For straight-skewed bridges, the internal intermediate cross-frame diagonal forces tend to be negligible.

[e] Modified from an A to an F considering the grade for the C and C&S bridges.

Table 5.7. Generalized tub-girder bridge scores.

Response	Sign of Error	Geometry	Analysis Method	
			Traditional 2D-Grid	1D-Line Girder
Major-Axis Bending Stresses	NA	C	B	C
		S	B	B
		C & S	B	C
Girder Torques	NA	C	D	D
		S	**F**	**F**
		C & S	**F**	**F**
Vertical Displacements	NA	C	A	B
		S	B	B
		C & S	B	B
Top Flange Lateral Bending Stresses	Positive (Conservative)	C	**F**	**F**
		S	**F**	**F**
		C & S	**F**	**F**
	Negative (Unconservative)	C	A	A
		S	A	A
		C & S	A	A
TFLB & Internal CF Forces	Positive (Conservative)	C	**F**	**F**
		S	**F**	NA[a]
		C & S	**F**	**F**
	Negative (Unconservative)	C	B	A
		S	C	NA[a]
		C & S	C	D
Girder Layover at Bearings	NA	C	NA[b]	NA[b]
		S	B	B
		C & S	B	B

[a] The component force equations report negligible forces on the internal CF forces in straight tub-girders.

[b] Magnitudes should be negligible for bridges that are properly designed & detailed.

5.5 Analysis Assessment Summary

Table 5.7 shows the synthesis of the analysis scores for the tub-girder bridge responses for traditional 2D-Grid and 1D-Line girder methods at large. This table addresses the accuracy of the calculations for major-axis bending stresses, girder torques, vertical displacements, girder layovers at the bearings and bracing system forces.

5.5.1 Major-Axis Bending Stresses, Vertical Displacements and Girder Layovers at Bearing Lines.

In these categories the letter grades are dominated by B grades, the 1D line-girder falls into the C grade for exceptional cases but this is expected as the complexity of response is not completely represented in the model. In summary the simplified analysis

methods show good agreement in the prediction of major-axis bending stresses, vertical displacement and girder layovers at the supports. For tub-girder bridges the lack of accuracy is expected from the line-girder analysis as the interaction between girders cannot be modeled.

5.5.2 Girder Internal Torques

The torsional properties of the tub-girders are used to take advantage of the individual girder behavior. However, the prediction of the torsional behavior is complex as it involves the interaction of several components including support diaphragms, external intermediate cross-frames, top flange lateral bracing system, etc. In consequence the lack of modeling accuracy of each of these components adds up and in the estimations fall into the F grade.

The torque behavior is more difficult to predict accurately as the complexity of the bridge increases. Uniform bracing, reduced interaction between adjacent girders and accurate modeling of support diaphragms provide improvements to the tub-girder bridge behavior and in consequence better torque estimations. Bridges with complex deck geometry, non-uniform bracing, multiple cross-frame interaction between girders, skewed supports, high eccentric vertical loading, etc., must consider the use of 3D FEA for an accurate representation of the torsional behavior. Line-girder and 2D-grid analysis methods still provide approximate estimations of the girder torques but the accuracy on the components forces depending on the girder torques are impacted.

The estimation of the torsional moments due to skew using simplified analysis methods is a main contribution of this dissertation. In consequence, the torsional moment estimate is evaluated for the skewed bridges analyzed for this research. Section 5.6 shows the results for the torsional moments and discusses the bridge behavior including the potential sources of error.

5.5.3 Bracing Forces

Several of the estimated bracing forces fall into F grades. The errors are mainly caused by the low accuracy on the torque estimates. However, the majority of the

estimations fall into the conservative categories meaning that the simplified methods still provide usable estimates for these cases.

Appendix A shows the results from the application of the component force equations to a previously published tub-girder example and compares with the responses from the 3D FEA. The worst case errors reported would be assigned a B grade. However, as mentioned in the appendix, this girder has a favorable geometry, such as symmetry, uniform bracing spacing, uniform and non-eccentric vertical loading and, since it is a single girder, it does not involve any interactions with other bridge components. In many cases encountered in practice, the behavior involves the interaction between the multiple girders. This causes the behavior to be more complex and difficult to estimate via simplified methods.

5.6 Evaluation of Simplified Estimates of the Torsional Moment

This dissertation studied 18 tub-girder bridges, 10 of them had skewed supports. Table 5.8 summarizes the main geometric characteristics of the study bridges with skewed supports. Of these, the first 5 bridges are straight and skewed bridges and the remaining 5 are curved and skewed bridges.

Table 5.8. General description of skewed study bridges.

Bridge ID	Span Length	Curvature Radius	Deck Width	Skew Angles	Number of Girders
XTCSN3	206 ft, 275 ft, 206 ft	–	43 ft	–	2
NTSSS1	150 ft	–	30 ft	15°, 15°	2
NTSSS2	150 ft	–	30 ft	30°, 30° 0°, 0°	2
NTSSS4	150 ft	–	30 ft	16°, -16° 0°, 0°	2
ETSSS2	205 ft	–	56.5 ft	33.4°, 33.4°	3
NTSCS5	150 ft	400 ft	30 ft	10.7°, -10.7°	2
NTSCS29	225 ft	820 ft	30 ft	15.7°, 0° 0°, 0°	2
ETCCS5a	183 ft, 161 ft	765 ft	36.2 ft	0°, 4.8°, 0°	2
ETCCS6	160 ft, 207 ft	814 ft	50.5 ft	0°, 39.2°, 0°	2
NTCCS22	250 ft, 250 ft	713 ft	30 ft	20.1°, 0°, 0° 0°, 0°, 0°	2

Each of the following subsections illustrates the bridge layout and presents the torsional moment for the bottom-most girder in the layout (Girder 1). An explanation of when the simplified procedures provide accurate estimations or not, based on the quantitative and conceptual sources of errors, is included for each bridge.

The benchmark torsional moments are obtained by integrating the 3D FEA stresses over the cross-section of the tubs. The 1D line-girder analysis results are obtained using the recommendations from Chapter 3 to account for the effects of skew. For some of the curved and skewed bridges, the torsional moments are shown for the zero skew (radial) case to compare to the curvature effects.

5.6.1 XTCSN3

The XTCSN3 bridge is an straight and unskewed bridge (tangent bridge). Figure 5.2 illustrate the XTCSN3 bridge layout. Figure 5.3 illustrate the torsional moment for Girder 1. The torsional moment of this bridge is caused by the eccentric vertical loading which results on a uniformly distributed torsional moment. The 1D line-girder analysis relies on Eqs. 2.5 and 2.6 to evaluate the torsional moments by substituting the M/R by a constant distributed torsional moment equal to *ew*, where e is the eccentricity of the applied vertically distributed load *w* (See Fig. 2.18).

Figure 5.2. Plan view of XTCSN3.

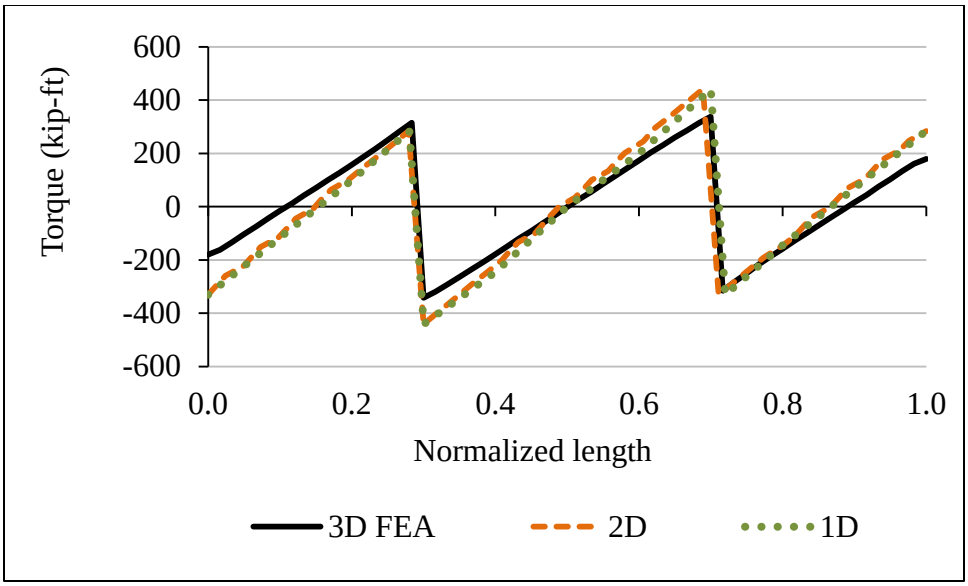

Figure 5.3. XTCSN3 Torsional moment for Girder 1.

The torsional moment distribution is represented accurately by both the simplified analysis methods. Minor differences are attributed to the estimation of the eccentricity and the applied load.

5.6.2 NTSSS1

Figure 5.4 illustrates the NTSSS1 bridge with parallel skewed supports. According to the procedures discussed in Chapter 3, the bridge is subjected to constant torsional moments due to discrete torques at the supports. The comparisons of the simplified methods to the 3D FEA illustrated in Figure 5.4 suggest that additional actions cause a different torsional moment distribution along the length of the bridge.

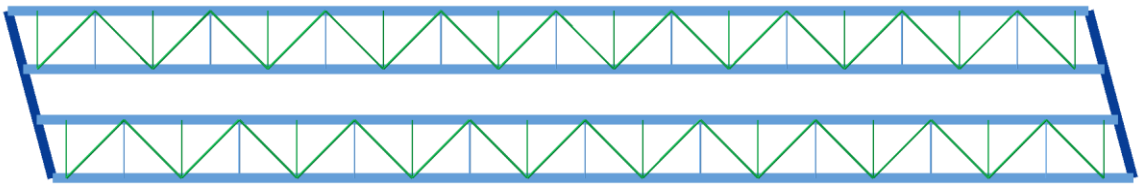

Figure 5.4. Plan view of NTSSS1.

The bracing internal forces are believed to create additional torsional effects. The parabolic-like torsional moment diagrams corresponds to additional torques with a parabolic-like distribution similar to the strut forces for a bridge like this as seen in

Figure A.24 for NTSSS2 in Appendix A. For the NTSSS1, the effect of the internal bracing on the torsional moments is more noticeable as the torsional moments due to skew are relatively small when compared to curved bridges or bridges with more skew.

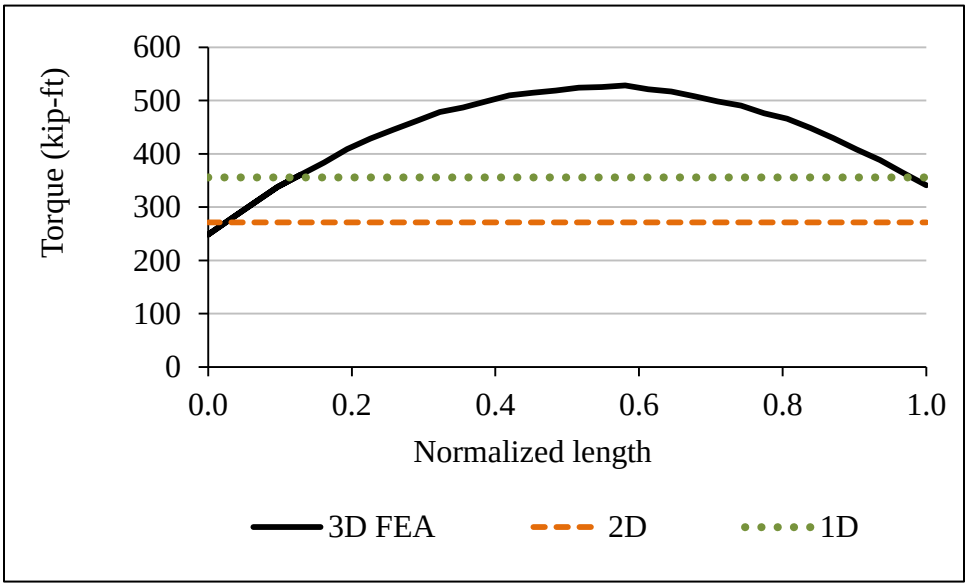

Figure 5.5. NTSSS1 Torsional moment for Girder 1.

5.6.3 NTSSS2

Figure 5.6 illustrates the plan view of the NTSSS2 bridge which has similar geometry as NTSSS1 but with parallel skew of 30°.

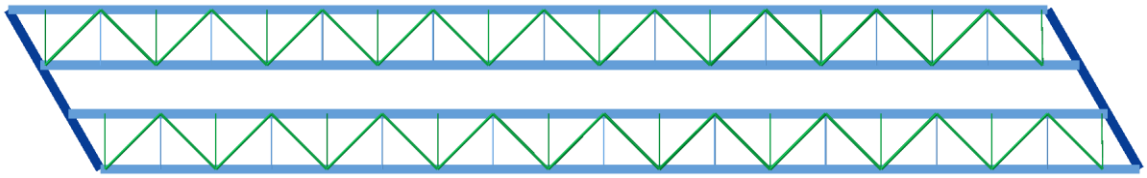

Figure 5.6. Plan view of NTSSS2.

The torsional moment distributions are shown in Figure 5.7 for the 3D FEA and the simplified analysis methods. As in the previous case, the torsional moment, as predicted by the refined analysis method, follows a parabolic-like distribution. For this case, the parabolic-like effects are relatively smaller when compared to the maximum torques due to skew. As discussed previously, the parabolic-like effects are believed to be caused by the internal bracing forces.

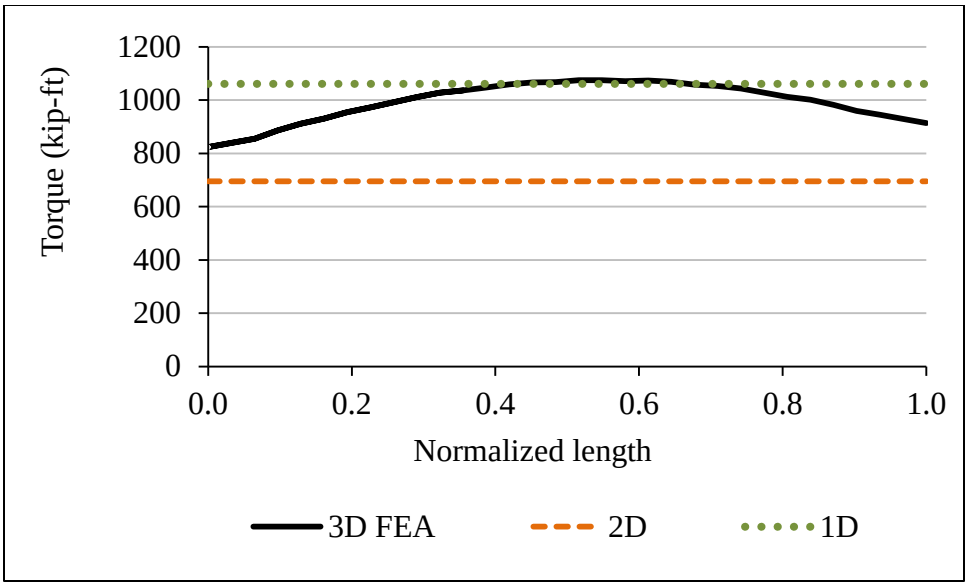

Figure 5.7. NTSSS2 Torsional moment for Girder 1.

5.6.4 NTSSS4

The NTSSS4 bridge is illustrated in Figure 5.8. The bridge has equal but opposite skewed supports (+16° and -16°). This case illustrates the mechanism explained in Figure 3.6b in which the girders experience rigid body rotations with no additional torque due to the skewed supports.

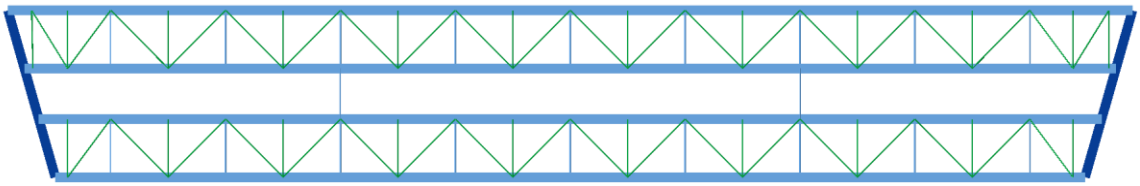

Figure 5.8. Plan view of NTSSS4.

The torsional moment distributions predicted by the 3D FEA and the simplified analysis methods are illustrated in Figure 5.9. For this case, the torsional moments are affected by the interaction between girders caused by the external intermediate cross-frames. The 1D method fails to predict these interactions as it regularly neglects the girder interactions. The 1D method could include the effects of the girder interactions if Section 2.3.3 is used to evaluate the forces and associated torsional moment caused by the external intermediate cross-frame forces.

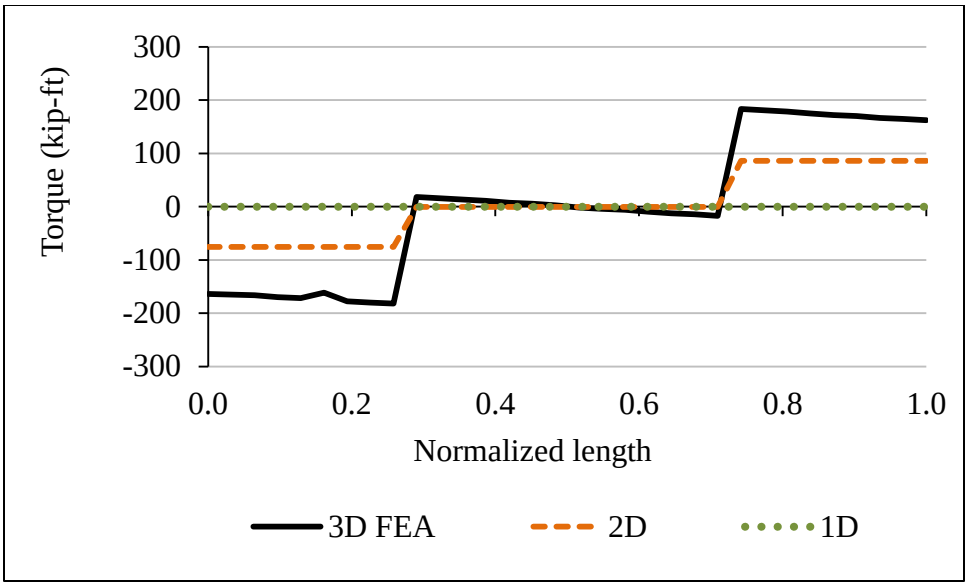

Figure 5.9. NTSSS4 Torsional moment for Girder 1.

The 2D-grid analysis is capable of including these effects provided that the external intermediate cross-frames are included in the model. The magnitude of the torsional moments caused by the interaction of the external intermediate cross-frames is small when compared to the NTSSS1 and NTSSS2 results. The differences of the 2D-gird results have been attributed to the modeling characteristics of the grid which neglect to region within the cross-section of the girders. This effect results on increased length and, consequently, reduced stiffness which may affect the transverse load transfer that originates the torsional moments on Figure 5.9.

The effect on the torsional moments due to the external intermediate cross-frames is also evident for curved bridges. However, for curved bridges, the magnitude of the torsional moments is several times larger than the effect of the external intermediate cross-frame and the interactions can be safely neglected.

5.6.5 ETSSS2

The ETSSS2 study case corresponds to the Sylvan Bridge located in Multnomah Co., OR. The bridge under construction is shown in Figure 4.6 and 4.7 and the layout is shown in Figure 5.10. The bridge has several skewed external intermediate cross-frames used during construction to control relative vertical displacements.

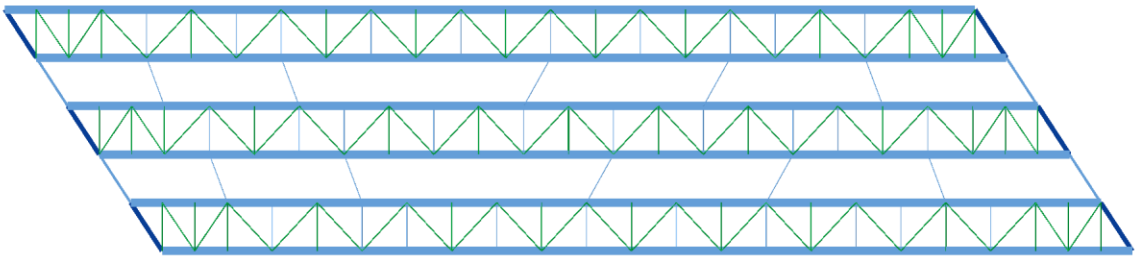

Figure 5.10. Plan view of ETSSS2.

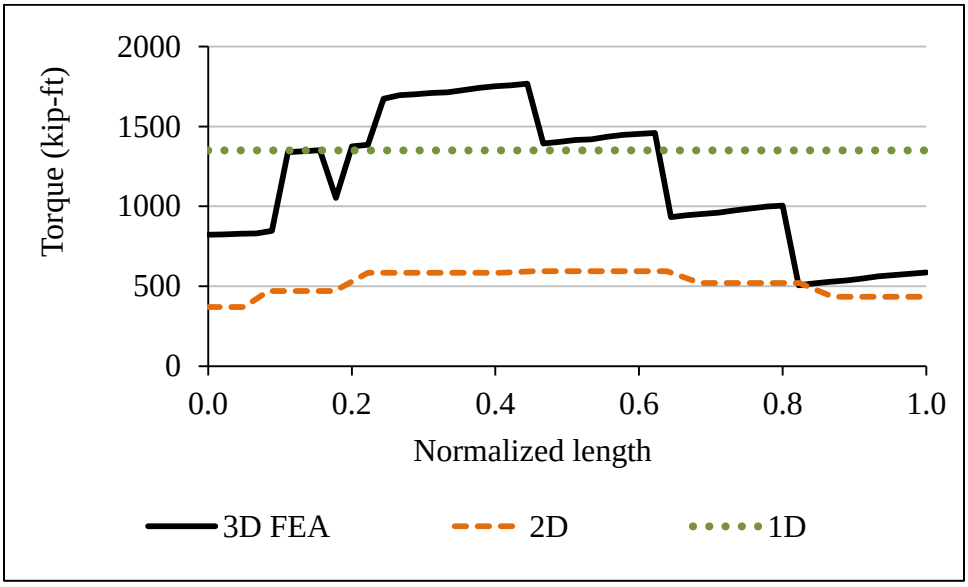

Figure 5.11. ETSSS2 Torsional moment for Girder 1.

The external intermediate cross-frames develop interaction between girders which directly affect the torsional moment magnitudes as shown in Figure 5.11. For this case, the interactions between girders occur at different relative positions along the girder spans since the external intermediate cross-frames are skewed. A bridge with such complexity would require a refined analysis to properly estimate the behavior including the torsional estimations. The 2D-gird results approximate the behavior of the external intermediate cross-frames by predicting changes on the torsional moments. However, these interactions are not sufficiently accurate as the model that represents the external intermediate cross-frame may lack of the required strength to provide a transverse load path for the development of larger additional torques as those predicted by the 3D FEA. Additional analysis were performed to predict this behavior with better accuracy by estimating the properties of the external intermediate cross-frames by different methods,

however, the interactions were not successfully achieved. In consequence, the lack of accuracy is assumed to be caused by the skewed external intermediate cross-frame configuration, the numerous cross-frames and the regions within the girder cross-section.

5.6.6 NTSCS5

The curved and skewed bridge NTSCS5 is shown in Figure 5.12. The bridge has equal but opposite skew angles to provide a configuration with parallel supports. The skew configuration is equivalent to Figure 3.6b including curvature and measuring the angles from the radial lines. The skew configuration results on rigid twist rotations but zero skew effects on the torsional moment distribution as discussed previously on Section 3.1.2.

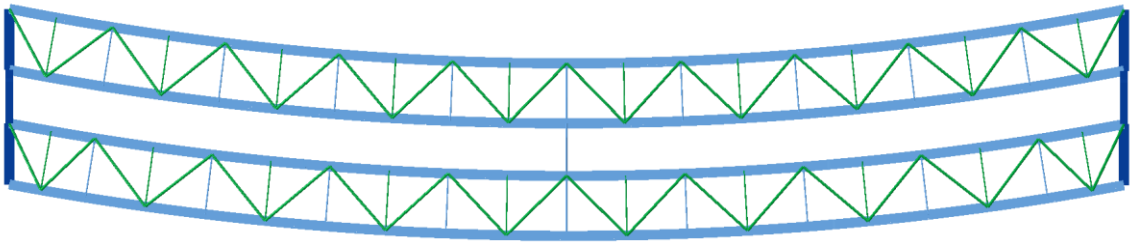

Figure 5.12. Plan view of NTSCS5.

Figure 5.13 illustrates the torsional moment distribution for the original configuration as predicted by the 3D FEA and the 1D and 2D simplified analysis methods. Figure 5.14 show the results for the 3D FEA and 1D for the sensitivity study bridge with radial supports but keeping the same overall geometry. As expected, both torsional moment distributions have negligible differences as the torque due to skew is negligible.

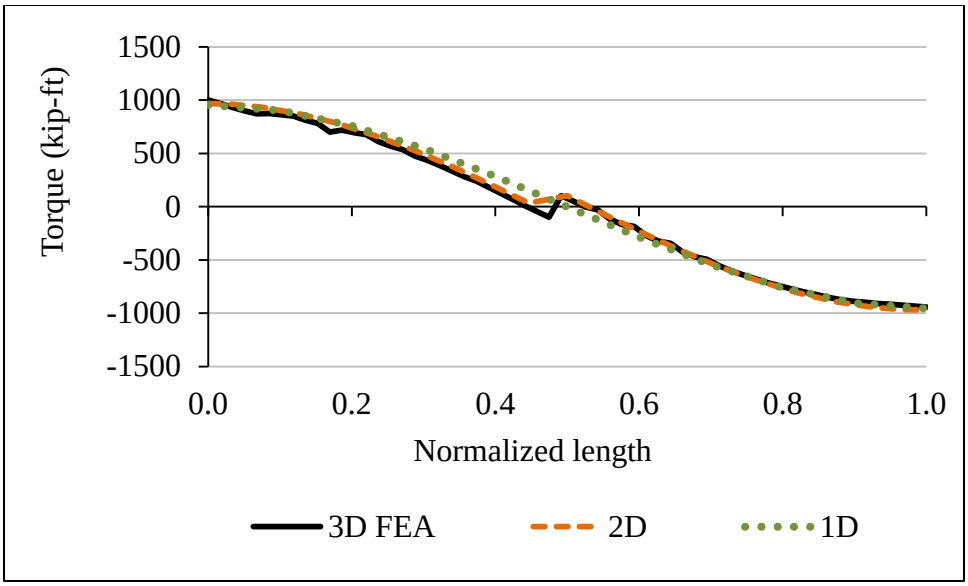

Figure 5.13. NTSCS5 Torsional moment for Girder 1.

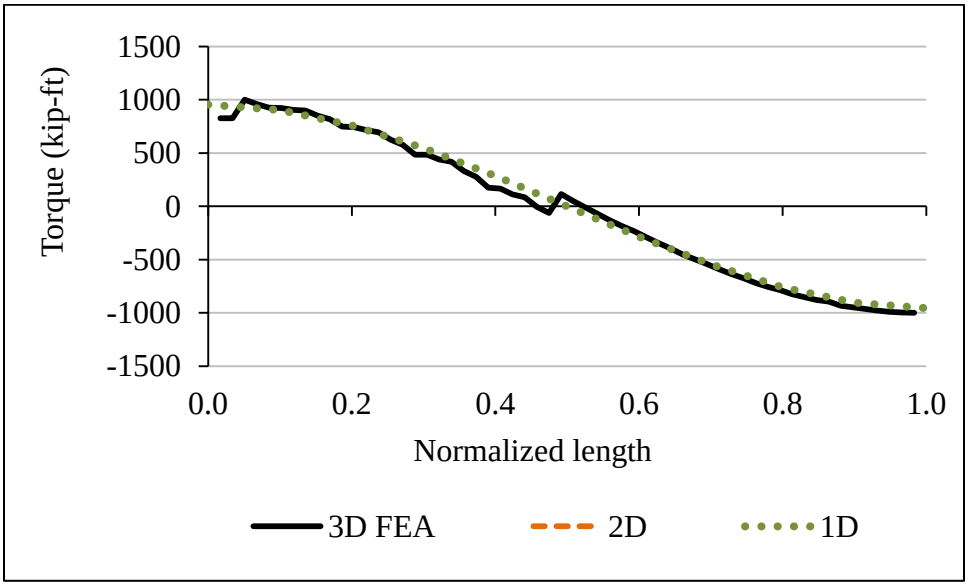

Figure 5.14. NTSCS5 Torsional moment for Girder 1 for radial sensitivity case (0° skew).

At 0.5 of the normalized length an external intermediate cross-frame interconnects the girders. The effect of this external intermediate cross-frame is noticeable as a change in the internal torques. The 1D method does not reflect this effect as it ignores the external cross-frames. In contrast, the 2D-grid methods includes the effect of the external intermediate cross-frame interaction in the torsional moment estimation.

5.6.7 NTSCS29

The NTSCS29 bridge shown in Figure 5.15 illustrates a curved and skewed support configuration. The left support is skewed 15.7° to create a parallel configuration in which the right support keeps the radial support.

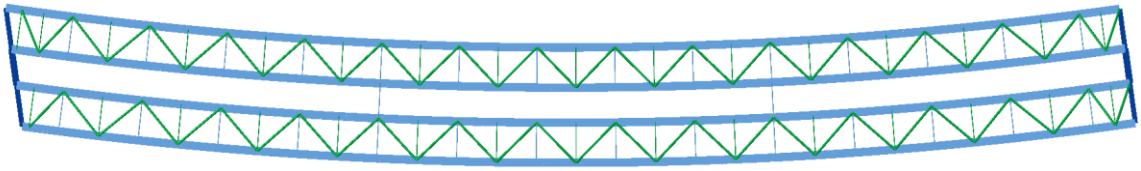

Figure 5.15. Plan view of NTSCS29.

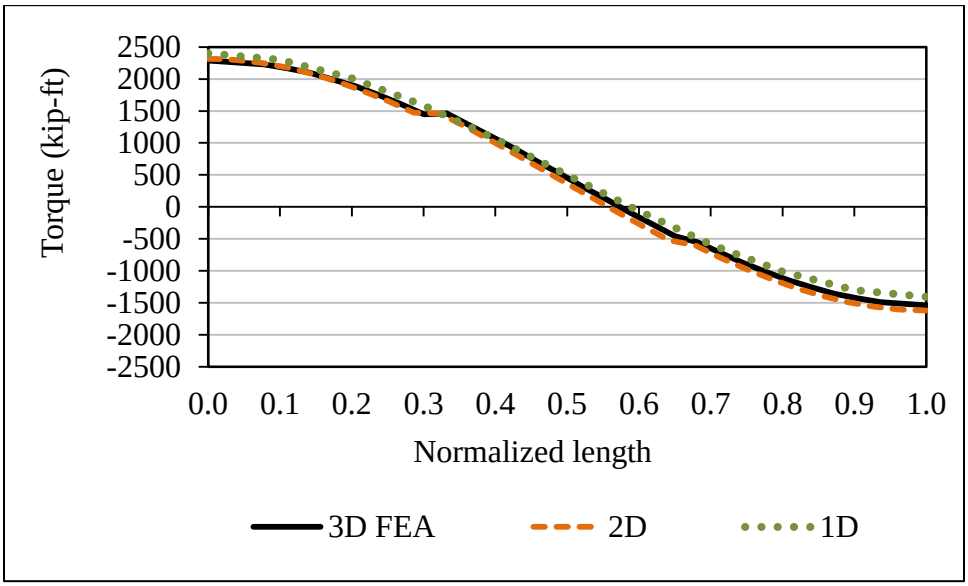

Figure 5.16. NTSCS29 Torsional moment for Girder 1.

Figure 5.16 illustrates the torsional moments for the configuration shown in Figure 5.15 for the 3D FEA and 2D and 1D simplified analysis methods. Figure 5.17 illustrate the torsional moments from 3D FEA and 1D estimations for the sensitivity study bridge with the same general configuration but with both radial supports. The skewed case in Figure 5.16 is similar to 5.17 but the diagram is shifted upwards as the result from the additional torque due to skew.

The 1D analysis method ignores the effects of the external intermediate cross-frames which are barely noticeable as minor changes on the torsional moments for the 3D FEA and 2D-grid results. This effect is small relative to the curvature effects.

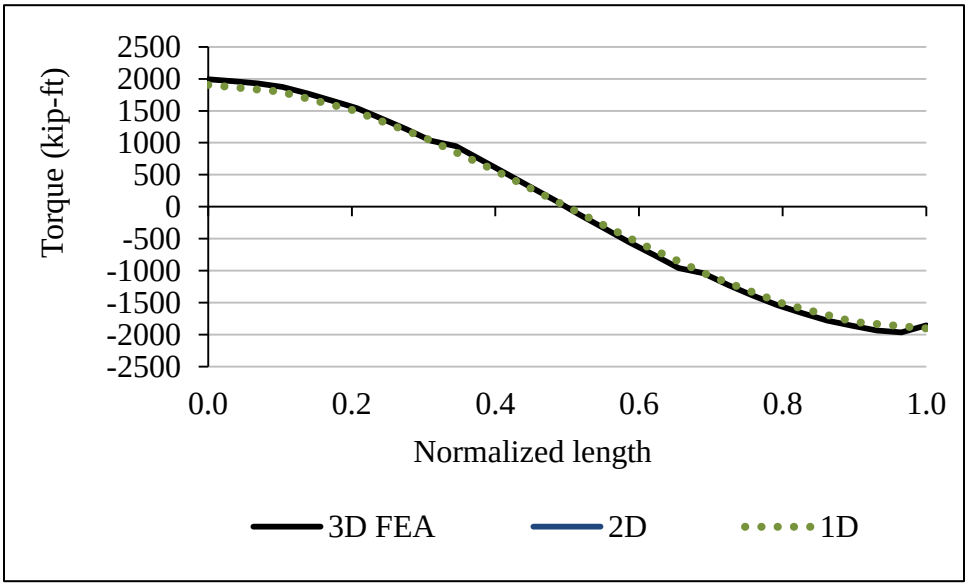

Figure 5.17. NTSCS29 Torsional moment for Girder 1 for radial sensitivity case (0° skew).

5.6.8 ETCCS5a

Figure 5.18 illustrates the plan view of the existing ETCCS5a bridge. ETCCS5a is located at the SR 9A and SR 202 interchange in Duval Co. FL, the bridge has an intermediate skewed support of 4.8°. The bridge has a Pratt truss configuration for the top flange lateral bracing system.

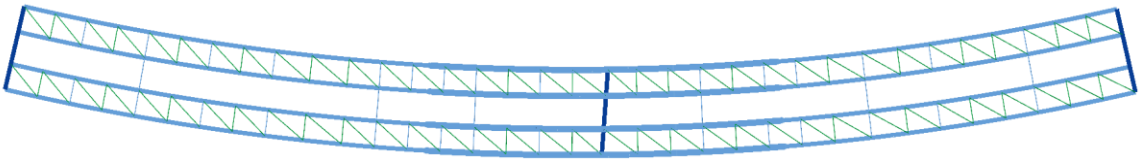

Figure 5.18. Plan view of ETCCS5a.

For this case, the intermediate skewed pier is skewed and the span lengths are similar (183 ft and 161 ft). In consequence, the effects of skew are negligible, as the girder bending rotation at the pier is close to zero and the skew angle is small.

Figure 5.19 illustrates the torsional moments as predicted by the 3D FEA and the simplified analysis methods. For this case, the simplified analysis methods fail to predict

the response accurately as consequence of the Pratt top flange lateral bracing configuration. Pratt layout configurations tend to produce diagonal and strut forces with the same sign (tension or compression) along the length of the bridge producing internal lateral loads. This results on additional torques at each panel which are not easily predicted by the simplified analysis methods. In consequence, when Pratt configurations are used, the analysis should consider the use of a refined analysis.

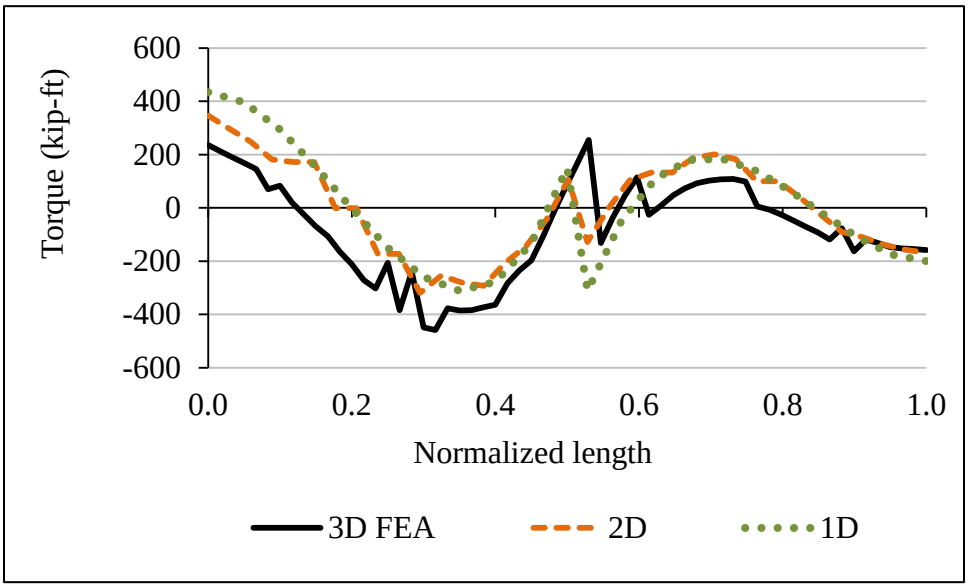

Figure 5.19. ETCCS5a Torsional moment for Girder 1.

5.6.9 ETCCS6

The exterior phase of ETCCS6 bridge layout is shown in Figure 5.20. ETCCS6 is the Magruder Blvd. bridge over I-64 in Hampton, VA. The bridge phase studied has an intermediate skewed pier with skew angle of 39.2°. The bridge design does not include an external support diaphragm at the intermediate skewed pier connecting the girders.

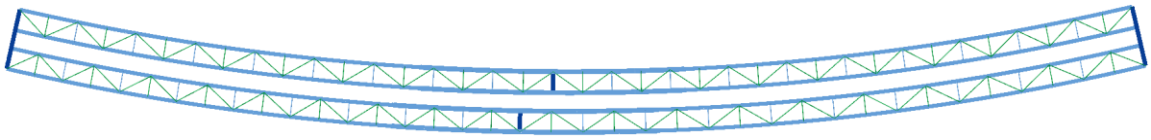

Figure 5.20. Plan view of ETCCS6.

The lack of external support diaphragm at the intermediate pier prevents the skew mechanism to create an additional torsional moment. In consequence, the behavior of the

bridge cannot be represented accurately by the simplified analysis methods as shown in Figure 5.21 and could potentially under or overestimate the behavior. The torsional moment reduction by the removal of the support diaphragm requires a more refined analysis to capture the behavior accurately.

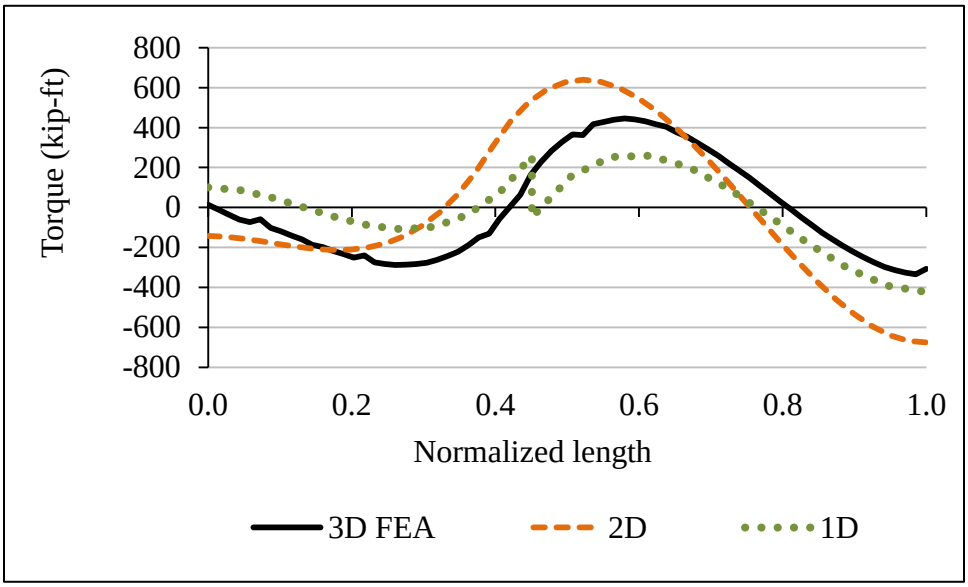

Figure 5.21. ETCCS6 Torsional moment for Girder 1.

5.6.10 NTCCS22

Figure 5.23 illustrates the NTCCS22 bridge previously discussed for the evaluation of the torsional effects due to skew in continuous span bridges. The bridge has one skewed support of 20.1° making the left abutment parallel to the central pier.

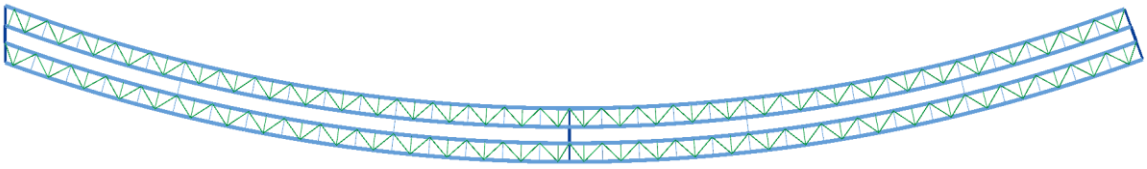

Figure 5.22. Plan view of NTCCS22.

Figure 5.23 illustrates the torsional moment distribution as predicted by the 3D FEA and the 2D and 1D simplified analysis methods for the configuration shown in Figure 5.23. Figure 5.24 illustrate the torsional moments as predicted by the 3D FEA and 1D for the sensitivity study case with radial supports.

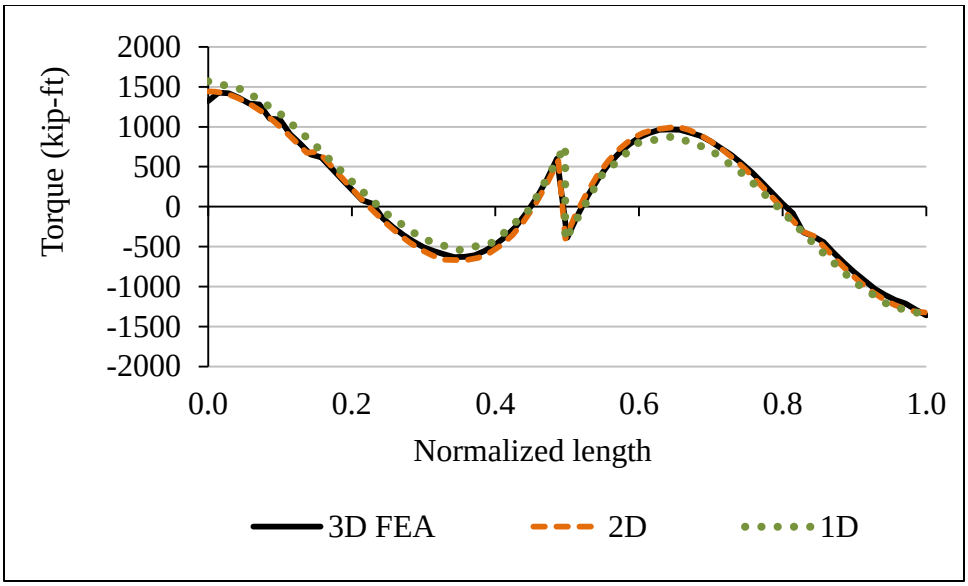

Figure 5.23. NTCCS22 Torsional moment for Girder 1.

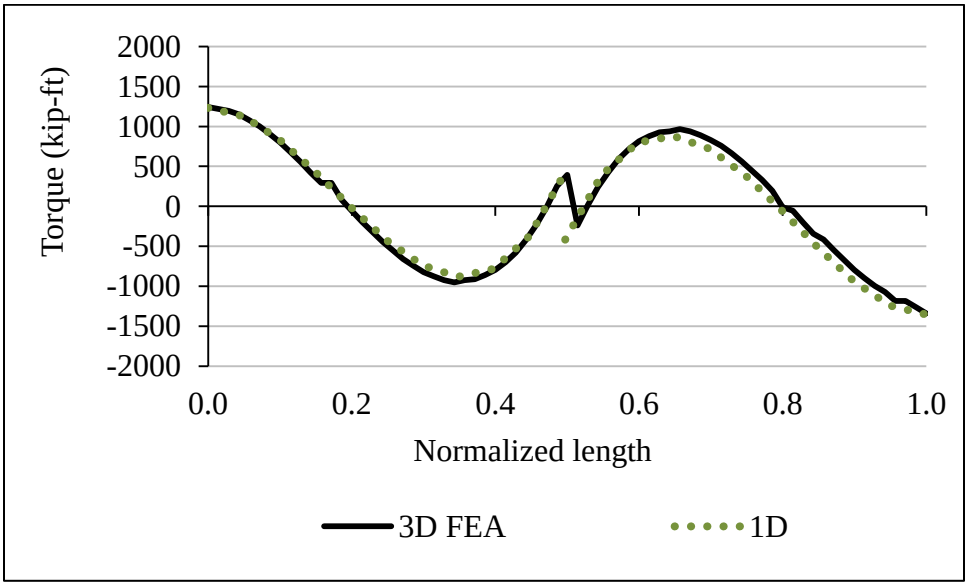

Figure 5.24. NTCCS22 Torsional moment for Girder 1 for radial sensitivity case (0° skew).

When compared to the radial case in Figure 5.24, the left span torsional moment diagram in Figure 5.23 is shifted upwards as a result of the skewed supports. The right span remains mostly unchanged for both cases.

The 1D analysis method predicts the behavior of the skew accurately when the improvements proposed in Chapter 3 are included. Minor differences are identified at the

locations of the external intermediate cross-frames. The 2D-grid method also predicts the behavior accurately including the minor torque changes at the external intermediate cross-frame locations.

5.6.11 Summary of Torsional Moment Estimates

Table 5.9 summarizes the results from the torsional estimates of the skewed studied bridges from the 1D line-girder analysis method using the developments of Chapter 3.

The sources of errors in the estimation of the torsional moments on the studied bridges are summarized as

- External intermediate cross-frames cause additional torsional effects which are usually ignored by 1D analysis methods.
- Larger errors are expected as the number of external intermediate cross-frames increase. The use of skewed external intermediate cross-frames increases the errors.
- Lack of external support diaphragm at intermediate piers.

Additionally, for the studied bridge using Pratt top flange lateral bracing system, evidence was found that suggested that the simplified analysis methods would experience accuracy problems evaluating the girders torsional behavior.

Previous to the developments presented in this dissertation, the effects of skewed supports could not be quantified by 1D analysis methods. The girder internal torsional moments involve interaction between the internal supports which would require a higher level of analysis to estimate the effects with better accuracy, however the 1D analysis method still provide useful estimations provided the above characteristics are avoided.

Table 5.9. Torsional moment estimations summary

Bridge ID	Main Bridge Characteristic	Summary
XTCSN3	Tangent bridge	The torsional moments are caused by the eccentric vertical loads.
NTSSS1	Moderate skew	The internal bracing causes additional torques. This effect is comparable in magnitude to the torques due skewed supports.
NTSSS2	Large skew	The internal bracing causes additional torques. This effect becomes less important as the torques due skewed supports increase.
NTSSS4	Equal but opposite skew	The mechanism for equal but opposite skew estimates rigid twist rotation and zero torque. Effects due to external intermediate cross-frame are not estimated.
ETSSS2	Multiple skewed external intermediate CF	The multiple skewed external intermediate cross-frames cause interaction between girders. The torsional moment distribution is not estimated accurately.
NTSCS5	Equal but opposite skew	The mechanism for equal but opposite skew estimates rigid twist rotation and zero torque. The effects of the external intermediate cross-frame are small relative to the maximum estimated torques at the supports.
NTSCS29	Curved and skewed	The effects of curvature and skew are captured accurately by the simplified methods. The combined effects are confirmed to be additive.
ETCCS5a	Pratt TFLB	The TFLB layout causes a torsional behavior difficult to capture accurately.
ETCCS6	No diaphragm at skewed intermediate pier	The lack of diaphragm at the intermediate pier alleviates the torsional moments but a refined analysis is necessary to estimate the bridge behavior.
NTCCS22	Continuous span	The effects of curvature and skew on continuous spans are captured accurately by the simplified analysis methods. A skewed support only affects the spans adjacent to such support.

CHAPTER VI.

EVALUATION OF CONTRUCTION CONDITIONS

The erection of tub-girder bridges often encounters difficulties due to their multiple components and high torsional stiffness. In comparison, I-girders are more flexible and the erector is able to use this characteristic to facilitate the construction through a variety of erection procedures.

Due to their relatively high stiffness, the default choice for the erection of tub-girders is the "No-Load-Fit" procedure. The No-Load-Fit erection procedure assumes that all field splices, cross-frames and diaphragms connections are made at a non-deflected or no-load geometry. This usually means that during steel erection the tub-girders are sufficiently shored to maintain the no-load geometry. In practice, it is not always possible to provide all the necessary temporary supports; so, the erection needs to consider the possibility of overcoming displacements due to the steel self-weight load. In addition, even when sufficient vertical supports are provided, the girders can experience significant rotations resulting in unexpected and problematic configurations. To avoid the issues due to the relative displacements between girders, the external intermediate cross-frames are sometimes detailed to fit the deformed geometry under steel dead load or "Steel-Dead-Load-Fit". This practice requires the consideration of the relative vertical displacements at this stage which may affect the cross-section profile.

Once all the steel girders have been erected and connected, the concrete deck is cast. The girders must be able to support the weight of the wet concrete, equipment and construction loads. This is the most critical phase since the bridge composite action is not achieved until the concrete cures. During this stage the maximum displacements are expected and, therefore, the girders are cambered to accommodate these displacements and to provide the desired final deck elevation. Also, it is during this stage that the relative vertical displacements and rotations must be controlled via external cross-frames to avoid excessive girder rotations that may impact the acceptable tolerance on the concrete deck thickness during the deck placement. An alternate approach requires

controlling the relative vertical displacements and rotations by the use of girder cambers and/or deck haunches rather than by external intermediate cross-frames. This practice, however, requires that the displacement responses are correctly evaluated, therefore, the relative displacements affecting the deck thickness are included on the camber and/or deck haunches. This prevents the use of external intermediate cross-frames and reduces the undesired effects on the accuracy of the simplified analysis methods.

During the construction stages the bearing reactions must be checked to prevent uplift. The bearing uplift can cause overloading to the adjacent bearings possibly causing premature damage. Support uplift is caused by the torsional effects of skew, curvature, eccentric loading and construction errors. Section 4.4.1.1 provides the Torsion Index for an early evaluation of uplift and overturning due to curvature.

The following sections discuss in more detail the above points for steel erection fit-up, relative displacements during concrete deck placements, and bearing behavior. The fit-up scenarios considered in the following discussions are unique of the characteristics of each bridge. However, a general procedure is presented to estimate the associated effects. Finally, the effects of skew interactions in these issues are discussed.

6.1 Steel Erection Stages

In order to identify the scenarios in which the steel-erection fit-up issues arise, the following developments examine erection procedures of two parametric study tub-girder bridges. The erection procedures presented are a part of the combined effort for the research project NCHRP 12-79 (NCHRP, 2011). The NCHRP 12-79 project team provided erection engineering plans based on experience from actual bridges with similar characteristics and current common standards of care.

The parametric bridges in this study consider simple and continuous-spans with span lengths of 150 ft to 350 ft. Steel bridges are usually fabricated and shipped in several parts also known as “field sections”. The crane capacity, the job site and transportation constraints often limit the sizes of the sections. For this reason, steel-bridges are usually erected in several field sections of reduced length.

Provided the number of field sections, several steel erection procedures can be chosen depending in the site constraints, available equipment and the preferred practice of the erector. As an example, two erection schemes are shown in Figures 6.1 and 6.2 for the parametric study bridges NTSCS29 and NTSCS22.

Figure 6.1 illustrates one approach for the erection of the simple-span bridge NTSCS29 which considers the use of temporary supports for the entire steel erection procedure. Once all the field sections have been erected and the external intermediate cross-frames placed the temporary supports are removed. The use of temporary supports during the entire process shown in Figure 6.1 reduces the displacements during erection and, in consequence, requires minimum effort to overcome displacements due to the bridge self-weight during construction.

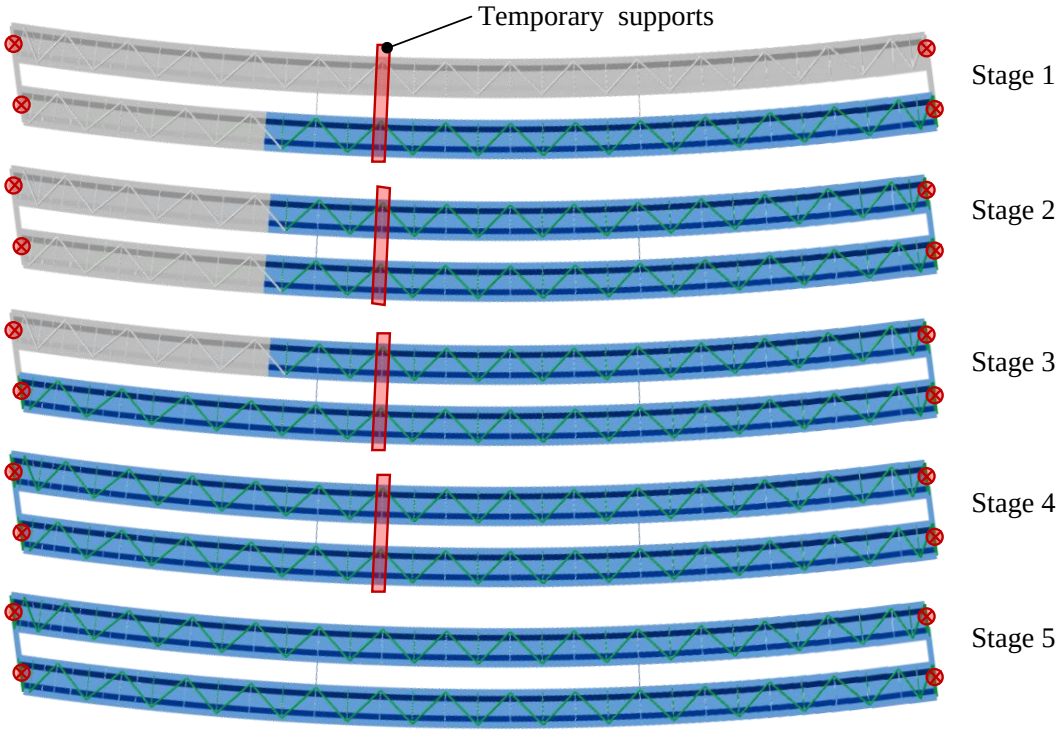

Figure 6.1. NTSCS29 intermediate steel erection stages.

Figure 6.2 illustrates the erection stages of the continuous-span bridge NTSCS22 and the location of the temporary supports. This erection scheme assumes that temporary supports are removed before the bridge is fully erected due to job site constrains requiring the minimum interruption of the traffic flow below. Since tub-girder bridges are

commonly detailed for No-Load-Fit, the erection procedure requires overcoming the displacements due to self-weight. The No-Load-Fit detailing requires that the structure is supported during the entire erection process in its approximate no-load geometry.

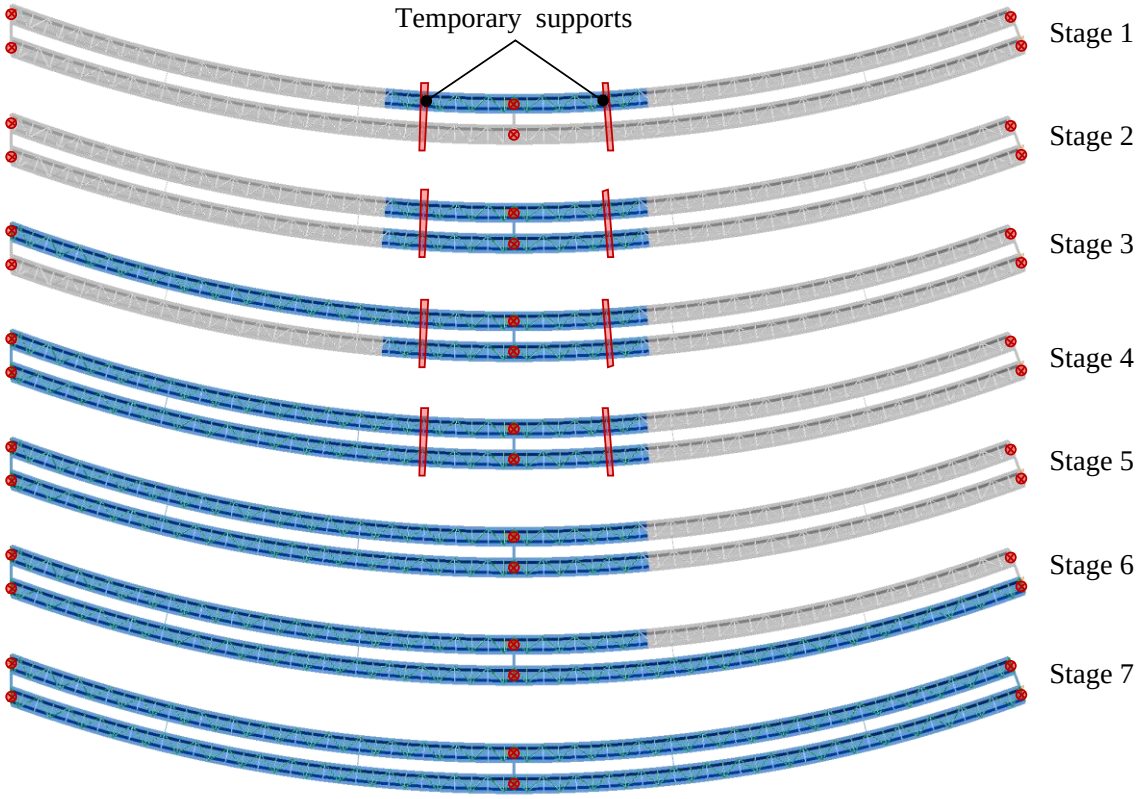

Figure 6.2. NTCCS22 intermediate steel erection stages.

The erection schemes shown in Figures 6.1 and 6.2 consider for most of the stages that two field sections of each girder are connected or spliced on the ground. This creates longer field sections to be lifted together to reduce the amount of work done far from the ground level. These erection procedures are selected based on the NCHRP 12-79 project team experience in similar bridges.

For the two erection procedures, the field sections can be lifted and tilted by the erection cranes to the positions where they can be connected stress-free and then released. This occurs during the intermediate stages prior to the final steel erection stage. However, difficulties could occur on the last erection stages when all field sections have been

erected and the last elements to be connected are the external intermediate cross-frames and the support diaphragms.

In summary, the problematic steel erection fit-up scenarios in tub-girder bridges usually involve the lack of fit at the last stages when the temporary supports are either removed or not capable of restraining girder twist rotations. The following section discusses two erection scenarios and illustrates the processes to estimate the associated fit-up forces.

6.2 Steel Erection Fit-up

During erection it is assumed that as long as there is a point of support, such as piers or other girders, it is simple to overcome the displacement incompatibilities. However, when dealing with tub-girders, the amount of force required overcoming the displacements could potentially exceed the capacity of the girders or the field equipment.

Different scenarios may occur during the erection process that may require a fit-up analysis. A fit-up analysis is the one made for evaluating the displacements during the erection stages and the associated forces required to overcome these displacements in order to be able to complete the connections. The stress levels that may arise due to the forces applied to the connecting elements should be kept below the yielding capacity of the parts.

The possible critical scenarios occur at the last stages of the steel erection when most of the girder splices have been erected and connected. During the initial stage, the girders can be moved to perform connections as the temporary supports and the erection cranes facilitate the connecting procedure. As more field sections are connected, the system stiffness starts to build up, making it harder to complete the remaining connections. Due to the nature of the high torsional and lateral stiffness of the individual tub-girders, any movement required at this stage for connecting two components requires a significant force to overcome even small displacements.

During steel erection the following example scenarios could occur:

- Lack of fit at the bearing line: In this case, the girders are sitting in the bearings, the external end diaphragm is the last element to be connected. The girders tend to rotate due to the torsional effects of curvature or skew and they must be brought together to make the connection.
- External intermediate cross-frame placement: In this case all girders are completely erected and the external intermediate cross-frames need to be placed.
- Drop in segment: For this case, the last connection happens at an intermediate location.

The first two fit-up scenarios can be evaluated by following a simplified process. The third scenario requires evaluation of the specific partial stages displacements and requires further reanalysis.

The support diaphragm and external cross-frame fit-up scenarios need to be taken into account for curved and/or skewed bridges, where relative displacements and rotations are expected. Tangent bridges could experiment these effects when the eccentric loads applied to the bridge can cause additional rotations. The following discussions are focused on recommending a fit-up process calculation.

6.2.1 Lack of Fit at the Bearing Line

For curved and/or skewed tub-girder bridges the rotations at the supports are expected to be small due to the high girder torsional stiffness, however, this also means that overcoming the displacements would require important force levels that need to be evaluated. For this scenario, the tub-girders are already connected and siting in the supports. The curvature and or skew induced girder rotation is as shown in Figure 6.9.

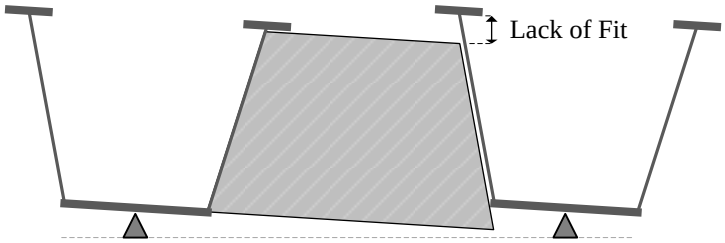

Figure 6.3. Lack of fit displacements due to girder rotation at the bearing line.

At this stage, the girders are transferring the vertical loads to the supports but the torque in the girders is expected to be null as no torsional fixity mechanism is in place. To connect the girders, it is necessary to rotate the girders to the final horizontal location and perform the connection. In summary, there are two ways to achieve this: pulling the left girder upwards and pushing the right girder down or pulling the girders left and right.

The fit-up forces required to connect the girders should generate torsional moments equivalent to the individual girder torque at the bearing line T_1 on girder 1and T_2 on girder 2 (see Fig. 6.4) to bring the girders to the connecting position.

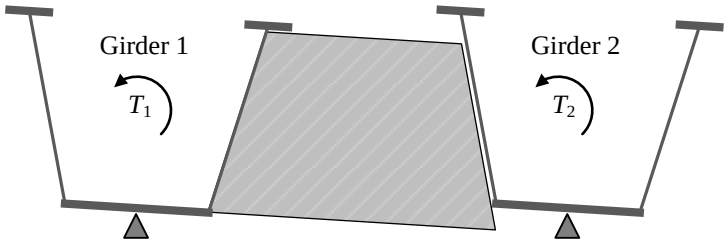

Figure 6.4. Set of forces required to connect the girders.

The torques T_1 and T_2 acting on the girders are equivalent to the torques obtained from the girder analysis. For a simple estimation, the 1D line-girder M/R Method and the T_S Eqs. 2.4 and 3.9 provide basic estimates for these torques.

The NTCCS22 bridge results presented in Appendix A illustrates the fit-up forces calculation. The following discussions evaluate the fit-up forces for the scenario discussed where the radial abutment external diaphragms, far right of Figure 6.11, is the last element to be connected. The girders are sitting on the supports and all intermediate supports have been removed allowing the girders to rotate as in Figure 6.9.

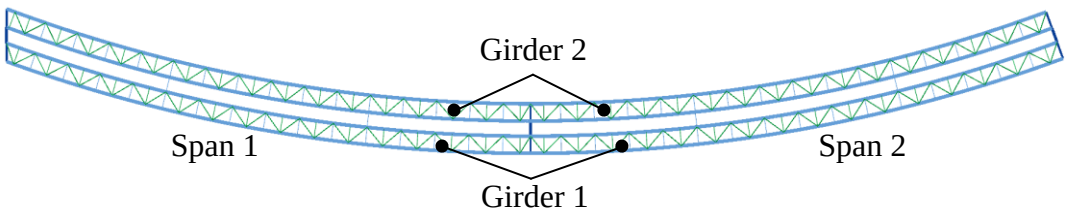

Figure 6.5. NTCCS22 Bridge Layout.

According to the 1D line-girder results for the steel dead load, at the radial abutment girder the torsional moments are 512 kip-ft for girder 1 and 463 kip-ft for girder 2. These are the torsional moments that need to be applied to bring the girders to the adequate position. Figure 6.12 illustrates a set of forces necessary to generate the required torsional moments to connect the girders for the case where the radial abutment is the last element to attach. The forces required to bring the girder to a fit-up condition are shown as F_1 and F_2 and are estimated by knowing the fit-up force application point distances d_1 and d_2 as

$$F_i = \frac{T_i}{d_i} \tag{7.1}$$

where i represents the girder 1 or 2. The figure shows a set of forces which require only vertical forces, the actual set of forces is specific of the job conditions. For example, in order to reduce the 128 kip load, a horizontal load with magnitude of 56 kip could be used instead.

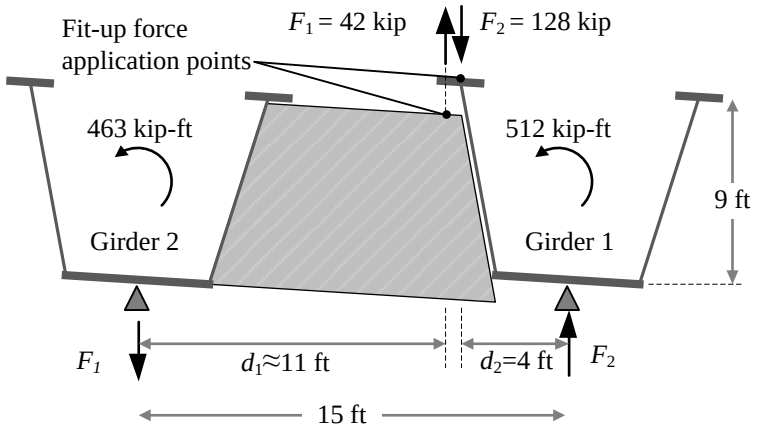

Figure 6.6. Set of forces required to connect the girders on the radial abutment of NTCCS22.

This development presents the worst case scenarios where the girders have been allowed to fully rotate, in practice, this type of scenarios are avoided by the use of temporary supports. However, the forces estimated serve as indication of the level of forces expected.

6.2.2 External Intermediate Cross-Frame Placement

For the second scenario the external intermediate cross-frames are added once the girders have been completely erected. This is not the ideal situation as the girders are now restrained at both ends and the associated stiffness makes more difficult to overcome the displacements at the cross-frame locations than when the cross-frames are added before the diaphragms. This scenario, however, has a simple solution based on the intermediate equations developed by Helwig et al. (2007) for external intermediate cross-frames.

The horizontal and vertical forces shown in Figure 6.13 are equivalent to the forces required to connect the girders at the moment of the cross-frame placement.

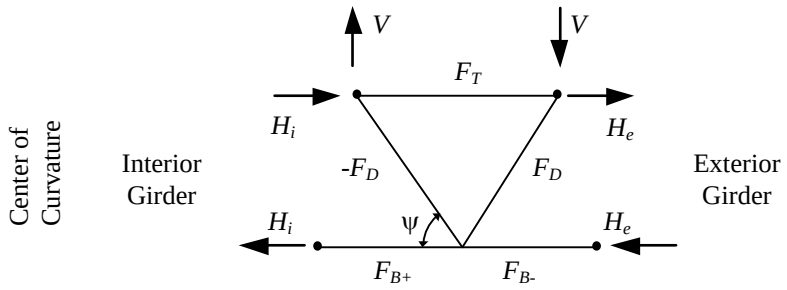

Figure 6.7. External intermediate cross-frame forces and fit-up forces.

The forces on the external diaphragm top chord, F_T, bottom chord F_B and diagonals F_D are defined in terms of the external intermediate cross-frame component forces defined in Chapter 2. The external cross-frame forces are

$$H_i = F_D \cos\psi - F_T \tag{6.2}$$

$$H_e = F_D \cos\psi + F_T \tag{6.3}$$

$$V = F_D \sin\psi \tag{6.4}$$

These equations provide an estimate of the lateral and vertical forces needed to connect the cross-frames. In the practice the amount of force necessary should be compared to that of the available equipment in the field, and preparations should be made to provide adequate supporting and time to avoid erection difficulties. The external

intermediate cross-frames depend on the amount of relative vertical displacement and rotations. If during erection the temporary supports restrain vertically displacements but not the rotations, the equations should be input with zero displacement and the expected relative rotation.

Appendix A shows the results from NTSCR1 bridge that illustrates the fit-up forces calculation for this scenario. Figure 6.14 shows the bridge layout and the fit-up analysis is performed assuming that both support diaphragms have been connected and the external intermediate cross-frame at the midspan is about to be connected.

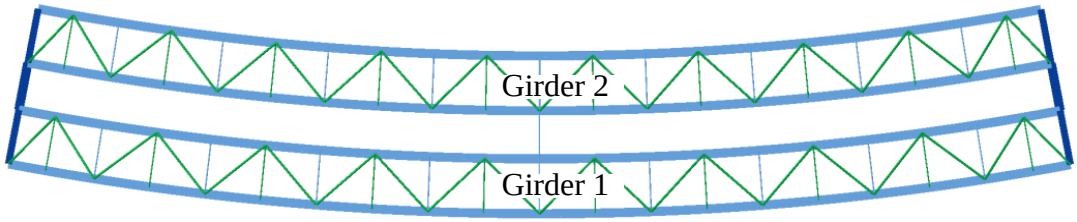

Figure 6.8. NTSCR1 Bridge Layout.

Figure 6.15 shows the external forces H_i, H_e and V from the external intermediate cross-frame and the associated distances. In Figure 6.15 a is the tub-girder width and h_K is the cross-frame bottom to top chord distance. To bring the girders to a position where the external cross-frames can be connected, a set of forces capable of generating an equivalent torsional moment should be applied.

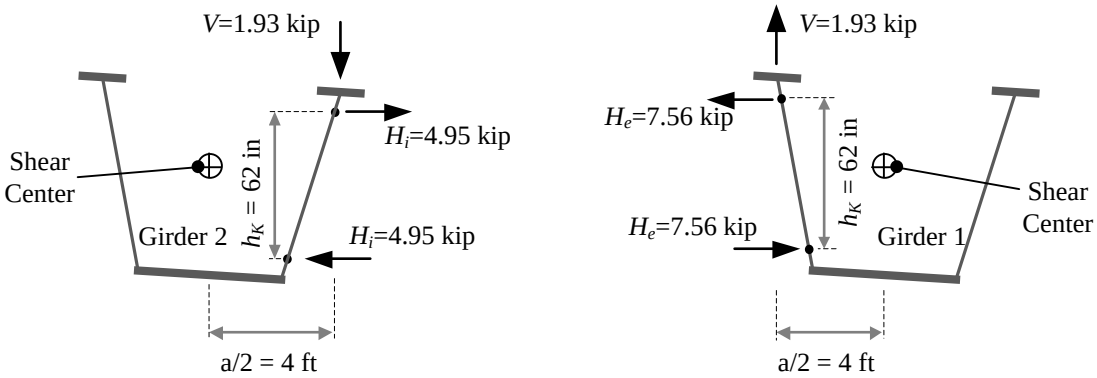

Figure 6.9. External forces on the girders required to connect the external cross-frame.

Form Figure 6.15 the required torsional moments are:

$$T_1 = H_e h_K - V\frac{a}{2} = 7.56 \cdot 62 - 1.93 \cdot \frac{96}{2} = 376\text{kip} \cdot \text{in} = 31.4\text{kip} \cdot \text{ft}$$

$$T_2 = -H_i h_K - V\frac{a}{2} = -4.95 \cdot 62 - 1.93 \cdot \frac{96}{2} = -399\text{kip} \cdot \text{in} = -33.3\text{kip} \cdot \text{ft}$$

Girder 2 must be rotated an additional amount with respect to the associated rotation originated from curvature only by applying a torsional moment T_2. The rotation due to curvature on Girder 1 must be reduced by applying the torsional moment T_1. Depending on the procedure used to connect, the associated fit-up forces can be calculated based on the torsional moments T_1 and T_2.

An alternate solution to this problem relies on detailing the external intermediate cross-frames to fit the geometry of the displaced bridge under steel dead load. The procedure is referred as Steel-Dead-Load-Fit for the cross-frames. This procedure reduces the forces due to displacement incompatibilities but requires evaluation of the bridge behavior possibly recurring to refined analysis methods.

6.2.3 Shoring

The above scenarios are dependent on the shoring provided for the erection stages. Since the tub-girder bridges are generally detailed for a No-Load-Fit they are expected to stay at a zero load configuration, meaning that enough temporary supports such as shoring towers and lifting cranes should be available during construction. In other cases, it is expected that during the bridge construction, the erector is ready to deal with the displacement incompatibilities.

The simplest solution, but not the most economically preferred, uses shoring towers to guarantee the no-load configuration. The number of shoring towers and location is defined by the amount of allowable displacement, splice locations and the erection stage and is highly dependent on the specific job conditions.

6.3 Concrete Deck Placement

Once the girders have been successfully erected, the next construction stage involves the casting of the concrete deck. In this stage, the girders are the only elements supporting the entire load as the temporary supports are usually removed.

When the concrete deck is cast, the bridge may experience significant displacements of larger than $L_{as}/300$, and once the deck cures the displacements are permanent. These displacements and rotations under concrete deck dead load must be accurately evaluated via the methods described previously in order to provide an adequate girder camber and prevent undesired concrete deck profile (see Fig. 3.10). To achieve the final desired elevations, the girders generally are cambered to accommodate the relative girder displacements. This usually involves vertical and rotational camber but since the combination of both vertical and rotational camber is not desired (NSBA, 2006), a possible solution for deck thickness control is the inclusion of external intermediate cross-frames.

6.3.1 Deck Thickness Control

As a result of the eccentric loading, curvature and skew, differential vertical displacements between girders are expected. These can cause undesired changes in the slab profile which may lead to uneven loads in the cross-section and deficiencies in the composite action of the system.

Helwig et al. (2007) developed equations to control the maximum permissible deviation of the slab thickness. By fixing the value of the critical or allowable relative vertical displacement to $\Delta_{max} = 0.5$ in, Helwig et al. provide an approximate equation to determine the maximum external intermediate cross-frame spacing, L_{max}, as

$$L_{\max} = \left[\frac{0.6}{\frac{5w\beta_0 (a+c)}{384EI}\left(\frac{EI}{GJ} - 3\right)} \right]^{1/3} \tag{6.5}$$

where w is the distributed vertical load per unit length, β_0 is the span subtended angle, a is the tub-girder top width, c is the girder spacing, E and G are the steel elasticity and shear moduli and I is major-axis moment of inertia and J is the torsional constant of the girder.

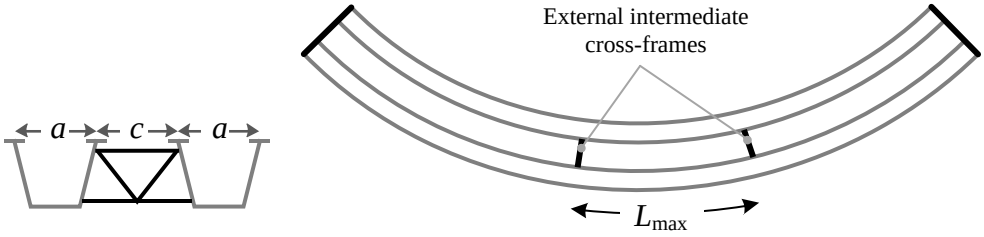

a) Cross-section b) Plan view

Figure 6.10. External intermediate cross-frame spacing.

The above equation is based on simply-supported girder behavior. However this approach provides a conservative solution to continuous-span bridges since the development is based on simple-span displacements, and the displacements are expected to be smaller for a comparable continuous-span. During the design stages the use of external intermediate cross-frames should consider the additional forces that these transmit to the internal cross-frames. Also, the use of external intermediate cross-frames limits the accuracy of the line-girder analysis method.

Relative vertical displacements larger than 0.5 in can be accommodated in the girder cambers and vertical haunches. In consequence, the external intermediate cross-frames can be avoided to control the relative girder vertical displacements. However, this practice relies in accurate vertical displacements and twist rotations predictions by the analysis method.

6.3.2 Phased Construction

Twin tub-girder bridges are the most common configuration in practice. This is mainly because they are commonly used as narrow ramps in highway interchanges. The maximum number of girders built at once is usually 3. Bridges with more than 3 tub-girders are often built in longitudinal phases, with two to three girders in each phase, connected by closure pours. This type of construction takes advantage of the girder

torsional stiffness which allows narrow units and the construction scheme brings benefits for replacement bridges as they allow opening one section to traffic while the remainder of the bridges is constructed.

From the construction engineering point of view it becomes essential to correctly estimate the girders final configurations in order to provide a uniform and leveled closure pour. This is the common problem with phased construction of any type of bridges. This type of construction scheme does not permit the use of external intermediate cross-frames between phases as the constructed phase is subjected to a total dead load having an important difference on displacement between the already constructed phase and the new one.

6.4 Bearing Behavior and Uplift Prevention

The geometric characteristics of the tub-girders provide diverse alternatives for positioning the bearings. In some cases, the designer can opt for a twin bearing configuration to take advantage of the bottom-flange dimensions and reduce the amount of load transferred to the bearings. Figure 6.17 illustrates an example of the single and twin bearing configurations.

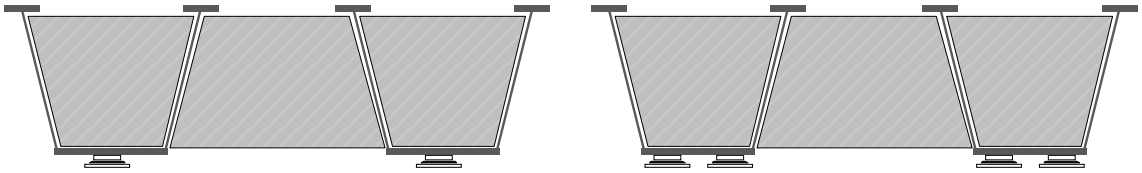

a) Single bearing configuration b) Twin bearing configuration

Figure 6.11. Single and twin bearing configuration for tub-girder systems.

In cases with girder torsional moments, the twin bearing configuration could lead to undesired problems as overload of one bearing and in some extreme cases to support uplift.

The ETSSS2 bridge utilizes the double bearing configuration shown in Fig. 6.17b. Since this bridge has skewed supports the girders are subjected to twist rotations which trigger uplift at the supports. The support uplift redistributes the reaction forces. Since the bearings are not capable of restraining the vertical movement, the reaction in one of the

twin supports is significantly increased. The 3D FEA analysis provided the vertical reactions shown in Figure 6.18 which indicated negative (uplift) reactions. The 3D FEA analysis was switched to unidirectional supports to prevent the development of false tie downs at the bearings.

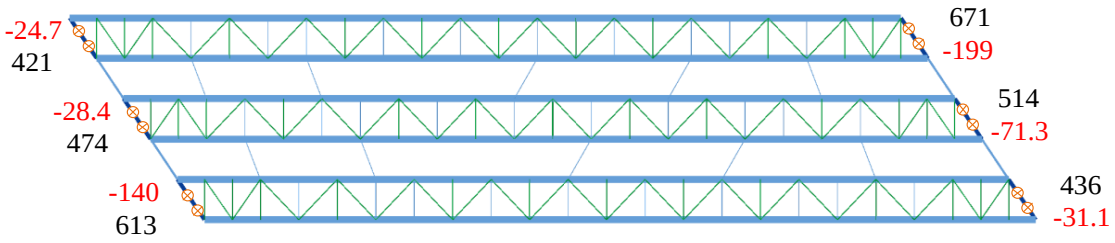

Figure 6.12. Vertical reactions in kip from the 3D FEA.

The field observations in this bridge did not report uplift. However, the analysis reported very small upward displacements that could have been overshadowed by several factors occurring during construction such as the inherent flexibility of the bearing pads, camber effects, etc. The effects of imminent bearing uplift, as those described herein, are only captured when the 3D FEA is used or by modeling the actual bearing offset on the 2D-grid.

1D line-girder analyses are unable to correctly report the behavior of twin bearings. Traditional 2D-grid models require modifications to the grid to locate the bearings at their correct locations which allows accounting for the twin bearing effect. Figure 6.19 shows a simplified grid model accounting for twin bearings spaced a distance *d*. A rigid element should be used between the twin bearings.

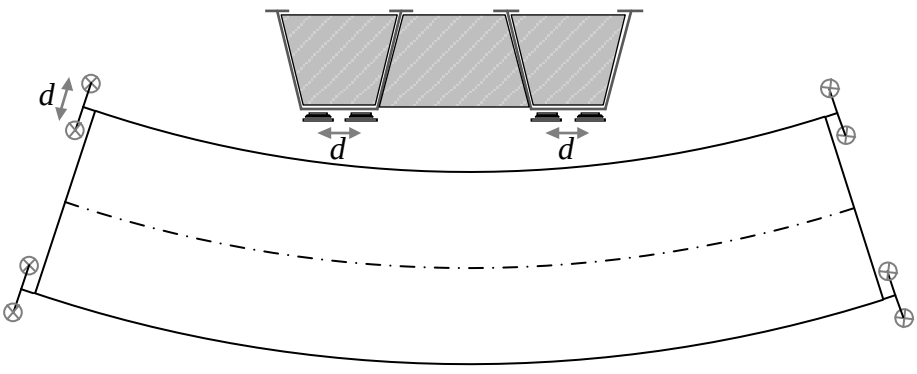

Figure 6.13. Grid modeling of the twin bearing systems on tub-girders.

This modification provides an estimation of the effects of the support system which in some cases may experience upward reactions (negative reactions), mainly due to the high torsional moments transferred to the supports. When negative reactions result from the analysis, it is necessary to consider this upward force on the bearing design. If the bearing is not capable of resisting upward forces the system may be experiencing imminent uplift at the supports. In practice, due to multiple variables and expected imperfections, the uplift may not be noticeable but must be considered in the analysis by removing the support with negative reaction and re-analyzing the model.

In addition, any individual bearing on a twin configuration in the tub-girder bridges should be designed to resist the total load vertical reaction force and the advantages expected by dividing the reaction halfway in a twin bearing configurations may be lost. The use of twin bearing system on tub-girder bridges subjected to any torsional loads or eccentric loading is highly discouraged as it requires further analysis and the resulting design may not be able to take advantage of a reduced design load.

6.5 Skew interactions

The effect of skewed supports directly impacts the girder torsional moments and rotations. The tub-girder behavior when skewed supports are present is described in Chapter 3. Additionally, the skewed supports make adjacent girders have different span lengths, which then results in different bending and torsional stiffnesses of the girders. Also, the skewed support line diaphragm has an increased length, resulting potentially in a reduced stiffness when compared to a radial line support diaphragm. Therefore, the Equations 2.29 and 2.30 must use the skewed length to estimate the appropriate strength and stiffness. The skew induced girder rotations, torsional moments and different initial geometries affect:

- The support diaphragm lack-of-fit forces: in addition to the increased moments, the associated lengths are affected.
- The forces required to connect the external intermediate cross-frames: the displacements and rotations are directly affected and these are input to the forces equations.

- The relative vertical displacements and rotations during deck placement: due to changes on adjacent girder stiffness.

Due to the complexity of the interaction between girders with skewed supports, the use of external cross-frames should be studied and the use of skewed external intermediate cross-frames avoided. However the use of external intermediate cross-frames may bring additional forces that would not benefit the design. Alternate methods to control the girder relative vertical displacements that affect the slab profile should be used, these include accommodating the relative displacements with girder haunches and modifying camber of the girders.

CHAPTER VII.

CONCLUSIONS

7.1 Summary

This dissertation addresses the construction engineering of tub-girder bridges. Tub-girder bridges have advantages over other steel girder systems since their torsional properties are multiple times higher that of a comparable open section girder. They rely on the quasi-closed and reduced cross-section distortional characteristics of the girders provided by the top flange lateral bracing system and internal cross-frames, these characteristics simplify the analytical representation of the system.

Simplified mechanisms and 1D, 2D and 3D analytical studies are used to evaluate and provide estimations of the effects of skewed supports on tub-girder bridges during steel erection and concrete deck placement. The effect on the bracing components and the interactions with the top flanges are studied to provide estimates of the additional forces due to interactive effects.

Additionally, the 3D analytical studies are used to evaluate the accuracy of the simplified analysis methods for the prediction of construction conditions.

7.2 Research Contributions

An important original contribution of this research is that the data generated constitutes the first systematic study on a large set of curved and skewed tub-girder bridges using consistent advanced 3D FEA models to model construction forces and deformations. As such, the results of this research can serve as a benchmark for current and future improvements in methods of analysis and design for the construction engineering of curved and skewed tub-girder bridges. In the current research, this data has been used in both straight and curved tub-girder bridges to provide the following contributions.

7.2.1 Effects of Skew on the Girder Internal Torque

The main contribution of this research is the evaluation of the torsional effects of skewed supports to the girder response and the possibility of estimating the associated forces on the tub-girder components using simplified 1D analysis methods. This is possible by the study of simplified mechanics models which result in equations for the evaluation of the additional torque caused by the skew for both simple and continuous-span bridges.

The interaction of skewed supports and rigid bearing line diaphragms creates a mechanism in which the major-axis bending rotation (ϕ_y) on the girder are restrained by the diaphragm causing a twist (ϕ_x) to the girders. In spite of the diaphragms not being physically rigid, treating the bearing line diaphragms as rigid provides a good estimate of the girder internal torques. Equation 7.1 estimates the girder twist (ϕ_x) at the support as a function of the girder bending rotation (ϕ_y) and skew angle (θ). The major-axis bending rotation at the support (ϕ_y) is estimated by line-girder analysis.

$$\phi_x = -\phi_y \tan(\theta) \tag{7.1}$$

The skew induced girder twist rotations are expected to vary linearly along the span of the bridge. Therefore, the girder twist at a position *s* along the span is proportional to the skew induced rotation at the left and right supports, ϕ_{x1} and ϕ_{x2}, as

$$\phi_x(s) = \phi_{x1} - (\phi_{x1} - \phi_{x2})\frac{s}{L} \tag{7.2}$$

The effects of skew equations assume skew angles measured with respect to a line perpendicular to the bridge centerline, i.e., a curved bridge with radial supports has zero skew angle.

7.2.1.1 Simple-Span Straight Tub-Girder Bridges

The skew creates discrete girder torques at the supports. The torques are calculated at each support (1 and 2) resulting on a torsional moment distribution assumed constant and equal to the sum of the discrete torques. The girder torsional moments are

estimated by multiplying the girder torsional stiffness *GJ/L*, or the mechanical equivalent for multiple cross sections along the span length, by the relative girder twist rotation $\phi_{x1}+\phi_{x2}$. The resulting torsional moment due to skewed supports in terms of the major-axis bending rotations ϕ_{y1} and ϕ_{y2} is

$$T_S = -\frac{GJ}{L}\left(\phi_{y1}\tan\theta_1 + \phi_{y2}\tan\theta_2\right) \tag{7.3}$$

where *G* is the shear modulus, *J* is the torsional constant of the girder, *L* is the span length and θ_1 and θ_2 are the skewed supports angles.

7.2.1.2 Curved and Skewed Tub-Girder Bridges

In curved and skewed bridges, Eq. 7.3 is used to estimate the additional effect due to skewed supports. The torsional effects due to skew are supplementary to those caused by the curvature. The torsional moments and twist rotations are estimated by

$$T(s) = T_C(s) + T_S \tag{7.4}$$

$$\phi_x(s) = \phi_{x,C}(s) + \phi_{x,S}(s) \tag{7.5}$$

where $T_C(s)$ is given by Eq. 7.6 and simplifies to Eq. 7.7 for simple-span bridges, $\phi_{x,C}(s)$ is given by Eq. 7.8.

$$T_{C0} = \frac{1}{L}\int_0^L \frac{M(s)}{R}(L-s)\,ds \tag{7.6}$$

$$T_C(s) = \frac{wL^3}{24R} - \frac{ws^2(3L-2s)}{12R} \tag{7.7}$$

$$\phi_{x,C}(s) = \frac{1}{R}\left(1+\frac{EI}{GJ}\right)\Delta(s) \tag{7.8}$$

In these equations, *w* is the uniformly distributed vertical load, *M*(*s*) the major-axis bending distribution, *R* is the curvature radius, *I* the girder moment of inertia and Δ(*s*) the vertical displacement estimated by line-girder analysis.

7.2.1.3 Continuous-Span Bridges

For evaluating the skew effects on continuous-span bridges, Eqs. 7.1 provides the girder twist at each on the skewed supports on the bridge. The torsional moment along the span is equal to the sum of the discrete torques at the supports adjacent to the span and is estimated by Eq. 7.3. The torsional moments do not transfer to the contiguous span. For intermediate skewed piers the skew induced twist and rotations are also proportional to the bending rotation at the support. This means that in a continuous-span bridge, the intermediate skewed pier causes two equal in magnitude but opposite in sign torsional moments for the spans adjacent to the pier.

7.2.1.4 Skew-Curvature Torsion Index

A Skew-Curvature Torsion Index, I_{SC}, is provided for the estimation of the portion of torsion associated to the skewed supports. For a simple-span implementation, the equation simplifies to

$$I_{SC} = \frac{J}{I}\frac{\tan\theta_1 + \tan\theta_2}{2.675\alpha} \tag{7.9}$$

where α is the girder subtended angle and all the other terms have been previously defined. For unskewed configurations the skew-curvature index yields a zero value, for straight and skewed bridges the index is undefined. Intermediate values of the index provide the ratio of the skewed support effects to the maximum torque due to curvature.

This equation provides a clear value to help understand when the effects of skew are important for curved and skewed bridges and can be used on the early stages of the geometric design to assess the amount of skew effects and define the bending and torsional properties, I and J, to limit the amount of skew torsional moment. Despite the equation being developed for simple-span bridges, it provides an estimate of the combined effects if applied to the individual spans of a continuous bridge.

To estimate the total girder torque distribution $T(s)$ based on the I_{SC} index, the torsional moment due to curvature $T_C(s)$ can be shifted an amount equal to $I_{SC} \cdot T_{C0}$ as

$$T(s) = T_C(s) + I_{SC} T_{C0} \tag{7.10}$$

where T_{C0} is the torque at the support for simple-span curved bridge equal to $wL^3/(24R)$. As with previous developments, this is a conservative estimate since the interaction of the external intermediate cross-frames is ignored in the development.

The equations presented are essential for 1D line-girder analysis methods since the effects of skew are not captured otherwise. Even though 1D line-girder analysis is not the most common approach for the design of the bridge, it is still used to estimate the behavior of the bridge in the early stages of the design process.

7.2.2 Effects of Skew on Bracing Component Forces

The benefits of the tub-girder behavior are achieved in part by the various bracing components in the system. In the past, several contributions have been made to the State of the Art and it is possible to evaluate the forces due to the bending, torsional and distortional loads on the bracing by the use of a set of component force equations.

As part of this research, the bracing force equations are evaluated to study the possibility of changes to include the torsional effects induced by the skewed supports. The skewed support effects are shown to predominantly influence the girder twist rotations and torsional moments. The effects on the distortional loads are shown to be negligible for skew angles used on the tub-girder bridges studied in this dissertation. The effects of skew may be estimated individually for each girder by estimating the overall girder twist rotations and the corresponding torsional moments assuming that the bearing line diaphragms are rigid. The corresponding torques can then be input to the component force equations developed by Fan and Helwig (1999 & 2002) to determine the component forces. The corresponding twist rotations including skew effects and vertical displacements from a line-girder or a grid analysis without external cross-frames are input to Helwig et al. (2007) to determine the external intermediate cross-frame forces.

In summary, when skew is present the top flange lateral bracing would experience a change in the input shear flow and the external intermediate cross-frames would experience changes in the input girder twists used to evaluate the forces on its

components. The effects of skewed supports on tub-girder cross-section distortion have been shown to be negligible.

7.2.3 Top Flange Stresses and Localized Effects Due to Bracing Interactions

The tub-girder top flanges experience additional stresses due to the forces induced by the top flange lateral bracing. Previous work has provided equations to include the lateral bending stresses that result from the interaction of the lateral components at the work points of the top truss.

The research work studied the effects on the axial stresses induced by the longitudinal components of the load generated by the top truss interaction. The effect on the axial stresses is proportional to the top flange lateral bracing diagonal forces. These forces are dependent on the girder bending moments and, typically to a larger extent, on the girder torsional moments. These torsional moments depend on the curvature radius and skew angles.

The local increment in the girder flange longitudinal normal stresses due to the above diagonal forces is often disregarded since most of the analytical observations have been made on curved and radial and tangent bridges. On curved and radial bridges this effect is minimal at the location of maximum stresses and on tangent bridges the effects are negligible. However, on straight and skewed bridges the torsional effects are approximately constant and the effect of the interactive forces too, this means that at the locations of maximum stress the increments on the stresses are noticeable and important.

To address the above interactive force effects, a solution is presented to include the changes on the axial stress by means of an additional sawtooth stress which is superimposed on the bending stress f_b calculated using the girder cross-section major-axis bending moment. The magnitude of this sawtooth stress is proportional to the residual force P equal to the difference of the longitudinal components of the diagonals forces $D_{Tot,i}$ and $D_{Tot,j}$ given by

$$P = D_{Tot,i} \cos\alpha_i - D_{Tot,j} \cos\alpha_j \tag{7.11}$$

where α_i and α_j are the angles of two consecutive diagonals measured from the centerline of the flange. The load *P* acts longitudinally at the truss work point and creates a stress equal to *P* divided by the area of the top flange. The sawtooth stress creates tension to one side of the juncture of the diagonal with the flange and compression on the other. For simplicity, the stress is distributed in half to each side of the flange, resulting on a variation similar to the one shown in Fig. 7.1.

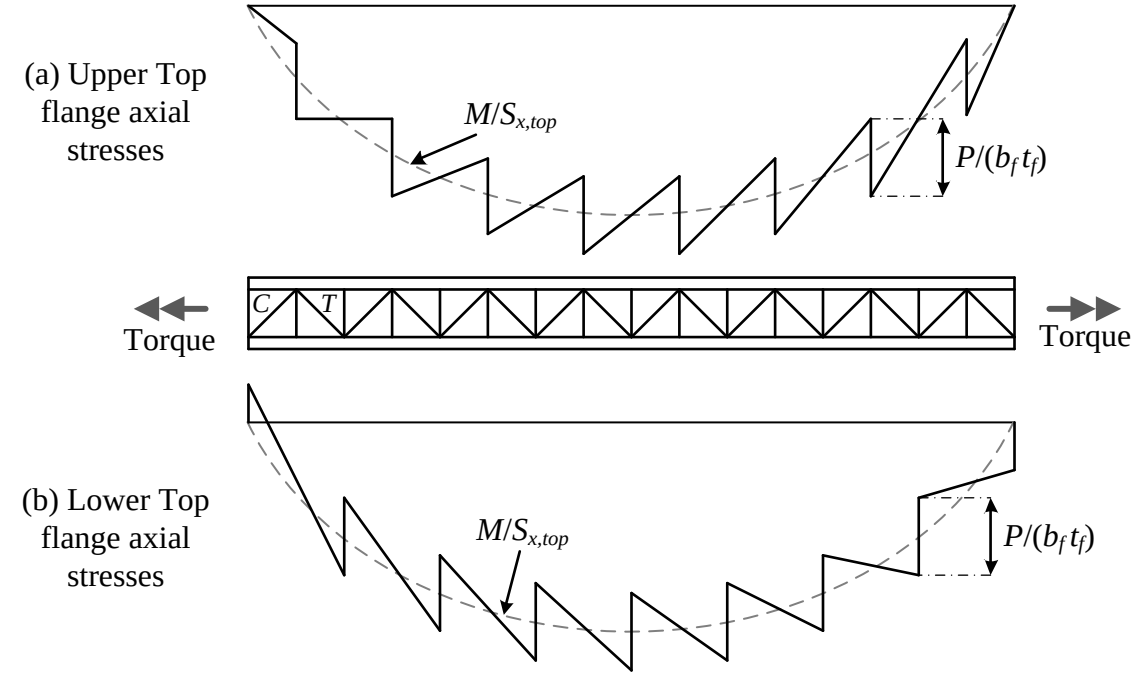

Figure 7.1. Top Flange sawtooth major-axis bending stresses due to the top flange lateral bracing interactive forces

The total flange normal stress is determined as

$$f_{b,TFLB} = f_b \pm \frac{P}{2b_f t_f} \tag{7.12}$$

where b_f and t_f are the top flange thickness and width.

7.2.4 Assessment of the Simplified Analysis Methods

This dissertation presents the assessment of the 1D line-girder and 2D-grid analysis methods for tub-girder bridges. The evaluation is based on comparisons with refined 3D FEA benchmark results.

The simplified analysis methods provide flexibility for the design process and the level of analysis is an important decision in the process. The simplest analysis methods are used at the early stages of design to pre-dimension the girders and components so the accuracy of these should be well known to reduce the number and complexity of design iterations. The analysis methods selection is also based on the bridge characteristics based on the assumption that regular geometries are relatively easier to model by the simplified methods.

The comparisons were carried for a set of existing and parametric bridges. The categories used for the evaluation are the major-axis bending stresses, girder torques, vertical displacements, top flange lateral bending stresses, bracing components forces and girder layover at bearings. The assessment summary dictates that:

- The major-axis bending stresses, vertical displacements and girder layover at bearings are properly estimated by any simplified analysis method, the 2D-grid analysis provides better estimations as the lack of accuracy is expected from the line-girder analysis as the interaction between girders cannot be modeled.
- The top flange lateral bending stresses are conservatively estimated.
- The top flange lateral bracing and cross-frame component forces are dependent on the bending and, mostly, on the torsional response; therefore, the errors are mainly caused by the low accuracy on these estimates. The bracing components evaluation often ranks as conservative.
- The torsional moment diagrams reveal that the general behavior is captured correctly and that the interaction between girders is a source of error since the simplified analysis methods have limited modeling capabilities for the interaction between girders. In consequence, the girder

torsion is estimated accurately provided that the interactions between girders are limited and that the tub-girder bridge geometry is uniform.

The sources of errors in the estimation of the torsional moments on the studied bridges are summarized as

- External intermediate cross-frames cause additional torsional effects which are usually ignored by 1D analysis methods.
- Larger errors are expected as the number of external intermediate cross-frames increase. The use of skewed external intermediate cross-frames increases the errors.
- Lack of external support diaphragm at intermediate piers.

Additionally, for the studied bridge using Pratt top flange lateral bracing system, evidence was found that suggested that the simplified analysis methods would experience accuracy problems evaluating the girders torsional behavior.

For bridges, involving irregular top flange lateral bracing system, external intermediate cross-frames skewed layouts, flexible support diaphragms which do not meet the stiffness requirements, bridges using special support systems or integral abutments, and other bridges not meeting the AASHTO (2011) requirements, the 2D-grid is unable to provide accurate solutions and a 3D FEA analysis is necessary.

7.2.5 Identification of Construction Issues

The contributions of this research for tub-girder construction are the identification of typical problematic scenarios and the quantitative force estimations to help deciding the adequate erection procedure. The scenarios identified are the bearing diaphragm and external intermediate cross-frames fit-up. The fit-up force calculation process uses simplified models to estimate the forces required to overcome the displacement incompatibilities.

Furthermore, the effects of the skewed supports are identified as additional displacements caused by the bending rotation and torsional compatibility. The developments in this dissertation provide simplified estimations of the skew induced

displacements that can affect the construction. These can be estimated by means of Eqs. 7.1 and 7.2.

$$\phi_x = -\phi_y \tan(\theta) \tag{7.1}$$

$$\phi_x(s) = \phi_{x1} - (\phi_{x1} - \phi_{x2})\frac{s}{L} \tag{7.2}$$

7.3 Recommendations for Future Work

This research provides information for the evaluation of the impact of skew effects during the construction stages of tub-girder bridges. It provides an assessment of analytical tools for the construction engineering of curved and skewed tub-girder bridges. There are a number of areas that merit further study. These are:

- Assessment of skew effects on live load responses. It is believed that for live loads the analysis of the bridge can be addressed as any other steel deck bridge. However, the effects on the complex details and the number of connections of the tub-girders bracing components may be subjected to the effects of fatigue loads. Some bracing components loading is highly reduced after the bridge reaches its composite characteristic, however, the effects on components away from the deck such as the bottom connections of the internal cross-frame and their connection plates may become important.
- The tub-girder support diaphragms and external intermediate cross-frames are detailed for locations matching the steel dead load. Specific studies that evaluate this procedure need to be evaluated as well as the possibility of the use of other detailing procedures.
- The scope of this study focused only on the steel erection and on single-stage concrete deck placement. Studies on sequential deck placement and early gain of strength of the concrete and the effects of skew should be studied to evaluate the performance of the analysis methods and general bridge behavior. The deck placement under the skewed end should be

studied for the effects of localized forces and additional layover. In addition, the early gain of strength changes the torsional stiffness of the bridge and thus the simplified torsional mechanisms should be reevaluated.

- The analysis of a bridge via a 1D analysis could be improved by a the inclusion of the additional shear forces due to the effects of external cross-frames, as is done for I-girder bridges using the V-Load method. An analogous application of the V-Load method to tub-girder bridges would provide a better understanding of the effects of the interactive forces in the torsional moments.
- Study the effects of the Pratt top flange lateral bracing layout to improve the component force equations accuracy and, if possible, take advantage of the internal bracing force interaction with the torsional response of the girder.
- Provide more specific guidelines to control the detailing procedures to take advantage of fit-up at different load conditions and the specification of girder cambers that prevent the use of external intermediate cross-frames.

APPENDIX A.

DETAILED DATA ANALYSIS

This appendix illustrates detailed analytical results of five tub-girder bridges. Each bridge is presented in a subsection with specific displacement, top-flange stresses, torsional moments and top flange lateral bracing forces.

Table A.1 shows the summary of the geometry of the bridges under study. These results are shown to help illustrate the discussions and exemplify the calculation procedures presented in Chapters 2 and 3. The bridges selected are four parametric bridges: (1) curved and radial, (2) straight and skewed, (3) curved and skewed and (4) continuous span. An additional existing straight and skewed bridge is presented which illustrates more complex geometry and layout.

The displacements, stresses, torsional moments and bracing forces are presented for the non-composite total dead load unless otherwise noted. No load factors are applied to the results. The equations in this appendix refer to the original numbering presented in the main body of the dissertation.

Table A.1. General description of detailed data analysis bridges.

Bridge ID	Description	Span Length	Curvature Radius	Deck Width	Skew Angles	Number of Girders
NTSCR1	Simple-Span, Curved, Radial Supports	150 ft	400 ft	30 ft	0°, 0°	2
NTSSS2	Simple-Span, Straight, Skewed Supports	150 ft	–	30 ft	30°, 30°	2
NTSCS29	Simple-Span, Curved, Skewed Supports	225 ft	820 ft	30 ft	15.7°, 0°	2
NTCCS22	Continuous-Span, Curved, Skewed Supports	250 ft, 250 ft	713 ft	30 ft	20.1°, 0°, 0°	2
ETSSS2	Simple-Span, Straight, Skewed Supports	205 ft	–	56.5 ft	33.4°, 33.4°	3

A.1 NTSCR1 Parametric Bridge

A.1.1 Description

This bridge is a simple-span, curved and radially supported parametric case. The top flange lateral bracing layout is illustrated in Figure A.1. Unless otherwise noted, the results are shown for the exterior girder (Girder 1) which is the girder with the largest radius of curvature.

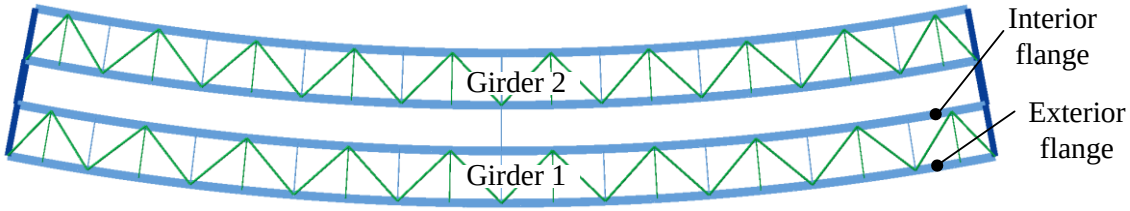

(L_1 = 150 ft / R = 400 ft / *deck width* = 30 ft)

Figure A.1. NTSCR1 Bridge Layout.

This bridge exemplifies the application of the M/R Method and how the torsional moments compare to other analysis methods. This case shows the sawtooth effects on the major-axis bending stresses on a curved bridge and how the implementation of this technique compares to the skewed cases. The effects of the external intermediate cross-frames and the internal cross-frames effects are also presented.

A.1.2 Displacements

The vertical displacements are readily available for the 2D-grider analysis and 1D line-girder analysis. The radial or lateral displacements for the 2D-grid analysis are a result of the girder twist rotations from the grid analysis. On the other hand, the 1D line-girder method relies on the M/R Method to evaluate the lateral displacements by calculating the girder twist rotation, $\phi_{x,C}(s)$, due to curvature in terms of the vertical displacement $\Delta(s)$ as

$$\phi_{x,C}(s) = \frac{1}{R}\left(1 + \frac{EI}{GJ}\right)\Delta(s) \tag{2.7}$$

where E and G are the steel elastic and shear modulus, R is the curvature radius, I is the moment of inertia and J is the St. Venant torsional constant of the girder. Figures A.2 and

A.3 illustrate the vertical and relative radial displacements for the three different approaches.

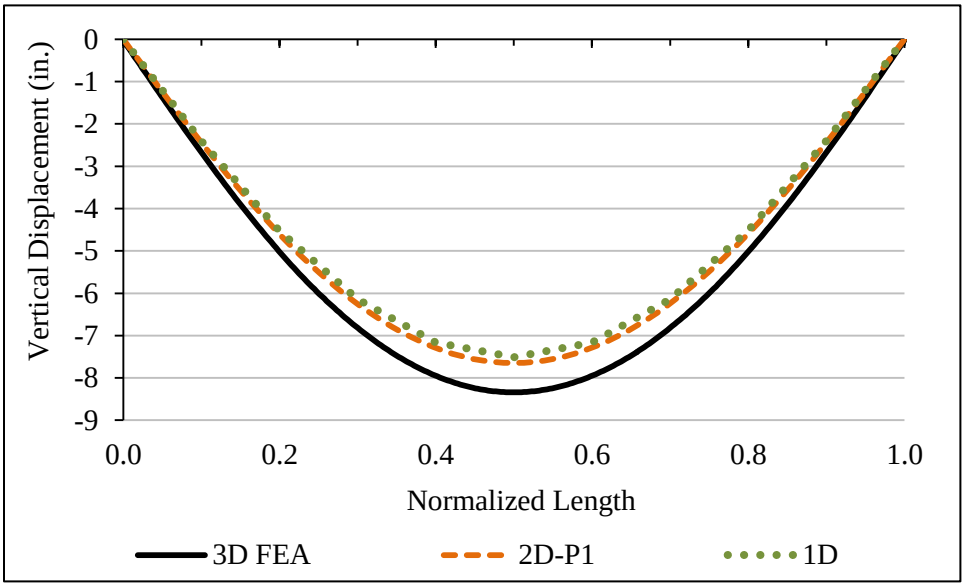

Figure A.2. Girder 1 centerline vertical displacements.

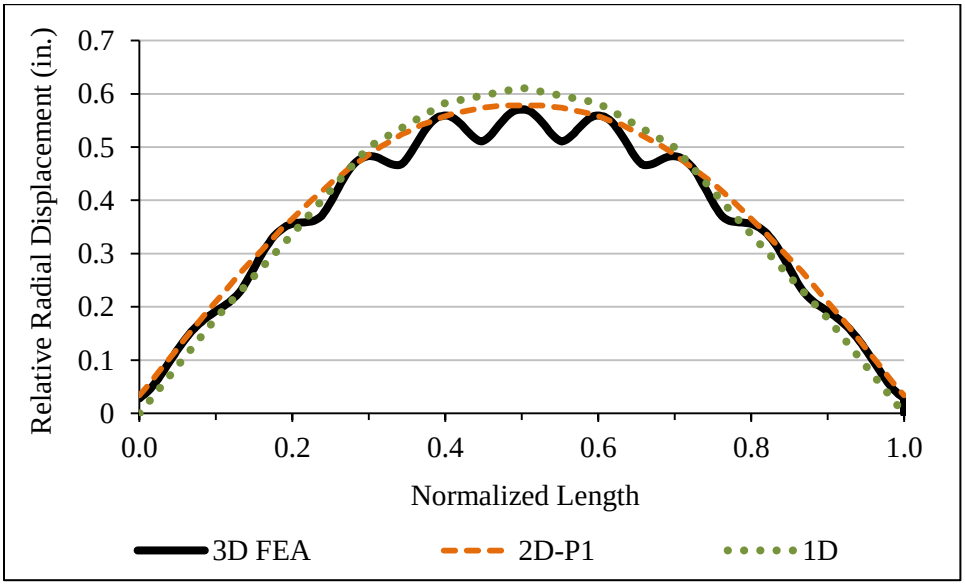

Figure A.3. Girder 1 relative lateral displacements.

The minor differences between analysis methods are due to the level of discretization of the model. In general, the results show a good agreement between all methods.

A.1.3 Top Flange Major-Axis Bending Stresses

The major-axis bending stresses results for the 3D FEA exhibited a sawtooth shape due to the interaction of the top flange lateral bracing system. The interaction is unaccounted on traditional 2D analysis and improvements on the analysis were discussed in Chapter 3. The improvements consist of including the effects of a force *P* defined as

$$P = D_{Tot,i}\cos\alpha_i - D_{Tot,j}\cos\alpha_j \tag{3.19}$$

where $D_{Tot,i}$ and $D_{Tot,j}$ are the total axial forces acting on consecutive diagonals and α_i and α_j are the angles of the diagonals. The force *P* causes a reduction of the axial stress on one side of the top truss work point and an increase at the other side. For simplicity it can be assumed that half of the force *P* acts as compression and the other half as tension. Therefore, for the top flange lateral bracing work points, the top flange maximum axial stress can be found as

$$f_{b,TFLB} = f_b \pm \frac{P}{2b_f t_f} \tag{3.23}$$

Figures A.4 and A.5 illustrate the top flange major-axis bending stresses on the exterior and interior top flanges of Girder 1 (see Fig. A.1). The axial stresses exhibit the sawtooth behavior due to the interaction of the top flange lateral bracing system.

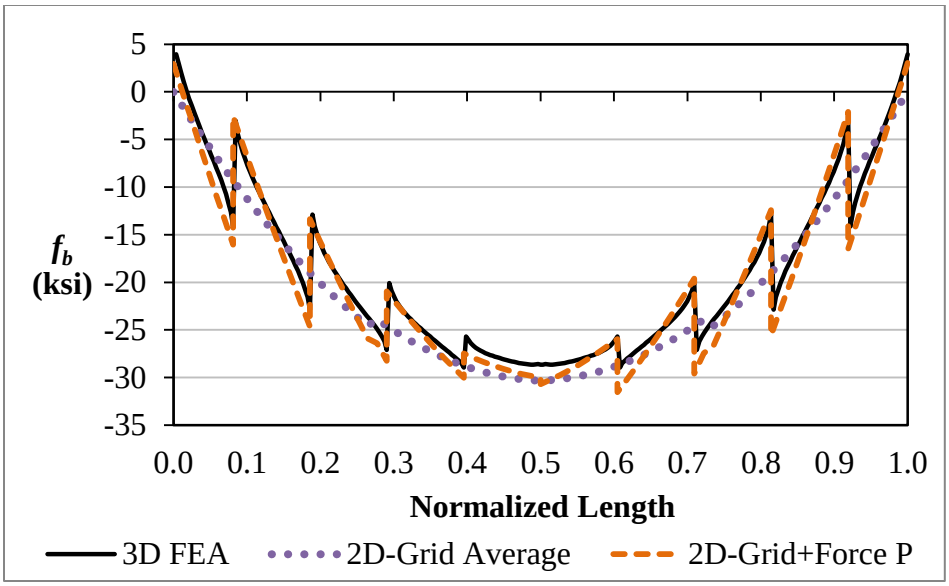

Figure A.4. Girder 1 top flange major-axis bending stresses at the exterior top flange.

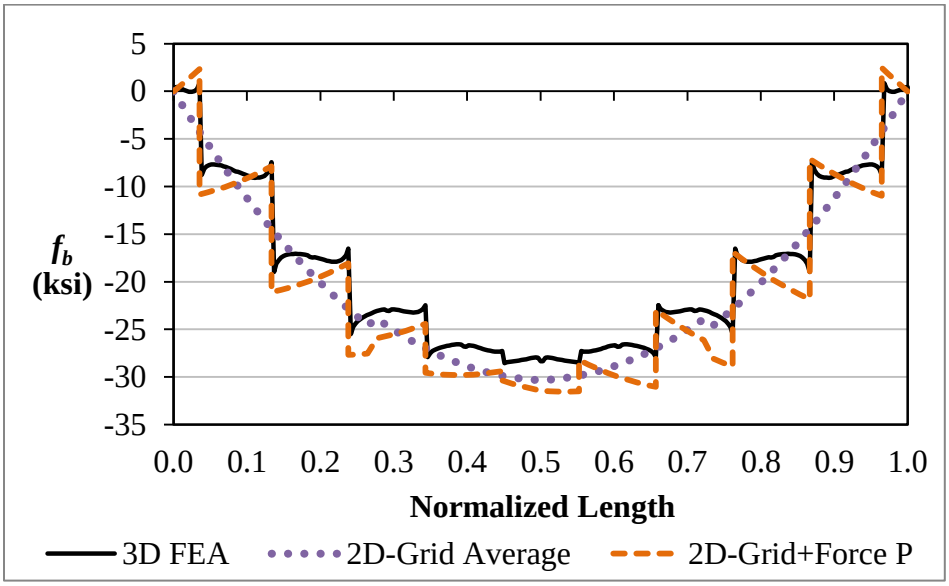

Figure A.5. Girder 1 top flange major-axis bending stresses at the interior top flange.

In the Figures A.4 and A.5 the sawtooth magnitude varies along the length of the bridge with maximum values close to the support. This effect is caused by the variation of the axial forces on the top flange lateral bracing diagonals shown in Fig. A.8 and these are mainly dependent of the torsional moment distribution shown in Fig. A.7.

A.1.4 Top Flange Lateral Bending Stresses

The top flange lateral stresses are calculated for the unbraced locations of the bridge where the stresses are expected to be higher. The results from 2D-grid are then only reported at the unbraced locations of the bridge. The 3D FEA analysis results, however, shows a more continuous variation of the lateral stresses.

The lateral stresses are calculated as a function of the lateral component of the vertical load and the effect of the strut force on the flange as shown in Eqs. 2.30 and 2.32.

$$f_{\ell,p} = \frac{0.6ps^2}{b_f^2 t_f} \tag{2.30}$$

$$f_{\ell,Bend} = \frac{1.5s}{b_f^2 t_f} S_{Bend} \tag{2.32}$$

The top flange lateral bending stresses are calculated as a function of the lateral component of the vertical load, the effect of the strut force on the flange and the effect of the lateral force due to curvature. A third component is exclusive of curved bridges and is additional to the stresses previously discussed. The additional stress due to curvature is described by Eq. 2.31.

$$f_{\ell,M/Rh} = \frac{0.6Ms^2}{Rhb_f^2 t_f} \tag{2.31}$$

Figure A.6 shows the lateral stresses on the girder top flanges from the 3D FEA and the calculated stresses for the 2D-grid analysis. As with other results, the equations report conservative estimates as the equations base their development on simplified estimations which do not consider the interaction with other components such as the webs.

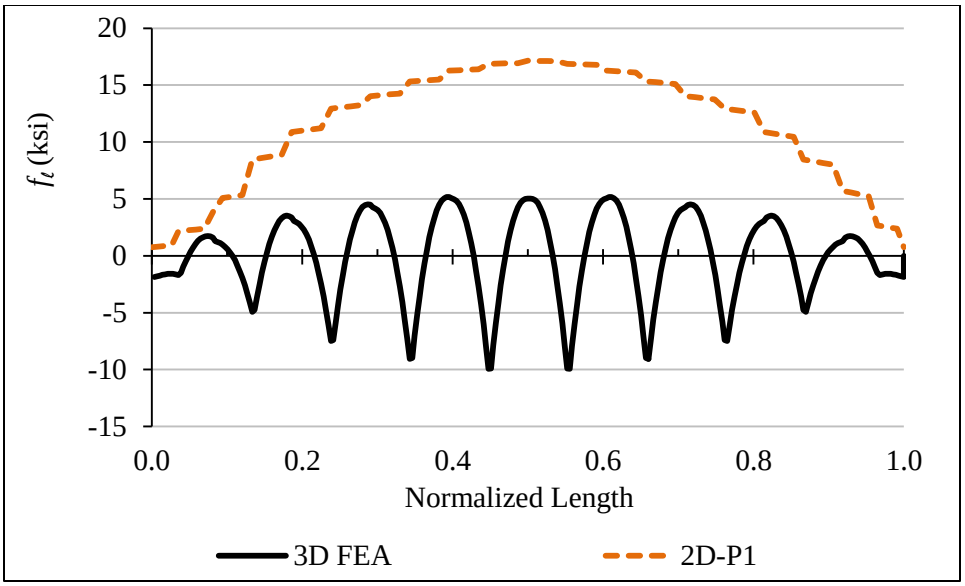

Figure A.6. Girder 1 top flange lateral bending stresses at the exterior top flange.

The effect of curvature results in a curved distribution of stresses between bracing points shown in Fig. A.6. Figure A.20, in contrast, shows a linear variation between points for the straight and skewed case.

A.1.5 Torque Due to Curvature

The torsional moment estimations for the 3D FEA, 2D-grid and M/R Method for 1D line-girder analysis are shown in Figure A.7. These results show good agreement in the magnitude and distribution of the torsional moments and only slight differences are evident at the midspan or 0.5 of the normalized length, where an internal intermediate cross-frame is present between girders.

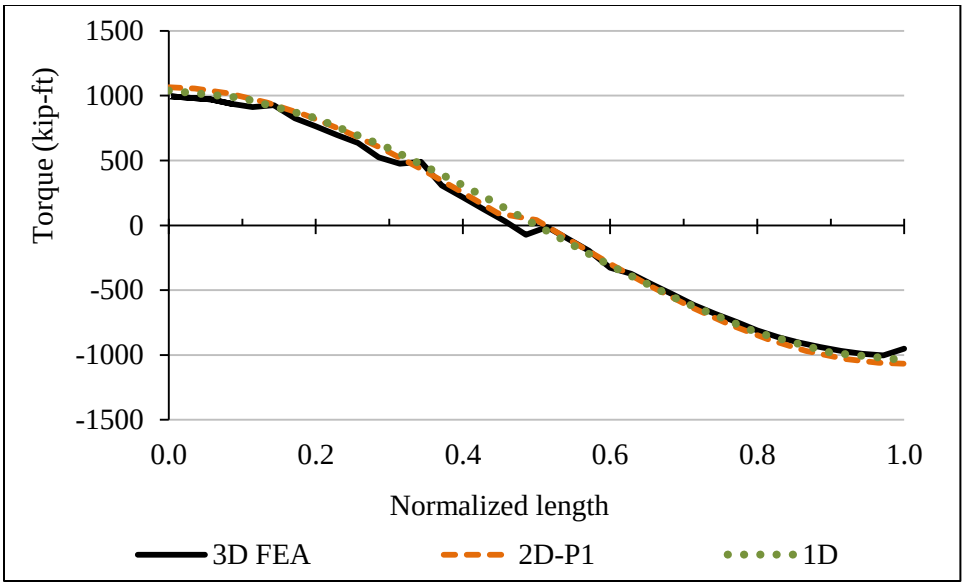

Figure A.7. Girder 1 torsional moments.

The 2D-grid analysis provides results directly from the analysis while the 1D method uses the M/R equations. For a simple-span case the, torsional moment distribution results on Eq. 2.6

$$T_C(s) = \frac{wL^3}{24R} - \frac{ws^2(3L-2s)}{12R} \tag{2.6}$$

This equation relies on the known major-axis bending moment distribution of a simple-span bridge. For continuous span bridges the equation may yield incorrect predictions since the equation is found by the integration of the bending moment distribution of a single span. However, Eq. 2.6 provides a conservative estimate of the maximum torsional moment in the span when $s = 0$.

A.1.6 Top Flange Lateral Bracing Diagonals and Struts

The axial forces on the diagonals are shown for Girders 1 and 2 in Figures A.8 and A.9. The differences between the girder forces are due to the reduced girder lengths that has large impact than the reduced curvature. The forces are separated by negative and positive values. The forces are represented as points and joined by lines for presentation purposes. The offset along the length of the bridge are the result of the point

where the result was reported for each method: for the 3D FEA at the midpoint of the element, for the 2D at the truss work point and for the 1D at the tenth point.

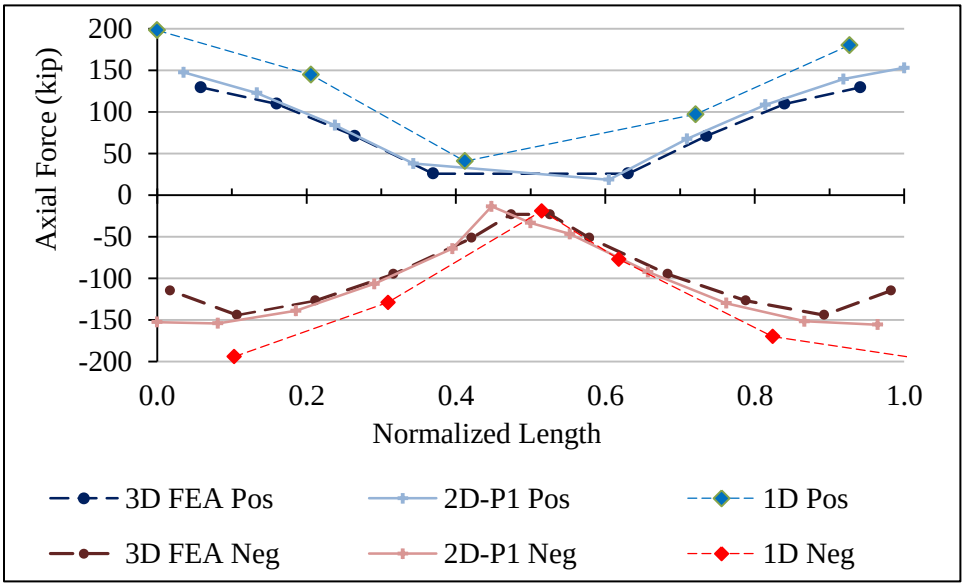

Figure A.8. Girder 1 top flange lateral bracing diagonals axial forces.

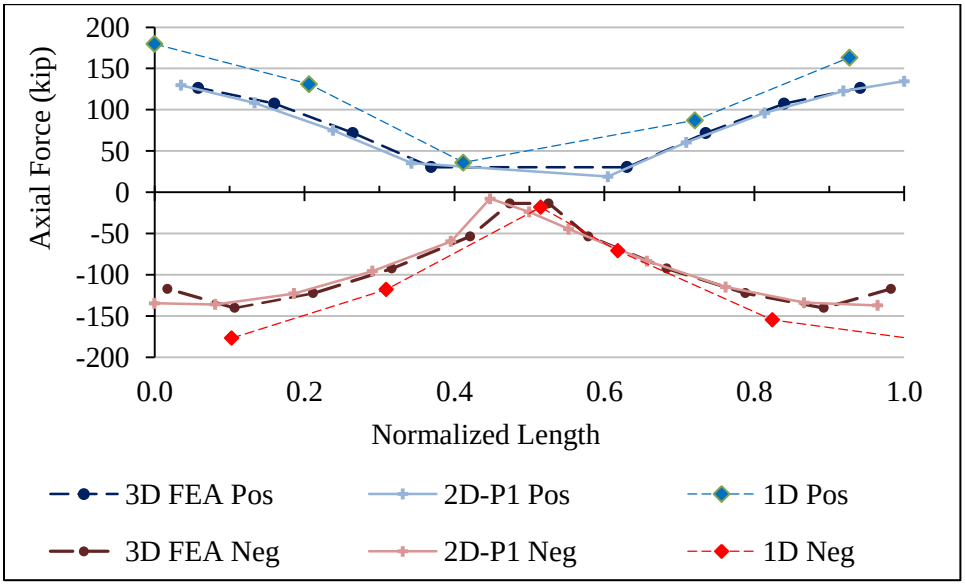

Figure A.9. Girder 2 top flange lateral bracing diagonals axial forces.

Figures A.10 and A.11 illustrate the axial forces on the struts on both girders. At the locations where internal cross-frames are present, the 3D FEA plot reports two forces corresponding to both sides of the cross-frame top chord. The difference on the forces is the result of the load transferred by the cross-frame diagonal. The 2D-grid and 1D

line-girder include the effect of the internal cross-frame but only report the maximum value at each location. The maximum strut forces are appropriately captured in cases where the forces are additive. However, when the internal cross-frame force is subtracted little accuracy is shown.

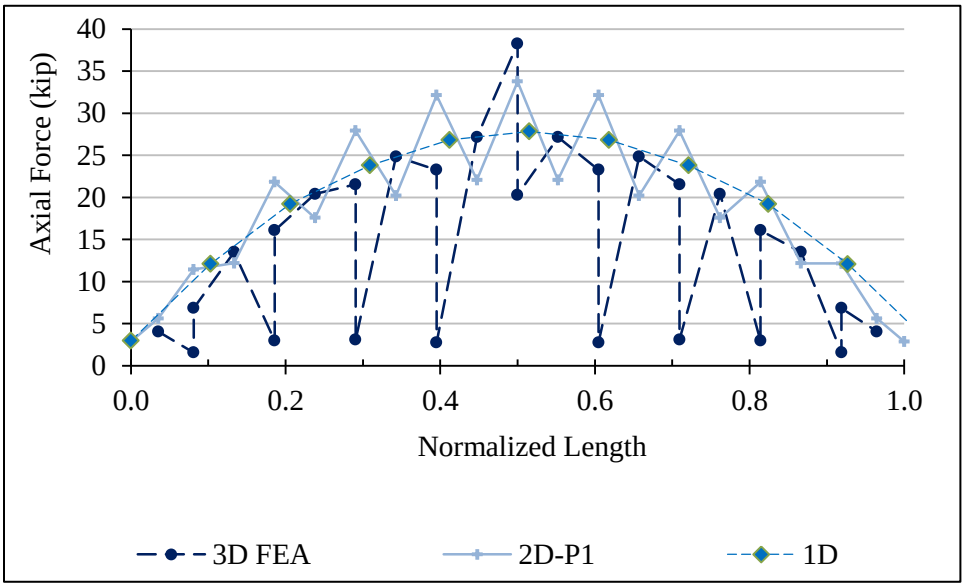

Figure A.10. Girder 1 top flange lateral bracing struts axial forces.

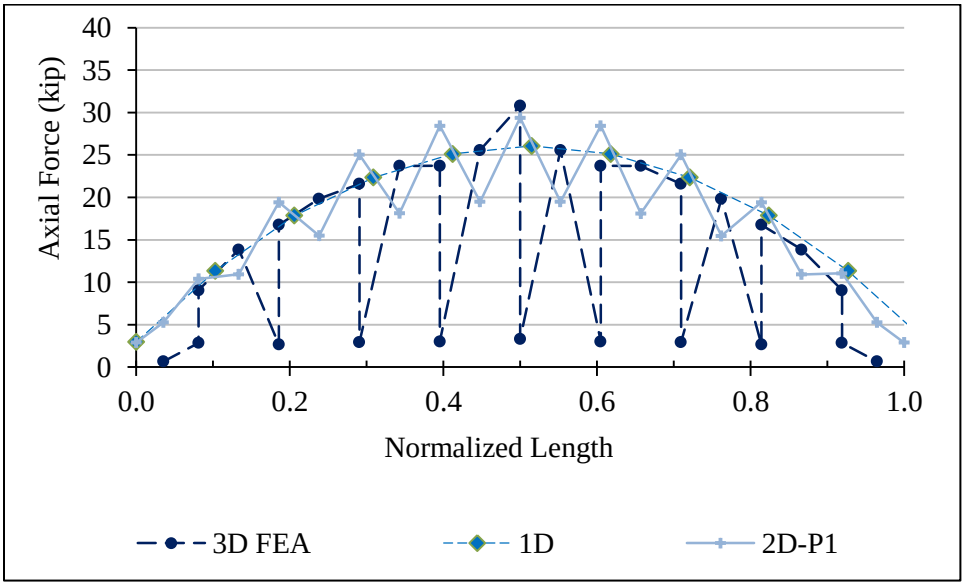

Figure A.11. Girder 2 top flange lateral bracing struts axial forces.

At 0.5 of the normalized length on Figures A.10 and A.11 a surge on the strut forces on the girders occurs. The increase from the average force at the 0.5 location is

approximately 12 kip for Girder 1 (exterior) and 5 kip for Girder 2 (interior). This is caused by the interaction between girders due to the external intermediate cross-frame.

The calculation of the external cross-frames and the forces acting on the girders are shown next based on the equations presented in Chapter 2. The external intermediate cross-frame internal forces F_T, F_D and F_B and the associated external reactions H_i, H_e and V are shown in Figure A.12.

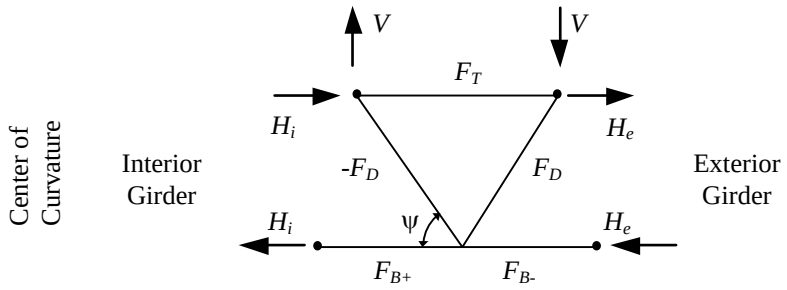

Figure A.12. External intermediate cross-frame internal forces and external reactions.

The forces in Fig. A.12 depend on the relative vertical displacements and rotations at the external intermediate cross-frame location. These are calculated from a 1D line-girder or a 2D-grid analysis without external intermediate cross-frames. For the NTSCR1 bridge, the displacements and rotations at the cross-frame location calculated using a 2D-grid analysis without external intermediate cross-frames, the tub-girder dimensions and average mechanical properties are shown in Table A.2. The associated forces are calculated next.

Table A.2. Total dead load displacements, dimensions and mechanical properties for the calculation of the NTSCR1 external intermediate cross-frame forces.

Variable	Value	Variable	Value
$\phi_{w,int}$	0.00726	$\phi_{w,ext}$	0.00814
$\Delta_{w,int}$	6.64 in	$\Delta_{w,ext}$	7.37 in
$\Delta_{w,rel}$	0.728 in	β_0	21.5°
E	29000 kip/in²	G	11154 kip/in²
I_{avg}	173044 in^4	J_{avg}	105182 in^4
L	1800 in (150 ft)	R	4800 in (400 ft)
L_i	1766 in	L_e	1834 in
a	96 in	c	84 in
h_k	62 in	ψ	55.9°
$A_{diagonal}$	8.82 in²	A_{strut}	8.82 in²

The intermediate parameters are

$$L_K = h_K \cos\psi + L_T \sin\psi = 62\cos(55.9°) + 48\sin(55.9°) = 74.5 \tag{2.24}$$

$$\frac{EI}{GJ} = \frac{29000 \cdot 173044}{11154 \cdot 105182} = 4.28$$

$$K_{e0} = 1 + \left(1 + \frac{EI}{GJ}\right)\left(1 - \cos\frac{\beta_0}{2}\right) = 1 + (1 + 4.28)\left(1 - \cos\left(\frac{21.5°}{2}\right)\right) = 1.092 \tag{2.25}$$

$$K_{e1} = \frac{L_i + L_e}{a + c} = \frac{1766 + 1834}{96 + 84} = 20 \tag{2.26}$$

$$\begin{aligned} K_{e2} &= K_{e0}K_{e1}\frac{L_i^3 + L_e^3}{12(EI/GJ)}\sin\psi + 2L_iL_eL_K \\ &= 1.092 \cdot 15\frac{1766^3 + 1834^3}{12(4.28)}\sin(55.9°) + 2 \cdot 1766 \cdot 1834 \cdot 74.5 = 4.60 \times 10^9 \end{aligned} \tag{2.27}$$

The forces on the external cross-frame diagonals, F_D, and top and bottom chords, F_T and F_B, are calculated as

$$F_D = 4GJ\frac{\left(L_i\phi_{w,ext} + L_e\phi_{w,\text{int}} - K_{e1}\Delta_{w,rel}\right)}{K_{e2}}$$
$$= 4\cdot 11153\cdot 105182\frac{\left(1766\cdot 0.00814 + 1834\cdot 0.00726 - 20\cdot 0.728\right)}{4.60\times 10^9} = 13.4\text{kip} \quad (2.21)$$

$$F_T = \frac{4GJ\left(\phi_{w,ext} + \phi_{w,\text{int}}\right) - F_D L_K\left(L_e - L_i\right)}{h_k\left(L_i + L_e\right)}$$
$$= \frac{4\cdot 11153\cdot 105182\left(0.00814 + 0.00726\right) - 13.4\cdot 74.5\left(1834 - 1766\right)}{62\left(1766 + 1834\right)} = 18.1\text{kip} \quad (2.22)$$

$$F_B = \pm F_D\cos\psi - F_T$$
$$= +13.4\cos(55.9°) - 18.1 = -10.6\text{kip} \quad (2.23)$$
$$= -13.4\cos(55.9°) - 18.1 = -25.6\text{kip}$$

The resulting forces acting on the girder are given by

$$H_i = F_D\cos\psi - F_T = 13.4\cos\left(55.9°\right) - 18.1 = -10.6\text{kip} \quad (6.2)$$

$$H_e = F_D\cos\psi + F_T = 13.4\cos\left(55.9°\right) + 18.1 = 25.6\text{kip} \quad (6.3)$$

$$V = F_D\sin\psi = 13.4\sin\left(55.9°\right) = 11.1\text{kip} \quad (6.4)$$

The resulting forces H_i, H_e and V are shown in Figure A.13. The forces are shown as external forces acting on the external intermediate cross-frame and the girders. Figure A.13 illustrates how the forces from the external cross-frame are transmitted to the girders affecting the internal cross-frames and the girder torsional moments.

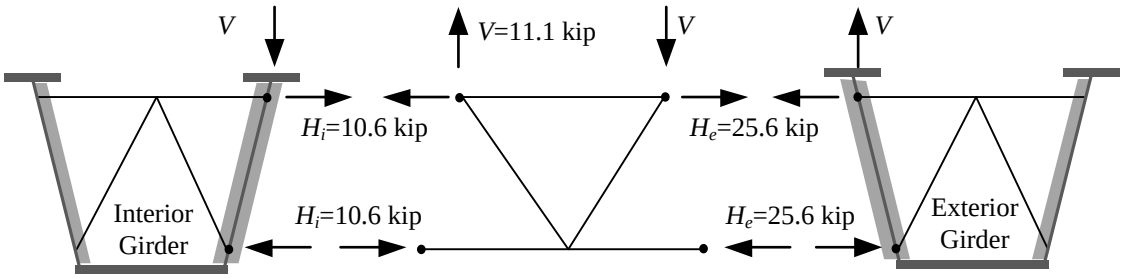

Figure A.13. Forces acting on the external intermediate cross-frame and girders.

The external intermediate cross-frame forces act on the girder connection plates, webs and internal cross-frame. From the 3D FEA results, the internal cross-frame top chord experienced an increase on the forces of approximately 12 kip on Girder 1 and 5 kip for Girder 2. These force increments are approximately half of the predicted H_i and H_e forces from the 3D FEA. This effect is expected as the external cross-frame forces are distributed into the connection plates, webs and the internal cross-frames. For simplicity, a design based on simplified methods should consider that the internal cross-frame is capable of resisting the full load amount originated from the external intermediate cross-frame.

A.1.7 Steel Erection Fit-Up Forces

One of the possible scenarios where fit-up issues may be encountered during steel erection is closely related to the developments shown previously. This scenario involves connecting the external intermediate cross-frame once the end diaphragms have been connected at the supports. For this case, the forces required to connect the girders are proportional to the forces shown in Figure A.13 but calculated for the steel erection stage displacements.

Table A.3. Steel dead load displacements, dimensions and mechanical properties for the calculation of the NTSCR1 external intermediate cross-frame forces.

Variable	Value	Variable	Value
$\phi_{w,int}$	0.00200	$\phi_{w,ext}$	0.00230
$\Delta_{w,int}$	1.81 in	$\Delta_{w,ext}$	2.082 in
$\Delta_{w,rel}$	0.272 in		

To bring the girders to a position where the external cross-frame can be connected a set of forces capable of generating an equivalent torsional moment should be applied. Figure A.14 shows the external intermediate cross-frame forces and the associated distances.

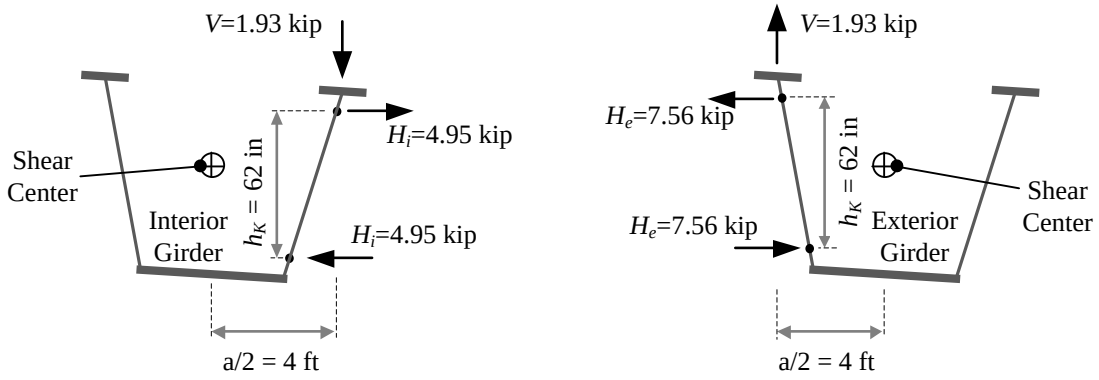

Figure A.14. External forces on the girders required to connect the external cross-frame.

Form Fig. A.14 the required torsional moments are:

$$T_{\text{int}} = -H_i h_K - V\frac{a}{2} = -4.95 \cdot 62 - 1.93 \cdot \frac{96}{2} = -399\text{kip} \cdot \text{in} = -33.3\text{kip} \cdot \text{ft}$$

$$T_{ext} = H_e h_K - V\frac{a}{2} = 7.56 \cdot 62 - 1.93 \cdot \frac{96}{2} = 376\text{kip} \cdot \text{in} = 31.4\text{kip} \cdot \text{ft}$$

Girder 2 (interior) must be rotated an additional amount with respect to the associated rotation originated from curvature only by applying a torsional moment T_{int}. The rotation due to curvature on Girder 1 (exterior) must be reduced by applying the torsional moment T_{ext}. Depending on the procedure used to connect, the associated fit-up forces can be calculated based on the torsional moments T_{int} and T_{ext}.

A.1.8 External Intermediate Cross-Frame Effect on the Girder Torsional Moment

As calculated in the previous section, an additional discrete torque is added to the girders at the cross-frame location as the consequence of the external intermediate cross-frame. The discrete torques causes an increase to the first half of the torsional moment

diagram and a decrease to the other half. The magnitudes of these increments are equivalent to half the torsional moments $T_{int,TDL}$ and $T_{ext,TDL}$.

Form Fig. A.13 the required torsional moments are:

$$T_{\text{int},TDL} = -H_i h_K - V\frac{a}{2} = -10.6 \cdot 62 - 11.1 \cdot \frac{96}{2} = -1190\text{kip}\cdot\text{in} = -99.2\text{kip}\cdot\text{ft}$$

$$T_{ext,TDL} = H_e h_K - V\frac{a}{2} = 25.6 \cdot 62 - 11.1 \cdot \frac{96}{2} = 1057\text{kip}\cdot\text{in} = 88.1\text{kip}\cdot\text{ft}$$

For the NTSCR1 bridge, the torques due to the external intermediate cross-frame interaction are less than 5 % of that of the maximum torque due to curvature (approximately 1000 kip-ft) and may be neglected for simplicity. However, in cases where the external intermediate cross-frame controls larger displacements this torque is expected to be important with respect to the torques due to skew or curvature and must not be neglected. Similarly, for straight and skewed bridges, this torque must be accounted as the effect of the external intermediate cross-frame must be the main source of torsional moment in the system.

A.2 NTSSS2 Parametric Bridge

A.2.1 Description

NTSSS2 is a parametric simple-span, straight and skewed bridge. This is the base case for the study of skew effects. The top flange lateral bracing layout is illustrated in the Figure A.15. All results are shown for Girder 1 which is the lower girder on Figure A.15 layout. Results on the Girder 2 are similar.

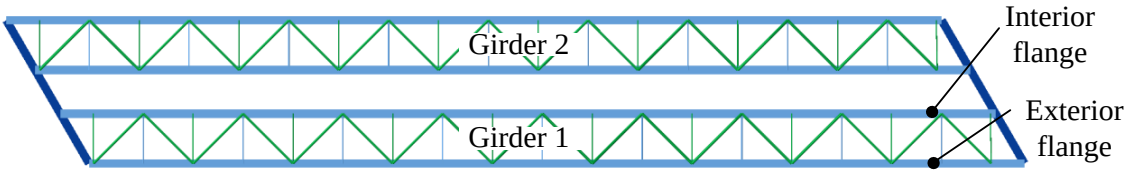

(L_1 = 150 ft / *deck width* = 30 ft / θ_1 = 30°, θ_2 = 30°)

Figure A.15. NTSSS2 Bridge Layout.

The topics highlighted for this bridge are the estimations of twist rotations and torsional moments due to skew, the top flange sawtooth axial stresses and the effect of the eccentric connections of the top flange lateral bracing.

A.2.2 Displacements

The vertical displacements and relative lateral displacements are shown in Figures A.16 and A.17. Results are shown for the 3D FEA, 2D-grid analysis from program P1 and 1D calculations. The vertical displacements are reported at the girder centerline. These relative lateral displacements shown are the difference of the average of the two top flanges to the bottom flange centerline lateral displacements. The displacements are in units on inches and the results are shown in the plots with respect to the bridge length normalized to 1.

The 2D analysis include the skew in the grid model while the effects on the 1D line-girder analysis method is accounted via the Equations 3.4, 3.5 and 3.10 that help evaluate the girder twist rotation and consequently the relative lateral displacement.

$$\phi_y = \frac{wL_g^3}{24EI_g} \tag{3.4}$$

$$\phi_x = -\phi_y \tan(\theta) \tag{3.5}$$

$$\phi_x(s) = \phi_{x1} - (\phi_{x1} - \phi_{x2})\frac{s}{L} \tag{3.10}$$

The results show good agreement and the differences between the analysis methods are inherent to the level of detail and discretization.

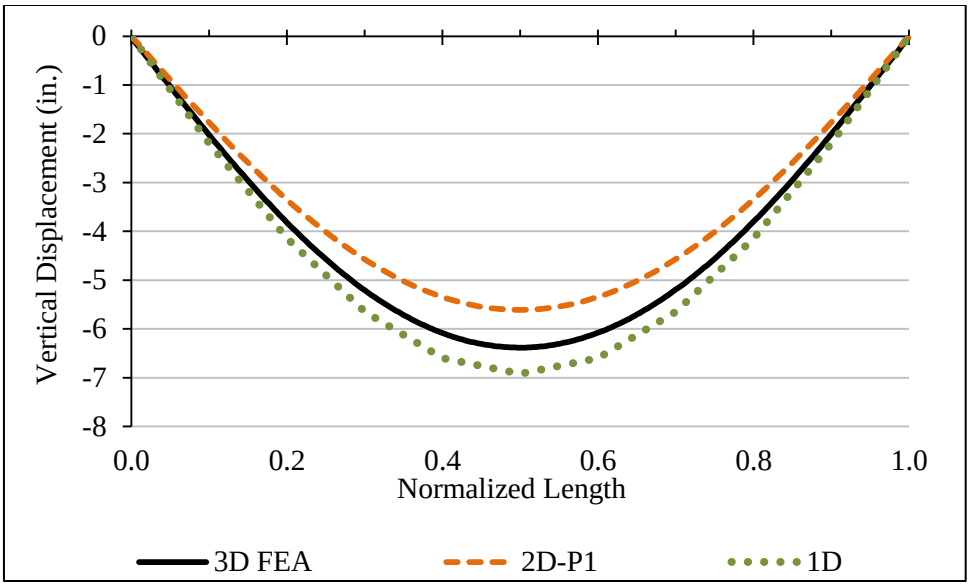

Figure A.16. Girder 1 centerline vertical displacements.

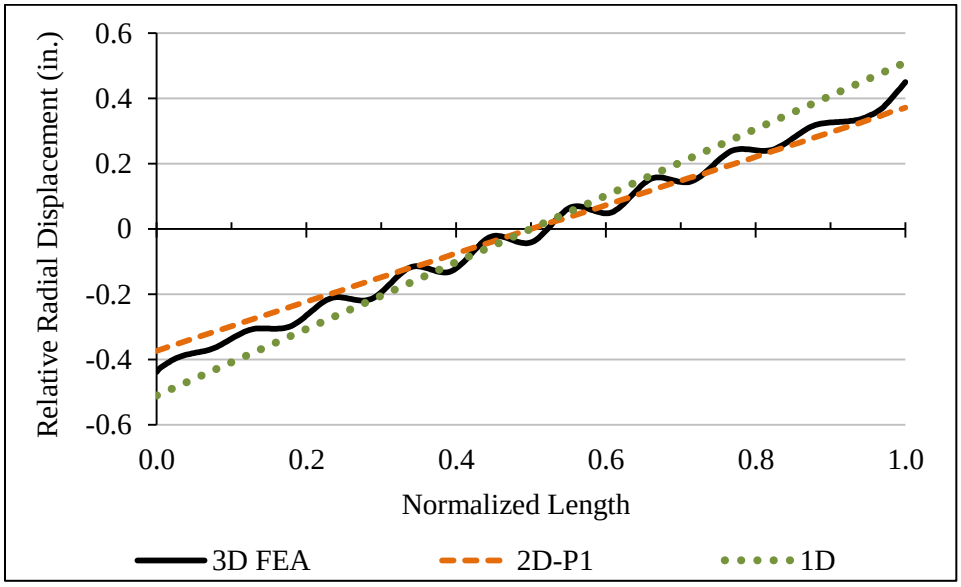

Figure A.17. Girder 1 relative lateral displacements.

A.2.3 Top Flange Major-Axis Bending Stresses

Figures A.18 and A.19 show the 3D FEA results and the 2D-grid analysis results (labeled "2D-P1") with and without the additional effect of the force *P* (labeled "2D+force P").

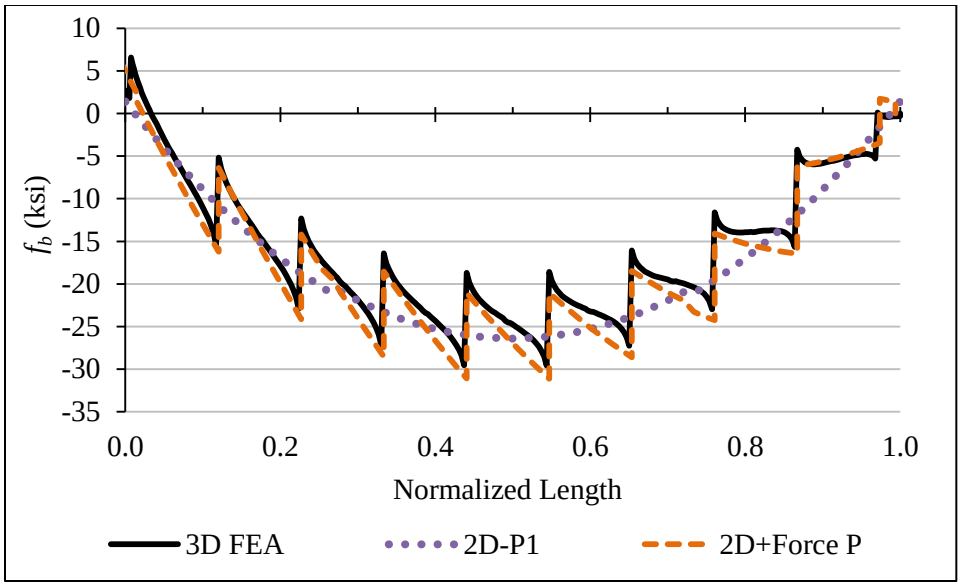

Figure A.18. Girder 1 top flange major-axis bending stresses at the exterior top flange.

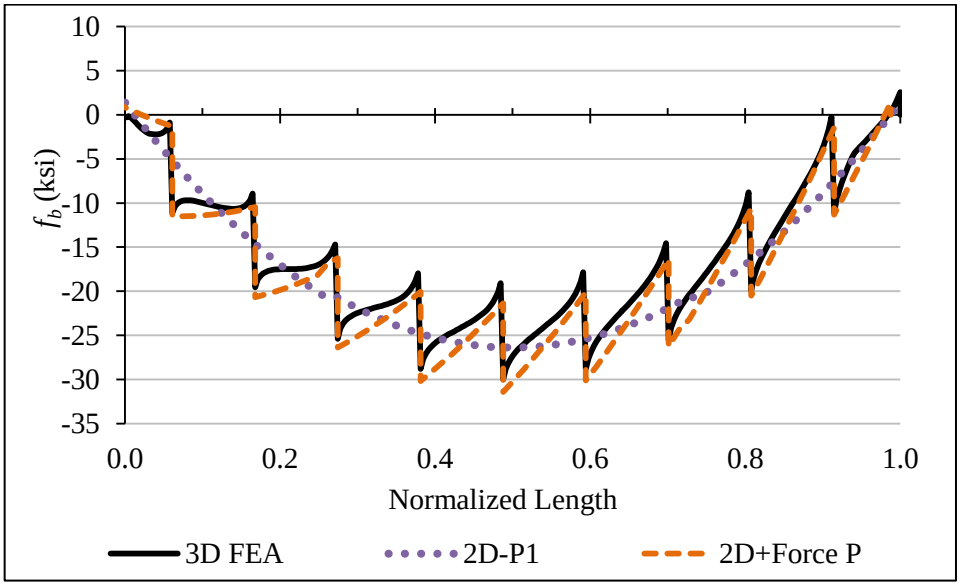

Figure A.19. Girder 1 top flange major-axis bending stresses at the interior top flange.

The magnitude of the correction provided by the forces *P* is dependent on the forces on the diagonals which for this case are approximately constant (see Fig. A.23) as they depend mainly in the torsional moment distribution (see Fig. A.21). This causes an approximately uniform sawtooth stress change along the entire length of the bridge. For

curved cases, the distribution of the torsional moment varies and the sawtooth stress change is not uniform in size, as is shown in the results for the NTSCR1 bridge.

A.2.4 Top Flange Lateral Bending Stresses

Figure 6.4 shows the top flange lateral bending stresses for the 3D FEA and 2D analysis. The results from 1D method are omitted.

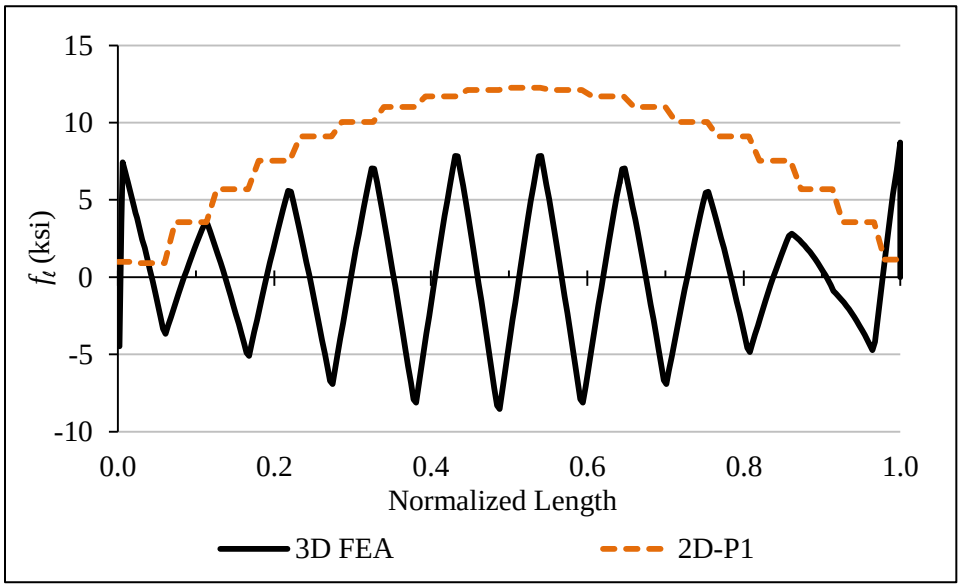

Figure A.20. Girder 1 top flange lateral bending stresses.

A spike on the stresses is observed close to the supports (normalized lengths equal to 0 and 1). This is due to the lack of continuity of forces originated by the top flange lateral bracing system.

A.2.5 Torque Due to Skew

The girder torsional moment estimations for 1D methods are based on the developments discussed in Chapter 3. The estimations of the 2D method are taken from the grid analysis which inherently includes the skew in the model.

At each support the torque is estimated as

$$T_S = -\frac{GJ_g}{L_g}\phi_x \tag{3.8}$$

And the total torque in this case of parallel support is twice of the calculated by Eq. 3.8. Figure A.21 shows the torsional moments for the NTSSS2 Bridge as originally designed with 30° of skew on both supports and Figure A.22 shows the results from the sensitivity study with 15° of skew on both supports.

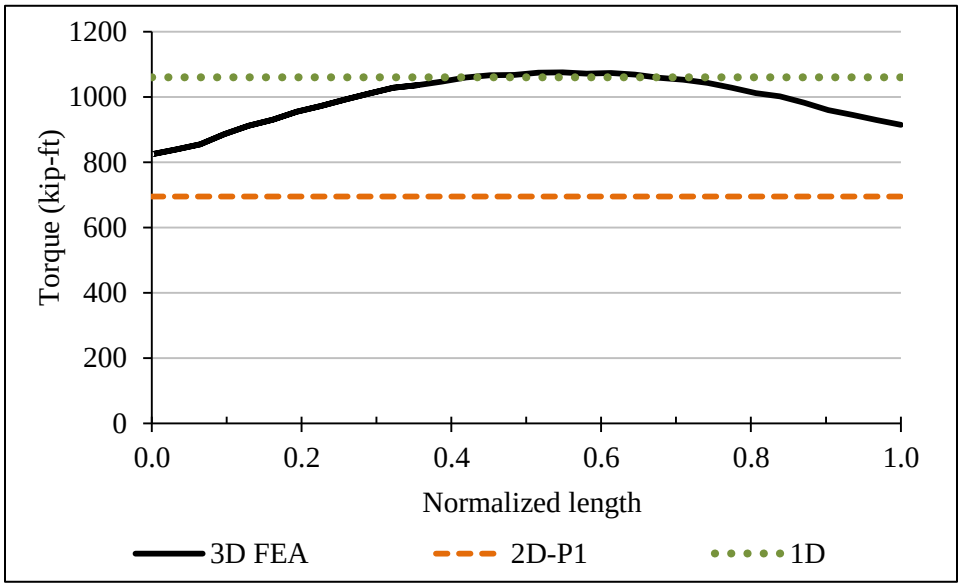

Figure A.21. Girder 1 torsional moments for the actual skewed case (30° skew).

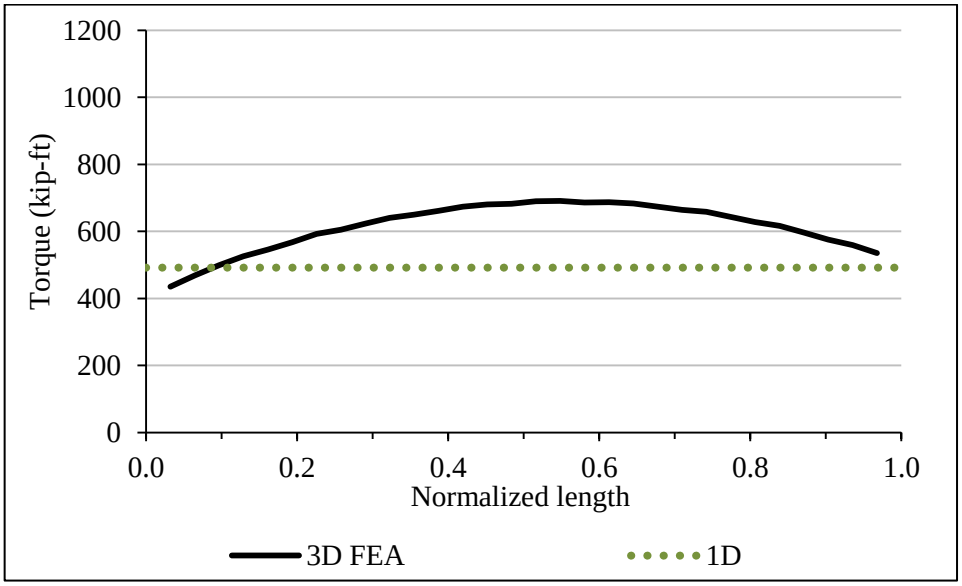

Figure A.22. Girder 1 torsional moments for the reduced skew sensitivity case (15° skew).

The torsional moment distributions are captured differently by the simplified analysis methods. The 3D FEA results exhibit a parabolic torsional moment distribution as a result of the small interactions of the top flange lateral bracing. The 1D simplified method assumes a constant torque, as also shown by the 2D-grid method.

The differences on the torsional moment estimations are due to the modeling of the diaphragms, eccentric loading and due to the discretization level of the bridge. The torsional moment obtained by Eq. 3.9 for the 1D line-girder method is still a close approximation of the behavior of the bridge, useful for the evaluation of the bracing forces.

The parabolic-like distribution of the torsional moment from the 3D FEA in Figures A.21 and A.22 are the result of additional internal torsional moments with a parabolic-like distribution. This evidences that these additional internal moments are caused by the TFLB strut lateral forces which follow a similar distribution as shown in Figure A.24. This response is exhibited in straight bridges where the only source of torsional moments is the skewed supports. In bridges subjected to curvature, this internal effect is not noticeable as the curvature effects are larger in magnitude.

For the NTSSS2 sensitivity case with 15° of skew results shown in Figure A.22 additional effect on the torque becomes more important as the torsional moment due to skew decreases. The shape also suggests correlation with the girder major-axis bending moment. The additional internal effect remains close in magnitude as in the original case with 30° of skew. This confirms that as the skew increases, this effect is less noticeable. Additional work is needed to quantify these effects and improve the accuracy of the 1D analysis method, however, the method still provide useful information on an estimation of the torsional effects due to skew.

A.2.6 Top Flange Lateral Bracing Diagonals and Struts

The axial forces of the top flange lateral bracing system are shown in Figures A.23 and A.24.

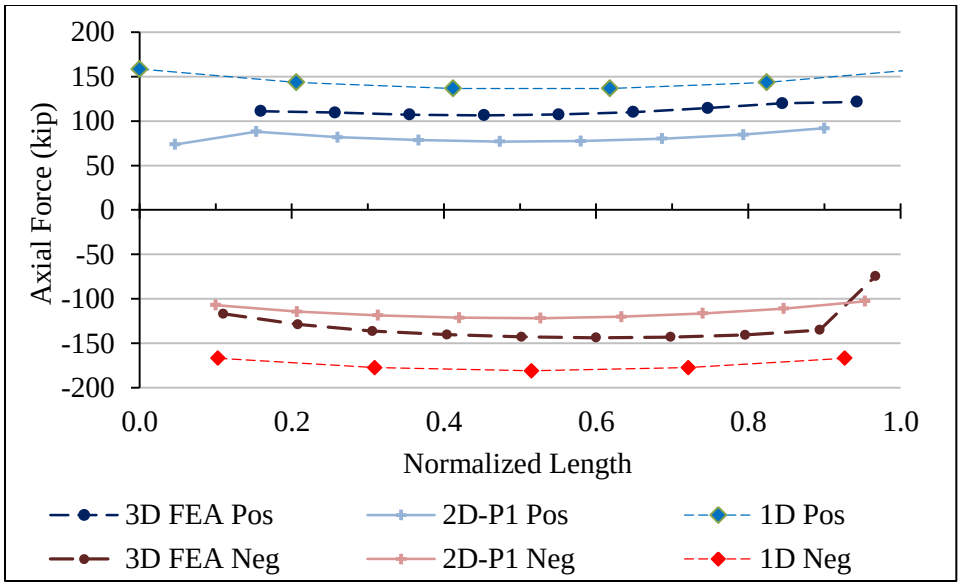

Figure A.23. Girder 1 top flange lateral bracing diagonals axial forces.

The 1D and 2D simplified methods use expressions that assume that the interaction occur solely within the top flanges of the tub-girder and the top truss. This assumption removes the possible interaction of the webs on the force distribution, so the estimates are slightly conservative for this case regardless of the approximate torsional moment estimations. Section A.5.6 illustrates a case where the forces on the diagonal, as predicted by the 2D-grid method are unconservative. Note that the 3D FEA includes the forces on the two components of the internal cross-frames and resulting in two values being shown in Fig. A.24 every other reporting point.

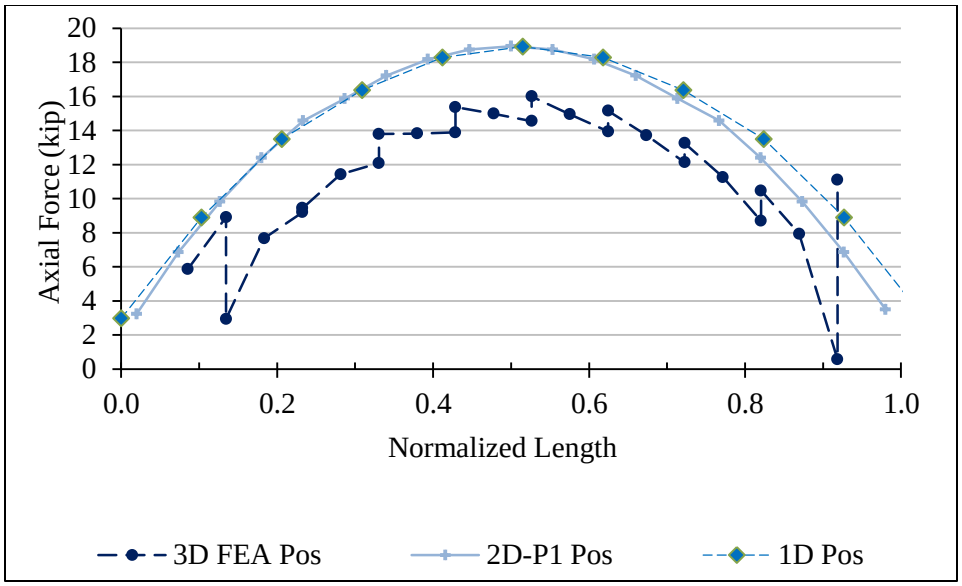

Figure A.24. Girder 1 top flange lateral bracing axial forces strut forces.

Close to the 0.9 normalized lengths, the 3D FEA results exhibit forces that are not correctly estimated by the simplified analysis methods. This is caused by the lack of continuity of the top flange lateral bracing at these locations. For the simplified methods to estimate the behavior accurately it is necessary that the bridge geometric details provide the continuity of the load paths.

Figure A.25 shows the details of top flange lateral bracing the NTSSS1 and NTSSS2 bridges. The NTSSS1 bridge bracing results are not presented in this appendix but this case is shown here for illustration purposes. The top truss must be connected to the end diaphragm by a diagonal to provide the necessary load path to avoid undesired stresses and for the applicability of the simplified methods of analysis and the respective component force equations. The solution for these cases requires a variation on the panel sizes to accommodate an additional panel to finish the top flange lateral bracing system using a diagonal rather than a strut as shown in Fig. A.25.

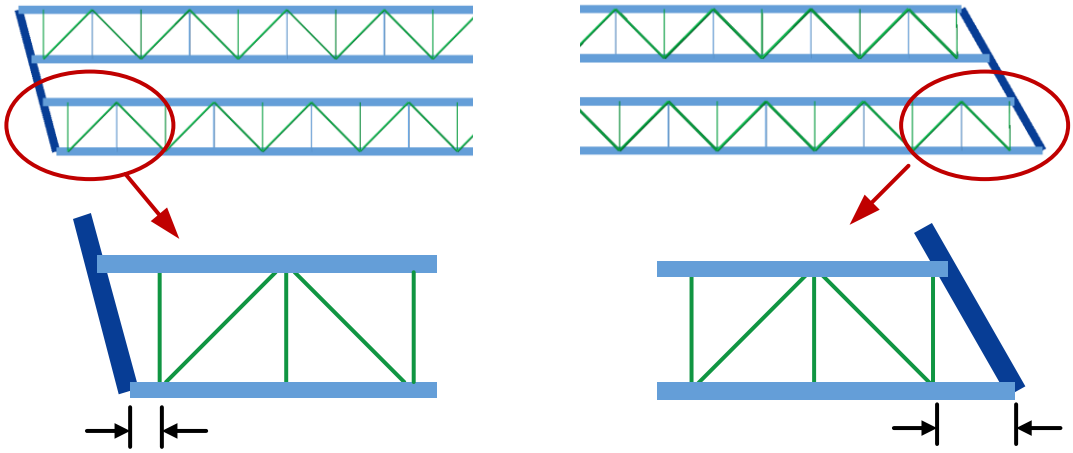

a) NTSSS1 (15° skew) **b) NTSSS2 (30° skew)**

Figure A.25. Undesired eccentric top flange lateral bracing detail in NTSSS1 and NTSSS2 bridges.

A.3 NTSCS29 Parametric Bridge

A.3.1 Description

NTSCS29 is a parametric simple-span, curved and skewed bridge. This is the base case for the combined curvature and skew effects. The top flange lateral bracing layout is illustrated in the Figure A.26. All results are shown for the exterior girder (Girder 1) which is the lower girder on Figure A.26.

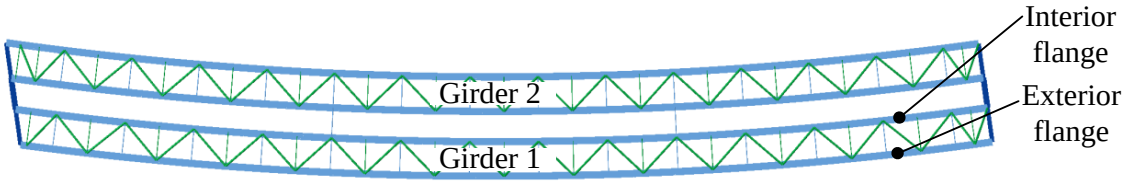

(L_1 = 225 ft / R = 820 ft / *deck width* = 30 ft / θ_1 = 15.7°, θ_2 = 0°)

Figure A.26. NTSCS29 Bridge Layout.

A.3.2 Displacements

The vertical displacements and relative lateral displacements are shown in Figures A.27 and A.28.

The effects of skew on the 1D line-girder analysis method is accounted via the Eq. 3.12 that helps evaluate the girder twist rotation and consequently the relative lateral

displacement. The results show good agreement on the estimation of the skew effects at the left support. The differences along the length of the bridge are caused by the external intermediate cross-frames and the inability of the M/R Method to evaluate their effects.

$$\phi_x(s) = \phi_{x,C}(s) + \phi_{x,S}(s) \tag{3.12}$$

The results show good agreement and the differences between the analysis methods are inherent to the level of detail and discretization.

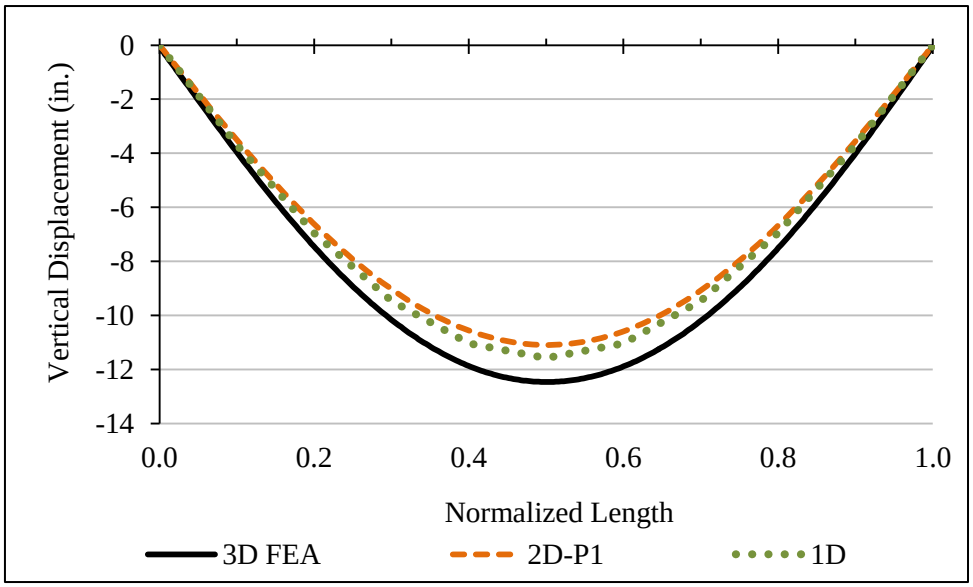

Figure A.27. Girder 1 centerline vertical displacements.

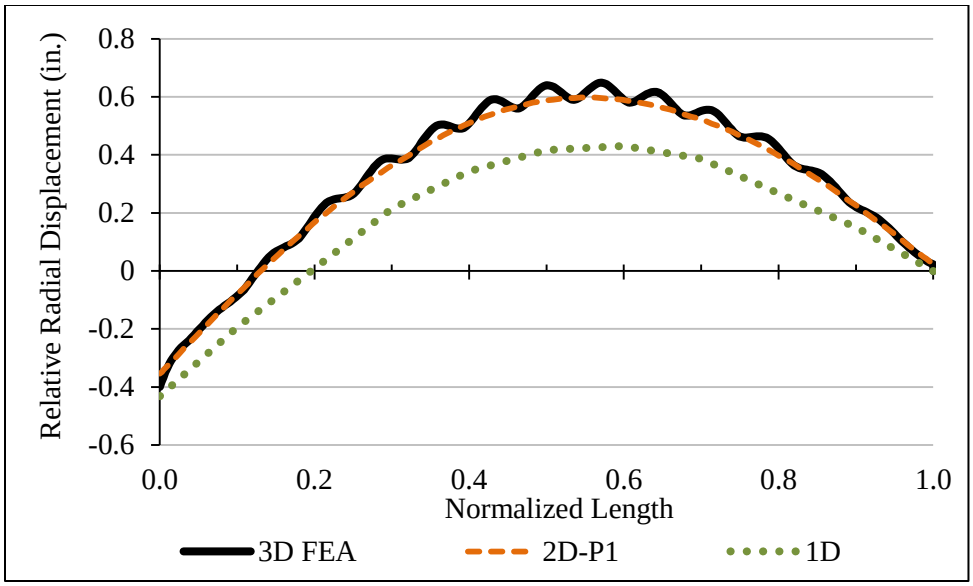

Figure A.28. Girder 1 relative lateral displacements.

A.3.3 Top Flange Major-Axis Bending Stresses

Figures A.29 and A.30 show the 3D FEA results and the 2D-grid analysis results (labeled "2D-P1"). The additional effects of the force *P* are shown for the simplified analysis methods.

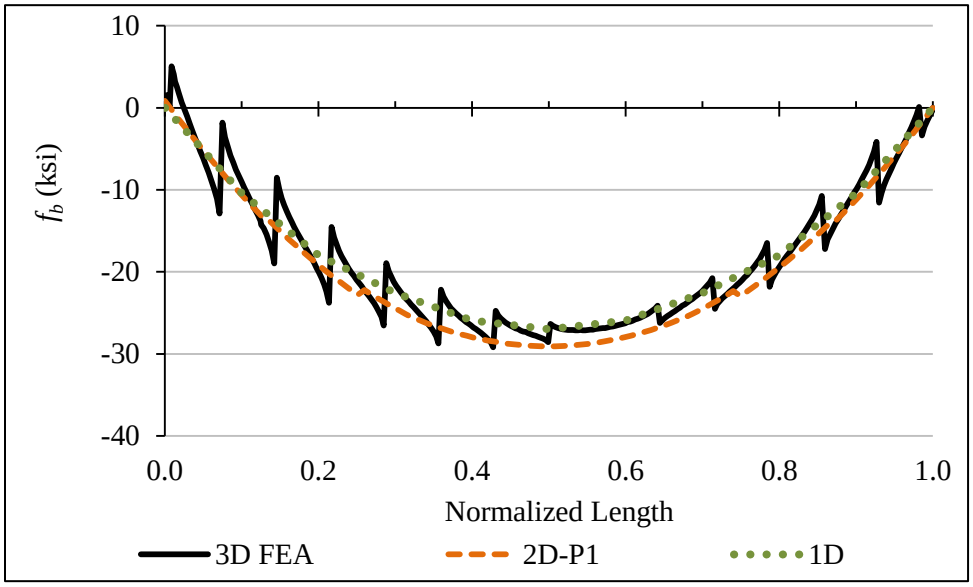

Figure A.29. Girder 1 top flange major-axis bending stresses at the exterior flange.

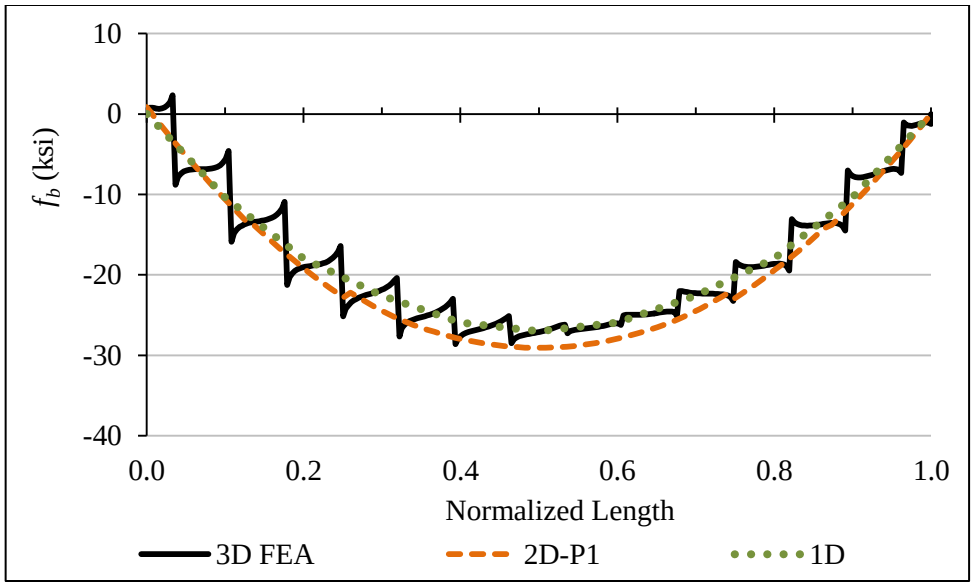

Figure A.30. Girder 1 top flange major-axis bending stresses at the interior flange.

A.3.4 Top Flange Lateral Bending Stresses

Figure A.31 shows the top flange lateral bending stresses for the 3D FEA and 2D analysis. The results from 1D method not shown.

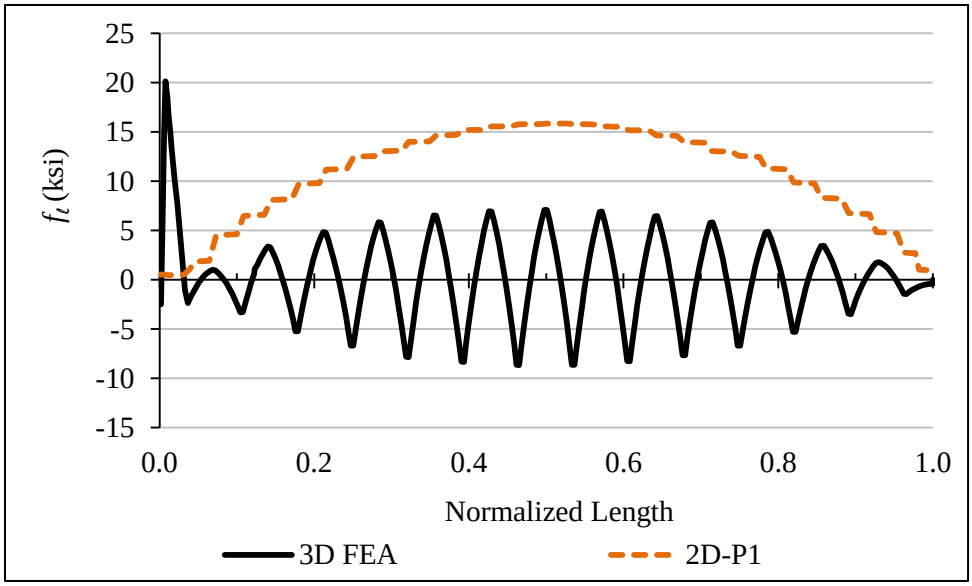

Figure A.31. Girder 1 top flange lateral bending stresses at the exterior top flange.

A spike on the stresses is observed close to the left support (normalized length equal to 0). This is due to the lack of continuity of forces originated by the top flange lateral bracing system.

A.3.5 Torque Due to Skew and Curvature

The girder torsional moment estimations for 1D method are based on the developments discussed in Chapter 3 summarized in Eq. 3.11 which include the torsional moment distribution due to curvature, $T_C(s)$, plus the additional torque due to skew T_S. The estimations of the 2D method are taken from the grid analysis which inherently includes the skew in the model.

$$T(s) = T_C(s) + T_S \tag{3.11}$$

Figure A.32 illustrates the torsional moments in Girder 1 obtained from the integration of the 3D FEA stresses and the M/R Method and torque due to skew estimates with the torsional moment T_S due to skew. Figure A.33 illustrates the radial case without the effects of skew from the 3D FEA and 1D estimations.

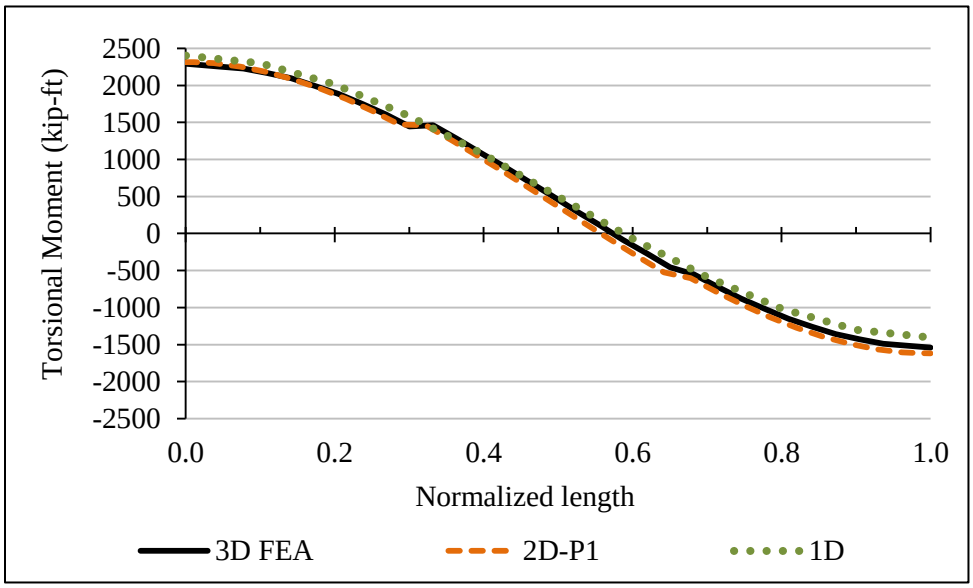

Figure A.32. Girder 1 torsional moments for the actual skewed case (15.7° skew).

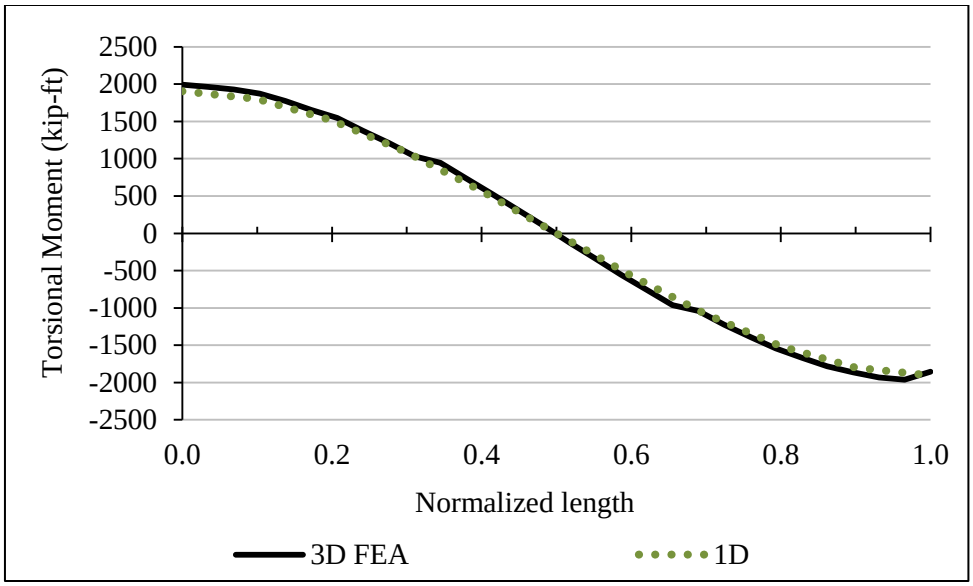

Figure A.33. Girder 1 torsional moments for the radial sensitivity case (0° skew).

This bridge has two external intermediate cross-frames as illustrated in Fig. A.26. The cross-frames influence the torsional response due to the shear transmitted between the girders. Figure A.32 and A.33 show that the torque estimated by Eq. 3.11 is very close to the torque from the 3D FEA when the bridge does not have external intermediate diaphragms. In the case where the external intermediate diaphragms exist, the approximate equations still give an upper bound estimate of the torsional response appropriate for design calculations.

A.3.6 Top Flange Lateral Bracing Diagonals and Struts

The axial forces of the top flange lateral bracing system are shown in Figure A.34. Figure A.35 illustrate the axial forces on the struts on Girders 1. At the locations where internal cross-frames are present, the 3D FEA plot reports two forces corresponding to both sides of the cross-frame top chord.

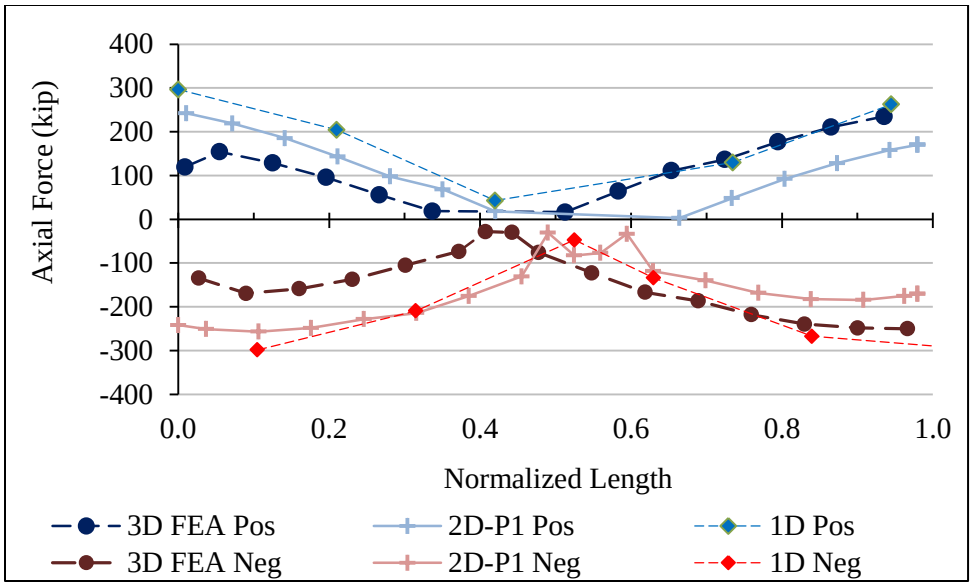

Figure A.34. Girder 1 top flange lateral bracing diagonals axial forces.

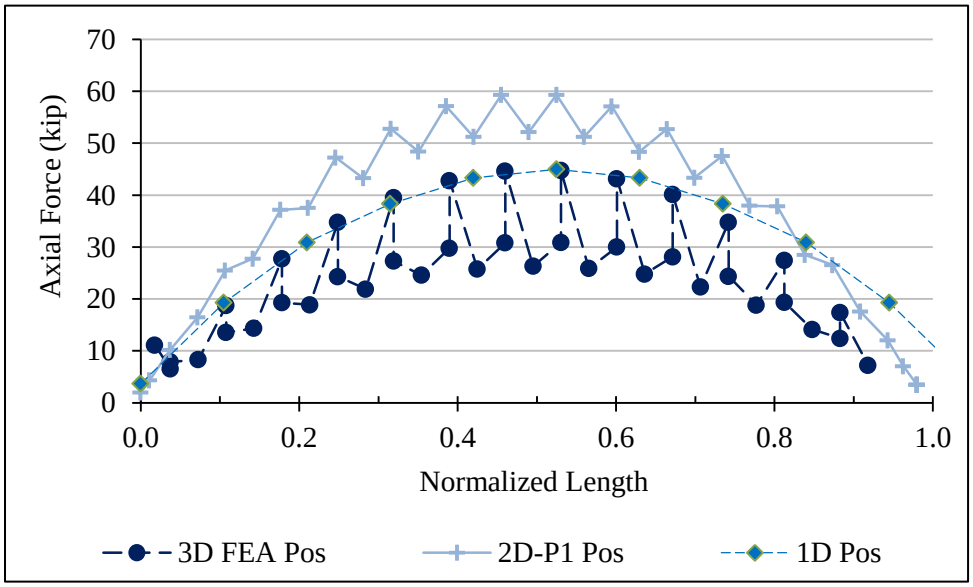

Figure A.35. Girder 2 top flange lateral bracing struts axial forces.

A.3.7 Steel Erection Stages

Figure A.36 illustrates the erection stages of NTSCS29. Each girder is fabricated in 3 parts or field sections. The field sections allow parts of reduced length that can be transported from the fabrication shop to the job site with relative simplicity.

The erection Stages 1 and 2 consider that two field sections on each girder are connected or spliced on the ground. This creates a longer field section of about two thirds of the girders total length. Then, these are lifted to the right abutment and temporary supports shown in Figure A.36. The last field sections are lifted and connected in Stages 3 and 4 keeping the temporary supports. In Stage 5 the temporary support is removed completing the steel erection sequence. Several steel erection procedures can be chosen depending in the site constraints, available equipment and the preferred practice of the erector. The erection scheme selected represents an approach to common practice.

The erection scheme shown uses temporary supports that provide reduced displacements during erection. These conditions are known as no-load-fit detailing and are the preferred steel erection scheme for tub-girder bridges. The no-load-fit requires zero or small displacements during the steel erection. The temporary supports are removed once all the field sections elements have been connected.

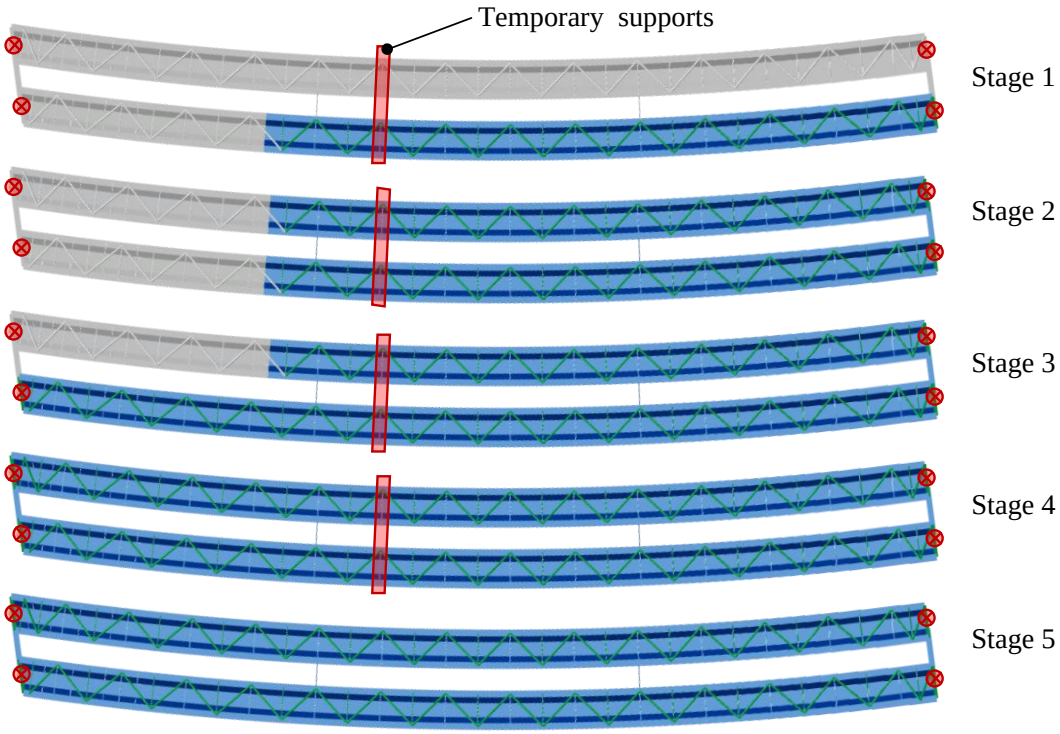

Figure A.36. Intermediate steel erection stages.

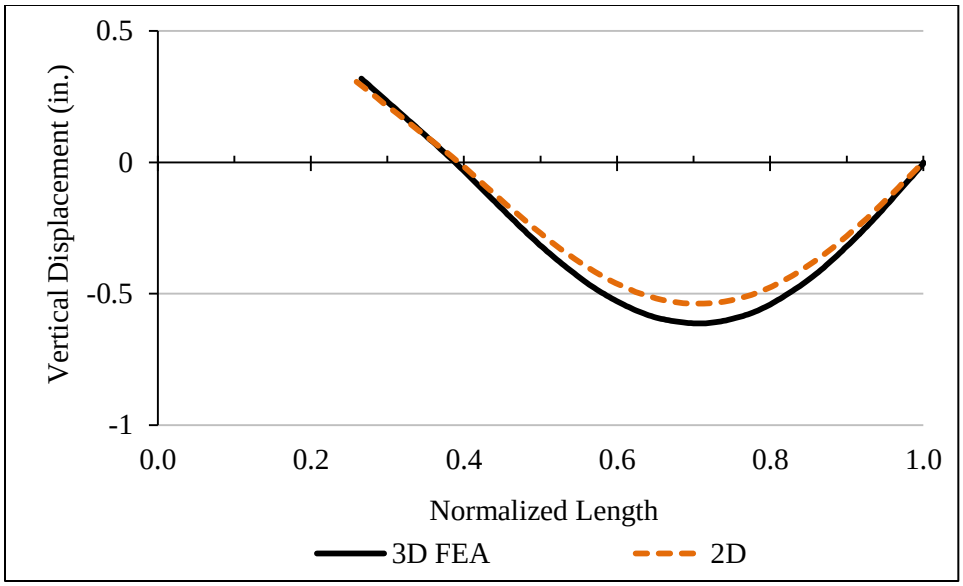

Figure A.37. Girder 1 vertical displacements for Stage 2 under steel dead load.

Figures A.37, A.38 and A.39 illustrate the evolution of the displacements during the steel erection Stages 2, 3 and 5 for Girder 1. Figures A.40, A.41 and A.42 illustrate the stress evolution during the same steel erection stages. All the displacements and stresses are shown for unfactored steel self-weight load.

The maximum displacements during the partial steel erection stages and the final steel erection are 0.7 in to 5.0 in respectively. These result on a ratio of less than 0.2. There is no clear ratio value to define the number of temporary supports for a no-load-fit erection scheme but the smaller the ratio the more appropriate the no-load-fit detailing scheme is.

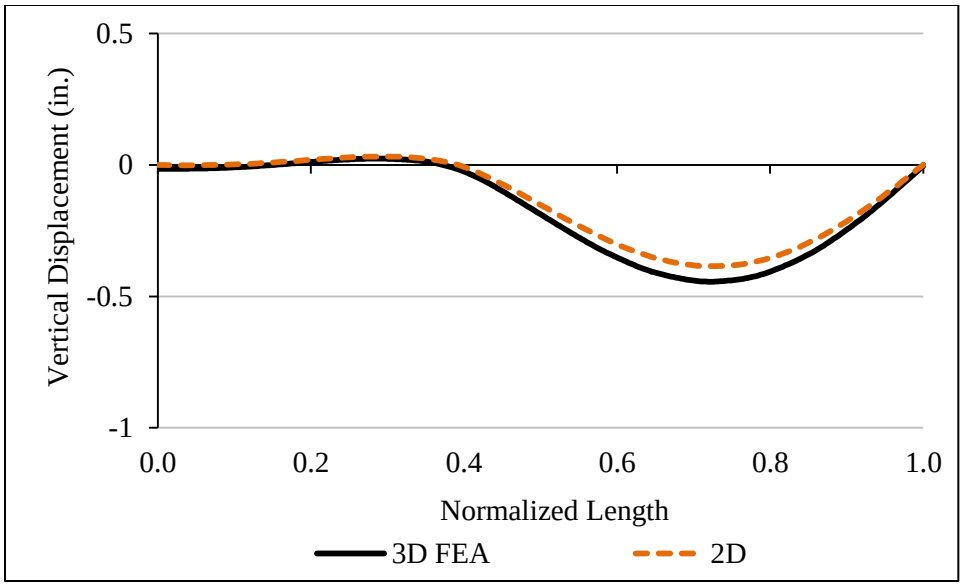

Figure A.38. Girder 1 vertical displacements for Stage 3 under steel dead load.

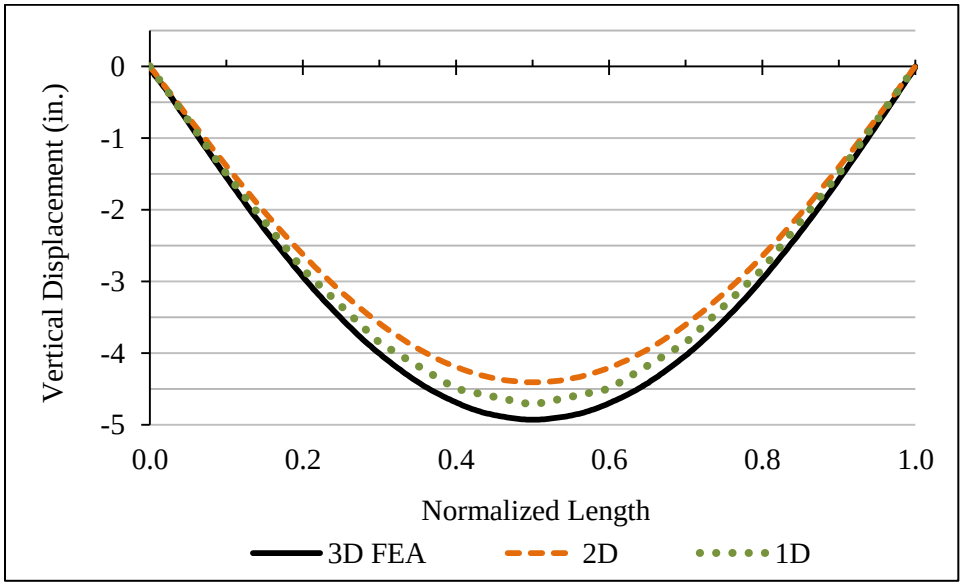

Figure A.39. Girder 1 vertical displacements for Stage 5 under steel dead load.

The relative vertical displacement at the splice location (0.26 the normalized length) is around of 0.3 in during the partial steel erection Stages 2 and 3 in Figures A.37 and A.38. At Stage 3, the girder splices can be easily performed since the girders are not experiencing large displacements.

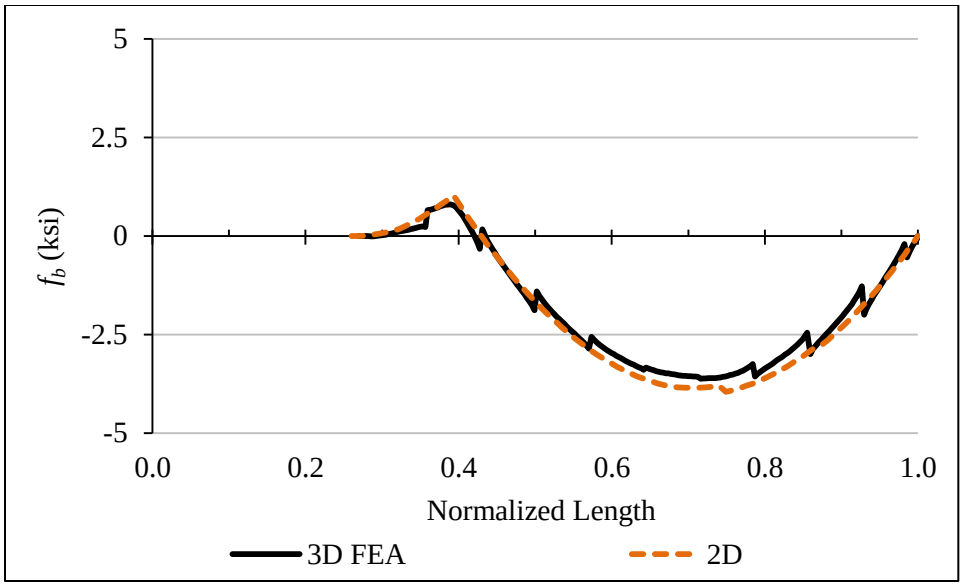

Figure A.40. Girder 1 top flange major-axis bending stresses for Stage 2 under steel dead load.

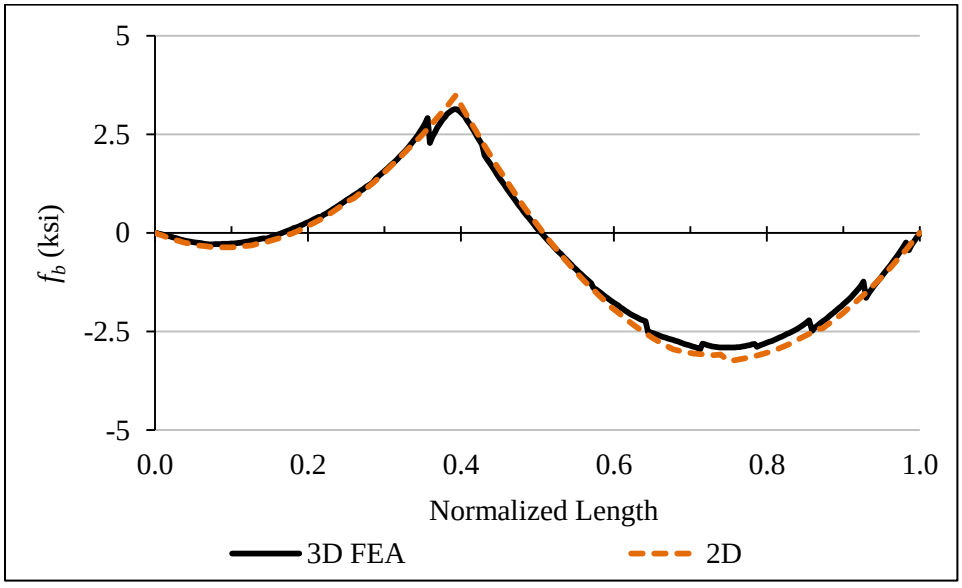

Figure A.41. Girder 1 top flange major-axis bending stresses for Stage 3 under steel dead load.

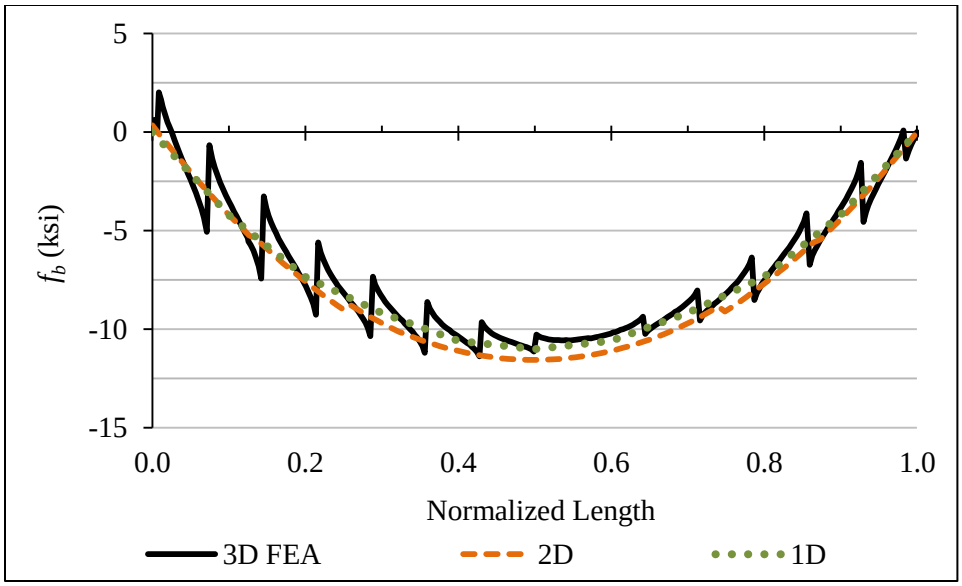

Figure A.42. Girder 1 top flange major-axis bending stresses for Stage 5 under steel dead load.

In terms of stresses, between stages 2 and 3 in Figures A.40 and A.41, the stress at the splice location goes from zero to approximately 0.8 ksi. This difference indicates the upper bound stress that the girders could experience under an erection scheme that requires displacing the girders to the common location in Stage 3 to perform the connection. In practice, the girder to be connected can be lifted and inclined by the cranes to a location which does not require additional stress to perform the splice. Once the splice is connected the girder is released to let it sit in the supports. At this moment, the splice self-weight brings the connection point to the expected displacement and stress level.

For tub-girder bridges, the problematic steel erection fit-up scenarios usually involve the lack of temporary supports and often occur at the external intermediate cross-frames and support diaphragms locations. During intermediate stages, the girders can be moved and inclined to bring the girders at an appropriate location to perform the connection with reduced effort. However, external intermediate cross-frames and diaphragms may need to overcome additional girder rotations resulting in increased forces due to the higher rotational stiffness of tub-girders.

A.4 NTCCS22 Parametric Bridge

A.4.1 Description

The NTCCS22 is a two-span continuous, curved bridge with one skewed support. The top flange lateral bracing layout is illustrated in Figure A.43. The left abutment of the bridge is skewed 20.1° and it is parallel to the radial intermediate pier. The right abutment is oriented radially. This bridge has one skewed and one radial spans and provides insight into the effect of skew between multi-span bridges. The results presented in this section are shown for the girder with the largest radius of curvature or Girder 1.

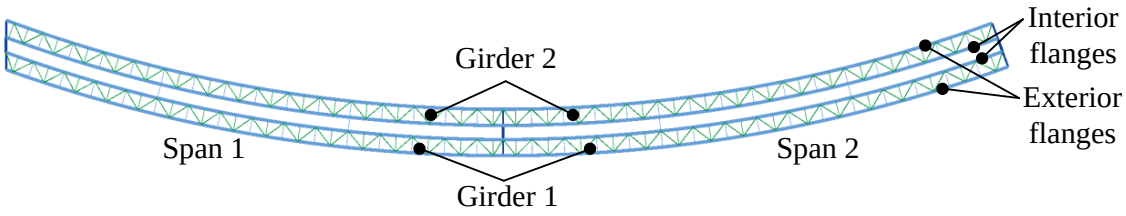

(L_1 = 250 ft, L_2 = 250 ft / R = 713 ft / *deck width* = 30 ft / θ_1 = 20.1°, θ_2 = 0°, θ_3 = 0°)

Figure A.43. NTCCS22 Bridge Layout

In the following sections the displacements, stresses, torsional moments and top flange lateral bracing forces are presented. Additionally, the fit-up forces are evaluated for the diaphragm connection scenario.

A.4.2 Displacements

The vertical and relative radial displacements are shown in Figures A.44 and A.45 for Girder 1. The left span experiences reduced vertical displacements with respect to the right span. This is direct consequence of the relative shorter span length due to skew.

Figure A.45 illustrates the top to bottom flange relative radial displacements as estimated by the 3D FEA, 2D-grid and 1D analysis methods. In this case, the skew causes an initial layover at the left support. The estimation by the 1D line-girder assumes a layover due to skew equal to

$$\phi_x = -\phi_y \tan(\theta) \tag{3.5}$$

which varies linearly along the left span to a zero layover at the intermediate pier. This layover is superimposed to the girder twist rotations calculated using the M/R Method given by

$$\phi_x = \frac{1}{R}\left(1+\frac{EI}{GJ}\right)\Delta \tag{2.7}$$

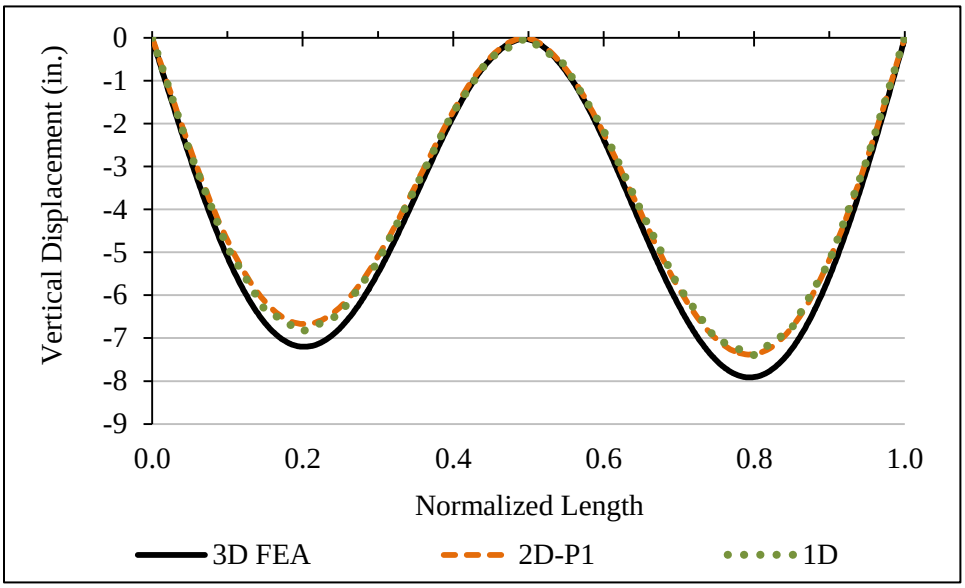

Figure A.44. Girder 1 centerline vertical displacements.

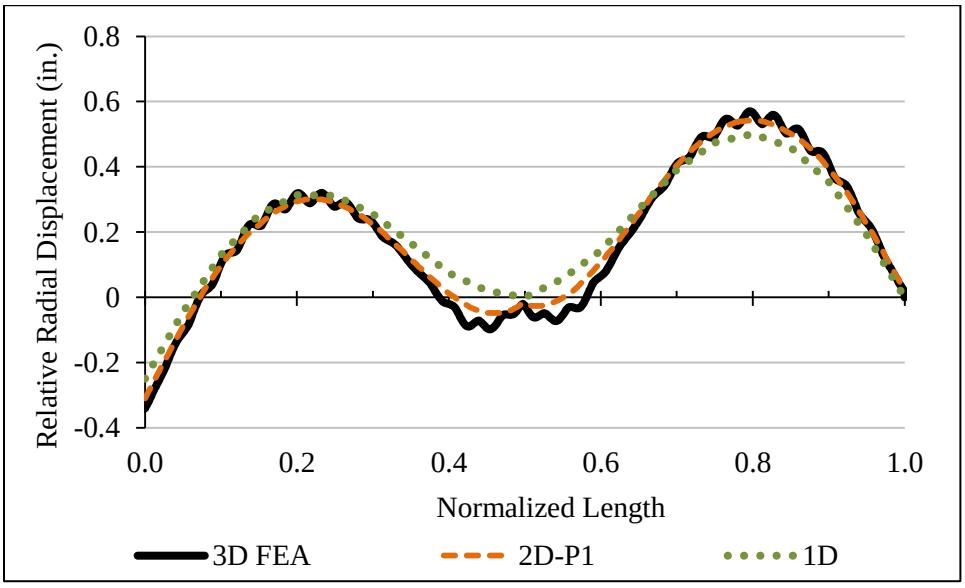

Figure A.45. Girder 1 relative lateral displacements.

The displacements show good agreement between analysis methods. Traditional 1D analysis methods do not account for the twist due to skew and the developments presented in this dissertation allow an appropriate estimation of the effects using the 1D line-girder method. The estimation assumes that the skew effects do not directly affect the displacements of the unskewed span. The skew, however, affects the second span indirectly when the span lengths change due to the skew.

A.4.3 Top Flange Major-Axis Bending Stresses

The top flange major-axis bending stresses for Girder 1 are shown in Figures A.46 and A.47. The results for both top flanges exhibit the effect of the sawtooth stresses but these barely affect the average bending stresses. In practical applications, the magnitude of the sawtooth stress can be evaluated at the points of maximum torsional moment to decide if they impact the estimations of the top flange major-axis bending stresses. Regardless of the sawtooth stresses, the simplified analysis methods provide an appropriate estimation of the major-axis bending stresses.

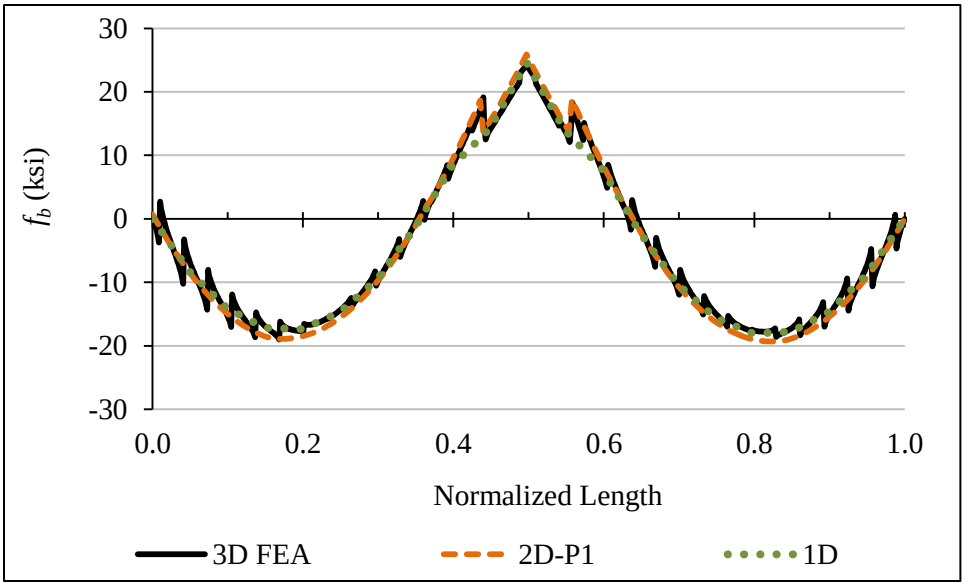

Figure A.46. Girder 1 top flange major-axis bending stresses at the exterior top flange.

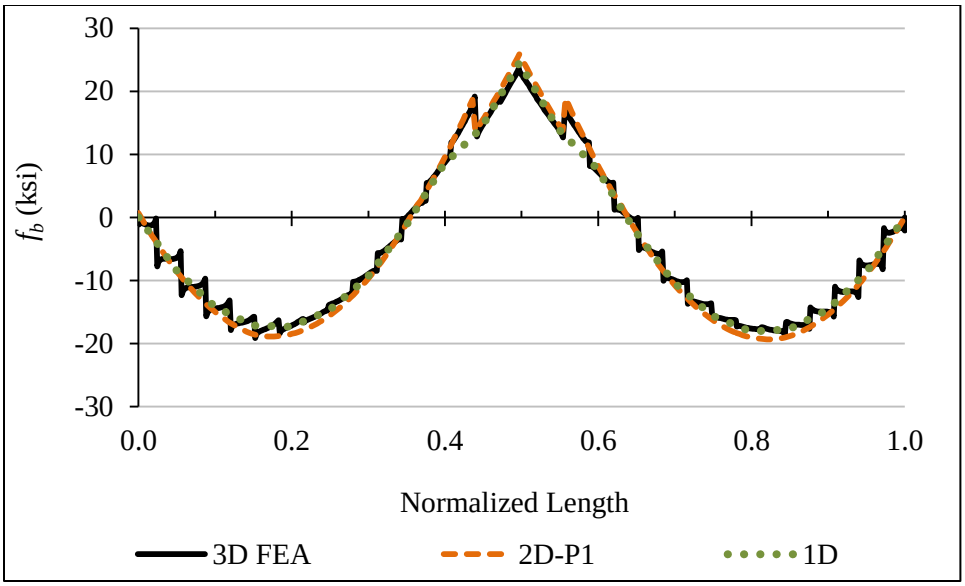

Figure A.47. Girder 1 top flange major-axis bending stresses at the interior top flange.

A.4.4 Top Flange Lateral Bending Stresses

Figure A.48 illustrates the top flange lateral bending stresses. These show conservative estimates from the 2D-grid method. The stresses are calculated as discussed previously including the effects from curvature, lateral component of the vertical load and the force due to the top flange lateral bracing strut.

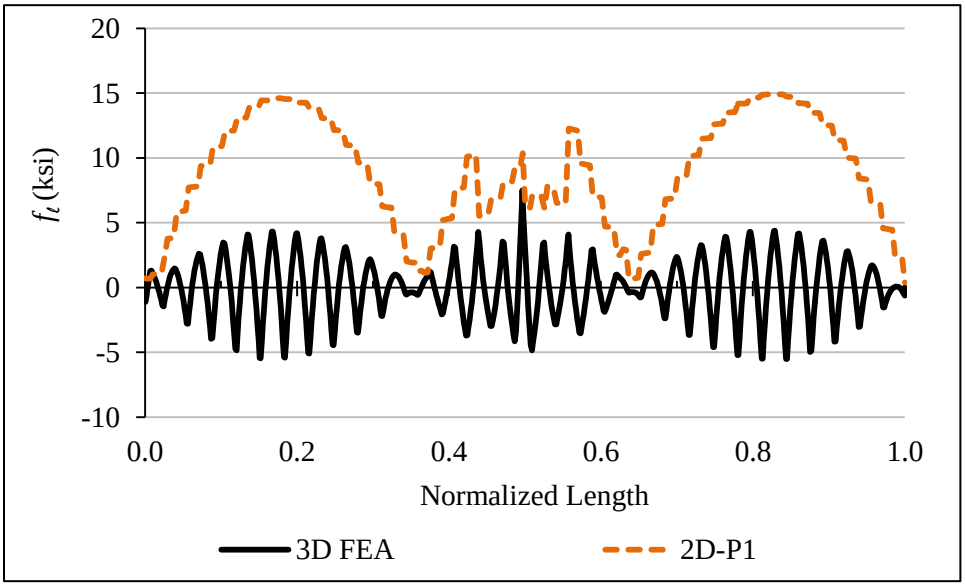

Figure A.48. Girder 1 top flange lateral bending stresses at the exterior top flange.

A.4.5 Torque Due to Skew and Curvature

As discussed previously for the estimation of the relative lateral displacements, the skew only directly affects the skewed span. For the torsional moments this assumption remains valid as the radial supports on the intermediate pier acts as a torsionally fixed support. Figure A.49 shows the torsional moment distribution on Girder 1 of the sensitivity study bridge with zero skew and Figure A.50 shows the original study case bridge NTCCS22. The torques estimated by the 2D method are the result of including the skew in the grid. The torque calculated using 1D line-girder is based on the estimations given by the equation

$$T_S = -\frac{GJ_g}{L_g}\phi_x \tag{3.8}$$

and the assumption that the skew only affects the left span. Figures A.49 and A.50 differ only on the left span by a constant torque calculated for the 1D method equal to 325 kip-ft.

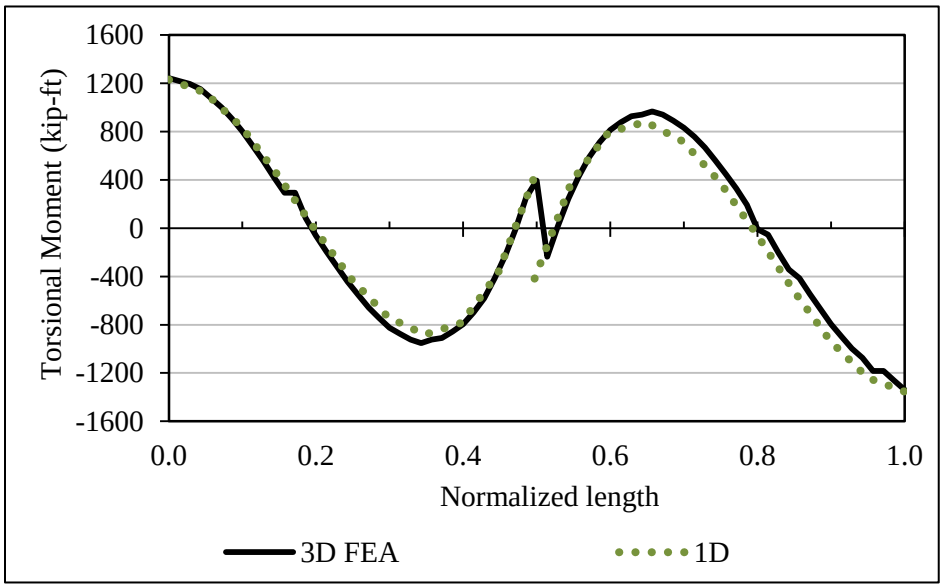

Figure A.49. Girder 1 torsional moments for the radial sensitivity case (0° skew).

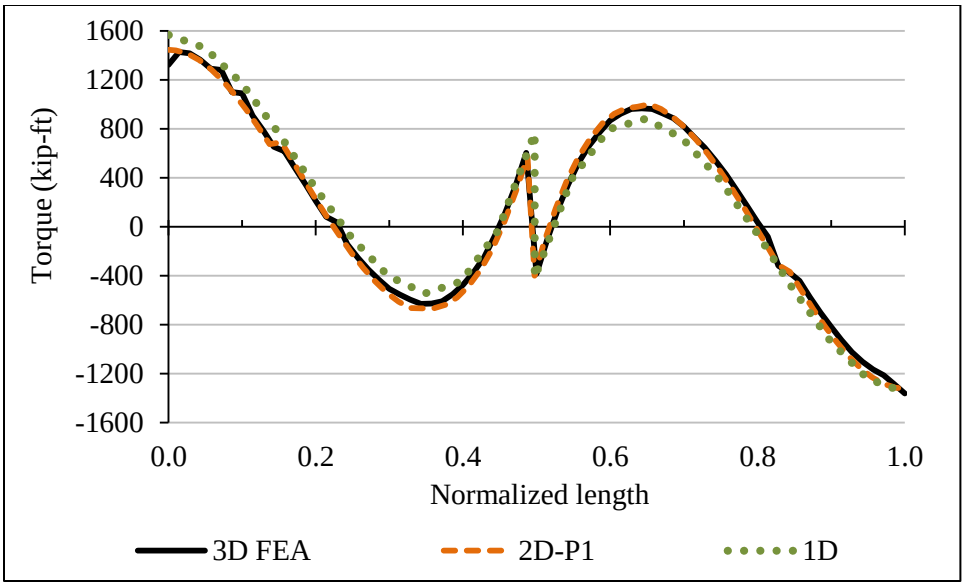

Figure A.50. Girder 1 torsional moments for the actual skewed case.

These estimations show good agreement between analyses methods and shows that the effect of the skew remains on the left span and has little effect on the right span.

For bridges where the intermediate pier is skewed, the twist rotations and torsional moments are affected on both spans. The twist rotations are dependent on the skew angle and the amount of bending rotation at this location. Therefore, the skew effects are not noticeable when the bending rotation at the support is negligible as in two-span bridges with similar span lengths.

A.4.6 Top Flange Lateral Bracing Diagonals and Struts

The top flange lateral bracing diagonals and strut forces for Girder 1 are shown in Figures A.51 and A52. The estimations of the axial forces are conservative when compared to the 3D FEA.

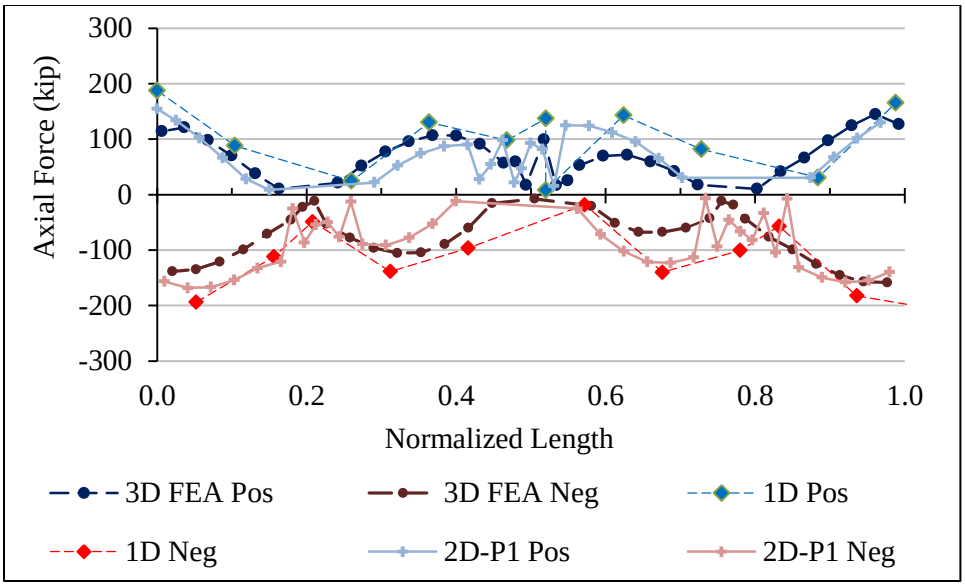

Figure A.51. Girder 1 top flange lateral bracing diagonals axial forces.

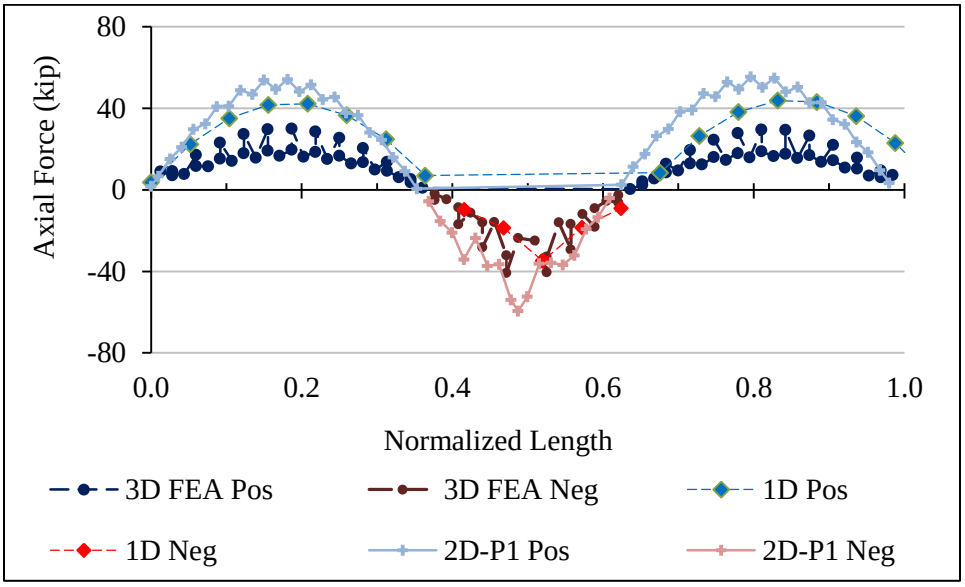

Figure A.52. Girder 1 top flange lateral bracing struts axial forces.

As discussed previously, the developments of the bracing forces are based on the assumption that other components of the bridge do not contribute to resist the forces that the bracing helps resist.

A.4.7 Steel Erection Stages Analysis

Figure A.53 illustrates the erection stages of NTSCS22 bridge and the location of the temporary supports. The total two span length of each girder is fabricated in 5 field sections.

In the erection Stages 1 and 2 the field sections are lifted onto the intermediate pier and the temporary supports. For the remaining stages two field sections of each girder are spliced on the ground. This creates longer field sections of about two fifths of the girders total two-span length. In the Stages 3 and 4 the double field sections are lifted to the right-hand abutment and connected to the central pier field sections. Stage 5 assumes that the temporary supports are removed before continuing with the erection of the remaining field sections. This step is selected arbitrarily in order to create a hypothetical erection constraint. The last field sections are lifted and connected in Stages 6 and 7.

The erection scheme shown in Figure A.53 uses temporary supports that provide reduced displacements during the first erection stages. For the last erection stages, the lack of temporary supports creates larger displacements. However, the higher tub-girder stiffness allows for a reduced amount of vertical displacements.

Figures A.54 and A.55 illustrate the evolution of the displacements during the steel erection Stages 6 and 7 for Girder 2. Figures A.56 and A.57 illustrate stress evolution during the same steel erection stages. All the displacements and stresses are shown for unfactored steel self-weight load.

In this case, the displacements during the partial steel erection stages are comparable to those on the final steel erection stage. The maximum displacements during the last partial steel erection stages and the final steel erection are 3.6 in to 2.7 in respectively. These result on a ratio larger than 1.0. This ratio is beyond any definition for a no-load-fit erection scheme.

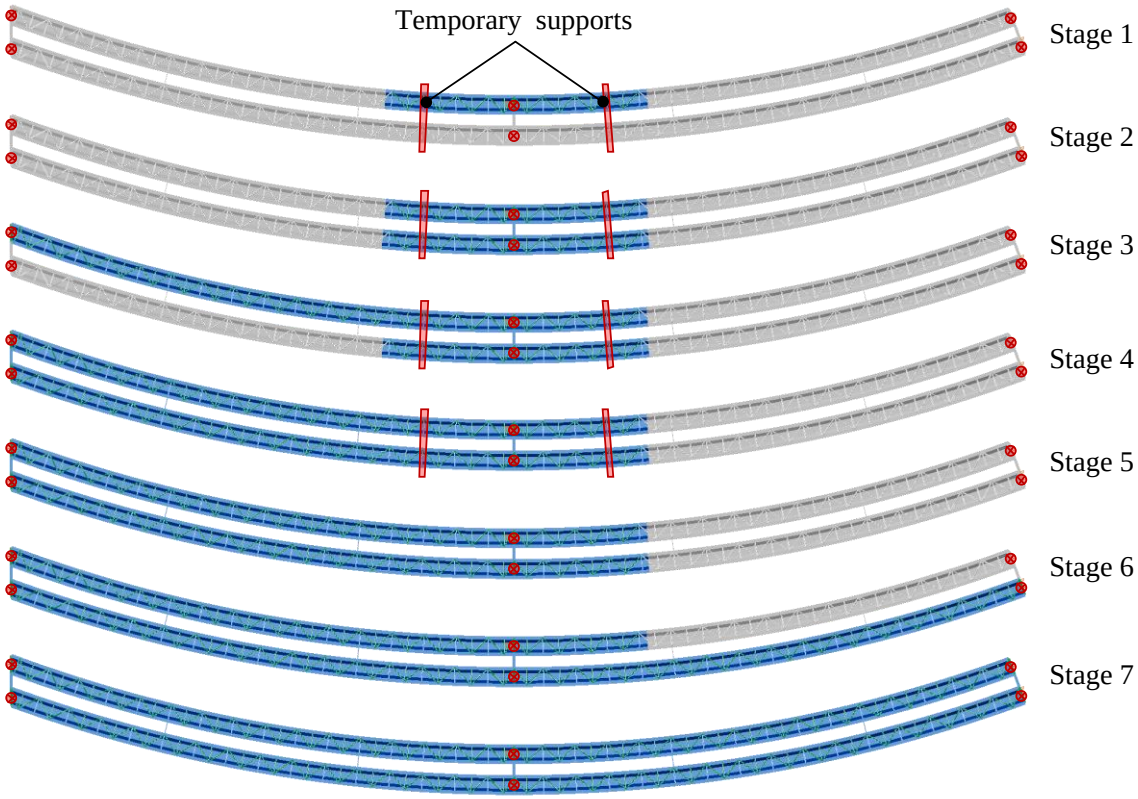

Figure A.53. Intermediate steel erection stages.

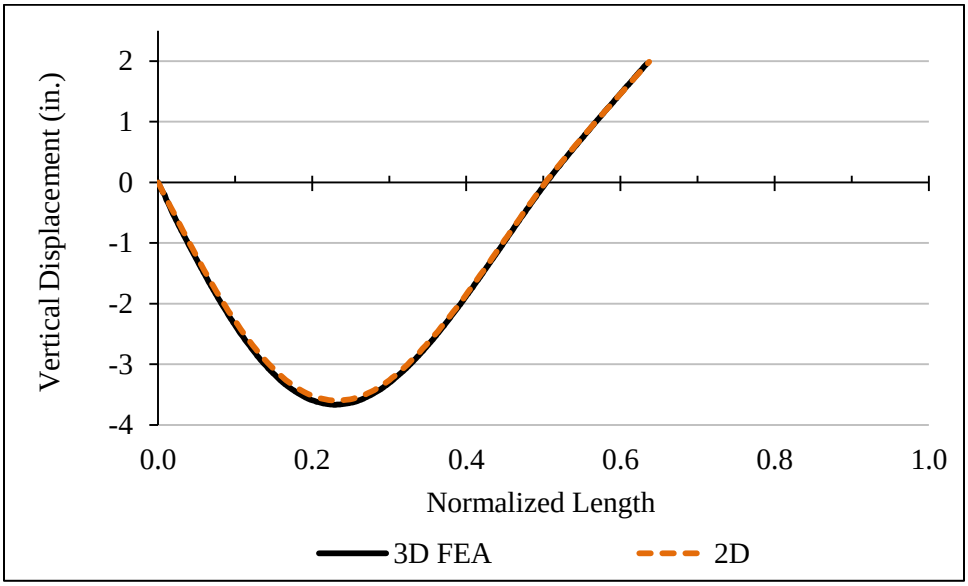

Figure A.54. Girder 2 vertical displacements for Stage 6 under steel dead load.

From Figures A.54 and A.55 the vertical displacements at the splice location (0.63 the normalized length) are 1.8 in for Stages 6 and –1.3 in for Stage 7. The relative

displacement is more than 3 in. However, in practice the girder to be connected can be lifted and inclined by the cranes to a location which does not require additional stress to perform the connection regardless of the relative displacements and rotations. Once the splice is connected the girder is released to let it sit in the supports.

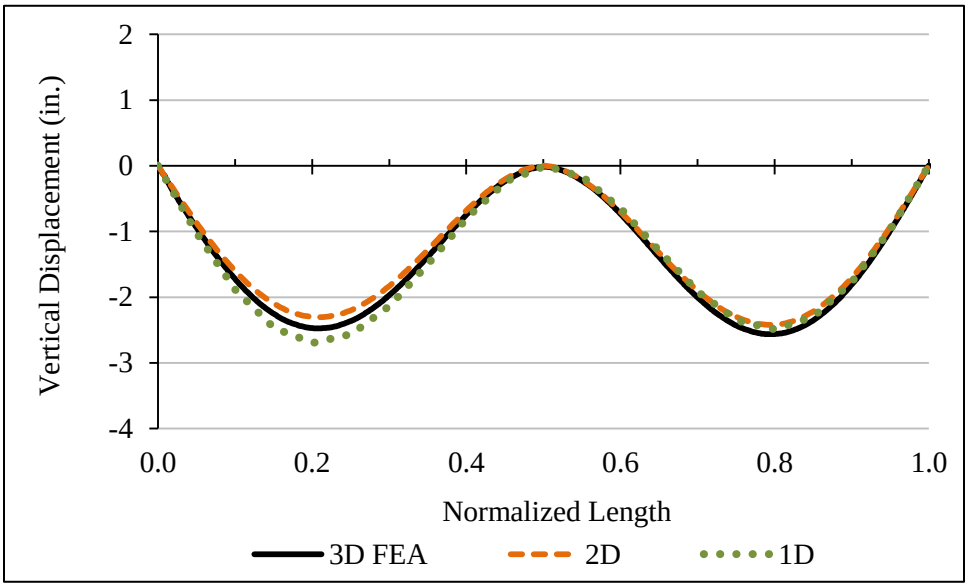

Figure A.55. Girder 2 vertical displacements for Stage 7 under steel dead load.

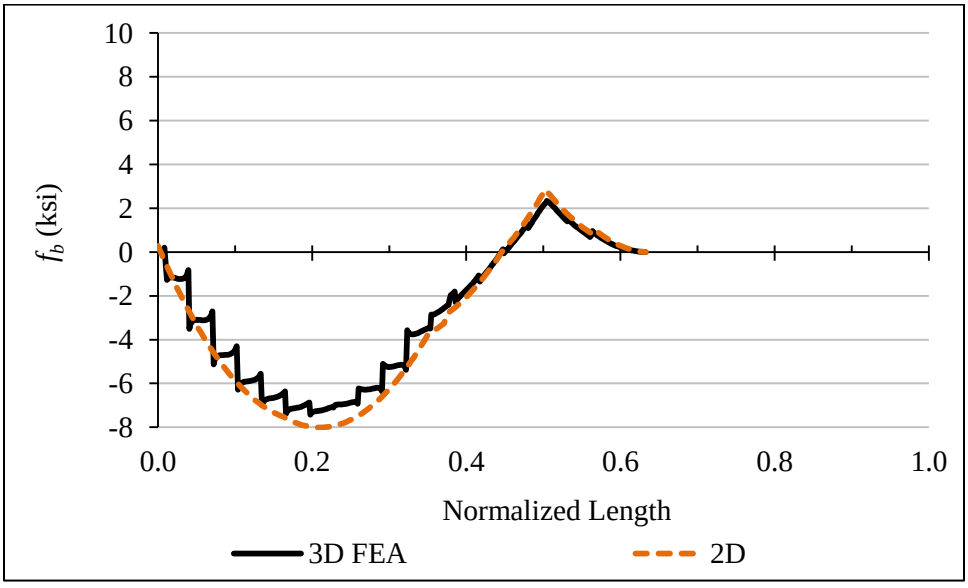

Figure A.56. Girder 2 top flange major-axis bending stresses for Stage 6 under steel dead load.

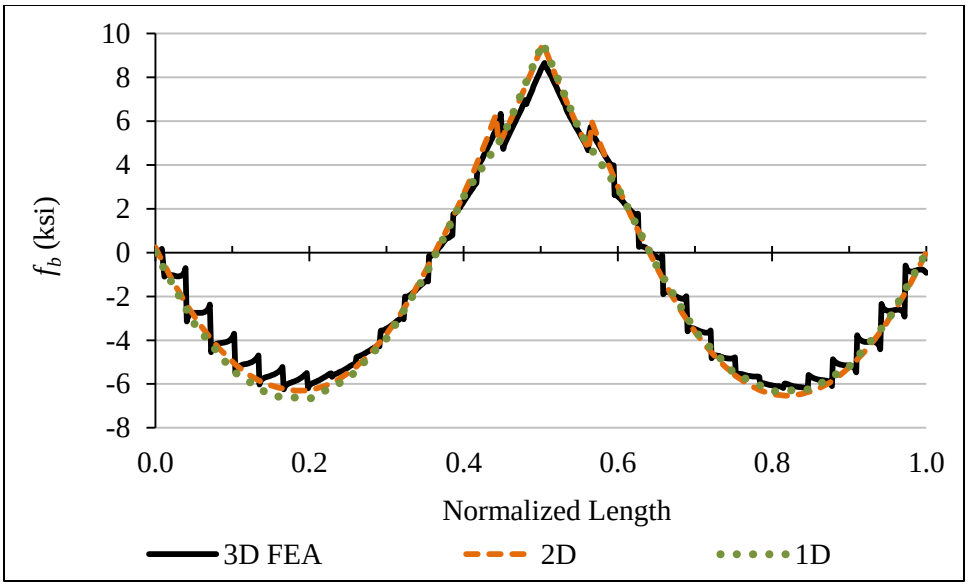

Figure A.57. Girder 2 top flange major-axis bending stresses for Stage 7 under steel dead load.

Between stages 6 and 7 in Figures A.56 and A.57, the stress at the splice location goes from zero to approximately 2.0 ksi. This value indicates the upper bound stress that the top flange of the girders could experience under an erection scheme that requires displacing the girders to the common location in Stage 7. However, as discussed earlier, the erection would follow a procedure in which the girder would be lifted and inclined to perform the connection at an unstressed position and then released.

After the girders are released, the external intermediate cross-frames and diaphragms may need to overcome additional girder rotations to perform the connections. The following section discusses lack of fit at the support diaphragm location to estimate the fit-up forces.

A.4.8 Steel Erection Fit-up forces

This case is studied for fit-up analysis for one possible scenario in which the one of the abutment external diaphragms is the last element to be connected. The scenario assumes that all girder splices have been connected, that the girders are sitting on the supports, the temporary supports have been removed and the support diaphragm is the last element to be connected.

In this steel erection stage, the girders torsional moments are zero at the abutment and therefore, the girders need to be brought to the configuration where they develop an equivalent torque in order to be connected. According to the 1D line-girder results for the steel dead load, at the skewed abutment the torsional moments are 590 kip-ft for Girder 1 (exterior girder) and 602 kip-ft for Girder 2 (interior girder). On the radial abutment the girder torsional moments are 512 kip-ft for Girder 1 and 463 kip-ft for Girder 2. Depending on the diaphragm to be connected last, these are the torsional moments that need to be applied to bring the girders to the adequate position.

Figure A.58 illustrates a set of forces to generate the required torsional moments to connect the girders for the case where the radial abutment is the last element to attach. The figure shows one set of forces which require only vertical forces, the actual set of forces is specific of the job conditions. For example, in order to reduce the 128 kip load, a horizontal load with magnitude of 56 kip could be used instead.

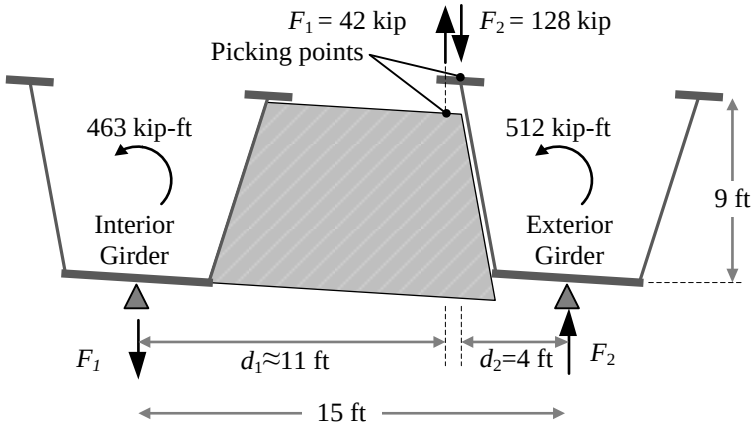

Figure A.58. Set of forces required to connect the girders on the radial abutment of NTCCS22.

On the skewed abutment a similar set of forces can be evaluated, besides the changes in the torsional moment magnitudes, the associated lengths are expected to change due to the skew but the resulting set of forces is larger than the forces at the radial abutment.

The above developments present the worst case scenarios where the girders have been allowed to fully rotate, in practice, these types of scenarios are avoided by the use of temporary supports. The forces estimated serve as indication of the level of forces expected

A.5 ETSSS2 Existing Bridge

A.5.1 Description

The ETSSS2 is one phase of the Sylvan Bridge over the Sunset Highway in Multnomah Co. OR. The phase is a three tub-girder simple-span, straight and skewed bridge. The top flange lateral bracing layout is illustrated in Figure A.59. All results are shown for Girder 1. The torsional moment distribution is shown for the three girders. The girders are numbered bottom to top on the layout on Figure A.59.

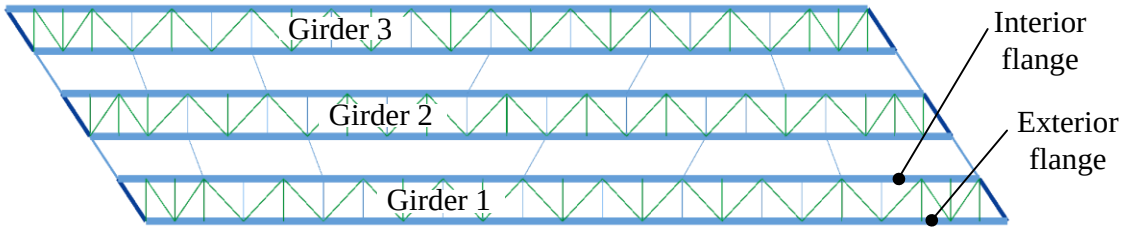

(L_1 = 205 ft / *deck width* = 56.5 ft / θ_1 = 33.4°, θ_2 = 33.4°)

Figure A.59. ETSSS2 Bridge Layout.

This bridge exemplifies the calculation of the torques due to skew using the 2D-grid and 1D line-girder analyses. The effect of the several external intermediate cross-frames on the girder torques is presented. Additionally, the bridge uses double bearings and therefore their effect on the accuracy of analytical methods is discussed.

A.5.2 Displacements

Figure A.60 illustrates the vertical and relative lateral displacements for Girder 1. As shown in Fig. A.61, double girder bearings do not help control the lateral displacements as the girders rotate with respect to the bearing line and the skew causes a layover.

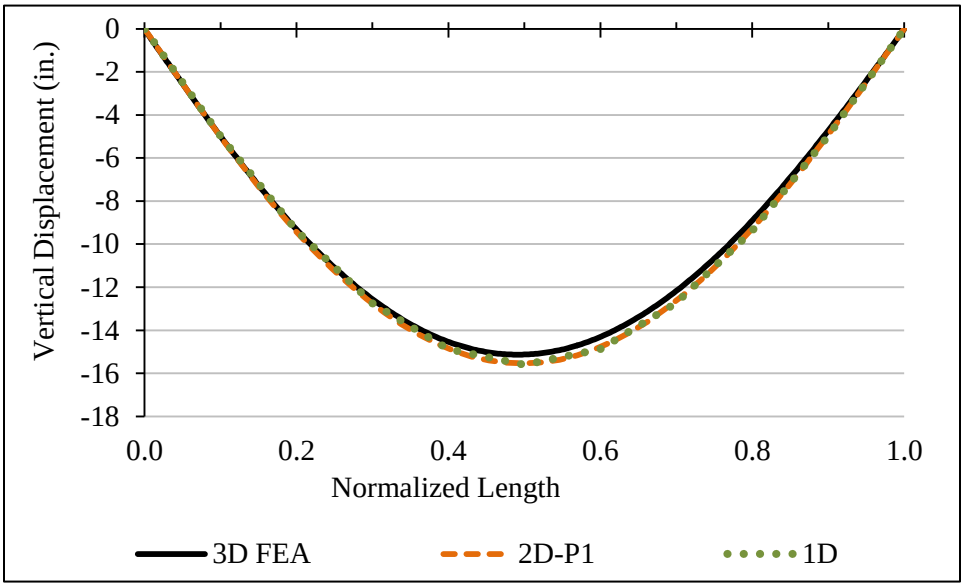

Figure A.60. Girder 1 centerline vertical displacements.

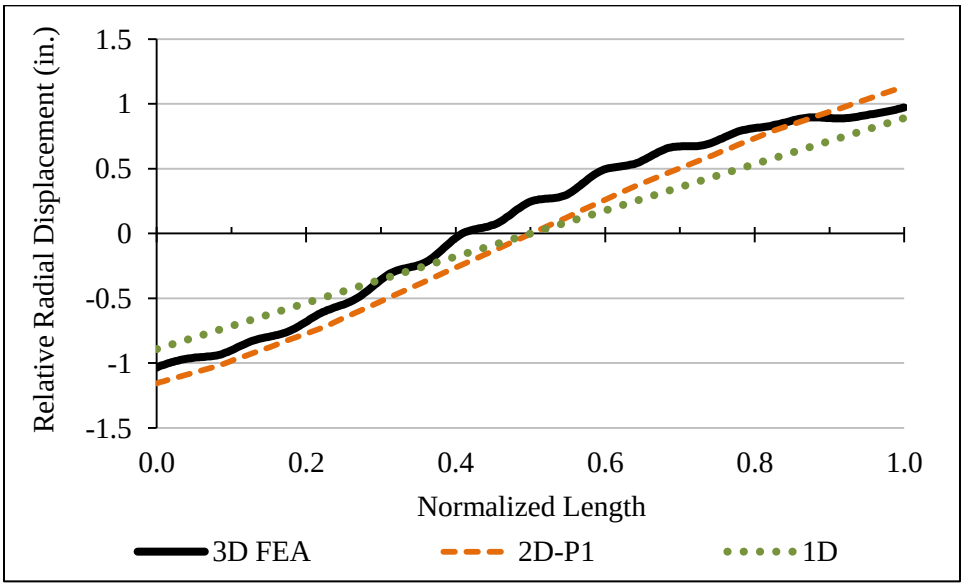

Figure A.61. Girder 1 relative lateral displacements.

The simplified analyses show good agreement with the 3D FEA. The 2D-analysis includes the skew on the grid and the 1D line-girder uses the approach discussed previously. The numerous external intermediate cross-frames show negligible impact on the displacement estimations.

A.5.3 Top Flange Major-Axis Bending Stresses

The top flange major-axis bending stresses are shown in Figures A.62 and A.63 for both top flanges. The sawtooth effect is shown again and has a behavior similar to those discussed for the NTSSS2 bridge. For this case the sawtooth stresses are not calculated for the simplified analysis methods and only the average stresses are presented.

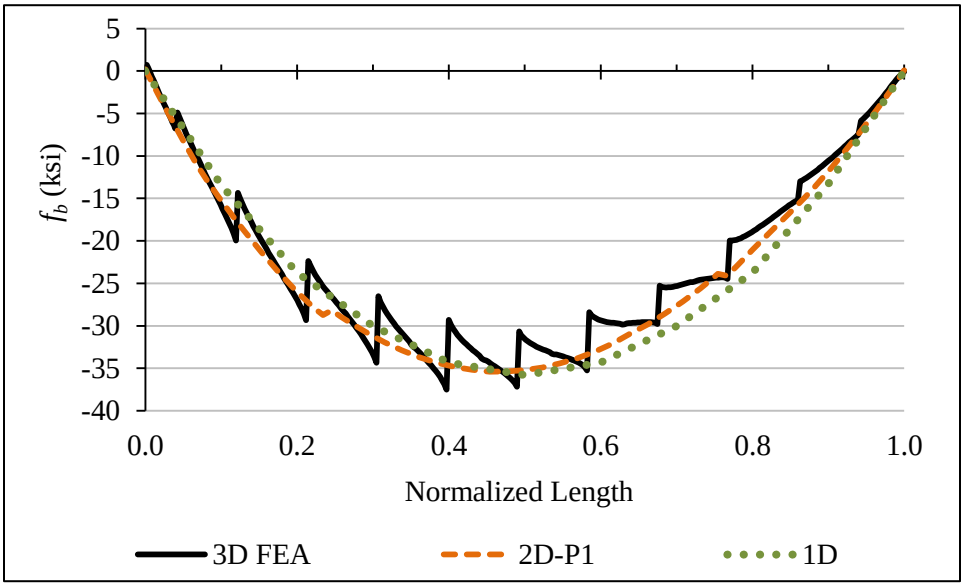

Figure A.62. Girder 1 top flange major-axis bending stresses at the exterior top flange.

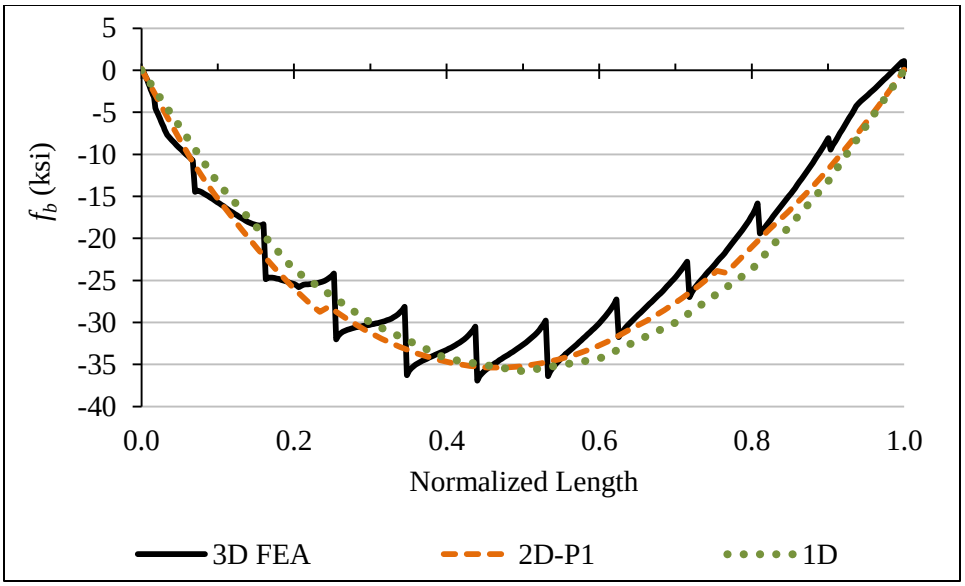

Figure A.63. Girder 1 top flange major-axis bending stresses at the interior top flange.

A.5.4 Top Flange Lateral Bending Stresses

Figure A.64 shows the top flange lateral bending stresses. The stress distribution is similar to those shown for the NTSSS2 bridge. The 3D FEA results do not exhibit increased stresses close to the supports since the top flange lateral bracing system begins with a diagonal rather than a strut as in NTSSS2.

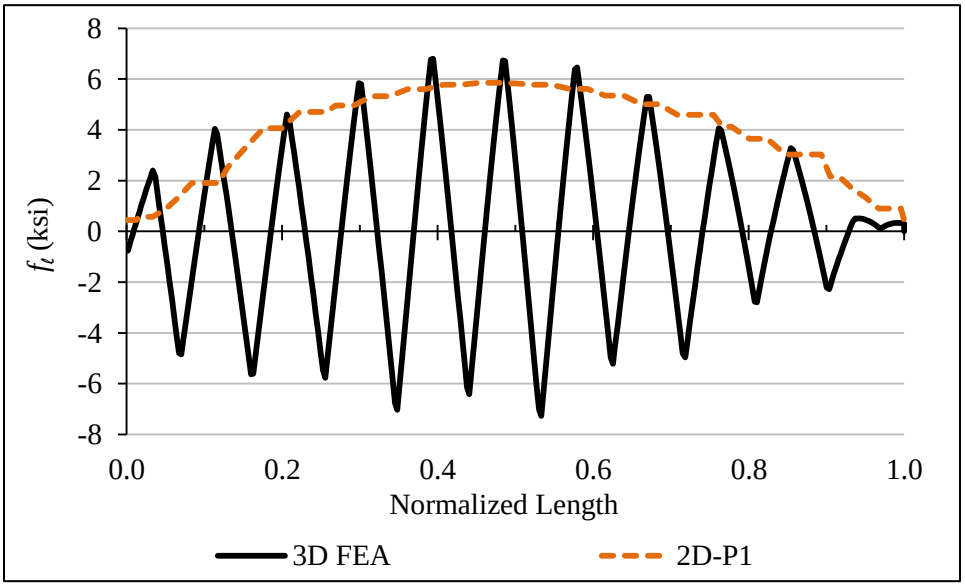

Figure A.64. Girder 1 top flange lateral bending stresses at the exterior top flange.

A.5.5 Torque Due to Skew

Figures A.65, A.66 and A.67 illustrate the torsional moments as calculated by the simplified method and the 3D FEA for the three girders on the bridge. The effect of the multiple external intermediate cross-frames is evident on the 3D FEA and barely noticeable on the 2D-grid method. The 1D line-girder method neglects all external intermediate cross-frame interaction unless it is included as discussed for NTSCR1.

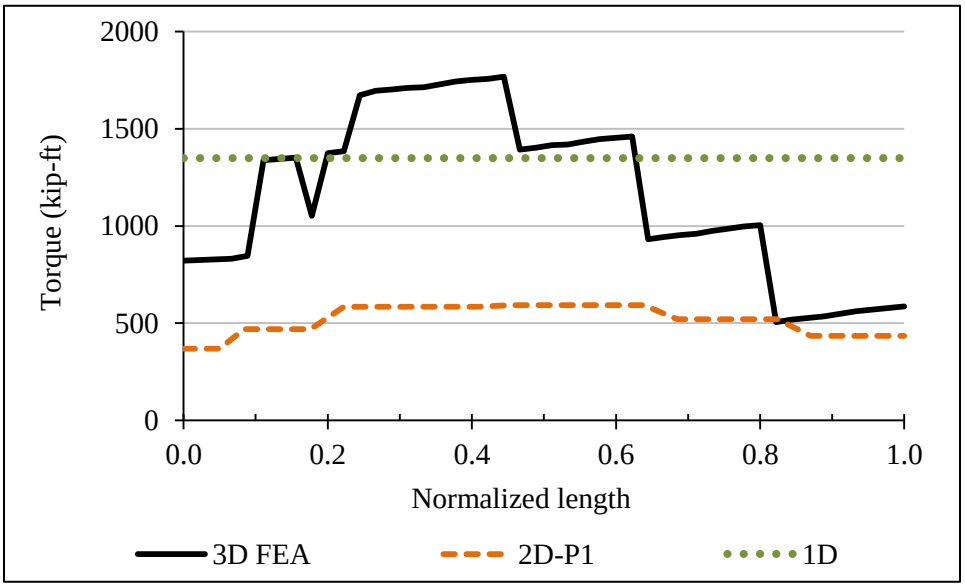

Figure A.65. Girder 1 torsional moments.

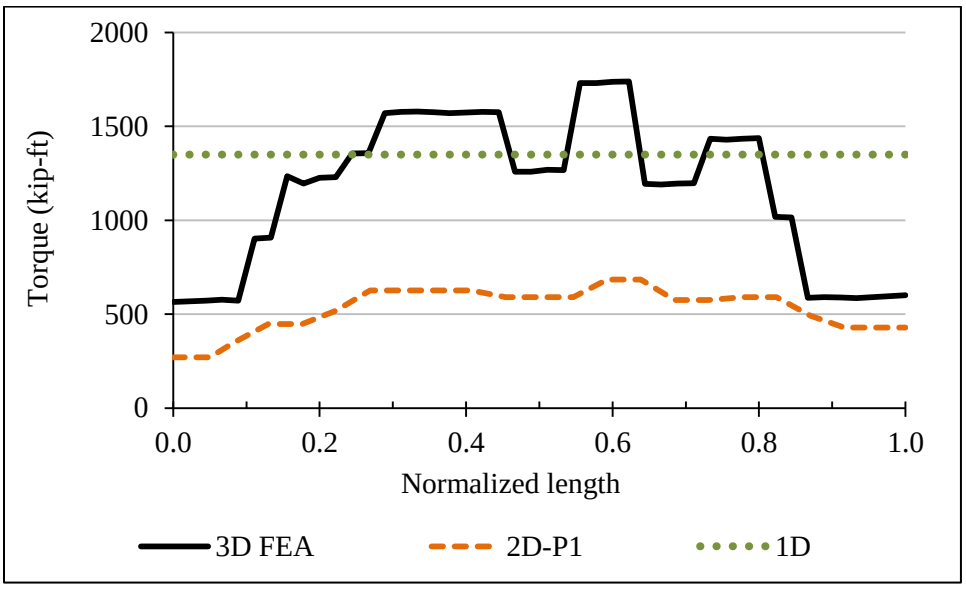

Figure A.66. Girder 2 torsional moments.

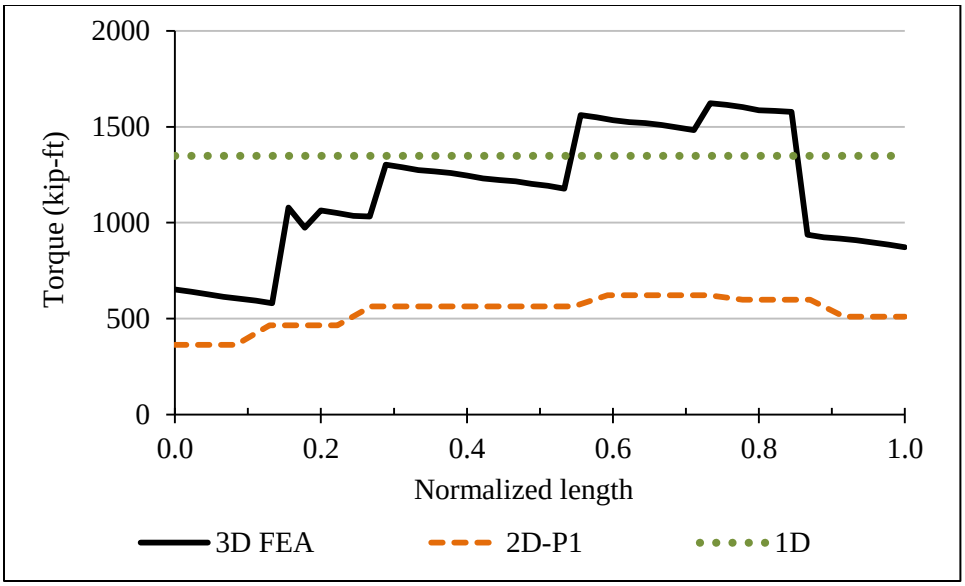

Figure A.67. Girder 3 torsional moments.

The external intermediate cross-frames are skewed and follow a non-uniform pattern. The layout shown in Figure A.59 shows that the external intermediate cross-frame are not tangent to the girders, non-parallel to the supports and have different skew angles.

At each external intermediate cross-frame location, the torsional moment presents an increase in magnitude. This is due to the force distribution between girders. The magnitude of the transferred force is proportional to the relative vertical displacements but, since the girders are interconnected at different relative locations along the spans, the transferred force is greater and harder to capture than for a bridge where the external cross-frames are used at similar relative locations along the spans.

A.5.6 Top Flange Lateral Bracing Diagonals and Struts

The top flange lateral bracing diagonals and struts forces on Girder 1 are shown in Figures A.68 and A.69. The accuracy of the forces on the diagonals on Figure A.68 depends in great measure on the torsional moment estimations. In consequence, the 2D-grid analysis method accuracy is poor since the torsional moment was underestimated. The 1D line-girder method has better accuracy but relies on the conservatism given by the component force equations.

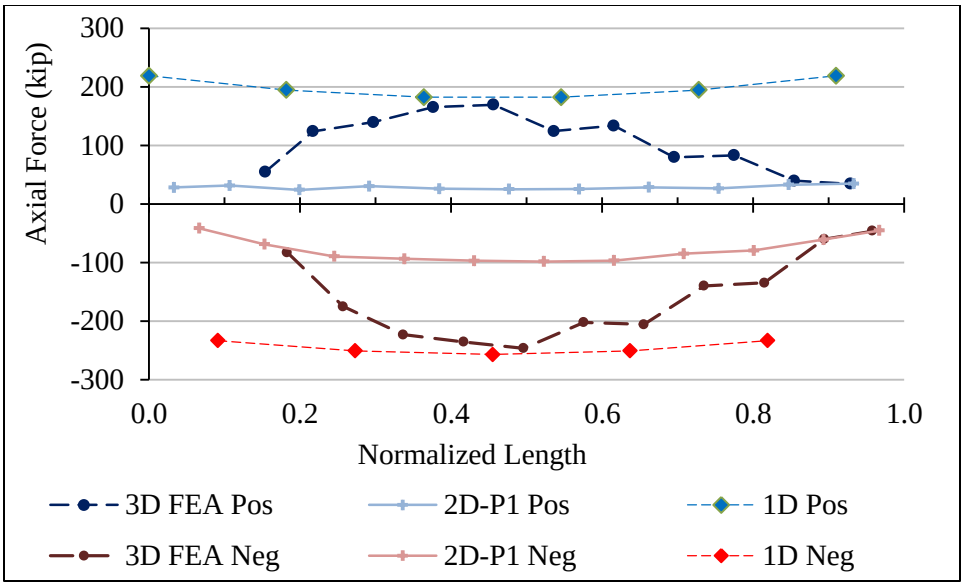

Figure A.68. Girder 1 top flange lateral bracing diagonals axial forces.

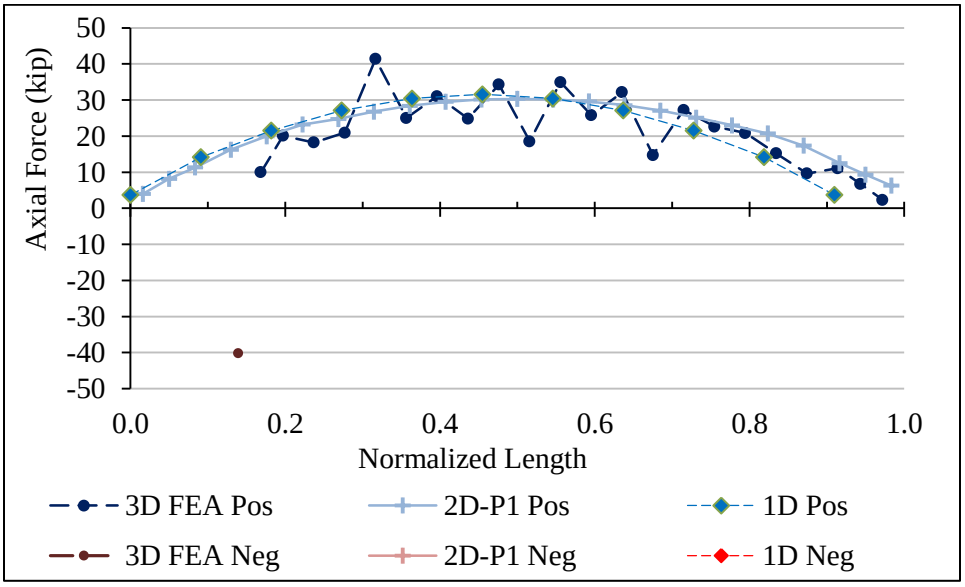

Figure A.69. Girder 1 top flange lateral bracing struts axial forces.

On Figure A.69, at the normalized length close to 0.14 the strut force as given by the 3D FEA experiences a negative force. At this location an external intermediate cross-frame connects and there is no internal cross-frame to handle this force and therefore the behavior cannot be predicted by the simplified analysis methods.

For the simplified methods to estimate the bridge behavior accurately, uniformity on the bridge layout is the preferred characteristic.

A.5.7 Twin Bearings

The ETSSS2 bridge utilizes a double bearing per girder. The benefits of this configuration allow the distribution of the load and permit a bearing design for a reduced load. However, when the girders are subjected to torsional moments, rotations can occur during the bridge erection that may trigger uplift at the supports. Support uplift may produce increases on the reactions and possible damage to the bearings.

The 3D FEA analysis provided the vertical reactions shown in Figure A.70 which indicated negative (uplift) reactions. The 3D FEA analysis was switched to unidirectional supports to prevent the development of false tie downs at the bearings.

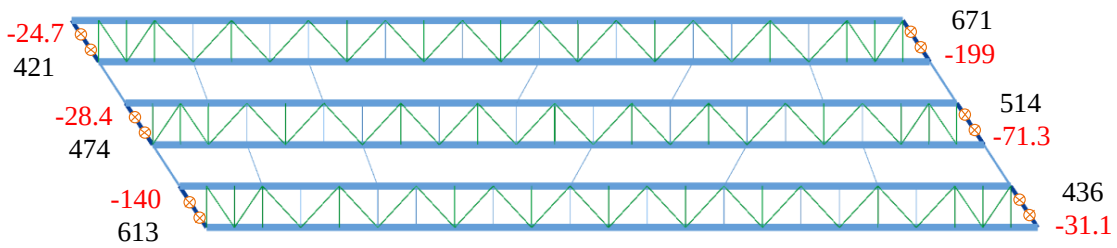

Figure A.70. Vertical reactions in kip from the 3D FEA.

The field observations in this bridge did not report uplift. However, the analysis reported very small upward displacements that could have been overshadowed by several factors occurring during construction such as the inherent flexibility of the bearing pads, camber effects, etc. The effects of imminent bearing uplift, as those described herein, are only captured when the 3D FEA is used or by modeling the actual bearing offset on the 2D-grid.

The ETSSS2 bridge exhibits several details that the simplified methods cannot model nor represent accurately. The most relevant issue is the estimation of the torsional moments caused by the presence of an irregular layout of external intermediate cross-frames. A bridge of such complexity should be analyzed using 3D FEA or the bridge layout should be modified so that the simplified methods can be implemented without the necessity of additional calculations.

APPENDIX B.

ANALYSIS VALIDATION

This appendix illustrates analytical results comparisons for the tub-girder top flange lateral bracing system component forces. For the purposes of these comparisons, the example published by Fan and Helwig (1999) is selected. The problem is a single three-span continuous curved tub-girder with radial supports. In the following, the geometry of the bridge is described first. Then the analysis results are summarized.

B.1 Girder Description

Figure B.1 illustrates the girder spans and cross section geometry. The girder has a total length of 640 ft and has a radius of curvature of R = 954.9 ft, corresponding to a 6° change in the subtended angle per 100 ft of length. The girder has two cross-sections, one for the positive moment region (P) and one for the negative moment region (N). The top flange lateral bracing system diagonals are WT6×13 sections and the struts are L4×4×5/6 sections. Both of these sections are constant for the entire bridge. A bottom flange longitudinal stiffener is located on the negative moment cross-section. The stiffener is a ST9×35 section. No internal cross-frames are specified. The top flange lateral bracing system uses an X-type layout with a panel size of 10 ft.

The girder is subjected to two uniform vertically distributed loads applied at the juncture of the webs with the top flanges. Each load is 1.65 kip/ft and represents the total concrete and steel self-weight.

B.2 Component Force Equations Result Comparisons

The girder is symmetric about the middle of the center span; therefore, the results are shown only for the first half of the bridge for simplicity. The bridge uses an X-type top flange lateral bracing system, and the responses are shown by grouping the diagonals that have the same inclination as X1 and X2. Note that the forces are generally not the same in any two diagonals of a given panel.

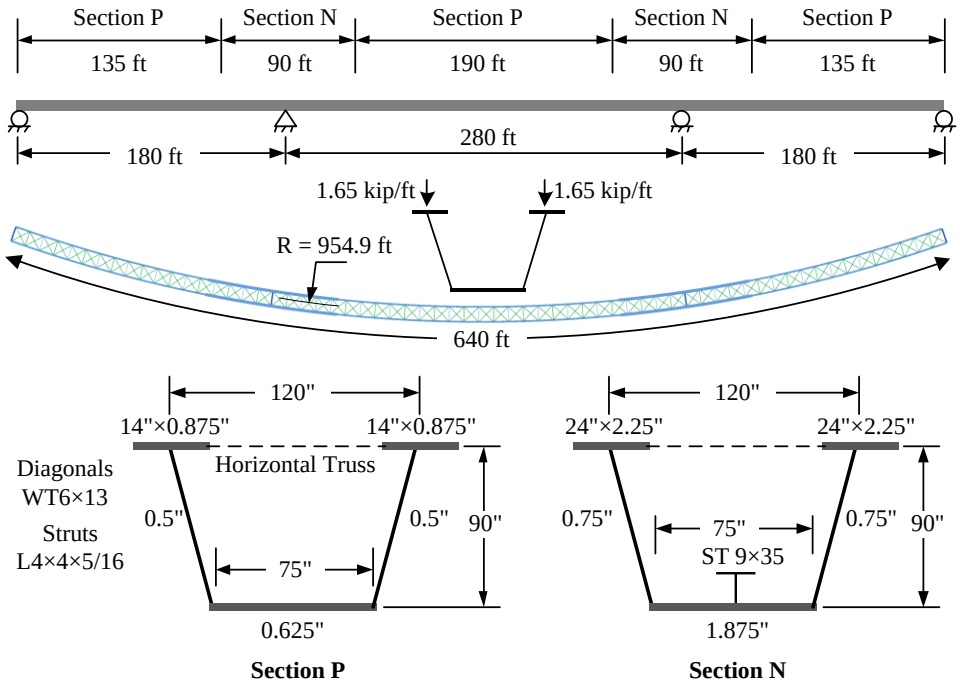

Figure B.1. Bridge geometry and plate dimensions.

The bridge is modeled and analyzed via 3D geometric non-linear elastic FEA using the ABAQUS Software (2011). In addition, the bracing component forces are calculated using a 1D line-girder analysis along with the M/R Method and the component force equations presented in Chapter 2. The analysis results are compared to the published values by Fan and Helwig and presented in the same graphical format.

Figure B.2 shows three plots for the axial forces in the top flange lateral bracing diagonals X1 and X2 and in the strut. The horizontal axis represents the position along the girder normalized with respect to the total girder length. The diagonals have a cross-section area equal to 3.82 in² and the struts 2.40 in², which results in a maximum stress of 13 ksi for the diagonals and 16 ksi for the struts.

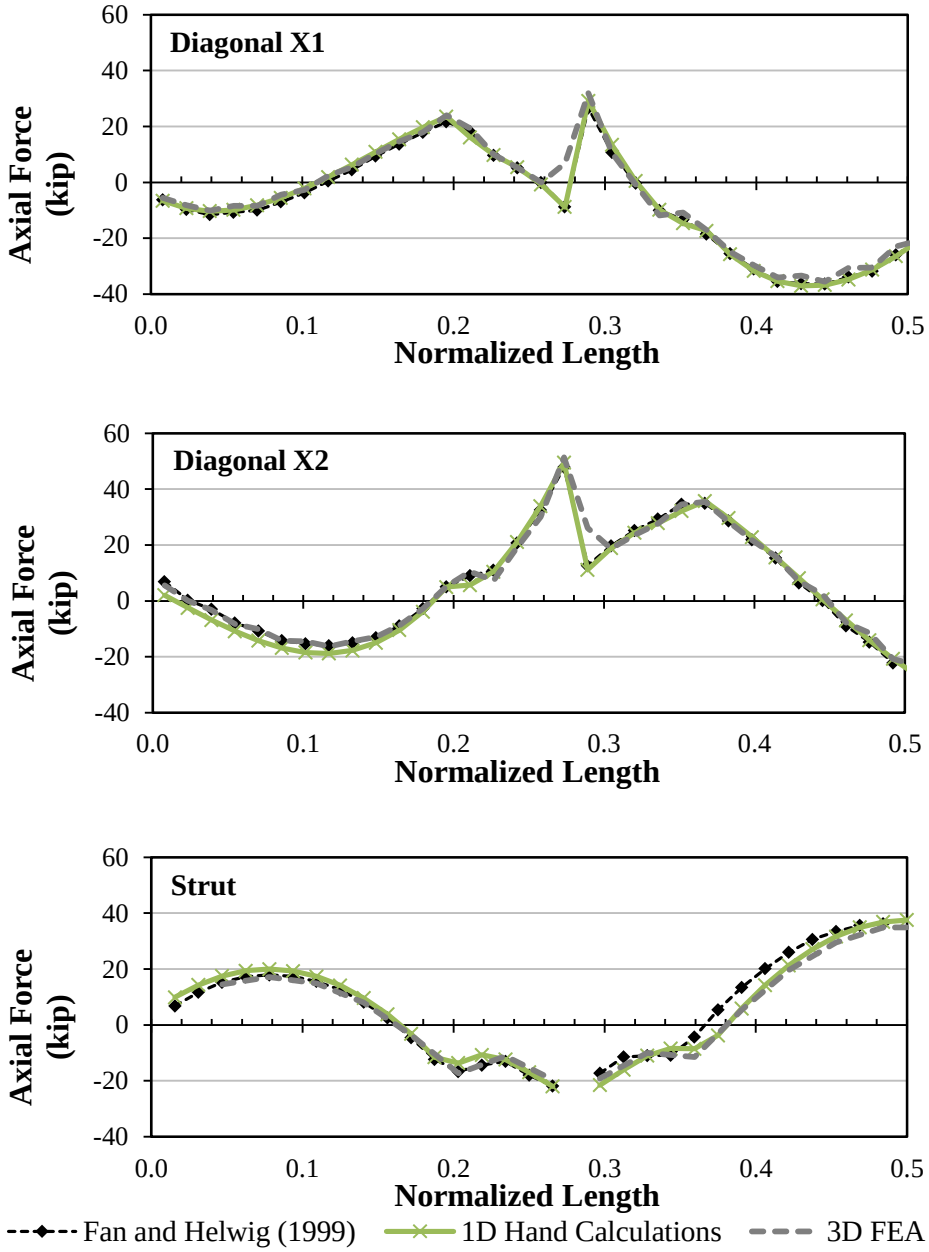

Figure B.2. Top flange lateral bracing diagonal and strut axial forces.

The intermediate pier is located at 0.29 of the normalized length. At this location, the forces on the diagonals exhibit differences due to the proximity to the support diaphragm. This localized interaction is not captured by the component force equations in Chapter 2.

B.3 Three-Dimensional FEA Results Comparisons

Fan and Helwig provide the bracing forces from a 3D FEA analysis, which are compared with the results from the ABAQUS simulations performed in this research. Figure B.3 shows the results from the two implementations of the 3D FEA to validate the modeling techniques used in this research.

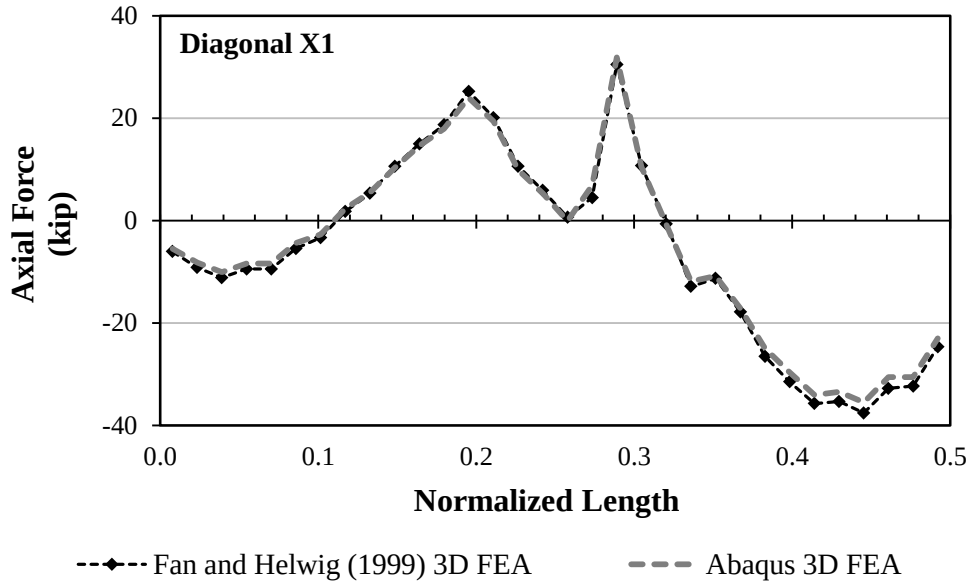

Figure B.3. Top flange lateral bracing diagonal X1 axial forces.

B.4 Analysis Validation Summary

The 3D FEA shows good agreement with the simplified procedures in distribution and magnitude. A mean error equal to 5 % is found when comparing the 3D FEA results to the implementation of the M/R Method and the component force equations in Chapter 2. When comparing the 3D FEA to the results published by Fan and Helwig the mean error is 5 %. The strut forces exhibit errors of 6 % and 7 % respectively. Likewise, the 3D FEA modeling techniques used in this research match the results of the 3D FEA implementation by Fan and Helwig within 3 percent of mean error.

The simplicity of the analyzed bridge system presents several advantages for the accuracy of the bracing component force equations. The beneficial characteristic of this bridge are

- Symmetry.
- Uniform bracing elements in cross-section and distribution.
- Absence of interaction with adjacent girders via support diaphragms and/or external intermediate cross-frames.
- Radial Supports.
- Lack of internal cross-frames.
- Uniform and non-eccentric vertical loading.

In practice, it is highly unlikely to have all these characteristics and in consequence, the simplified analysis methods and the application of the component force equations experience some degradation in their accuracy. Nevertheless, the simplified analysis method still provides useful estimates for design purposes. The simplified analysis errors are highly related to the deviation of the bridge geometry from the above ideal attributes.

APPENDIX C.

COLLECTED EXISTING BRIDGES

This appendix summarizes the overall characteristics of the existing tub-girder bridges collected from various owners and consultants. The figures show sketches of the overall deck plan geometry and bearing lines. The linear dimensions indicated in the sketches are provided in units of feet and all the angular dimensions are provided in degrees. All bridges are oriented concave upwards and the skew angle is measured from the radial lines, positive skew angles are measured counterclockwise.

Each of the bridge sketches in Figs. C.1 through C.6 has a title block containing the following information:

1. An identification label, composed of the letter "E" for "Existing" followed by the above symbols indicating the bridge category, and ending with the bridge number for that category, e.g., bridge "ETSCR1" in Figure C.3.
2. A description of the structure composed of the bridge name and/or location.
3. A summary of the basic geometry information about the bridge, enclosed in parentheses. For instance, in Figure C.3, the basic geometry information for the single ETSCR bridge includes:
    - The arc-span length of the bridge centerline,
    - The horizontal radius of curvature of the bridge centerline, and
    - The out-to-out width of the bridge deck perpendicular to the bridge centerline.

    This information is conveyed symbolically in the figure caption as "(LENGTH/RADIUS/WIDTH)." The other categories have similar but different basic geometry information. This information is summarized symbolically in each of their figure captions. The skew angle of the bearing lines is represented by the symbol θ. This angle is taken as zero when a bearing line is perpendicular to the centerline of the structure, that is, when the bearing line does not have any skew.

4. The symbol "*", at the end of the parentheses delimiting the basic geometry information, if the bridge has erection plans. No symbol is shown if the bridge does not have erection plans.
5. The organization that provided the drawings for each bridge. This information is delimited by square brackets, i.e., "[NHI]" in Figure C.3.

Other pertinent information is provided underneath the plan sketch of each of the bridges. This information includes data such as the number of girders in the bridge cross-section, whether test or field data is available for the structure, references to papers or reports containing test data or documentation of previous research on the bridge, and brief notes regarding successes or difficulties for certain bridges. Note that one scale is utilized for all the simple-span bridges, whereas a slightly smaller scale is used for all the continuous-span bridges.

(ETSSS 1) Sheffield Rd. Over The Green River, Great Barrington, MA
(139 / 49.6 / -15, -15) [Tensor]

Simple span, Three tub-girders

(ETSSS 2) Sylvan Bridge over Sunset Hwy, Multnomah Co. OR
(205/58.7/33.4,33.4), (205/58.7/33.4,33.4) [ODOT]

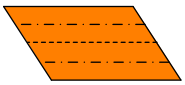

Simple span, Six tub-girders
Phased Construction

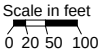

Figure C.1. Existing Tub-girder bridges, Simple-span, Straight with Skewed supports,(ETSSS #) Description (LENGTH / WIDTH / θ_{Left}, θ_{Right}) [Source].

(ETCSS 1) Rte. 853 / Division St. Over Naugatuck River, Ansonia, CT
(260, 190 / 67.8 / -22.9, -22.9, -22.9) [Tensor]

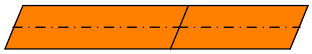

Two span continuous, Four tub-girders
Dramatically different span lengths

(ETCSS 2) US-75 Underpass at Churchill Way, Dallas TX
(139, 133, 100 / 83.0 / -34.1, -34.1, -34.1, -34.1) [HDR]

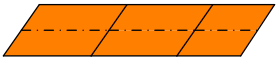

Three span continuous, Five tub-girders

(ETCSS 3) Bridge #564, Woodway Dr Overpass, Harris Co, TX
(140, 169, 121 / 69.2 / 30.2, 30.2, 30.2, 30.2) [Tensor]

Three span continuous, Four tub-girders

(ETCSS 4) Bridge #574, North Post Oak Rd Underpass, Harris Co, TX
(60.4, 124, 144, 138, 83.6 / 73.0 / -38, -38, -38, -38, -38, -38) [Tensor]

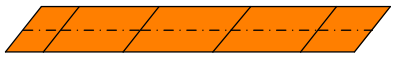

Five span continuous, Six tub-girders

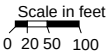

Figure C.2. Existing Tub-girder bridges, Continuous-span, Straight with Skewed supports, (ETCSS #) Description (LENGTH1, LENGTH2, … / WIDTH / θ_{Left}, …, θ_{Right}) [Source].

(ETSCR 1) NB Cross Island Pkwy to EB I495, Queens Co, NY
(101 / 484 / 25)* [HSSI]

Simple span, Two tub-girders

(ETSCR 2) Ramp M over I-71 NB, Hamilton Co, OH
(207 / 458, ∞ / 40) [ODOT]

Simple span, Two tub-girders

Figure C.3. Existing Tub-girder bridges, Simple-span, Curved with Radial supports, (ETSCR #) Description (LENGTH / RADIUS / WIDTH) [Source].

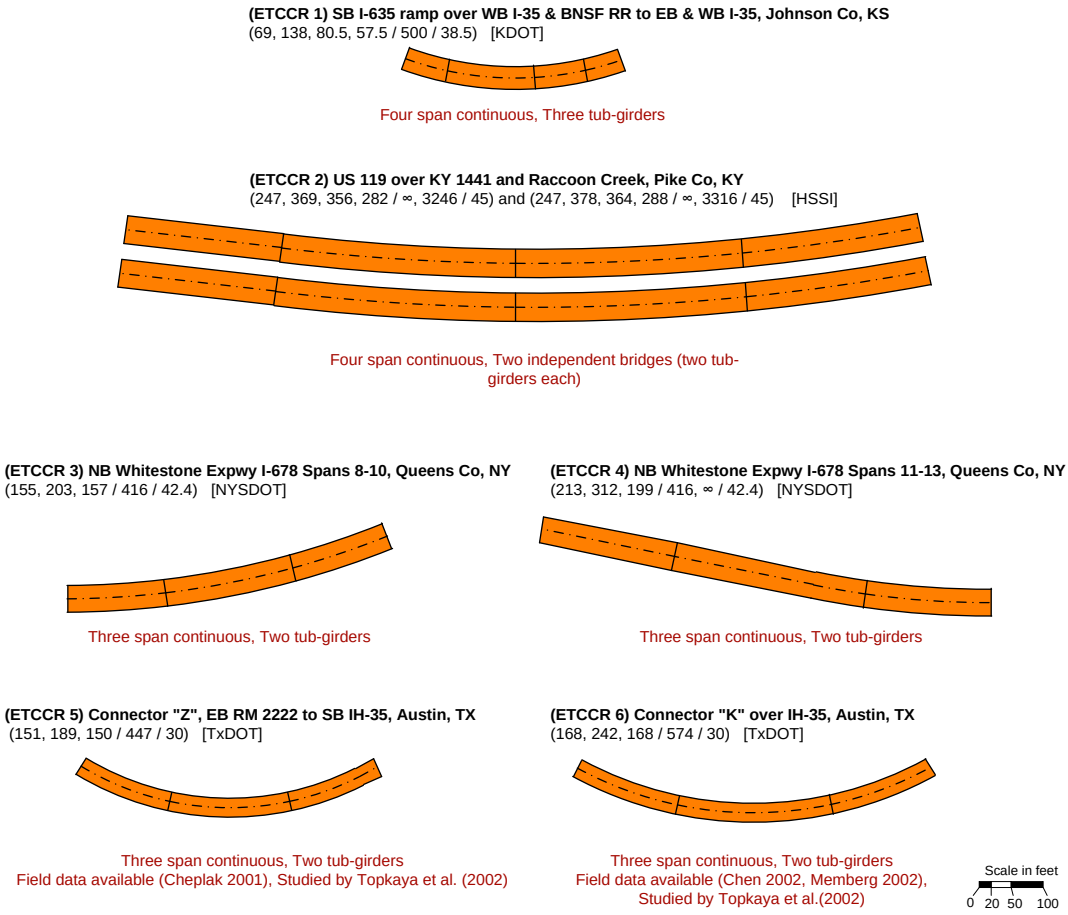

Figure C.4. Existing Tub-girder bridges, Continuous-span, Curved with Radial supports, (ETCCR #) Description (LENGTH1, LENGTH2, … / RADIUS1, RADIUS2, … / WIDTH) [Source].

(ETCCR 7) DC02 Spans 1&2 IH-30 PGBT Interchange, Dallas, TX
(164, 164 / 895 / 29) [HDR]

Two span continuous, Two tub-girders

(ETCCR 8) DC03 Spans 13&14 IH-30 PGBT Interchange, Dallas, TX
(155, 155 / 1010 / 29) [HDR]

Two span continuous, Two tub-girders

(ETCCR 9) DC03 Spans 15&16 IH-30 PGBT Interchange, Dallas, TX
(170, 170 / 1010 / 29) [HDR]

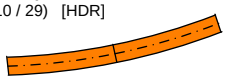

Two span continuous, Two tub-girders

(ETCCR 10) DC03 Spans 1, 2&3 IH-30 PGBT Interchange, Dallas, TX
(149, 189, 149 / 1010 / 29) [HDR]

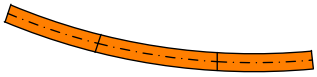

Three span continuous, Two tub-girders

(ETCCR 11) DC03 Spans 4&5 IH-30 PGBT Interchange, Dallas, TX
(167, 191 / 1010 / 29) [HDR]

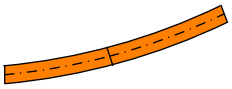

Two span continuous, Two tub-girders

(ETCCR 12) DC04 Spans 22&23 IH-30 PGBT Interchange, Dallas, TX
(165, 165 / 2060 / 29) [HDR]

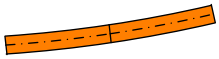

Two span continuous, Two tub-girders

(ETCCR 13) DC04 Spans 24, 25&26 IH-30 PGBT Interchange, Dallas, TX
(204, 254, 204 / 2060 / 29) [HDR]

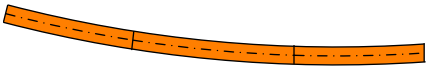

Three span continuous, Two tub-girders

(ETCCR 14) Connector EB North Beltway 8 to NB I-45, Houston, TX
(186, 286, 180 / 895 / 40.8) [TxDOT]

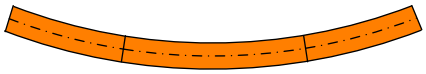

Three span continuous, Two tub-girders
Field data available (Fan 1999)

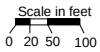

Figure C.4. (continued). Existing Tub-girder bridges, Continuous-span, Curved with Radial supports, (ETCCR #) Description (LENGTH1, LENGTH2, … / RADIUS1, RADIUS2, … / WIDTH) [Source].

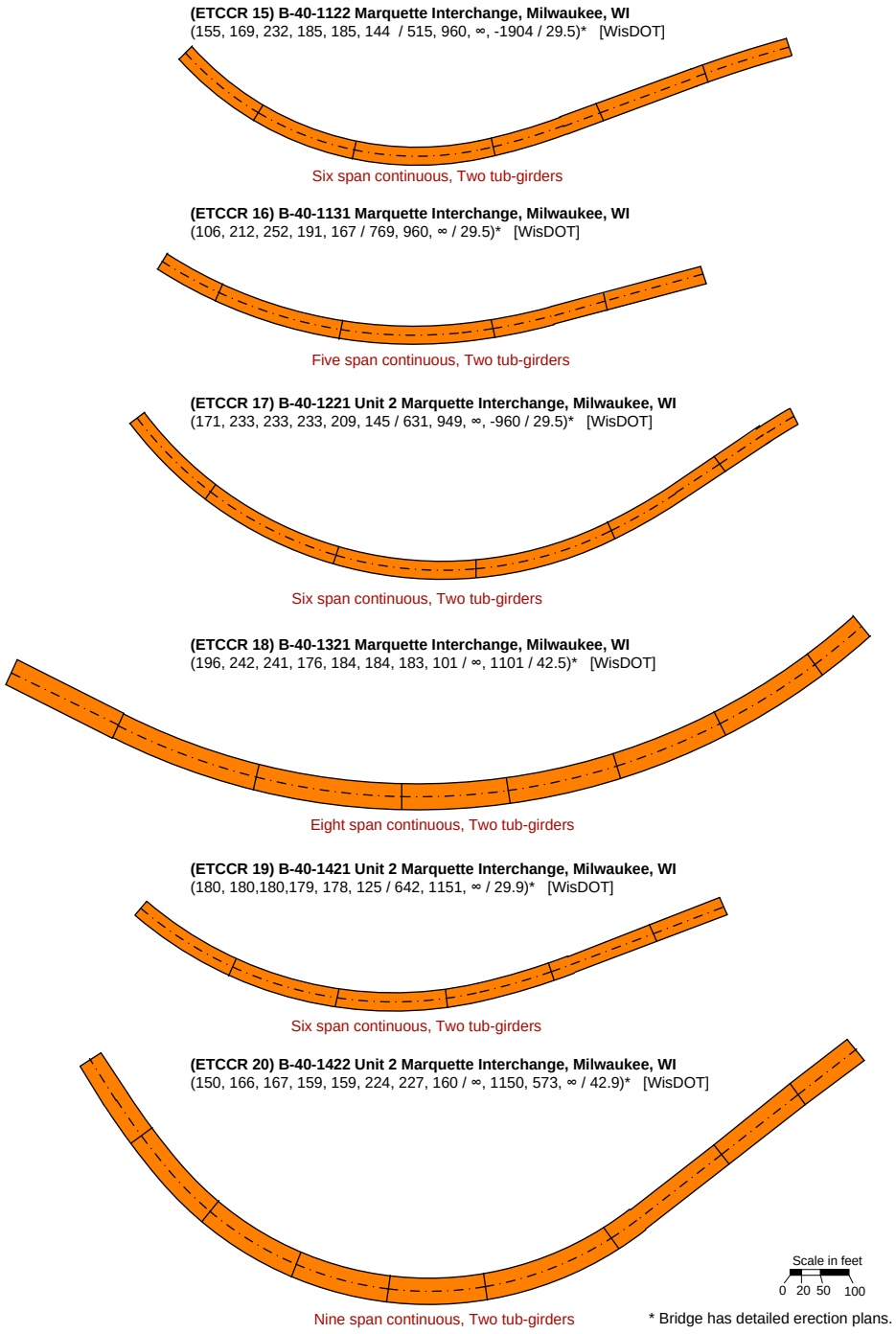

Figure C.4. (continued). Existing Tub-girder bridges, Continuous-span, Curved with Radial supports, (ETCCR #) Description (LENGTH1, LENGTH2, … / RADIUS1, RADIUS2, … / WIDTH) [Source].

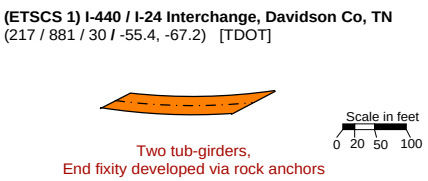

Figure C.5. Existing Tub-girder bridges, Single-span, Curved with Skewed supports, (ETSCS #) Description (LENGTH / RADIUS / WIDTH / θ_{Left}, θ_{Right}) [Source].

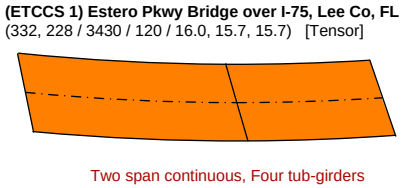

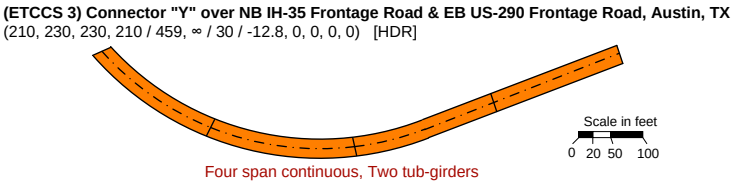

Figure C.6. Existing Tub-girder bridges, Continuous-span, Curved with Skewed supports, (ETCCS #) Description (LENGTH1, LENGTH2, … / RADIUS1, RADIUS2, … / WIDTH / θ_{Left}, …, θ_{Right}) [Source].

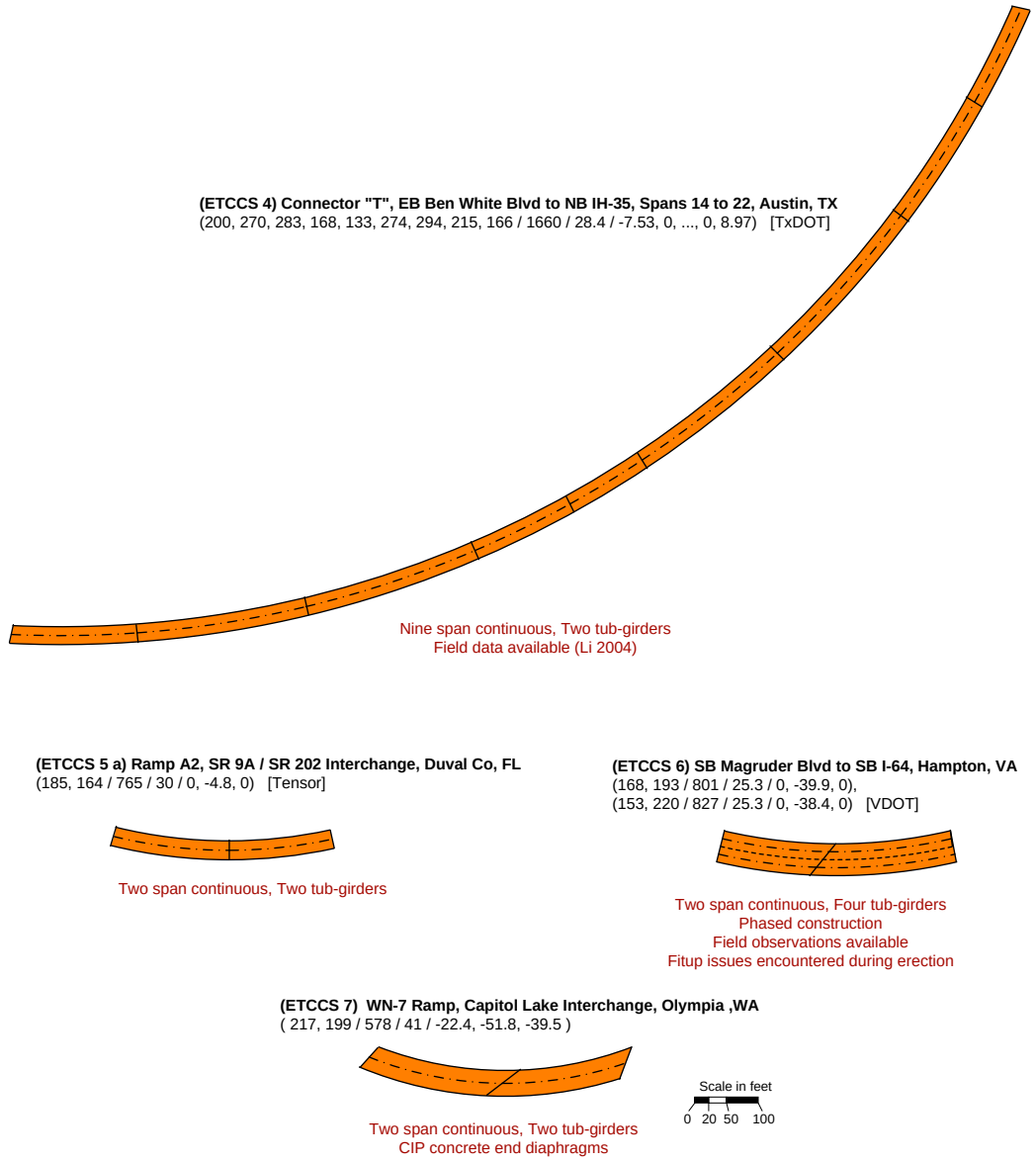

Figure C.6. (continued). Existing Tub-girder bridges, Continuous-span, Curved with Skewed supports, (ETCCS #) Description (LENGTH1, LENGTH2, … / RADIUS1, RADIUS2, … / WIDTH / θ_{Left}, …, θ_{Right}) [Source].

APPENDIX D.

EXECUTIVE SUMMARIES OF STUDY BRIDGES

This appendix provides executive summary of the bridges that were studied in the research. The bridges are grouped in their designated categories with their basic geometry information, key indices, and summary of the important observations. Table D.1 summarizes the main geometric characteristics of the bridges. The bridge layouts schematically illustrate the lateral boundary conditions.

Table D.1. General deck geometry of the analytical study bridges

Bridge ID	Span Length	Curvature Radius	Deck Width	Skew Angles	Number of Girders
XTCSN3	206 ft, 275 ft, 206 ft	–	43 ft	–	2
NTSSS1	150 ft	–	30 ft	15°, 15°	2
NTSSS2	150 ft	–	30 ft	30°, 30°	2
				15°, 15°	
				0°, 0°	
NTSSS4	150 ft	–	30 ft	16°, -16°	2
				10°, -10°	
				0°, 0°	
ETSSS2	205 ft	–	56.5 ft	33.4°, 33.4°	3
NTSCR1	150 ft	400 ft	30 ft	–	2
NTSCR2	150 ft	600 ft	30 ft	–	2
NTSCR5	300 ft	1360 ft	30 ft	–	2
NTCCR1	150 ft, 150 ft, 120 ft	268 ft	30 ft	–	2
ETCCR15	155 ft, 169 ft, 232 ft, 185 ft, 185 ft, 144 ft	515 ft, 960 ft, ∞, -1904 ft	29.5 ft	–	2
XTCCR8	160 ft, 210 ft, 160 ft	700 ft	40.5 ft	–	2
ETCCR14	189 ft, 291 ft, 183 ft	896 ft	40.8 ft	–	2
NTCCR5	350 ft, 350 ft, 280 ft	1380 ft	30 ft	–	2
NTSCS5	150 ft	400 ft	30 ft	10.7°, -10.7°	2
NTSCS29	225 ft	820 ft	30 ft	15.7°, 0°	2
				0°, 0°	
ETCCS5a	183 ft, 161 ft	765 ft	36.2 ft	0°, 4.8°, 0°	2
				0°, –10°, 0°	
				0°, 0°, 0°	
				0°, 10°, 0°	
ETCCS6	160 ft, 207 ft	814 ft	50.5 ft	0°, 39.2°, 0°	2
NTCCS22	250 ft, 250 ft	713 ft	30 ft	20.1°, 0°, 0°	2
				0°, 0°, 0°	

D.1 TCSN (Tub-girder, Continuous, Straight, No Skewed Supports)

XTCSN3 (L_1 = 206 ft, L_2 = 275, L_3 = 206 ft / w = 43 ft, 2 tub-girders)

Example Tub-Girder Bridge Design, Continuous-Span,

Straight, Zero Skew (NHI 2007)

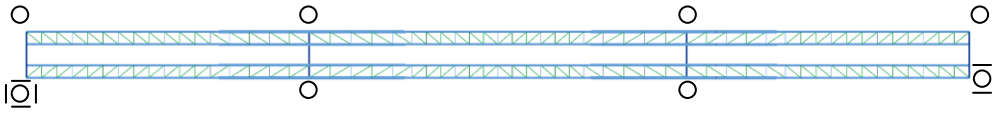

- I_{S1} = 0, I_{S2} = 0, I_{S3} = 0 / I_{L1} = 1.0, I_{L2} = 1.0, I_{L3} = 1.0 / I_{T1} = 0.5, I_{T2} = 0.5, I_{T3} = 0.5
- Internal torsional force caused by eccentric vertical loading.
- Pratt TFLB layout.

D.2 TSSS (Tub-girder, Simple-span, Straight, Skewed supports)

NTSSS1 (L_1 = 150 ft / w = 30 ft / θ_1 = 15°, θ_2 = 15°, 2 tub-girders)

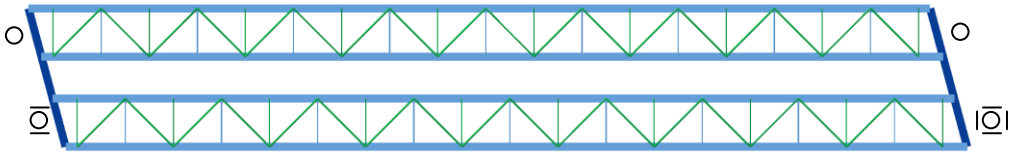

- I_{S1} = 0.03 / I_{L1} = 1.0 / I_{T1} = 0.5
- Torsion due to skew not captured by ordinary 1D analysis. Torque equations provided approximate torsional moment to apply to 1D model.
- 2D-Grid analysis prediction of the torsional moment depends on the model of the external end diaphragm; softer diaphragm causes underprediction of the torque.
- The torsional response is mostly insensitive to diaphragm plate thicknesses within a range of commonly used values on 3D FEA.
- The top flange major-axis bending stress distribution has a saw-tooth pattern matching the position of the TFLB locations.
- Plan layout does not permit the use of intermediate cross-frames.
- Constant torsional moment on the girders causing a constant force on the TFLB.

NTSSS2 (L_1 = 150 ft / w = 30 ft / θ_1 = 30°, θ_2 = 30°, 2 tub-girders)

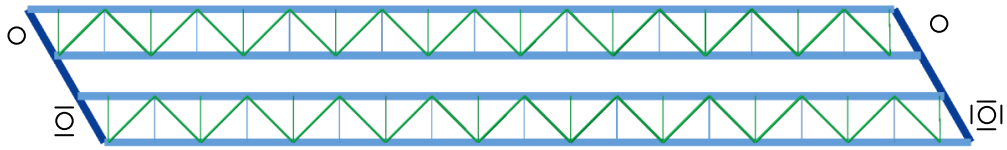

- I_{S1} = 0.06 / I_{L1} = 1.0 / I_{T1} = 0.5
- Increased skew angle with respect to NTSSS1, torsional effects increased.
- Same TFLB and top flange interaction as reported on NTSSS1.
- Sensitivity studies with skew variations of 0°, 15° and 30° show the correlation of skew and torsional moment.

NTSSS4 (L_1 = 150 ft / w = 30 ft / θ_1 = 16°, θ_2 = --16°, 2 tub-girders)

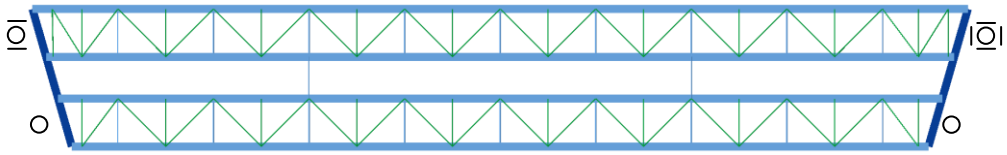

- I_{S1} = 0.03 / I_{L1} = 1.06 / I_{T1} = 0.48
- Due to the equal and opposite skew of the bearing lines, the girder torsional moment is zero, however, the girders exhibit a rigid body twist about their longitudinal axis.
- Girder twist rotation can cause fit-up and slab thickness issues if not accounted for.
- TFLB forces remain low due to rigid body rotation and zero torsional moment.
- No evidence of TFLB and top flange interaction since the sawtooth depends on the torsional moment in greater measure than on bending.
- Sensitivity studies with skew variations of 0° and 10° no direct torsional moment.

ETSSS2 (L_1 = 205 ft / w = 113 ft / θ_1 = 33.4°, θ_2 = 33.4°, 6 tub-girders, phased construction, two units of 3 girders each)

Sylvan Bridge over Sunset Hwy, Multnomah Co. OR

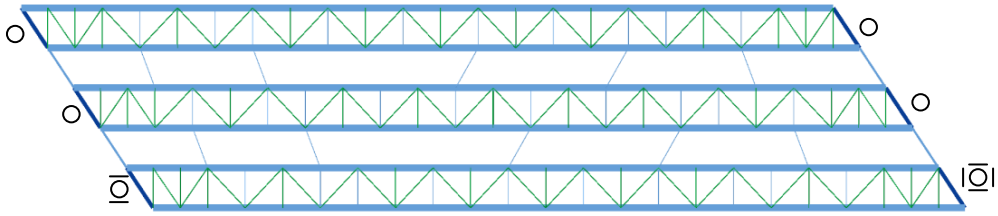

- I_{S1} = 0.13 / I_{L1} = 1.0 / I_{T1} = 0.5
- Cross-flames are used between girders during stages studied are flexible providing reduced torsional interaction as compared to rigid plate diaphragms.
- Double bearing configuration used at each girder end. Negative reactions found at one of each bearings.
- In 2D analyses the double bearing can be modeled by using an additional rigid member between the bearings.
- Skewed external intermediate cross-frames used only during construction. Offset at cross-frames bottom chords due to web slope.
- TFLB and top flange interaction is noticeable as saw-tooth shaped top flange major-axis bending stresses.

D.3 TSCR (Tub-girder, Simple-span, Curved, Radial supports)

NTSCR1 (L_1 = 150 ft / R = 400 ft / w = 30 ft, 2 tub-girders)

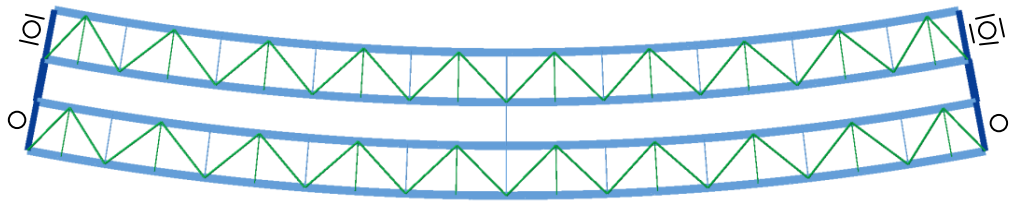

- I_{S1} = 0 / I_{L1} = 1.04 / I_{T1} = 0.83
- Effects of torsional forces are properly predicted by all the types of analysis.
- Intermediate external cross-frame at span center does not affect the vertical displacements or major-axis bending stresses predictions for 1D Line-Girder and 2D-Grid analyses.
- External intermediate cross-frame affects the forces on the internal cross-frame.
- TFLB and top flange interaction is noticeable as saw-tooth shaped major-axis bending stresses.

NTSCR2 (L_1 = 150 ft / R = 600 ft / w = 30 ft, 2 tub-girders)

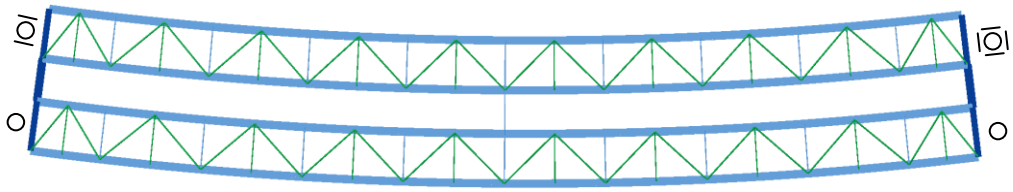

- I_{S1} = 0 / I_{L1} = 1.03 / I_{T1} = 0.72
- Reduced curvature with respect to NTSCR1 (higher curvature radius) proves reduced effects due to skew.
- TFLB and top flange interaction is noticeable as saw-tooth shaped major-axis bending stresses. When compared to NTSCR1 the saw-tooth height is reduced.
- External intermediate cross-frame interaction with the internal cross-frame is observed.

NTSCR5 (L_1 = 300 ft / R = 1360 ft / w = 30 ft, 2 tub-girders)

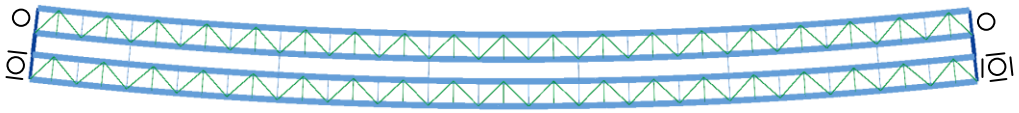

- I_{S1} = 0 / I_{L1} = 1.01 / I_{T1} = 0.87
- Longer span layout uses deeper tubs reducing the bottom flange width.
- Linear and Non-Linear 3D FEA analyses results report negligible differences.
- TFLB and top flange interaction is noticeable as saw-tooth shaped major-axis bending stresses.
- External intermediate cross-frame interaction with the internal cross-frame is observed.

D.4 TCCR (Tub-girder, Continuous-span, Curved, Radial supports)

NTCCR1 (L_1 = 150 ft, L_2 = 150 ft, L_3 = 120 ft / R = 268 ft / w = 30 ft, 2 tub-girders)

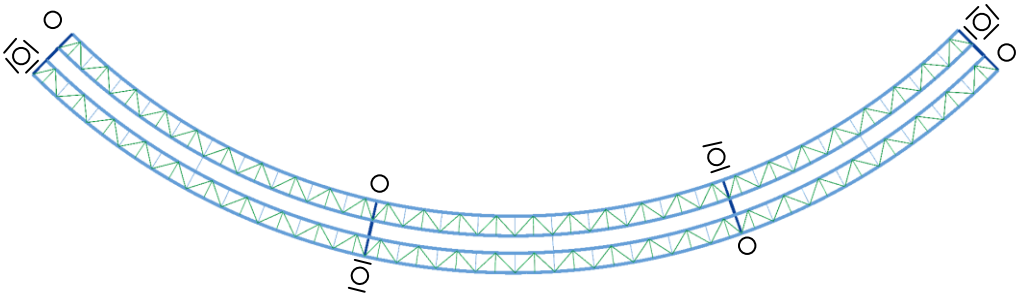

- I_{S1} = 0, I_{S2} = 0, I_{S3} = 0 / I_{L1} = 1.06, I_{L2} = 1.06, I_{L3} = 1.06 / I_{T1} = 1, I_{T2} = 1, I_{T3} = 0.82
- TFLB and top flange interaction is noticeable as saw-tooth shaped major-axis bending stresses. Interaction increased due to curvature.

ETCCR15 (L_1 = 155 ft, L_2 = 169 ft, L_3 = 232 ft, L_4 = 185 ft, L_5 = 185 ft, L_6 = 144 ft / R = 515 ft, 960 ft, ∞, -1904 ft / w = 29.5 ft, 2 tub-girders)

B-40-1122 Marquette Interchange, Milwaukee, WI

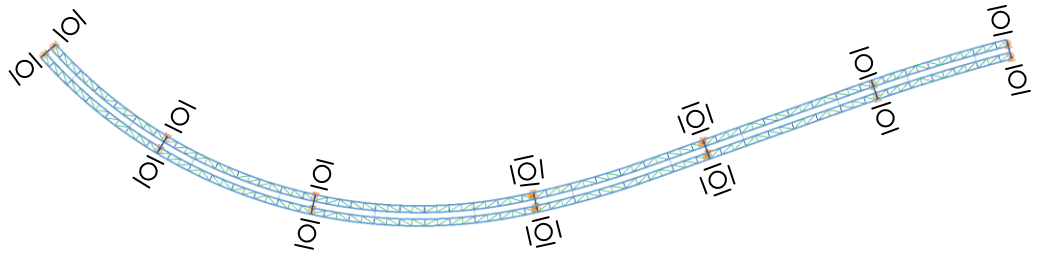

- I_{S1} = 0, I_{S2} = 0, I_{S3} = 0, I_{S4} = 0, I_{S5} = 0, I_{S6} = 0 / I_{L1} = 1.03, I_{L2} = 1.03, I_{L3} = 1.03, I_{L4} = 1.01, I_{L5} = 1.00, I_{L6} = 1.01 / I_{T1} = 0.79, I_{T2} = 0.85, I_{T3} = 1, I_{T4} = 0.66, I_{T5} = 0.50, I_{T6} = 0.57
- Bridge has alternating Pratt layout for TFLB and internal solid plate diaphragms.
- TFLB and top flange interaction is noticeable as saw-tooth shaped major-axis bending stresses. TFLB layout reduced the number of saw-tooth locations.

XTCCR8 (L_1 = 160 ft, L_2 = 210 ft, L_3 = 160 ft / R = 700 ft / w = 40.5 ft, 2 tub-girders)

Example Tub-Girder Bridge Design, Continuous-Span,

Curved, Radial Supports (Kulicki et al. 2005)

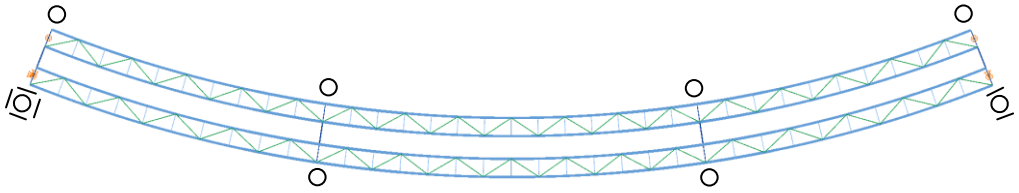

- I_{S1} = 0, I_{S2} = 0, I_{S3} = 0 / I_{L1} = 1.03, I_{L2} = 1.03, I_{L3} = 1.03 / I_{T1} = 0.64, I_{T2} = 0.74, I_{T3} = 0.64
- Double bearing per girder modeled as single bearing.
- TFLB and top flange interaction is noticeable as saw-tooth shaped major-axis bending stresses.

ETCCR14 (L_1 = 189 ft, L_2 = 291 ft, L_3 = 183 ft / R = 896 ft / w = 40.8 ft, 2 tub-girders)

Connector EB North Beltway 8 to NB I-45, Houston, TX

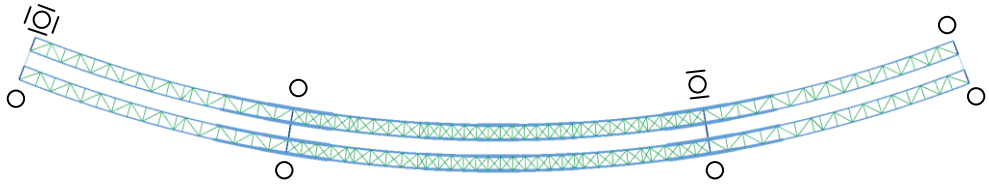

- I_{S1} = 0, I_{S2} = 0, I_{S3} = 0 / I_{L1} = 1.02, I_{L2} = 1.02, I_{L3} = 1.02 / I_{T1} = 0.66, I_{T2} = 0.88, I_{T3} = 0.65
- TFLB and top flange interaction is noticeable as saw-tooth shaped major-axis bending stresses at spans 1 and 3 with Warren-type top truss, no noticeable interaction at center span with X-type top truss system.

NTCCR5 (L_1 = 350ft, L_2 = 350 ft, L_3 = 280 ft / R = 1380 ft / w = 30 ft, 2 tub-girders)

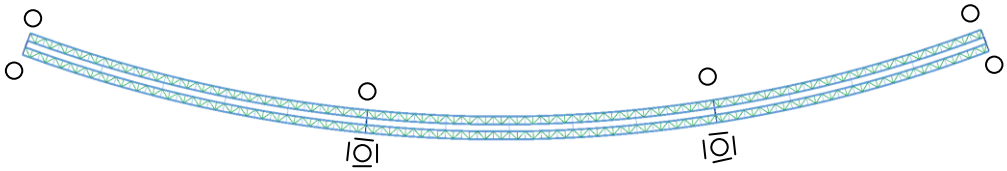

- I_{S1} = 0, I_{S2} = 0, I_{S3} = 0 / I_{L1} = 1.01, I_{L2} = 1.01, I_{L3} = 1.01 / I_{T1} = 1, I_{T2} = 1, I_{T3} = 0.82
- Linear and Non-Linear 3D FEA analyses results report negligible differences.
- TFLB and top flange interaction is noticeable as saw-tooth shaped major-axis bending stresses.

D.5 TSCS (Tub-girder, Simple-span, Curved, Skewed supports)

NTSCS5 (L_1 = 150ft / R = 400 ft / w = 30 ft / θ_1 = 10.7°, θ_2 = -10.7°, 2 tub-girders)

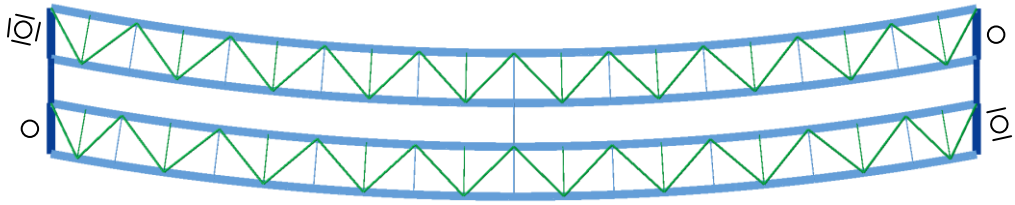

- I_{S1} = 0.02 / I_{L1} = 1.00 / I_{T1} = 0.81
- Lateral displacements start at non-zero value at skewed support locations. 2D-Grid matches the results.
- TFLB and top flange interaction is noticeable as saw-tooth shaped major-axis bending stresses.
- No additional torque due to skew.

NTSCS29 (L_1 = 225ft / R = 820 ft / w = 30 ft / θ_1 = 15.7°, θ_2 = 0°, 2 tub-girders)

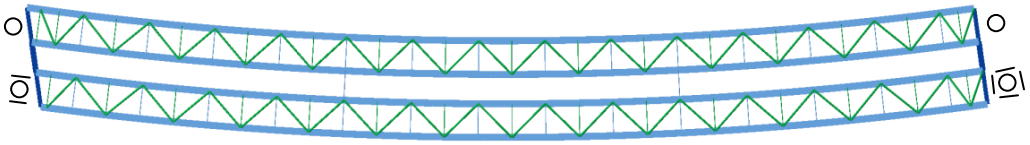

- I_{S1} = 0.02 / I_{L1} = 1.00 / I_{T1} = 0.84
- Lateral displacements start at non-zero value at skewed support location. 2D-Grid matches the results.
- TFLB and top flange interaction is noticeable as saw-tooth shaped major-axis bending stresses.
- Constant additional torque due to skew.
- Sensitivity study comparing to base radial case (0°) show that the constant moment due to skew is additive to the torque due to curvature.

D.6 TCCS (Tub-girder, Continuous-span, Curved, Skewed supports)

ETCCS5a (L_1 = 183 ft, L_2 = 161 ft / R = 765 ft / w = 36.2 ft / θ_1 = 0°, θ_2 = 4.8°, θ_3 = 0°, 2 tub-girders)

Ramp A2, SR 9A / SR 202 Interchange, Duval Co, FL

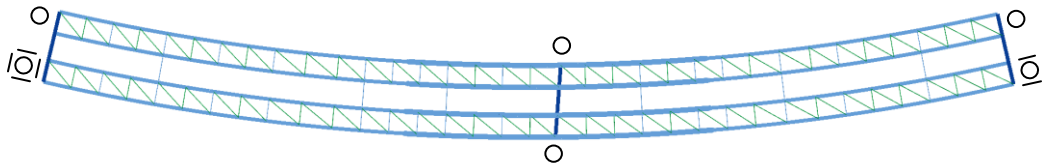

- I_{S1} = 0.01, I_{S2} = 0.01 / I_{L1} = 1.02, I_{L2} = 1.03 / I_{T1} = 0.70, I_{T2} = 0.67
- Intermediate skew increases the curvature effects on the left span while the skew counteracts the curvature on the left span. This effect is more noticeable when the angle of the skewed support is larger.
- TFLB and top flange interaction is noticeable as saw-tooth shaped major-axis bending stresses.
- Pratt TFLB
- Sensitivity studies with skew variations of 0°, 10° and -10° show the effect of skew angle sign on the estimations of the torsional moment due to skew.

ETCCS6 (L_1 = 160 ft, L_2 = 207 ft / R = 814 ft / w = 50.5 ft / θ_1 = 0°, θ_2 = 39.2°, θ_3 = 0°, 2 tub-girders)

SB Magruder Blvd to SB I-64, Hampton, VA

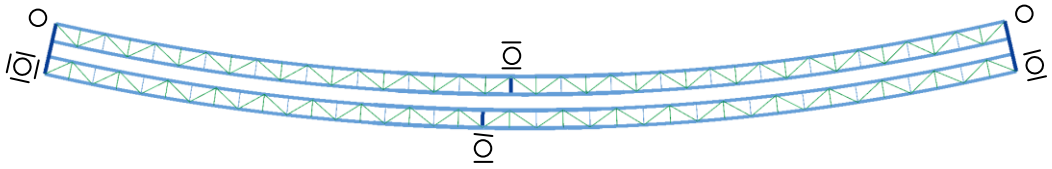

- I_{S1} = 0.06, I_{S2} = 0.05 / I_{L1} = 0.95, I_{L2} = 1.07 / I_{T1} = 0.70, I_{T2} = 0.84 (Stage 1 - Interior)
- I_{S1} = 0.06, I_{S2} = 0.04 / I_{L1} = 0.95, I_{L2} = 1.06 / I_{T1} = 0.68, I_{T2} = 0.95 (Stage 2 - Exterior)
- Staged construction of 2 tub-girders each.
- The lack of external diaphragms at the interior pier helps avoiding the torsional effects due to skew but girder rotations are increased.
- Heavily skewed intermediate supports must have collinear diaphragms and cross-frames to avoid geometric problems with sloped webs.
- Relative vertical displacements of the most extreme flanges have differences of 8in on the completed 4 tub-girder bridge mainly due to the increased relative length of the internal to external girders. These vertical displacements are usually accommodated in the camber but must be predicted accurately.
- TFLB and top flange interaction is noticeable as saw-tooth shaped major-axis bending stresses.

NTCCS22 (L_1 = 250 ft, L_2 = 250 ft / R = 713 ft / w = 30 ft / θ_1 = 20.1°, θ_2 = 0°, θ_3 = 0°, 2 tub-girders)

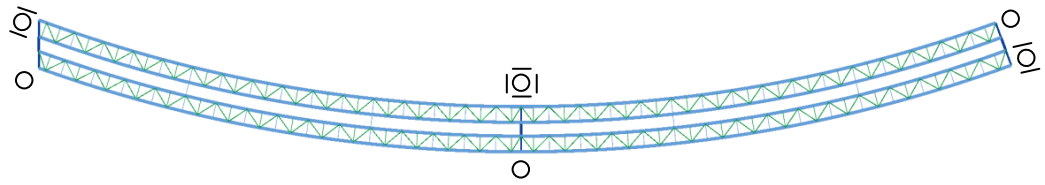

- I_{S1} = 0.02, I_{S2} = 0 / I_{L1} = 1.00, I_{L2} = 1.02 / I_{T1} = 0.98, I_{T2} = 1
- Lateral displacements start at non-zero value at skewed support location. 2D grid matches the results.
- Constant additional torque due to skew on first span. No effects on second span.
- TFLB and top flange interaction is noticeable as saw-tooth shaped major-axis bending stresses.
- Linear and Non-Linear 3D FEA analyses results report negligible differences.
- Sensitivity study comparing to base radial case (0°) verifies that the constant moment due to skew affects only the first span and null effects are observed on the second span.

REFERENCES

AASHTO (2010). "AASHTO LRFD Bridge Design Specifications." 5th Edition, American Association of State Highway and Transportation Officials, Washington, DC.

Bridgesoft, Inc. (2010). "STLBRIDGE, Continuous Steel Bridge Design" http://bridgesoftinc.com

Carnahan, J.D., Grubb, M.A., and Hartmann, J.L. (1997). "Four LRFD Design Examples of Steel Highway Bridges." Example 4, AISI, MI, 65 pp.

Chen, B.S. (1999). "Buckling of U-Shaped Girders with Top-Flange Lateral Bracing." M.S. Thesis, Department of Civil Engineering, The University of Texas at Austin, TX 122 pp.

Chen, B., Yura, J., Williamson, E., and Frank, K. (2005). "Top-Lateral Bracing Systems for Trapezoidal Steel Box-Girder Bridges." Technical Report 0-1898-4. Center for Transportation Research, University of Texas at Austin, TX, 134pp.

Cheplak, B., Memberg, M., Frank, K., and Yura, J. (2002). "Field Measurements of Diaphragm and Top Lateral Members of Three Trapezoidal Composite Box Girder Bridges." Research Report 0-1896-1, Center for Transportation Research, University of Texas at Austin, TX, 125pp.

Cheplak, B. (2001). "Field Measurements of Intermediate External Diaphragms on a Trapezoidal Steel Box Girder Bridge." MS Thesis, University of Texas at Austin, TX, 137pp.

Coletti, D., Fan, Z., Gatti, W., Holt, J. and Vogel, J. (2005). "Practical Tub Girder Design." National Steel Bridge Alliance.

Dabrowski, R. (1968). "Gekrümte dünnwandige Träger: Theorie und Berechnung." Springer-Verlag, Berlin, 1968.

Dabrowski, R. (1972). “Curved Thin-Walled Girders: Theory and analysis.” Cement and Concrete Association, London, 1972.

Fan, Z. (1999). “Field and Computational Studies of Steel Trapezoidal Box Girder Bridges.” Doctoral dissertation, Civil and Environmental Engineering Department, University of Houston, 300 pp.

Fan, Z. and Helwig, T. (1999). “Behavior of Steel Box Girders with Top Flange Bracing.” *Journal of Structural Engineering*, August 1999, ASCE, pp. 829-837.

Fan, Z. and Helwig, T. (2002). “Brace Forces Due to Box Girder Distortion.” *Journal of Structural Engineering*, V. 128, No. 6, June 2002, pp. 710-718.

Gaylord, E.H., Gaylord, C.N., and Stallmeyer, J.E. (1997). “Structural Engineering Handbook.” 4th Ed., McGraw-Hill Book Co., New York.

Grubb, M. (1984). “Horizontally Curved I-Girder Bridge Analysis: V-Load Method.” Transportation Research Record, No. 289, 1984, pp. 26-36.

Heins, C.P. (1975). “Bending and Torsional Design in Structural Members”, Heath and Company, Massachusetts.

Helwig, T., Yura, J., Herman, R., Williamson, E., and Li, Dawei (2007). “Design Guidelines for steel trapezoidal box girder systems.” Technical Report No. FHWA/TX-07/0-4307-1. Center for Transportation Research, University of Texas at Austin, TX, 84pp.

Kim, K. (2004). “Research on horizontally curved steel box girders.” Ph.D. Dissertation, Auburn University, Alabama.

Kim, K., and Yoo, C. H. (2006). “Brace forces in steel box girders with single diagonal lateral bracing systems.” *Journal of Structural Engineering*, V. 132 No. 8, ASCE, pp. 1212-1222.

Kollbrunner, C. F. and Basler, K. (1969). “Torsion in Structures.” Springer-Verlag, New York.

Kulicki, J. M., Wassef, W. G., Smith, C., Johns, K. (2005). "AASHTO-LRFD Design Example Horizontally Curved Steel Box Girder Bridge." NCHRP Project No. NCHRP 12-52, National Cooperative Highway Research Program, Transportation Research Board, National Research Council, 148 pp.

LARSA (2011). "LARSA 4D, The Complete Software for Bridge Engineering." http://www.larsa4d.com/products/larsa4d.aspx

Li, D. (2004). "Behavior of Trapezoidal Box Girders with Skewed Supports." Doctoral dissertation, Department of Civil and Environmental Engineering, University of Houston, Houston, TX, 251 pp.

MDX (2011). "MDX Software, The Proven Steel Bridge Design Solution." http://www.mdxsoftware.com/

Memberg, M., Yura, J., Frank, K., and Williamson, E. (2002). "A Design Procedure for Intermediate External Diaphragms on Curved Steel Trapezoidal Box Girder Bridges." Research Report 0-1898-1, Center for Transportation Research, University of Texas at Austin, TX, 119pp.

NCHRP (2011). "Guidelines for Analytical Methods and Erection Engineering of Curved and Skewed Steel Deck-Girder Bridges." NCHRP 12-79, National Cooperative Highway Research Program, Washington, DC, and Transportation Research Board, Washington, DC.

NHI (2007). "Load and Resistance Factor Design (LRFD) for Highway Bridge Superstructures." Design Manual, NHI Course No. 130081, 130081A-130081D, Publication No. FHWA-NHI-07-035, National Highway Institute, Federal Highway Administration, 1982 pp.

NHI (2011). "Analysis and Design of Skewed and Curved Steel Bridges with LRFD, Reference Manual." NHI Course No. 130095, Publication No. FHWA-NHI-10-087, National Highway Institute, Federal Highway Administration, 1476pp.

NSBA (2006). "Guidelines for Design Details." G1.4, AASHTO/NSBA Steel Bridge Collaboration American Association of State Highway and Transportation Officials, Washington, DC.

NSBA (2011). "Guidelines for Steel Girder Bridge Analysis." G13.1, AASHTO/NSBA Steel Bridge Collaboration American Association of State Highway and Transportation Officials, Washington, DC.

Okeil, A. M. and El-Tawil, S. (2004). "Warping Stresses in Curved Box Girder Bridges: Case Study." *Journal of Bridge Engineering*, ASCE, Vol. 9, No. 5, September 2004, pp. 487-496.

Ozgur, C. (2011). "Influence of Cross-Frame Detailing on Curved and/or Skewed Steel I-Girder Bridges." Ph.D. Dissertation, School of Civil and Environmental Engineering, Georgia Institute of Technology, Atlanta, GA

Poellot, W. (1987). "Computer-Aided Design of Horizontally Curved Girders by the V-Load Method." *Engineering Journal*, AISC, Vol. 24, No. 1, First Quarter 1987, pp. 42-50.

Simulia (2010). "Abaqus, Realistic Simulations" http://www.simulia.com

Topkaya, C. and Williamson, E. (2003). "Development of Computational Software for Analysis of Curved Girders under Construction Loads." Computers and Structures, 81, 2087-2098.

Tung, D. and Fountain, R. (1970). "Approximate Torsional Analysis of Curved Box Girders by the M/R-Method." *AISC Engineering Journal*, July 1970, AISC, pp. 65-74.

United States Steel Corporation (1965), "Highway Structures Design Book," ADUSS 88-1895-01, Vol. 1.

VITA

Juan Manuel Jiménez Chong was born in Xochimilco, México. He attended the National Autonomous University of México (UNAM) where he earned a B.S. in Civil Engineering in 2003 and a Master in Civil Engineering in 2005. He worked as structural engineer from 2004 to 2006. In 2007, he moved to the United States to attend the Graduate School of Civil and Environmental Engineering at Georgia Institute of Technology. Upon receiving her Master's degree in 2009, Juan Manuel continued his graduate studies pursuing a Doctoral Degree in Civil Engineering at Georgia Institute of Technology.